Wind Turbine Converter Reliability Analysis Under Realistic Loading

SERMED AB RIDHA ALSAADI

Wind Turbine Converter Reliability Analysis Under Realistic Loading

Sermed Alsaadi

Thesis submitted towards the
degree of Doctor of Philosophy

Department of Engineering
Durham University
United Kingdom
November 2024

Wind Turbine Converter Reliability Analysis Under Realistic Loading

Sermed Alsaadi

Abstract

Electricity generated by wind energy is getting increasing attention as a successful alternative to fossil fuel electricity generators. One of the challenges of wind energy is the reliability of the wind turbine power converter (WTPC) as its failure rate impacts the levelised cost of wind energy. The semiconductor devices have been found to contribute to the WTPC failure rate due to the thermomechanical stress generated by the cycling of their junction temperatures and differences in the thermal expansion coefficients of their internal layers. WTPC lifetime estimation models based on its semiconductors junction temperatures have become widely accepted by industry and academia.

The published articles in this field use wind turbine modelling to analyse the WTPC lifetime considering operating conditions and different wind turbine technologies. However, important modelling details are required to ensure results accuracy alongside a proper analysis method to develop valid conclusions. To emulate the actual WTPC loading, variable wind speed profiles covering a good range of wind speeds and turbulence intensities are essential for WTPC lifetime estimations. Also, the complexity of wind speed changes requires statistical analyses in order to assess WTPC reliability related to variable wind turbine operating conditions. Furthermore, the simulated parameters of modelled wind turbines have to be validated to ensure accurate outputs related to input wind speeds.

In this research, a new WTPC reliability analysis method is presented. It is based on testing hundreds of variable wind speed profiles and uses statistical tools to assess WTPC reliability against wind speeds and turbulence intensity. The method considers the simulated outputs of a validated wind turbine model for WTPC lifetime estimation. The model is demonstrated and tested for converter topologies and control systems that are widely deployed in wind turbine applications. In a contribution to this field, the research found that wind turbulence intensity shows a statistically significant impact on WTPC lifetime at a 95% confidence level in all tested models. In comparing the impact of wind turbine design factors on WTPC lifetime, the research found that WTPC with direct torque control is more impacted by increasing wind speeds and turbulence intensity, resulting in 91% of the lifetime of WTPCs controlled by field-oriented control. WTPC has been significantly developed in their design by implementing the three-level topology in the last ten years. In comparing converter topologies, the research found that 3L-NPC WTPCs lifetime achieves 2.7 to 3.9 times the lifetime of 2L-VSC depending on wind speed and turbulence intensity. This method can be utilised to select the converter topology and control system for a longer WTPC lifetime based on the specific wind speed profile of the proposed site. This method contributes a valid approach to assessing the reliability of future WTPC considering minor changes in the wind turbine model while the overall framework stays unchanged.

Dedication

This thesis is dedicated to the memory of my parents.

Declaration

The work in this thesis is based on research carried out in the Engineering Department, Durham University. No part of this thesis has been submitted elsewhere for any other degree or qualification and it is all my own work unless referenced to the contrary in the text.

Two papers were produced during the research project. This includes conference and journal papers. They are attached in Appendix A. The published papers titles are:

- Sermed Alsaadi, Christopher J Crabtree, Peter C Matthews, and Mahmoud Shahbazi. Understanding wind turbine power converter reliability under realistic wind conditions. IET Power Electronics, n/a(n/a), 2024.
- Sermed A.B.R. Alsaadi, Peter C. Matthews, and Christopher J. Crabtree. Control Strategy Assessment for Wind Turbine Converter Reliability. In IET Conference Proceedings, volume 2022, pages 230–234, 2022.

Acknowledgement

I would like to express my sincere thanks to my supervisors Prof Christopher Crabtree and Dr Peter Matthews, for their considerable support, advice, patience and above all encouragement throughout this research. A special thanks to Dr Mahmoud Shahbazi for his assistance in the research and publishing.

I like to thank the staff of the Engineering Department and colleagues for their cooperation and help during this research.

I want to thank my family, Zaman and Rasool, for their patience and travelling and special thanks to my sister, Rana, for encouraging me during this journey.

This research was made possible by funding from the UK Prosperity Partnership in Offshore Wind (EP/R004900/1) (npow.group.shef.ac.uk).

Contents

List of Figures

List of Tables

Nomenclature

a	Coffin-Manson model empirical constant
A_t	Wind turbine swept area
b	Coffin-Manson model empirical constant
C_p	Wind turbine power coefficient
$C_{LT,ds}$	Capacitor lifetime in the datasheet
C_{LT}	Capacitor lifetime
CI	Confidence interval
d	Diode
D_{bond}	Bond wire diameter
$D_{f,cycle}$	Damage to failure caused by one thermal cycle
$D_{f,VWSP}$	Damage to failure cause by one variable wind speed profile
D_{sh}	Wind turbine shaft damping constant
E_a	Activation energy
E_{off}	IGBT turn off energy
E_{on}	IGBT turn on energy
E_{rr}	Diode reverse recovery energy
f_g	Grid line frequency
f_m	Generator frequency
f_{sw}	Converter switching frequency
hr	Hour
i	IGBT

I_F Nominal diode current

I_g Grid line current

I_m Generator line current

I_t Power module terminal current

$I_{\alpha\beta}$ Thee phases current in $\alpha\beta$ frame

I_{abc} Thee phases current

I_{Cnom} Nominal IGBT current

I_{DC} DC Bus current

I_{dg} Grid direct current in dq frame

I_{dm} Generator direct current in dq frame

I_{qg} Grid quadrant current in dq frame

I_{qm} Generator quadrant current in dq frame

J_m Generator inertia

J_t Wind turbine rotor inertia

K_B Boltzmann constant

k_p PI integral gain

k_p PI proportional gain

K_{sh} Wind turbine shaft spring constant

L_g Grid filter inductance

L_s Generator stator winding inductance

LTR_{3L} Lifetime ratio of 3L-NPC to 2L-VSC wind turbine power converters

LTR_{DTC} Lifetime ratio of DTC to FOC wind turbine power converters

M Modulation index

$MTTF$ Mean time to failure

N_f Semiconductor's number of thermal cycles to fail

P_d Diode power loss

P_g Active power supplied to the grid

P_i IGBT power loss

P_m Generator power

P_p Generator pole pairs

P_t Wind turbine rotor mechanical power

P_{air} Power carried by wind

P_{cn} Conduction power loss

P_{sw} Switching power loss

Q_g Reactive power supplied to the grid

R Wind turbine rotor radius

R_F Diode on resistance

R_s Generator stator winding resistance

R_{CE} IGBT on resistance

$R_{th,Dev}$ Device thermal resistance

$R_{th,Hs}$ Heatsink thermal resistance

s_d number of diodes in converter circuit

s_i number of IGBTs in converter circuit

S_m Generator apparent power

s_{2L-VSC} Number of parallel converters in 2L-VSC topology wind turbine power converter

$s_{3L-NPCC}$ Number of parallel converters in 3L-NPC topology wind turbine power converter

T_C Capacitor temperature

T_j Junction temperature

t_Σ total delay in the control loop

$T_{C,ds}$ Capacitor temperature in the datasheet

T_{ct} Coolant temperature

t_{dq} Inner control loop time delay

$T_{j,max}$ Maximum value of junction temperature cycle

$T_{j,min}$ Minimum value of junction temperature cycle

T_{jSL} Simulated junction temperature by Simulink

T_{jSS} Simulated junction temperature by SemiSel

t_s Simulation sampling time

TSR Wind turbine tip speed ratio

TSR_{opt} Wind turbine optimal tip speed ratio

U Wind speed

U_{in} Cut-in wind speed

U_{out} Cut-out Wind speed

U_{rated} Wind turbine rated wind speed

V_B Chip blocking voltage

V_g Grid line voltage

V_m Generator line voltage

V_{abc} Thee phases voltage

V_{CE0} IGBT saturated collector emitter voltage

V_{CES} IGBT blocking voltage

V_{d_0} Diode saturated forward voltage

V_{DC} DC bus voltage

V_{dg} Grid direct voltage in dq frame

V_{dm} Generator direct voltage in dq frame

V_{ds} Capacitor datasheet voltage

V_{qg} Grid quadrant voltage in dq frame

V_{qm} Generator quadrant voltage in dq frame

z Confidence level

Z_{base} Per unit base impedance

$Z_{C,Dev}$ Device thermal storage

$Z_{C,Hs}$ Heatsink thermal storage

$Z_{th,Dev}$ Device thermal impedance

$Z_{th,Hs}$ Heatsink thermal impedance

Z_{th} Thermal impedance

Greek

$\alpha_{1..6}$ Bayerer model empirical constants

β Wind turbine blade angle

Δ_{Rel} Relative difference

θ Power factor angle

θ_e Generator rotor angle (electrical)

θ_g Grid voltage angle

λ Failure rate

λ_{2L-VSC} 2L-VSC wind turbine power converter failure rate

λ_{3L-NPC} 3L-NPC wind turbine power converter failure rate

λ_{GSC} Grid side converter failure rate

λ_{MSC} Machine side converter failure rate

μ Statistical mean value

ρ_{air} Air density

σ Statistical standard deviation

τ Torque

τ_{em} Electromagnetic torque developed by wind turbine generator

τ_t Torque developed by wind turbine rotor

ϕ_m Generator flux linkage

ω Angular speed

ω_e Generator rotor angular speed (electrical)

ω_g Grid line angular frequency

Acronyms

2L-VSC Two-level voltage source converter.

3L-ANPC Three-level active neutral point clamped.

3L-NPC Three-level neutral point clamped converter.

Al-CAP Aluminium Electrolytic Capacitor.

CTE Coefficient of thermal expansion.

DC Direct current.

DFIG Doubly fed induction generator.

DOWEC Dutch Offshore Wind Energy Converter.

DTC Direct torque control.

DUT device under test.

EESG Electrically Excited Synchronous Generator.

ESR Capacitor's equivalent series resistance.

FOC Fiel oriented control.

FRC Fully rate converter.

GaN Gallium nitride transistor.

GSC Grid side converter.

IGBT Insulated gate bipolar transistor.

IGCT Intigrated gate-commutated thyristor.

LCOE levelised cost of energy.

LV Low voltage.

LWK Reliability data of Landwirtschaftskammer Germany.

MLC-CAP Multilayer Ceramic Capacitor.

MMC Modular multilevel converter.

MPPF-CAP Metalized Polypropylene Film Capacitor.

MPPT Maximum power point tracking.

MSC Machine side converter.

MTTF Mean time to failure.

MV Medium voltage.

OPEX Project operation cost.

PC Power cycling test.

PDF Probability density function.

PI Proportional-integral controller.

PMSG Permanent magnet synchronous generator.

PMSM Permanent magnet synchronous machine.

PRC Partially rate converter.

pu Per unit value.

PWM Pulse width modulation.

RMSE Root mean square error.

RSC Rotor side converter.

SCADA Supervisory Control and Data Acquisition.

SCIG Squirrel cage induction generator.

SiC MOSFET Silicon Carbide Metal-Oxide Field Effect Transistor.

SPWM Sine wave pulse width modulation.

SVM Space vector modulation.

TC Thermal cycling test.

TSR Tip speed ratio.

VOC Voltage-oriented control.

VWSP Variable wind speed profile.

WSD Reliability data of WindStats survey in Germany.

WSDK Reliability data of WindStats survey in Denmark.

WTPC Wind turbine power converter.

Chapter 1

Introduction

1.1 Wind energy

Humans have exploited the power of the wind since the time of ancient civilisations. Sea ships were the first examples of how humans utilise wind power for commercial use. The extraction of mechanical power from wind continued to develop for other applications like water lifting and grinding. In modern history when electricity commercially started, electrical generators were driven by rotating mechanical power. This develops the idea of using windmills to generate electricity. In 1887, wind power was first used to generate electricity using a 10 meters high windmill with blades covered by sailcloth built by James Blyth, considered the first successful wind-operated electrical generator [1]. Professor Blyth used his windmill generator to charge batteries for night lighting in his holiday house. Wind turbines have become a major source of renewable electrical energy in the UK generating 85TWh, which equals 22.6% of UK electrical energy production in 2022 [2].

Over the past two decades (2000 to 2020), the issue of climate change started to get greater attention around the world. The relationship between increasing the level of CO_2 and global warming became more clear with the record-high temperatures and other impacted environmental conditions like north pole ice melting, increasing sea level, extreme worldwide weather, and dryness of rivers in many countries. All those became clear indications of what humans are going to face if they continue ignoring the impact of increasing CO_2 on the environment. Governments and organisations started to take actions to reduce the CO_2 footprint of industry, transportation, electricity generation, and many other human activities. The use of fossil fuel in electricity generation is responsible for more than 40% of CO_2 emissions related to energy generation [3]. Therefore, alternative sources of electricity generation are needed to reduce the global CO_2 footprint of electricity generation. One of these sources is wind energy which has a considerably low CO_2 footprint compared to other resources like fossil fuel and photovoltaics because the manufacturing process of photovoltaic produces higher CO_2 than the manufacturing of wind energy, wind energy is considered as a lower CO_2 footprint than photovoltaic. [4].

In addition to the global warming issue, renewable energy supports energy security against fuel price fluctuations and geopolitics [5].

These two reasons result in strong energy policies set by many governments to encourage

replacing fossil-fuel electricity generators with what are called renewable energy sources like wind, solar, tidal, biothermal, and geothermal. Wind energy appeared as a successful source of renewable energy for various reasons such as it can operate day and night, it can be installed onshore and offshore, and it has a competitive cost compared with other renewable energy sources. According to the International Energy Agency (IEA) Net Zero Emissions scenario for 2050, wind and solar will provide 70% of the electricity demand worldwide [6].

The Global Wind Report 2022 [7] shows a total of 93.7GW new wind power installed in 2021 added to the globally installed wind generators (total of 837GW) making the annual growth at 12%. The projection of global wind power based on the current growth will be 1,400GW by 2030 however it is required to reach 3,200GW of installed wind power by 2030 to meet the 2050 zero emissions scenarios. These numbers show an increasing global interest in wind energy and in the related research in this field by academia and industry for developing wind turbines towards more reliable and higher power sources of electricity.

1.2 Wind turbines

1.2.1 Fixed speed wind turbines

The early commercially produced wind turbines, called type 1 wind turbines [8], were built utilising the squirrel cage induction generator (SCIG). The fixed-speed generator is required to rotate at a speed which is slightly higher than its synchronous speed imposed by the grid frequency to generate electrical power. The SCIG consumes reactive power and therefore requires a reactive power source for its operation which is provided by a capacitor bank connected in parallel with the generator windings. A soft starter is deployed optionally in these wind turbines for smooth starting to avoid high transient currents when connecting to the grid [9]. The electrical system of this wind turbine, as shown in figure 1.1, does not contain a power converter therefore it is considered simple. It is also reliable, low-cost, and robust. However, the fixed-speed wind turbine has disadvantages because it operates at a fixed rotating speed. It cannot perform maximum power point tracking which limits the wind turbine's capacity factor [8]. Moreover, the fluctuation of wind speed is transmitted to the wind turbine mechanical system producing stress on the wind turbine blades and producing fluctuations in the supplied current to the grid.

1.2.2 Variable speed wind turbines

The mechanical power extracted from the wind by the wind turbine is related to the value of tip speed ratio (TSR) which is the ratio of the blade tip speed to the wind speed. The highest extracted power occurs at an optimum value of TSR (TSR_{opt}). Figure 1.2 shows the relationship between the turbine mechanical output power, in per unit (pu), and the turbine's rotational speed, in pu, for different wind speeds which shows that at each wind speed, the turbine's maximum power occurs at different rotating speeds. Therefore, aiming to extract the highest possible power from the wind over the wide range of available wind speeds, the wind turbine has to change its rotating speed according to the wind speed to improve its capacity

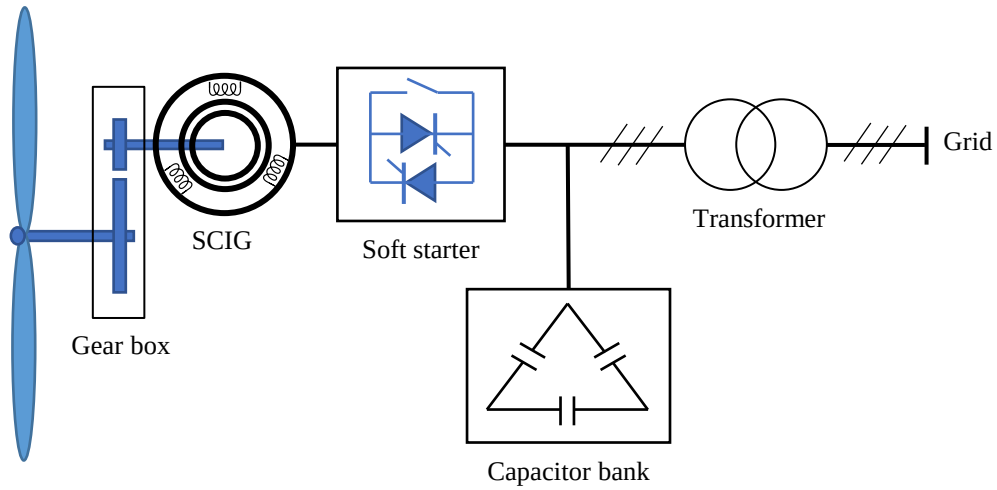

Figure 1.1: Fixed speed SCIG wind turbine

factor.

This advantage is achieved in wind energy by introducing the variable speed wind turbine. The optimum rotating speed is calculated according to the wind speed by the maximum power point tracking (MPPT) controller. A further advantage of the variable speed wind turbine is lowering the mechanical stress on the rotor blades allowing bigger blades to be installed and therefore higher power wind turbines to be produced [9]. To protect the wind turbine from high rotating speed, the pitch control system is introduced by controlling the blade attacking angle to reduce the developed torque when the wind turbine rotating speed reaches the designed rated value.

The advantages of the variable-speed wind turbine come with the cost of a more complex electrical system than the fixed-speed wind turbine. Methods were used in variable-speed wind turbines to control the generator speed like SCIG with variable rotor resistance in wind turbine type 2 [10]. The generator speed was controlled through external variable resistors connected to the rotor windings via slip rings. This technique provided a variable speed range of 10% of the wind turbine rotating speed. This method, however, involved extra power losses and could not control the reactive power produced by the SCIG, which became a requirement by the grid code.

The next generation of wind turbines, type 3, was based on the doubly-fed induction generator (DFIG) which could achieve control of the reactive power with an even higher variable speed range reaching 30% of the wind turbine rotating speed [10]. The DFIG requires an AC-DC-AC back-to-back power converter for the rotor windings circuit. The advantage of using the power converter in DFIG is to control the rotor field strength and frequency so the stator winding generates a fixed frequency current even with variable speed rotation besides the ability to control the machine's reactive power. The power converter became an essential part of the wind turbine electrical system for the DFIG wind turbine and the next wind turbine generator, type 4, which is based on the Permanent Magnet Synchronous Generator (PMSG) [8].

Power converters are also used with the variable speed SCIG and the Electrically Excited Synchronous Generator (EESG) wind turbines. The power converter in wind turbines enables a wide range of control over the generator speed and the wind turbine's active and reactive output power as per the grid code requirement.

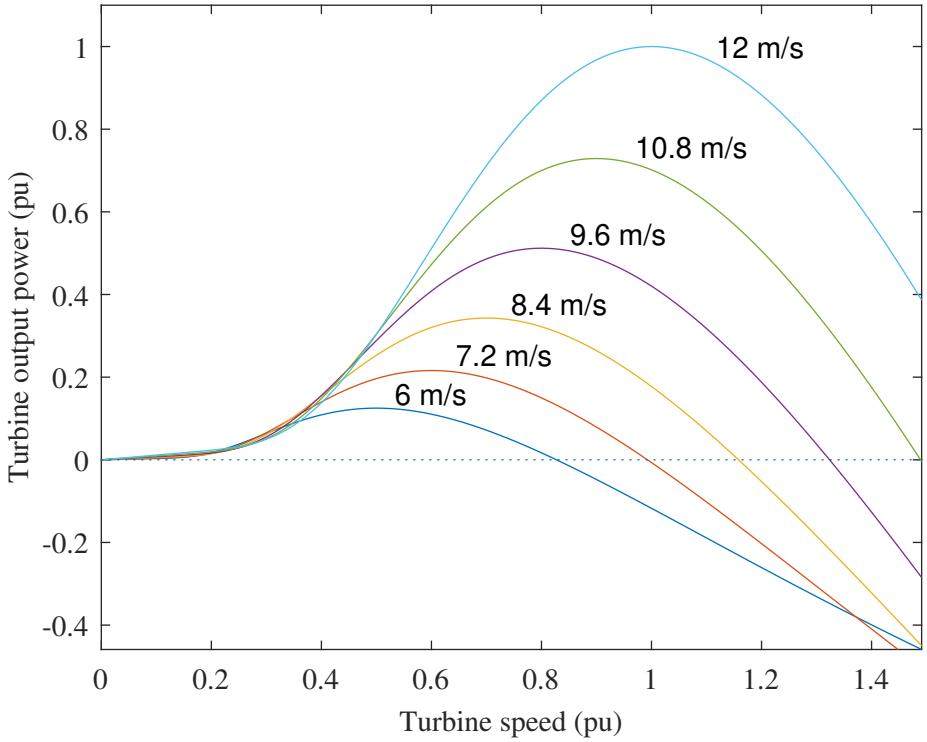

Figure 1.2: Wind turbine output power for different wind speeds

1.3 The power converter

The power converter is a multiport electronic circuit containing semiconductor switches that operate to facilitate the electrical energy exchange between two or more subsystems [11]. Power converters vary in design and the type of semiconductors used according to the application operating parameters, voltage, current, and frequency where they are deployed in various applications like motor speed control in industry, trains, and electric vehicles and as voltage regulators in power systems, home appliances, adapters, and renewable energy sources [12]. The three-phase two-level voltage-source converter (2L-VSC) is a widely deployed power converter in industry, power systems, and renewables [13]. This converter consists of six semiconductor switches which can be transistors or thyristors connected with reverse freewheeling diodes. Figure 1.3 shows a schematic diagram of the three-phase 2L-VSC using Insulated Gate Bipolar Transistors (IGBT).

1.3.1 Power converter operation

The power converter's semiconductor switches are operated in a systematic sequence to produce the required output parameters. The required voltage level is obtained by controlling the

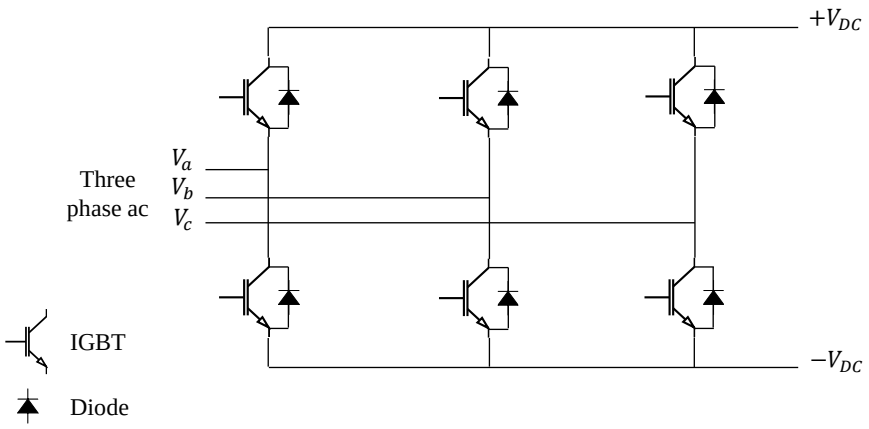

Figure 1.3: Schematic diagram of the three-phase 2L-VSC

switches on and off times [13]. This method is called Pulse Width Modulation (PWM) which is widely implemented in current power converters in industry and power systems. When PWM is used to generate sinewave output, it is called Sinewave PWM (SPWM) while other pulse modulations are also available to use with power converters like the Space Vector Modulation (SVM) [14]. The type of pulse modulation is chosen according to the applied control strategy and the converter design. During the operation of the power converter, power losses are produced due to the interaction between the semiconductor current and its internal parameters like resistance, threshold voltage, and capacitance [11]. The converter power losses impact its efficiency and produce heat that is required to be dissipated by a heatsink to protect the semiconductors from the damaging high temperature.

1.3.2 Power converters in wind energy

The deployment of power converters in wind turbines started when the variable-speed wind turbine was introduced to convert the variable frequency of the generator into a fixed frequency for the load [15]. A variety of wind turbine power converter (WTPC) designs appeared in wind turbines however the three-phase 2L-VSC became popular in this application due to its simplicity [16]. The power electronic industry introduced power modules dedicated to wind energy power conversion usually by including the transistor and the freewheeling diode in one power module. Examples of the available power modules are SKM800GA176D manufactured by SEMIKRON DANFOSS [17] and 5SNG0300Q170300 by Hitachi ABB [18]. They also introduced more advanced and compact power converter stacks which contain modular half-bridge or full-bridge power converters with their drives to be installed in wind turbines for easier installation and replacement like SKiiP 3 [19]. During the rapid development of wind turbines in the last 20 years, bigger wind turbines with higher power were introduced in the market. The generator type has evolved as well from SCIG to DFIG and then to PMSG. Each of those generators offers advantages over its predecessor however each of those requires changes in the wind turbine electrical system and mainly in the power converter circuit which affects the power converter design and semiconductor types.

Figure 1.4: SEMIKRON SKM800GA176D IGBT power module, as published in [17]

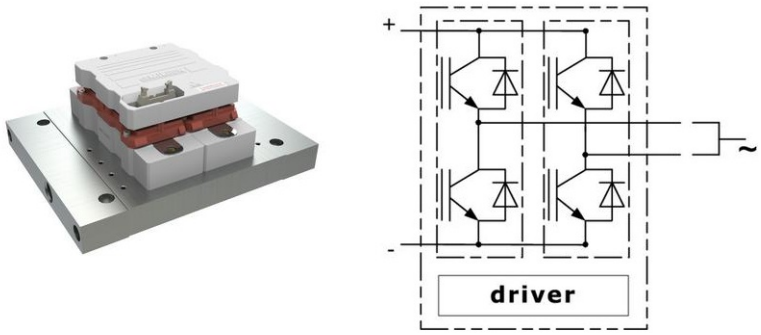

Figure 1.5: Power converter stack, as published in [19]

1.3.3 Fully rated power converter

A fully rated power converter (FRC) is required for the variable speed wind turbines with SCIG, EESG, or PMSG where the wind turbine generator's full power passes through the WTPC [20]. In this design, the WTPC consists of three main parts: the Machine Side Converter (MSC), the DC bus, and the Grid Side Converter (GSC). The MSC rectifies the generator current into DC and feeds it to the DC bus. The GSC works as an inverter producing a fixed frequency and voltage as required and supplies it to the grid transformer or the load. Figure 1.6 shows a fully rated WTPC deployed in a PMSG wind turbine.

1.3.4 Partially rated power converter

Wind turbines equipped with the DFIG require a partially rated power converter (PRC) in which only the generator rotor power passes through the WTPC while the generator stator power is delivered directly to the grid through the wind turbine three windings transformer [21]. The PRC consists of a rotor side converter (RSC), a DC bus, and a GSC. Figure 1.7 shows the power converter connection in the DFIG wind turbine.

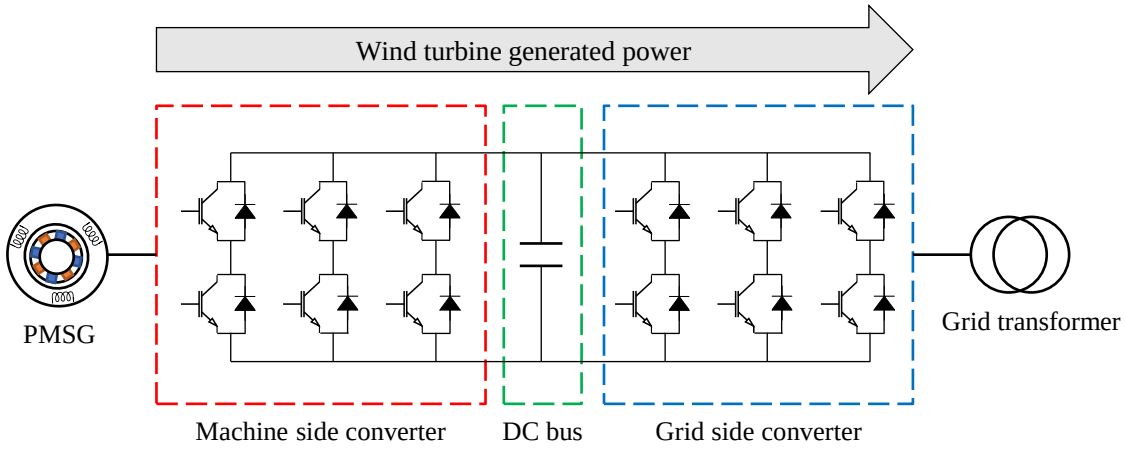

Figure 1.6: Fully rated power converter in PMSG wind turbine

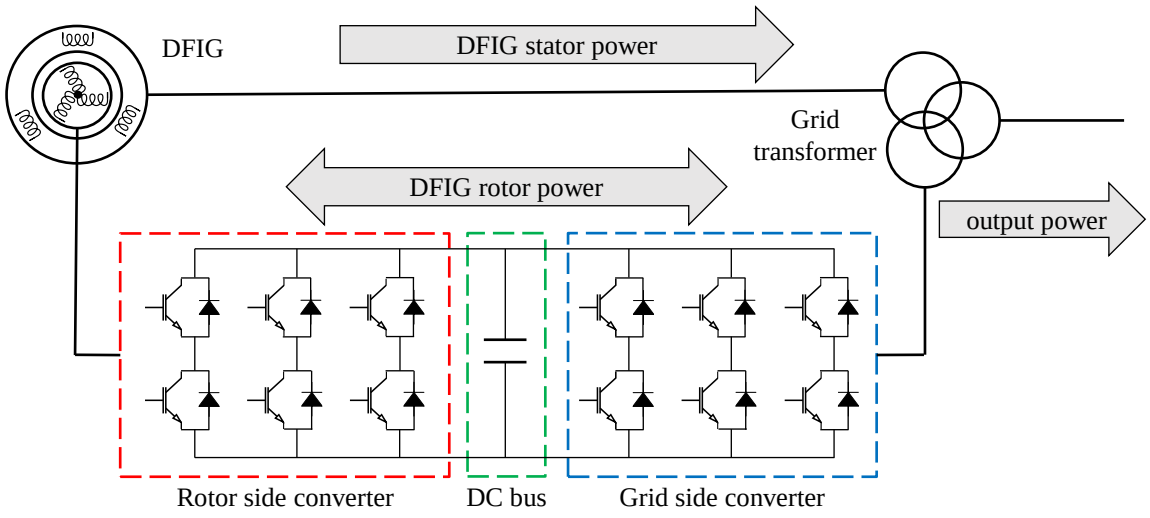

Figure 1.7: Partially rated power converter in DFIG wind turbine

1.3.5 WTPC control

The WTPC control system is an essential part of the wind turbine as it controls the conversion of most of the extracted power from the wind through all the wind turbine parts and aims that the delivered power meets the grid interconnection requirements [22].

In FRC used with PMSG, WTPC is controlled by two controllers one for MSC and the other controls GSC. A variety of control schemes were used with WTPC however a widely used scheme is controlling the GSC to stabilise the DC bus voltage and to control output reactive power while the MSC is controlled to extract the maximum available power from the wind turbine generator [23]. Similarly in PRC WTPC used with DFIG, WTPC is controlled by two controllers, for GSC and RSC. The GSC control regulates the DC bus voltage and controls output reactive power while the RSC control aims to keep the DFIG output frequency synchronised to the grid and controls output active power [24].

Vector control strategies like Field Oriented Control (FOC) and Direct Torque Control

(DTC) are widely used in WTPC for performance and protection capabilities [23]. Both control strategies, FOC and DTC, have advantages and drawbacks in their performance however in this research, the reliability impact on WTPC by both control strategies will be presented in Chapter 6.

1.4 Existing megawatt-scale wind turbines and their power converters

The PMSG is widely deployed in large multi-megawatt (6MW and bigger) wind turbines with many advantages including lightweight, reliability, and ease of maintenance [25]. PMSG can operate at low rotating speed therefore the direct-drive wind turbine is produced without the need for the maintenance-intensive gearbox which affects the wind turbine's cost and the nacelle weight [26]. Moreover, the PMSG does not require field current to induce the magnetic field since the permanent magnets provide it, making PMSG more efficient than wound rotor generators. In addition, PMSG is a brushless machine that requires less maintenance than DFIG. These advantages made PMSG a preferable generator for multi-megawatt wind turbines.

1.5 Future power converters for wind turbines

The rapid increase in wind turbine size and power urges power converter manufacturers to use different WTPC designs to adapt to the high power requirement [27]. Two strategies appeared in the WTPC industry to deal with the high power requirement in multimegawatt wind turbines. The first strategy is to continue using the existing low voltage (LV) WTPC which has a voltage rating below 1kV like the popular 690V wind turbines by paralleling converters within the WTPC to accommodate the high power requirements [25, 28]. This strategy benefits from working with the well-known technology of the 2L-VSC and providing high redundancy. If any paralleled converters fail, the others can continue to operate with lower power until the repair is done. An example of this arrangement is used in Gamesa G10x 4.5MW [29] where its WTPC contains 6 parallel power converters 770kW each. The advantages of this strategy are that the 2L-VSC requires relatively simple control and is simpler in maintenance while switching to higher voltage WTPC involves more system complexity and maintenance difficulties due to the higher voltage safety requirements.

The other strategy adopts increasing the wind turbine rated voltage by moving from LV to medium voltage (MV) (voltage range from 1kV to 35kV [30]) since increasing the converter voltage reduces the line current. However, for the WTPC to operate with MV wind turbines, the converter design and its semiconductor type have to change. In MV WTPCs, the converter topology changed to the three-level neutral point clamped converter (3L-NPC) to gain higher operating voltage as this converter topology enables the converter operating voltage at twice the semiconductor rated voltage [31]. The converter semiconductor is changed to the integrated gate-commutated thyristor (IGCT) for even higher voltage and high current capabilities than the IGBT used in 2L-VSC WTPC. A popular example of this converter is PCS6000 manufactured by Hitachi ABB company [32] which is deployed in wind turbines like GE HaliadeX 12 MW [33,34].

The supporters of this strategy claim that higher voltage WTPCs reduce the sizes and weights of the cables and transformer which reflects on the wind turbine nacelle weight and structure [35]. Also, they claim that MV WTPC with IGCT is more reliable than LV WTPC with IGBT [36]. In this research, the WTPC reliability comparison between both converters, the LV 2L-VSC and the MV 3L-NPC will be presented in Chapter 6.

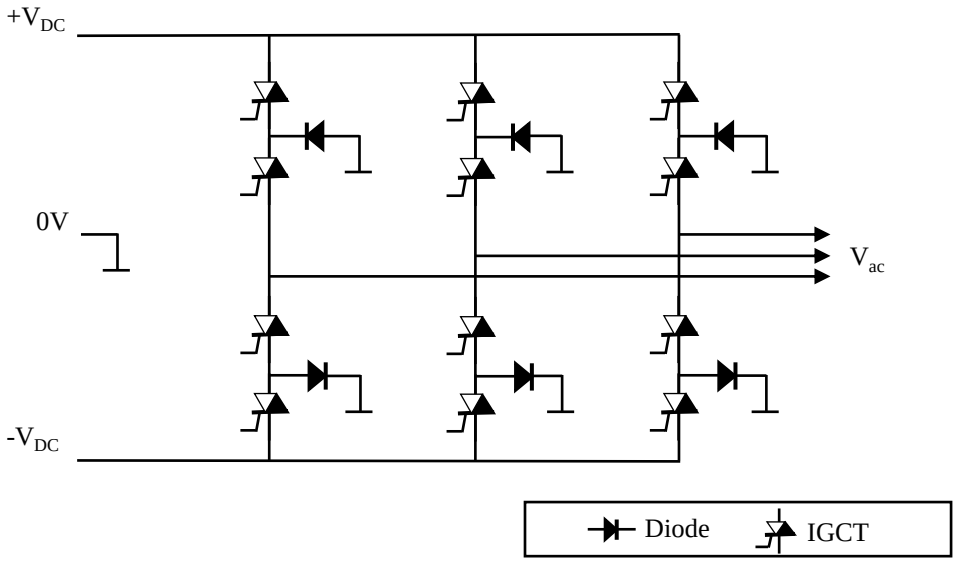

Figure 1.8: Schematic diagram of 3L-NPC using IGCTs

1.6 Wind turbine reliability

1.6.1 Introduction to reliability

The reliability of a machine is defined as the probability that the machine is functioning as expected for the specified time [37]. A number of failures might occur during the operating time of the machine where this number of failures is used to evaluate the machine reliability indicators. The reliability function (R) is used to evaluate the reliability of a machine, assembly, or component where $1 \geq R \geq 0$ and calculated by equation (1.1) [38].

$$R = 1 - Porbability\ of\ failure \tag{1.1}$$

One of the reliability indicators is the failure rate (λ) defined as the number of failures that occurred during a specified time calculated by equation (1.2). Machines usually contain assemblies and components that have failure rates which contribute to the machine's failure rate. The failure rate of the machine is equal to the summation of the failure rates of all its parts including subassemblies and components as expressed in equation (1.3) where λ_{p1},λ_{p2}, and λ_{p3} are failure rates of part1, part2, and part3. For the machine containing n parts, λ is the summation of the failure rates of all its parts calculated as in equation (1.4).

$$\lambda = \frac{\text{number of failures}}{\text{time}} \tag{1.2}$$

$$\lambda = \lambda_{p1} + \lambda_{p2} + \lambda_{p3} + ... \tag{1.3}$$

$$\lambda = \sum_{i=1}^{n} \lambda_{pi} \tag{1.4}$$

The machine failure rate changes in three age stages during the machine's lifetime, from when it started until it wore out. The early age stage of operation (burn-in), the useful life stage, and the end-of-life stage (wear out). The machine failure rate during the three stages of the machine lifetime can be illustrated by the bathtub curve as shown in figure 1.9. During the machine's useful life stage, the failure rate as a function of time ($\lambda(t)$) shows a steady value against time. Therefore, the exponential distribution is suitable to describe the probability of failure occurring in this age stage as in equation (1.5) where $F(t)$ is the probability of the failure occurring at time t [39]. Accordingly, the machine's reliability, $R(t)$, which is the complement of the probability of failure occurring is calculated as in equation (1.7) [40].

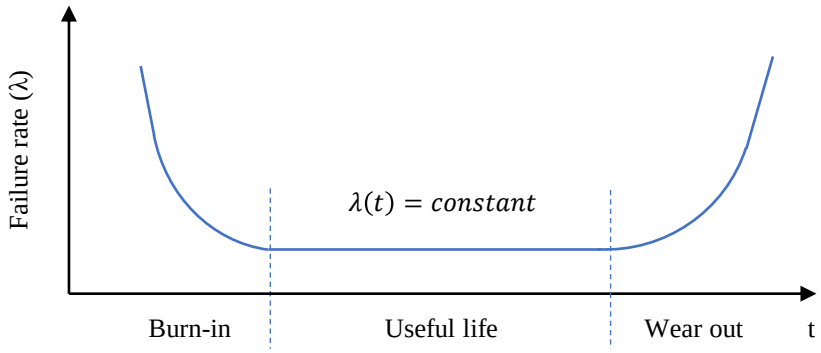

Figure 1.9: Bathtub curve

$$F(t) = 1 - e^{-\lambda t} \tag{1.5}$$

$$R(t) = 1 - F(t) \tag{1.6}$$

$$R(t) = e^{-\lambda t} \tag{1.7}$$

1.6.2 Mean Time to Failure and B10 indicators

The term "mean time to failure" (MTTF) is a reliability indicator used to evaluate the lifetime of a machine, subsystem, or component. MTTF is a statistical indicator used to describe the average time before the machine or component fails and is calculated as the integral of reliability function ($R(t)$) as in equation (1.8) [41].

Since $R(t)$ has exponential distribution, the MTTF value presents the estimated minimum time in which approximately 37% of the total number of the machines, or components, are

expected to have not failed. An example of that is if a wind farm includes 100 wind turbines each with MTTF of 20 years then after 20 years it is expected that at least 37 wind turbines will be in operation while 63 wind turbines might have failed.

$$MTTF = \int R(t)dt = \int e^{-\lambda t}dt = \frac{1}{\lambda} \tag{1.8}$$

Some industries found that the MTTF indicator is not a suitable indicator for the component lifetime because during that time most of the components (63% of the total) would have failed. Therefore, the bearings manufacturers presented the B_{10} indicator which estimates the time when 90% of the items have not yet failed but only 10% of them might have failed. The name B_{10} came from "Bearings" and the failed 10% of the total parts. Following the same distribution of reliability function ($R(t)$), B_{10} is calculated as in equation (1.10). Figure 1.10 shows the exponential distribution of the reliability function $R(t)$ with both B_{10} and MTTF occurring times indicated.

$$R(t = B_{10}) = e^{-B_{10}\lambda} = 0.9 \tag{1.9}$$

$$B_{10} = \frac{-\ln(0.9)}{\lambda} = \frac{0.105}{\lambda} \tag{1.10}$$

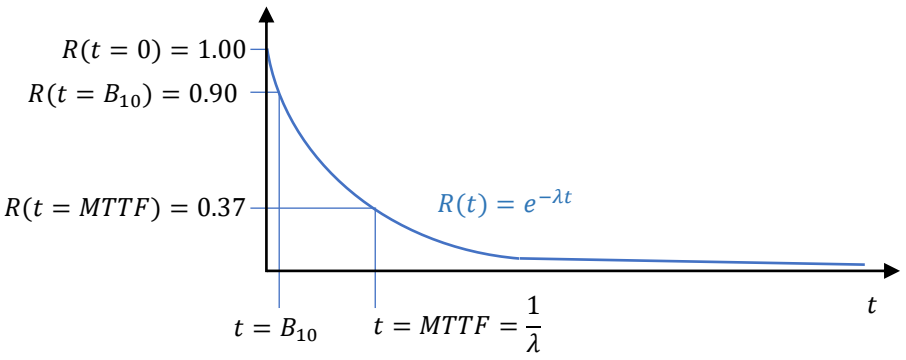

Figure 1.10: Exponential distribution of the reliability function

1.6.3 The cost of the unreliability

Like other machines, the wind turbine includes parts that can fail during their working life. The failing parts required unplanned maintenance to fix or replace them. This process adds two cost parts to the estimated cost of the generated energy units. The first part is for unplanned maintenance, including logistics and spare parts, while the second part is for wind turbine downtime [42]. Both cost parts become greater for offshore wind turbines due to the difficult maintenance, expensive transporting, and the relatively long time needed to wait until suitable weather conditions to repair [43]. The maintenance cost is added to the operating cost which will reflect on the price of the generated energy units. This extra cost works against wind energy

competing with other electricity sources.

1.6.4 Contribution of WTPCs to wind turbine reliability

Wind turbine reliability studies based on reliability data from the field show that failures of the wind turbine subsystems and parts vary in frequency and contribution to the wind turbine downtime [44]. The wind turbine includes a variety of subsystems depending on its size and technology however the main subsystems are the mechanical, electrical, and the structure. Field reliability data found that WTPC failures highly contribute to the wind turbine failure rate and downtime [45, 46].

1.7 Research aims and thesis structure

WTPC reliability impacts the cost of wind energy which affects wind's competitiveness against fossil fuel electricity generation that is responsible for 40% of the global CO_2 emissions. This research interest is in line with the requirement of the electrification of transportation and industry to reduce the CO_2 footprint to control climate changes. This research aims to improve the reliability of wind turbines by highlighting the WTPC failure impact factors and their interactions with the power converter design and control.

This research presents a new reliability assessment method based on the realistic operation of wind turbines considering different converter designs, control approaches, and wind characteristics. A further contribution to this field, this research proves the significant impact of wind turbulence intensity on WTPC reliability by statistical analyses. The research is guided by setting three research questions which represent the steps towards delivering the information and knowledge about WTPC reliability:

1. How can the reliability of existing wind turbine two-level voltage source converters be better understood?

2. How can the reliability of more complex converter topologies in wind turbine applications be estimated from knowledge of 2L-VSC systems?

3. How can the reliability of future wind turbine power converters be estimated?

This thesis is structured as follows: Besides the Introduction Chapter, this thesis also contains wind turbine power converters reliability in the literature which reviews related published articles from academia and industry in Chapter 2. Chapter 3 discusses the current techniques used in wind turbine power converter reliability analysis highlighting their advantages and drawbacks besides presenting the new method used in this thesis. Chapter 4 presents modelling wind turbine for the power converter reliability analysis. The model represents the widely deployed WTPC to address the first research question. Chapter 5 presents two more models, the direct torque control model and the 3L-NPC model to address the second research question. Chapter 6 presents the WTPC lifetime analysis against wind speed and turbulence intensity of the three developed models. The Chapter discusses the WTPC lifetimes of each model, compares the

models' WTPC lifetimes, and addresses the third research question. Finally, the thesis ends with Chapter 7 presenting the research conclusions and the proposed future work.

Chapter 2

WTPC Reliability in Literature

2.1 Introduction

After costly and frequent failures in the WTPC, groups of researchers from industry and academia joined the work of investigating the cause of failures and the impacting factors on WTPC reliability [47]. The published literature of this work and the following works in this field analysed WTPC reliability from three main topics. The first topic studied the impact of WTPC failure on the cost of wind energy by evaluating the failure contribution on wind turbine failure rate and downtime as in [38,44,48]. The second topic analysed the WTPC cause of failure to identify the responsible parts and to understand the failure mechanisms as in [49–51]. The third topic investigated the WTPC reliability impact factors related to wind turbine operation and converter design. Reliability impact factors like wind speed, generator type, and converter topology have been tested to understand how WTPC reliability can be improved as in [52–54].

The published articles on these three topics demonstrate academic and industry interests in understanding the cause and impacts of the WTPC's high failure rate. This Chapter reviews the related published literature on the three topics in the following sections. The cost impact of the WTPC failures in section 2.2, the cause of failure and failure mechanisms in section 2.3, and the WTPC reliability impacting factors in section 2.5.

2.2 Cost impact of WTPC failures

Unplanned failures add extra operational costs to cover the repairs and the system downtime. Accordingly, the cost of WTPC failures in wind turbines is added to the project operational expenditure (OPEX) which later reflects on the cost of the generated wind energy [48]. The cost impact of a part failure within an operating system is related to the part's failure rate, system downtime caused by the failure, and the cost of the repair [42]. Therefore, to evaluate the cost impact of WTPC failures on the cost of wind energy, it is important to review the WTPC failure rate within the running wind turbine, the downtime caused by WTPC failures, and the cost of the WTPC repairs.

2.2.1 Failure rate of WTPC within the wind turbine system

The published articles on wind turbine reliability considered breaking down the wind turbine system into subsystems and subassemblies for better analysing the reliability data to identify the cause of failures and their contribution to wind turbine downtime as in [36, 55]. An example of a wind turbine subsystem is the drive train which includes subassemblies like the gearbox, the generator, the bearings, the shaft, and the rotor hub.

At the early stage of wind turbine reliability analysis, the published paper by Spinato et al. [40] has analysed wind turbine reliability. The reliability data for over 11 years of more than 6000 onshore wind turbines and their subassemblies have been investigated. The paper data was collected from Landwirtschaftskammer Germany (LWK), WindStats survey in Denmark (WSDK), and WindStats survey in Germany (WSD). The reliability analysis of failures that occurred during the wind turbine's useful lifetime stage clarified interesting details of the wind turbine subassemblies' failure rates. The paper analysis showed that some wind turbine subassemblies, like the gearbox, achieved similar reliability when they were used in other applications. In contrast, other subassemblies like power converters achieved lower reliability in wind turbines compared to their reliability in other applications. Furthermore, the paper's survey revealed that the reliability of direct-drive wind turbines was not better than geared wind turbines. The identified reason was that the increased WTPC failure rate in the direct-drive wind turbines substituted the failure rate of the removed gearbox. Also, the same survey revealed that larger wind turbines showed lower reliability than smaller wind turbines due to the WTPC failures which made a conclusion that higher power WTPC suffers a higher failure rate than lower power WTPC.

The paper revealed interesting information about WTPC reliability mainly when it highlighted that WTPC reliability is poorer in wind turbine applications however further reliability analysis is required to clarify more details about the reasons causing the reliability drops in WTPC. Although the paper categorised wind turbines as large, small, old, and new however it did not categorise wind turbines according to the generator type which showed later a considerable reliability difference between FRC WTPC and PRC WTPC, used with PMSG and DFIG respectively as presented in [54]. Furthermore, the paper relied on the reliability data that included the failures of the electrical system together with the WTPC failures while later reliability analysis showed that WTPC parts vary in their failure rates as an example of that, the MSC dominated the failures of the WTPC as discussed in [56].

2.2.2 WTPC contribution to wind turbine failures and downtime

Further reliability analysis of wind turbine subassemblies is presented by Wang et al. in [44]. The paper analysed failure data of 350 onshore wind turbines collected from 10-minute Supervisory Control and Data Acquisition (SCADA) records. The data contained 35,000 downtime events, operational and maintenance contractor reports, and work orders with service reports. The analysis of the collected wind turbine failure data reveals that the WTPC is one of the highest failing subassemblies in wind turbines with a 13% contribution to the analysed wind turbine failures and appeared to be one of the highest contributors to wind turbine downtime with

18.4% of the total wind turbine downtime as presented by the paper diagrams shown in figure 2.1.

(a) Wind turbine subassemblies contribution to failure rate

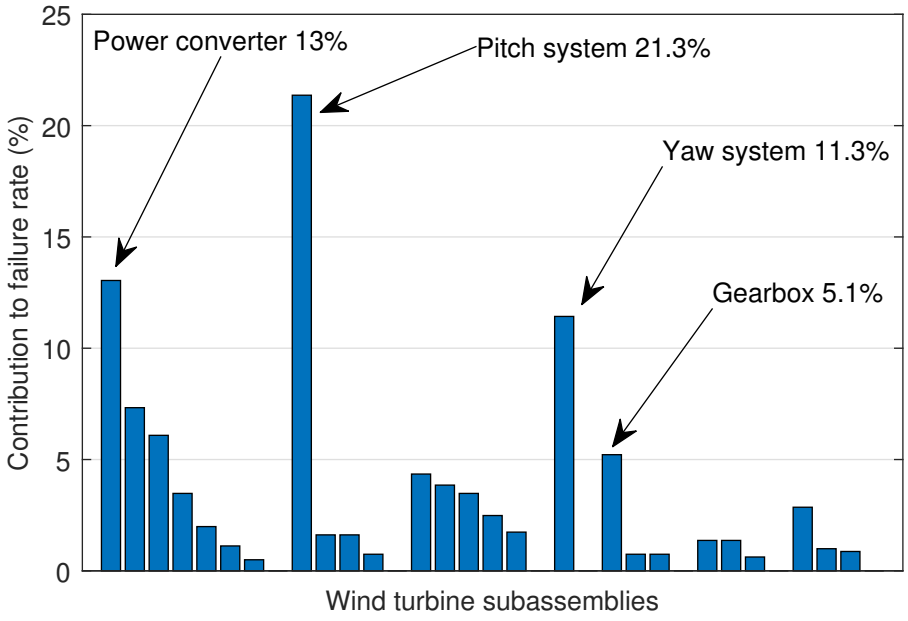

(b) Wind turbine subassemblies contribution to downtime

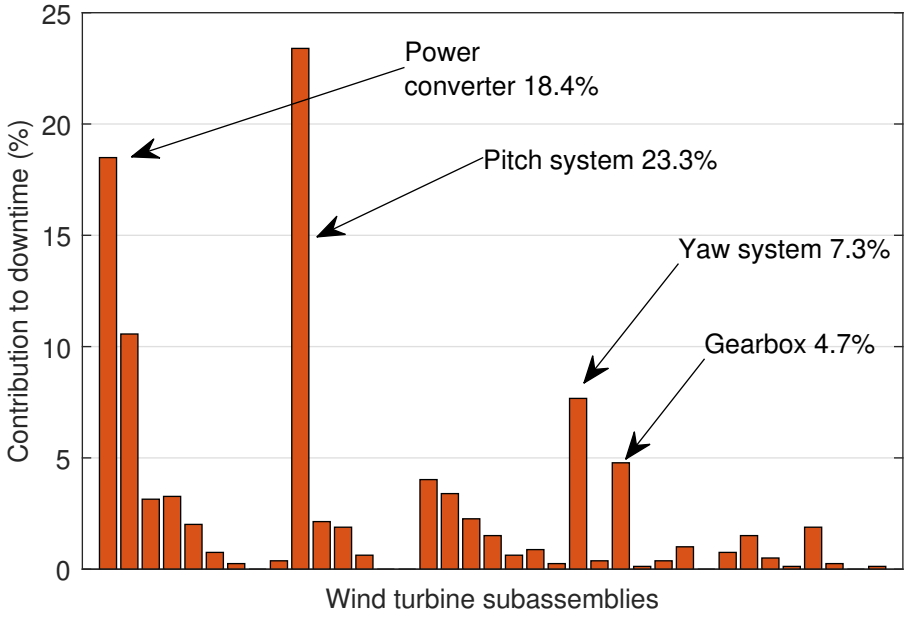

Figure 2.1: Wind turbine subassemblies' contributions to wind turbine failure, (a) failure rate and (b) downtime, reproduced from [44]

The database analysed by Wang et al. was more than 10 years old which can be doubted as invalid information for the current WTPC reliability assessment. However, a more recent wind turbine subassembly reliability analysis by J. Liang in [57] has also reviewed the reliability of WTPC based on more recent field reliability data. The paper used three data sources, Swedish,

AWE, and VTT. The paper presented the annual failure rate of the wind turbine assemblies where the annual failure rate of WTPC was around 15% in the three data sources. However, the contribution of WTPC failure to wind turbine downtime was different in each data, 14% in Swedish data, 12% in AWE, and 10% in VTT. The similarity of the WTPC failure rate indicates the consistency of this value which when compared to the 18.4% from the previously discussed paper indicates that not much WTPC reliability improvement has been achieved over the last 10 years. The variance of the downtime contribution can be understood as different data sources represented different geographical locations and different requirements affecting the needed time for the repair jobs. However, all three values present a considerable contribution to the wind turbine downtime affecting the annual wind energy production.

2.2.3 Impact of the WTPC failures on the cost of wind energy

The levelised cost of wind energy (LCOE) including the cost of WTPC failures is reviewed by Dao et al. in [48]. The paper studied field data of wind energy failure rates and the related downtimes from 18 public databases covering over 18,000 wind turbines equivalent to 90,000 wind turbine years. The sources of data were the Dutch Offshore Wind Energy Converter (DOWEC) project and the ReliaWind project which includes Landwirtschaftskammer Germany (LWK), WindStats Germany, and Windstats Denmark. The paper analysed the wind turbine subassembly failure data variations and compared offshore and onshore reliability data. The paper observed variation between downtimes and failure rates in the reliability data. However, the electrical subassembly which includes the WTPC was one of the top five reliability critical components of wind turbines across all analysed data. The cost of WTPC failure has been estimated based on the field maintenance logs and SCADA records which are then used to calculate the cost of wind turbine operation. The paper presented a mathematical model that shows the LCOE of wind energy as a function of failure rate and downtime. The results suggested that failure rates of the wind turbine subassemblies, including WTPC, have to be reduced to minimise the LCOE factor to 1 to reduce wind energy project OPEX.

2.3 Influencing parts to WTPC failure

The literature investigated the reliability of the stressed parts within the WTPC to identify the highly responsible part that caused the WTPC to fail. These parts are mainly the power semiconductors including the IGBTs and diodes in both MSC and GSC and the capacitors in the DC bus. Those parts have been investigated by analysing their reliability data from the field and studying their expected lifetimes by testing or modelling techniques. The following sections review related published articles reviewing the reliability of the DC bus capacitor and power semiconductors in the WTPC.

2.3.1 DC bus capacitor

A capacitor bank is usually connected to the WTPC DC bus. The function of the capacitor is to minimize the DC voltage ripple generated with the rectified AC voltage by both MSC and GSC.

(a) Subassemblies contribution to wind turbine failure

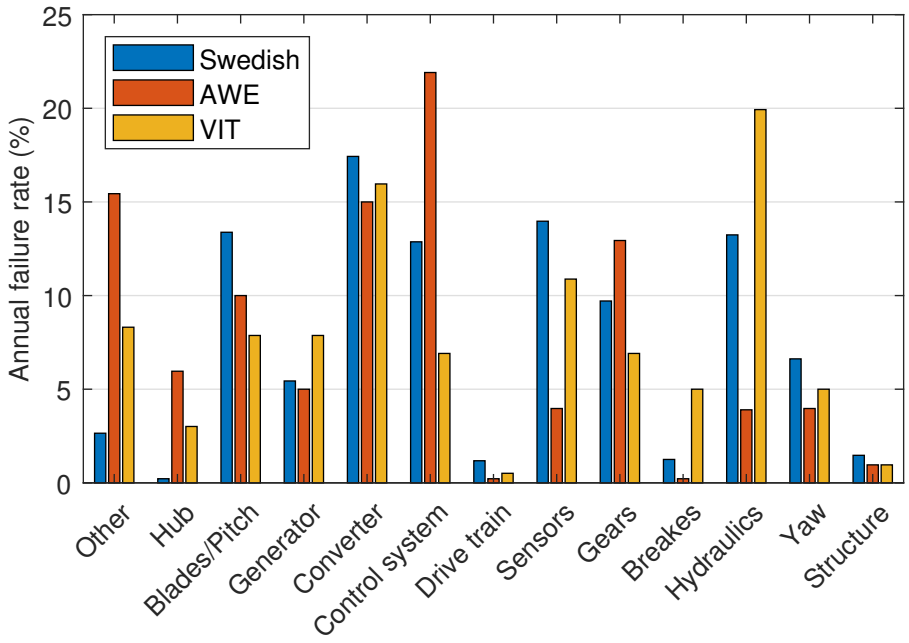

(b) Subassemblies contribution to wind turbine downtime

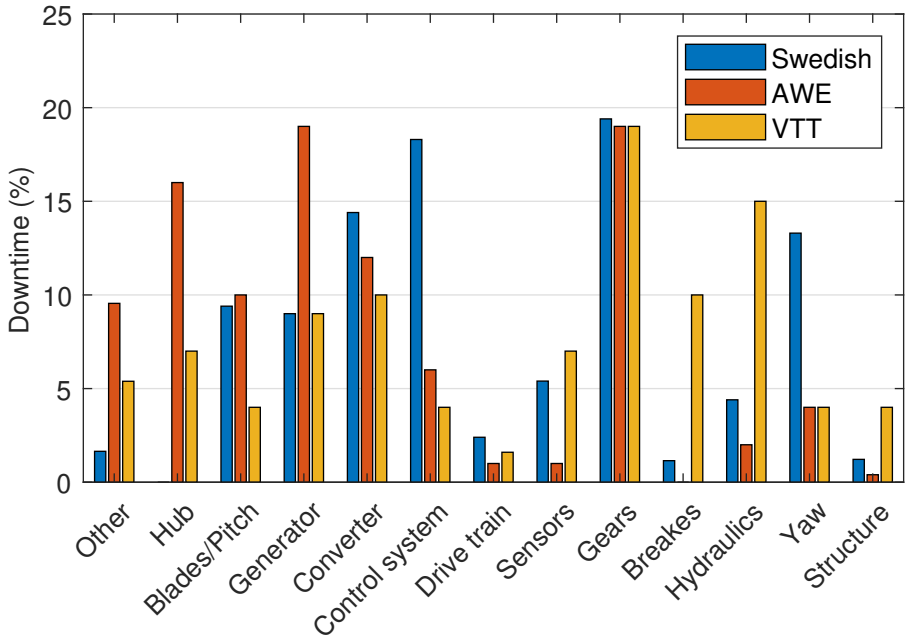

Figure 2.2: Wind turbine subassemblies' contributions to wind turbine failure, (a) failure rate and (b) downtime, reproduced from [57]

The DC bus voltage ripple produces charging and discharging currents that pass through the DC bus capacitor. Due to these currents and the applied voltage, the DC bus capacitor withstands thermal and electrical stresses causing the capacitor to age and fail. Published articles discussed the DC bus capacitor lifetime and its reliability factors in power converter applications including in wind turbines.

Wang and Blaabjerg in [58] have reviewed the reliability of the capacitor in the DC bus of the

AC-DC-AC converter which is the same configuration used in WTPC. The paper reviewed three types of capacitors used in the power converter DC bus, the Aluminium Electrolytic Capacitor (Al-CAP), the Metalized Polypropylene Film Capacitor (MPPF-CAP), and the Multilayer Ceramic Capacitor (MLC-CAP). The Al-CAP offers low cost, high capacitance and high voltage per volume unit but they suffer low durability [59]. The temperature affects Al-CAP lifetime as it causes the capacitor liquid to evaporate which increases the capacitor's internal equivalent series resistance (ESR) shown in figure 2.3. This effect increases with higher capacitor current as it generates more heat that increases the capacitor temperature. MLC-CAPs are smaller in size, operate at higher temperatures, and in a wider frequency range but they suffer sensitivity to mechanical stress and they are higher in cost [58]. Although MPPF-CAPs are bigger in size and have moderate operating temperatures they offer good capacitance, reliability, ESR, and cost, and are capable of withstanding high surge currents and voltage [60]. The comparison of the three capacitor types is shown in the table 2.1

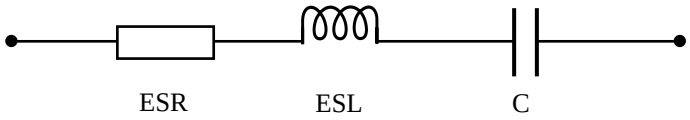

Figure 2.3: Capacitor equivalent circuit

Table 2.1: Capacitor type reliability details

	Al-CAP	MPPF-CAP	MLCC-CAP
Dominant failure modes	Open circuit	Open circuit	Short circuit
Dominant failure mechanisms	Electrochemical reaction & electrolyte vaporization	Dielectric losses & moisture corrosion	Flex cracking & insulation degradation
Critical stress	Temperature voltage current	Temperature voltage humidity	Temperature voltage vibration
Self-healing capability	Moderate	Good	No

The capacitor's lifetime is affected by the temperature and voltage as shown in the capacitor lifetime model expressed by equation (2.1) [58] where C_{LT} is scaled capacitor lifetime under operating conditions, $C_{LT,ds}$ is the datasheet estimated lifetime, V is operating voltage, V_{ds} is the datasheet voltage, T_C is the operating temperature, $T_{C,ds}$ is the datasheet temperature, n is empirical constant, E_a is the activation energy, and K_B is Boltzmann constant. The produced heat in the capacitor raises the capacitor temperature and produces thermal stress affecting the capacitor's lifetime.

$$C_{LT} = C_{LT,ds} \cdot \left(\frac{V}{V_{ds}}\right)^{-n} \cdot exp\left[\left(\frac{E_a}{K_B}\right) \cdot \left(\frac{1}{T_C} - \frac{1}{T_{C,ds}}\right)\right] \tag{2.1}$$

A method of estimating the DC bus capacitor lifetime in WTPC has been presented by Xue et al. in [50]. The paper modelled a 1.2MW PMSG wind turbine with 2L-VSC FRC WTPC and considered a variable wind speed mission profile as input for the model. The paper selected the Al-CAP type for the lifetime evaluation. The capacitor power losses were calculated according to the ripple voltage (ΔV) and the capacitor ESR which is imported from the capacitor datasheet. The capacitor power losses are calculated considering the harmonics of the ripple voltage as different frequencies have different power losses in the Al-CAP type [61]. The ripple voltage was calculated by equation (2.2) where P_{GSC} is the GSC power, f_g is the grid frequency, C_{DC} is the capacitor capacitance, and V_{DC} is the DC bus voltage.

The paper modelled the capacitor's internal temperature using a thermal equivalent circuit where the heat source is the capacitor power losses and thermal resistance is the sum of capacitor internal thermal resistance and case-to-air thermal resistance while the ambient temperature is the heat dissipation reference. The paper used the capacitor simulated temperature and the voltage in the lifetime model shown in equation (2.1). The paper concluded that higher power increases voltage ripple and therefore the capacitor temperature which is also increased due to the increase of ambient temperature. Therefore, the paper advises using cooling methods to improve WTPC capacitors' lifetime. The method of the paper did not consider the ripple current generated by the MSC without justification. However, the paper highlighted the major impacts on the reliability of the DC bus capacitor in FRC WTPC.

$$\Delta V \approx \frac{P_{GSC}}{2\pi f_g C_{DC} V_{DC}} \tag{2.2}$$

The reliability of the DC bus capacitor has been improved in the current WTPCs by utilising self-healing technology and paralleling multiple capacitors for redundancy like in PCS6000 WTPC [36].

2.3.2 Semiconductors

The semiconductor switches in converter circuits are transistors or thyristors working as active switches and diodes as passive switches. The IGBT became widely used in power converters in wind turbines and many other applications. IGBT has proven its performance in high-power converters due to its high operating current, voltage, and low controlling current requirement [62]. IGBT combines the advantages of bipolar transistors and field effect transistors.

For power converter circuits, the IGBT is fabricated as a power module combined with a parallel reverse diode. Different fabrication technologies were used resulting in two IGBT types, the bonded-wire power module and the press-pack power module. The diodes within the IGBT power module are constructed on the same base plate however the diode occupies a smaller area making its thermal resistance higher than the adjacent IGBT as shown in figure 2.4. Therefore, for a similar load current, the diode junction temperature will be higher and more affected by the power module current than the IGBT junction temperature.

The reliability analyses of semiconductors show that junction temperature fluctuation is highly impacting their lifetime. The differences in the semiconductor internal parts coefficient of thermal expansion (CTE) with changes in junction temperature produce mechanical stress between the semiconductor parts and in the soldering joints. Figure 2.4 shows the construction parts of the bonded wire IGBT [63] where attached layers are fabricated by different materials having different CTEs as shown in table 2.2.

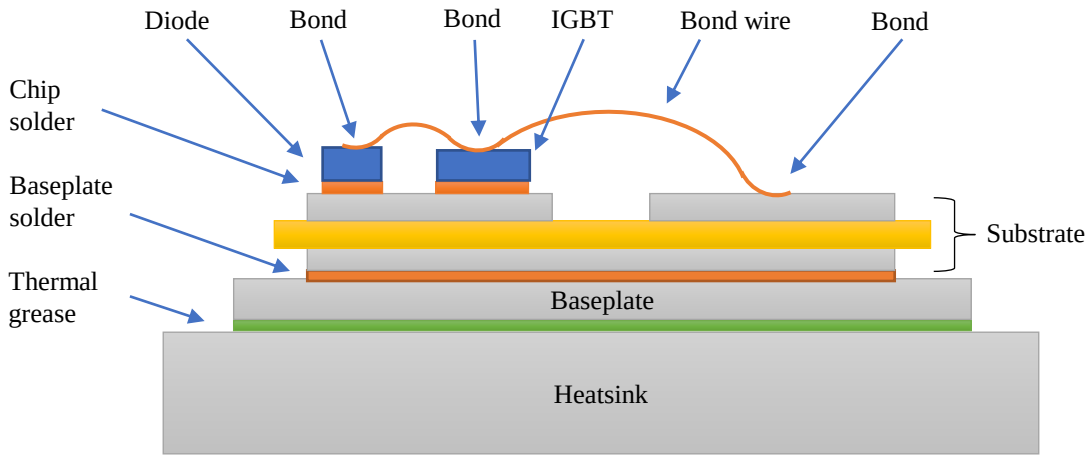

Figure 2.4: IGBT and reverse diode in IGBT power module [63]

Table 2.2: CTE of the materials in the IGBT power module

Material	Property	CTE (10^{-6} /K)
Al_2O_3	Ceramic	6.8
AlN	Ceramic	4.7
Al	Metal	23.5
Cu	Metal	17.5
Si	Semiconductor	2.6
Solder	Alloy	28

2.4 Failure mechanisms

The published literature on the WTPC reliability analysis based on the field-collected failure data shows that the periodic changes of the semiconductor junction temperature highly influence the semiconductor lifetime and then the WTPC failure rate. The semiconductor thermal cycling is considered the leading cause of failure of WTPC [20, 29, 64]. Due to the cycling in the semiconductor junction temperature and the differences in the coefficient of thermal expansion (CTE) of the internal attached parts, cycling mechanical stress develops between these parts causing fatigue [65].

Semiconductor failure mechanisms have been identified where the junction temperature is found to be the cause of most failure mechanisms of the power module as in table 2.3 [66]. These

mechanisms are reviewed by Ciappa in [67] where the paper focuses on the high-power IGBT modules which are similar to those used in the WTPC. The failure mechanisms are discussed in the following paragraphs

2.4.1 Bond wire

Bond wire failure in power semiconductors has been discussed in [67–69]. High-power modules of multichip IGBTs typically contain up to 800 bond wires around half of them are connected to the semiconductor active area, IGBTs and freewheel diodes and they are exposed to the temperature swing caused by the wire resistance heating and the heat dissipation from the semiconductor [67].

The diameter of bond wires connected to the emitter is usually in the range of 300μm to 500μm. The bond wire composition can vary according to the manufacturer however pure aluminium is used with adding a small amount of alloying materials such as magnesium or silicon for hardening or nickel to control corrosion. The bond wire current is limited by its melting point. The bond wire's maximum current capability is 25A for one cm length, 300μm diameter and 60A for 500μm diameter. However, in normal power module operating parameters the single aluminium bond wire current is limited to 10A where the maximum heat dissipation caused by the wire resistance is around 100mW to 400mW according to the bond wire diameter.

During the high-frequency switching operation, the skin effect causes the current density to be inhomogeneously distributed across the bond wire area. The bond wires are fitted on the aluminium metalisation by ultrasonic wedge bonding. Two failure mechanisms in power semiconductors are related to the bond wire, lift-off and heel cracking.

Bond wire lift-off

The bond wire lift-off mechanism has been discussed in [63, 67, 70]. It was observed that bond wire lift-off has been affecting the IGBT and freewheeling diode in power modules. However, bond wire lift-off with IGBT was mostly analysed since the test equipment uses DC current while the bond wire lift-off at the diode connection was ignored. Moreover, it has not observed a bond wire lift-off on the copper terminal side because there is no high swing in temperature at this point. Besides, the CTE difference between aluminium and copper is lower than the difference between aluminium and silicon.

The lift-off mechanism at the bonded point and the propagation of cracks within the joint with time is a complex problem. However, experiments show that the crack is initiated at the

Table 2.3: IGBT failure mechanisms

Wire-bonded IGBT modules	Press-pack IGBT modules
Bond wire lift-off	Fretting damage
Solder joint fatigue	Spring fatigue
Bond wire heal cracking	Spring stress relaxation
Aluminium reconstruction	Cosmic ray induced burnout
Cosmic array induced burnout	

bond wire tail and moves within the bond wire material until it lifts off completely.

Bond wire heel cracking

The bond wire lift-off mechanism has been discussed in [67,69,71]. The bond wire heel cracking is rarely observed in multichip IGBT power modules. However, it can be found after long lifetime tests and mainly in power modules with unoptimized bonding processes. The failure mechanism is also due to the effect of thermal stress. Effectively, the bond wire expanding and contracting due to temperature cycles are producing flexure fatigue. In 1 cm bond wire, the swing of $50°C$ makes 10μm displacement in the top of the bond wire loop which produces about $0.05°$ in the bending angle at its heel. The developed stress of this failure mechanism increases by the fast displacement of the bond wire within the silicon gel due to high viscosity. When the source of the heat comes from the bond wire current, heel cracking can be observed at the copper terminal joint as well as at the joints of the diode and IGBT.

2.4.2 Aluminium reconstruction

The aluminium reconstruction mechanism has been discussed in [67,72]. In the multichip IGBT power module, the thermal cycling of the IGBTs and freewheeling diodes produces periodical tensile and compressive stresses in the thin metalization film due to the CTE difference between the silicon chip and the aluminium. The stiffness of the silicon and the large difference between the two materials CTEs produce a large stress in the aluminium film which can be higher than its elastic limits during the switching operation of the device. The aluminium film stress relaxation can occur by grain boundary, plastic deformation, or by diffusion creep. The metalization strain rate is related to the temperature change. If the device is operating at its maximum junction temperature, the plastic deformation at the grain boundaries occurs due to the stress relaxation leading to cavitation effects or extrusion of the aluminium.

2.4.3 Solder fatigue and solder voids

This failure mechanism is discussed in [67,73,74] The fatigue of the solder alloy layer is considered the main failure mechanism of the IGBT power module. The solder between the base plate and the ceramic substrate is the most critical area, especially with the copper base plate. The thermo-mechanical stress caused by the temperature swing is the reason for this fatigue and mainly because of the high difference in CTE of the materials and the large interface area. The solder fatigue between the ceramic substrate and silicon chip is also happening.

The junction temperature of the IGBT and diode in the power semiconductor can be increased due to voids and fatigues-induced cracks which accelerates the other aging mechanisms like bond wire lift-off. Furthermore, a temperature gradient can be produced when the heat flows through a large amount of voids which reduces the chip heat dissipation. In the power semiconductor which has internal layers constructed vertically, the die attach is required to provide high thermal and electrical conductivity. The existence of voids obstructs the die heat flow but it does not affect the current flow. Therefore, voids impact the die attach thermal efficiency without a noticeable impact on the chip's electrical conductivity. To avoid producing

solder voids between chip layers during the fabrication process, a clean process and vacuum ovens are used besides good soldering temperature control. However, avoiding solder voids is still a challenge in the large plate soldering process.

2.5 WTPC reliability impacting factors

The literature on the reliability of WTPC has presented papers discussing the impacting factors affecting the lifetime of WTPCs. Those factors are related to the wind turbine operational conditions and to the wind turbine technology. The wind turbine operational conditions related to WTPC loading are wind speed, gust frequency, and wind turbulence; the wind turbine technology factors are the generator type, converter topology, and control system. The following sections present the literature related to those impacting factors on WTPC reliability.

2.5.1 Impact of wind speed

In variable-speed wind turbines, wind speed has a cubic relationship with the power. Therefore, wind speed develops a great effect on the WTPC loading by increasing its current. Accordingly, the WTPC power losses produced in its semiconductors increase and the junction temperatures increase which impacts the semiconductors' lifetimes. The relationship between wind speed and the estimated WTPC lifetime has been analysed in published literature such as in [47, 52, 53]. The published articles used different techniques to assess the WTPC reliability against wind speeds. However, more reliability analysis is required here considering the impacts of the realistic operation of wind turbines.

Xei et al. in [52] analysed the effect of wind speed on WTPC reliability. The paper modelled a 2MW PMSG direct drive variable wind speed wind turbine. Specifically, the paper modelled the wind turbine generator power, voltage, and frequency by applying four mathematical relationships related to the input wind speed ranges: below cut-in wind speed, between cut-in and rated wind speed, between rated and cut-out wind speed, and above cut-out wind speed. The modelled WTPC semiconductors' power losses were calculated by mathematical modelling of switching and conduction power losses. Accordingly, semiconductor junction temperatures were calculated based on the power losses and thermal impedances of the devices. The temperatures were used to calculate the semiconductors' failure rates which were then used to calculate the WTPC lifetime. The paper used hourly sampled wind speed time series for one year (8760 hr).

The paper used the developed mathematical model of WTPC lifetime and wind speed for fixed wind speed values from 2m/s to 20m/s with a 1m/s increment. For each wind speed, the paper modelled the corresponding WTPC lifetime. At the same time, the paper used the probability of that wind speed within the annual wind speed data to calculate the WTPC lifetime during the year. The paper concluded that the WTPC failure rate increases as wind speed increases until wind speed reaches the rated value where the WTPC failure rate becomes fixed until the cut-out wind speed. Figure 2.5 shows the paper's results for the MSC (Machine Side Converter), GSC (Grid Side Converter), and DC-link failure rates against wind speeds. The failure rate of the MSC was the highest followed by the GSC while the DC-link achieved the lowest failure rate.

The results' accuracy could have been impacted by the modelling method. For example, the paper did not consider the wind turbine dynamics as the calculation was based on assuming fixed operation parameters driven by constant wind speed. Furthermore, the paper did not consider the impact of junction temperature on the semiconductor parameters which would have a considerable impact on the semiconductor power losses and the related junction temperature.

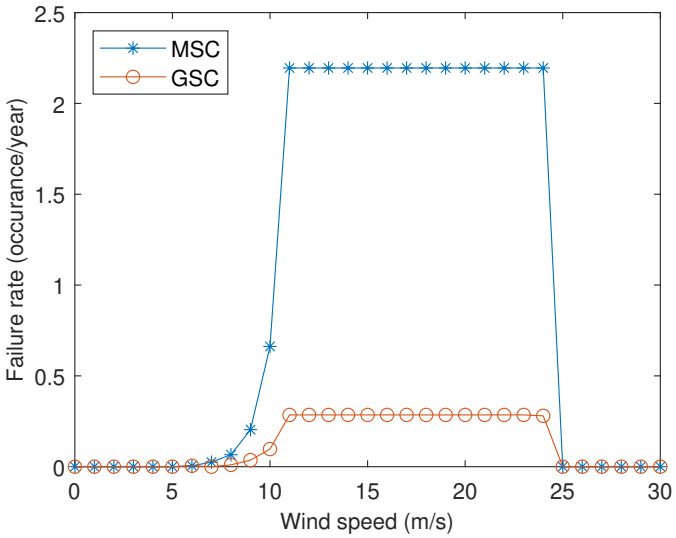

Figure 2.5: Impact of wind speed on WTPC reliability as published by [52]

2.5.2 Impact of wind gust and turbulence

Besides the wind speed, WTPC reliability is also impacted by other wind parameters like gust frequency and turbulence intensity [75, 76]. Wind turbulence intensity (TI) is an important parameter that can be extracted from the wind speed data. The TI of a variable wind speed profile is expressed as the percentage value of the standard deviation of wind speed measurements (U_σ) divided by the average wind speed ($\overline{U}$) [53], calculated as in equation (2.3).

$$TI = \frac{U_\sigma}{\overline{U}} \cdot 100\% \tag{2.3}$$

The effects of wind gusts and turbulences on the reliability of WTPCs have been rarely discussed. A few published articles introduced the possibility of a relationship between TI and WTPC reliability. Smith et al. in [75] examined the impact of gust frequency on the WTPC lifetime by simulating the thermal loading of the WTPC's semiconductors. The paper modelled a 2MW PMSG wind turbine connected to a 2L-VSC MSC and a DC source substituting the GSC. Synthetically generated wind speeds of constant and square wave time series were used in the simulation model to analyse the impact of wind speed and gust frequency on the MSC reliability. The simulation results showed that the thermal loading of MSC semiconductors was increased during low gust frequencies compared to during high-frequency gusts. Accordingly, the paper concluded that lower turbulence sites would have a more damaging impact on the WTPC. The paper would present more realistic results by using field-recorded wind speed rather than synthetically generated wind speed in the simulation model.

Isidor et al in [49] discussed the effects of interactions between wind roughness classes and the WTPC modulation method on the WTPC reliability. The paper modelled a 10MW grid-connected wind turbine with PMSG and 3L-NPC WTPC. The lifetime of 3L-NPC WTPC using thermal loading simulation with three variable wind speed profiles representing three different wind roughness classes and having the same average wind speed. The variable wind speed profiles were 16s in duration. The simulated junction temperatures of both MSC and GSC semiconductors showed the highest maximum junction temperature during the highest roughness class profile and the lowest maximum junction temperature during the lowest roughness class wind profile. Therefore, the estimated WTPC lifetime was longer at the lowest roughness class wind profile. Accordingly, the paper concluded that higher turbulence intensity wind decreases the WTPC lifetime.

This paper's conclusion conflicts with the findings of the previously discussed paper [75]. The paper concluded the impact of wind turbulence on WTPC reliability based on the simulation of only three 16s variable-wind-speed profiles. The wind speed varies within the wind profile in a complex phenomenon. Therefore, testing other wind profiles could produce different results even if the tested profiles have the same average wind speed and the same wind turbulence intercity. Therefore, the impact of wind turbulence intensity on WTPC reliability would be better judged by testing a large number of wind speed profiles and analysing the results. The paper also did not evaluate the impact of wind turbulence intensity on the WTPC lifetime which could help in better lifetime estimating related to the wind turbulence intensity besides the average wind speed.

Baygildina et al. in [77] assessed the thermal loading of the WTPC semiconductors against the dynamics of wind speed. The paper modelled a 1.5MW direct-drive PMSG wind turbine connected to 2L-VSC WTPC for reliability analysis. The paper tested a realistic 180s variable-speed-wind profile for estimating the WTPC lifetime based on the simulated semiconductor junction temperature. The visual comparison between the trends of junction temperature and the wind speed showed that the high-frequency wind speed changes did not affect the semiconductors' junction temperature variation. The paper claimed that the wind turbine dynamics filtered the fast wind speed changes and therefore the WTPC thermal loading was not impacted during the high-frequency wind turbulence. Accordingly, the paper linked the WTPC thermal loading to the rotating speed of the wind turbine. The paper found that it is reasonable to assume that low-frequency turbulence winds produce a higher damage rate to the WTPC. However, the paper's conclusion was based on the results of only one 180s variable-wind-speed profile without demonstrating further analysis to evaluate the results.

The reviewed articles tried to assess the relationship between WTPC reliability and wind turbulence intensity. However, they could not agree on a clear conclusion about the impact of wind turbulence on WTPC lifetime. They developed their conclusions based either on synthetically generated wind speed or a few realistic variable wind speed profiles of a short time. Furthermore, The papers came to different decisions and none of them presented a method to evaluate the impact of wind turbulence on WTPC lifetime.

2.5.3 Effect of converter topology on WTPC reliability

The wind turbine industry continues to increase the size and rated power of wind turbines. This increases the wind turbine capacity factor and reduces the cost of produced energy. The 2L-VSC operated at low voltage (LV) which is normally below 1kV due to the limitation of the semiconductor maximum operating voltage of the converter. In multimegawatt wind turbines, the high generator current is shared by multiple converters in parallel. An example of this arrangement is WTPC used in Gamesa G10X 4.5MW where six 2L-VSC converters are paralleled to share the generator power [78]. Other manufacturers decided to deploy higher voltage power converters to reduce the converter current which reflects on the sizes of the cables and grid transformer. The three-level neutral point clamped converter (3L-NPC) was introduced to be used in wind turbines. This converter provides higher voltage because of its design and also due to using IGCT instead of the IGBTs used with 2L-VSC which provides higher operating voltage. An example of this WTPC is the PCS6000 converter manufactured by Hitachi ABB company [79] and deployed in wind turbines like the GE Haliade X [33].

The introduction of 3L-NPC converters in wind energy opened the discussion on the WTPC reliability improvement in comparison to the widely popular LV 2L-VSC WTPC. The article by Bala et al. in [36] has described the PCS6000's performance capabilities and presented it as a better alternative to the existing IGBT-based 2L-VSC WTPCs. The operating voltage of the PCS6000 is 3.3kV AC and 5kV DC which is considerably higher than 690V AC and 1.15kV DC in the LV 2L-VSC. This MV voltage capability along with the high current capacity obtained by utilising the IGCT device and the converter topology. The outcome of this technology produced a powerful converter that can be installed as a WTPC in a 5MW wind turbine without paralleling. However, the paper admitted that the WTPC still need parallel converters to provide redundancy for any unexpected failure that can happen in the converter circuit which is described by the paper as an unavoidable situation. The paper presented reliability data collected from the field that showed a WTPC failure rate of 0.2 failures per turbine per year which can not be considered a big reliability improvement compared to the LV 2L-VSC which showed 0.23 failures per turbine per year according to [40]. The paper did not give details about the wind farm site location and the nature of the wind there and that can raise questions about how the reliability of the 3L-NPC can be assessed compared to the 2L-VSC and whether or not wind characteristics will be involved in this assessment.

2.5.4 Effect of generator type on WTPC reliability

The rapid development of the wind turbine industry brought different types of generators for deployment in wind turbines. The DFIG and PMSG dominate the generator types in the current multimegawatt wind turbines. The WTPC operating conditions and its rated power vary depending on which of the two generators is installed. In the DIFG wind turbine, the WTPC is a PRC power converter which carries up to one-third of the wind turbine output power while in PMSG, the WTPC is FRC and therefore it carries all the wind turbine output power.

The impact of this technology difference on the reliability of the WTPC is analysed by Carroll

et al in [54]. The paper compared the lifetime of the WTPC used with both generator types, the DFIG and PMSG. The paper analysed reliability data of 2,222 onshore wind turbines of the same rated power and same blade size but vary in their drive train including the generator type. The paper did not disclose the wind turbines' exact details due to information confidentiality requirements but mentioned the studied wind turbines' rated power was between 1.5 and 2.5 MW. The analysed reliability data were equivalent to 34 million turbine hours and were collected within the first five years of the wind turbine operation. The data populations between both generator types were 1,822 DFIG wind turbines (providing around 29 million turbine hours) and 400 PMSG wind turbines (providing around 4.5 million turbine hours). The failure rate analysis of the collected reliability data showed that the failure rate of the PRC was 0.106 and FRC was 0.593 failures per turbine per year. The paper also included the generator failure rates where DFIG was 0.123 and PMSG was 0.076. The reliability comparison between both wind turbine types shows that PMSG had a higher failure rate than DFIG as shown in the stacked failure rate diagram in figure 2.6.

The paper also analysed the cost of failures of both technologies according to three cost categories, minor repair, major repair, and major replacement. The cost of maintenance of FRC is higher than PRC due to the higher failure rate while the cost of maintenance of PMSG is lower than DFIG for the same reason. However, the overall cost of failures showed that the maintenance cost of FRC with PMSG is higher than that of the PRC with DFG. This conclusion was based on the comparison of onshore wind turbines where the maintenance cost of DFIG would be much higher if it was offshore deployed which could change the comparison results. The paper successfully highlighted the reliability issue of WTPC and showed how wind turbine maintenance cost is impacted by WTPC failures mainly in the FRC PMSG wind turbines.

The paper built the WTPC reliability comparison between DFIG and PMSG based on the onshore wind turbines. The offshore wind farm can bring different results mainly because of the impact of wind speed and turbulence intensity. Also, the maintenance cost of DFIG in the onshore wind farm is lower than the cost of similar maintenance in the offshore wind turbine. The DFIG is a slip-ring brush machine which needs regular maintenance compared to the PMSG. Therefore the total cost comparison could change to the advantage of the FRC WTPC because of the cost of the generator maintenance. Moreover, the paper did not explain possible reasons cause FRC achieved poor reliability than PRC in wind turbines.

2.5.5 Effect of generator speed on WTPC reliability

The move toward PMSG in wind turbines provided the possibility to eliminate the gearbox and use the direct drive wind turbine as PMSG can operate at low rotating speeds [9]. The removal of the gearbox reduces the nacelle weight and reduces the wind turbine mechanical maintenance. However, the low-speed generator can have an impact on the wind turbine electrical system mainly on the WTPC.

Zhou et al. in [80] have highlighted this impact. The paper modelled two wind turbines, direct drive and geared, both equipped with 2MW PMSG and 2L-VSC WTPC. The models' parameters were almost identical except for the generators' number of poles and impedance. The paper showed that both models' generators produce similar voltage, current, and power

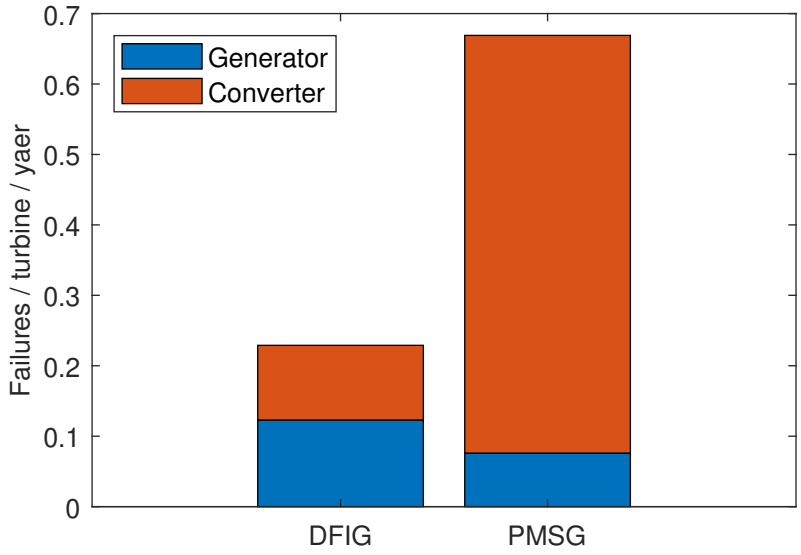

Figure 2.6: Failure rates of DFIG and PMSG wind turbines

related to constant wind speeds from cut-in to cut-out values. However, the simulation showed that WTPC power losses, conduction and switching, are greater in the low-speed generator and mainly in the diode. Therefore, the diode junction temperature of the low-speed generator model is higher in the average and cycling range than the diode in the high-speed generator model. Accordingly, the estimated WTPC lifetime is lower in the low-speed generator model. The paper's conclusion was based on a range of constant wind speeds which may not reflect the realistic operation of the wind turbine. Moreover, the WTPC reliability assessment was built based on the generator frequency rather than the generator speed as the paper title indicated. The generator frequency is related to both generator speed and the number of poles which can be a higher number than in the modelled generator. Therefore, the reliability impact of the direct-drive PMSG wind turbine on WTPC can be more influenced by the number of poles than the generator speed. Similarly, this paper also highlighted the WTPC reliability issue by trying to find a related factor that can be used to improve the WTPC reliability or to avoid a harmful impact.

2.6 Chapter summary

This chapter has reviewed the published work related to the reliability of WTPC. The literature shows that WTPC contributes highly to wind turbine failure rate and downtime. These repeated failures lead to unplanned maintenance which adds more cost to the project OPEX and therefore WTPC failures impact the cost of wind energy. The literature found that WTPC reliability is highly influenced by the power semiconductor lifetime. Semiconductor thermal loading was found to be the cause of most semiconductor failure mechanisms. Therefore, the reliability analysis of WTPC is mainly based on semiconductor thermal loading. This approach became widely accepted by academia and industry. The published work applied the semiconductor lifetime estimation to analyse the WTPC reliability and to understand the impacts of

different operational and design factors like wind speed, gust frequency, converter topology, and generator type. The reviewed papers commonly use the method of WTPC lifetime estimation based on semiconductor thermal loading. However, the literature did not consider validating semiconductor junction temperature obtained by simulation or calculation. Furthermore, the literature was mostly based on constant wind speeds or a few variable wind profiles to assess the impact of wind turbulence on wind turbine power converter lifetime which is unrealistic since wind keeps changing the speed. There is a need to develop a method capable of analysing WTPC lifetime concerning realistic wind conditions. The following chapter discusses the current techniques used in WTPC reliability analysis and highlights their advantages and drawbacks besides presenting the method used in this research.

Chapter 3

Techniques Used in WTPC Reliability Analyses

3.1 Introduction

The reliability analysis of WTPC is important for better estimating the cost of wind energy. It helps wind turbine manufacturers improve the WTPC lifetime reflecting on the wind turbine's overall reliability. Furthermore, WTPC reliability analysis helps wind farm operators plan for maintenance to reduce calls of unplanned maintenance due to unexpected failures by providing a more accurate estimate of the WTPC lifetime.

WTPC reliability analysis works on identifying the cause of failure and studies the parameters affecting the failure rate like operating conditions and wind design parameters. The WTPC power semiconductors were found to be likely the cause of WTPC failure due to the thermal loading [20, 81]. The thermal loading analysis of power semiconductors became a widely agreed approach to WTPC reliability analysis by academia and industry [29, 75, 82]. This approach can be applied in different converter topologies used in WTPC like the 2L-VSC, 3L-NPC, and modular multi-level converter (MMC) [83]. Furthermore, this reliability analysis approach is valid with a variety of semiconductors, like IGBTs, diodes [84], IGCTs [36], and Thyristors [49]. Therefore, analysing the WTPC semiconductors' junction temperature became a key factor in analysing its lifetime.

Researchers and industry used various techniques to approach semiconductor junction temperature related to wind turbine operating conditions or design parameters. Techniques like mathematical calculation, model simulation, and laboratory prototyping were used in WTPC reliability analysis. These techniques vary in their complexity, accuracy, and cost. This chapter discusses these techniques highlighting their advantages and gaps, and introducing the method developed in this research.

3.2 Reliability analysis based on lab tests

The lab tests used in power electronics reliability analysis by industry to evaluate their products' lifetime and by academia for reliability analysis research. In this field, lab experiments are

used for semiconductor lifetime estimation by accelerated damage tests or junction temperature measurements.

Accelerated damage tests are usually used to imitate the field operation conditions to collect relevant information for constructing the lifetime models. It is one of the techniques used to estimate the power electronic lifetime usually implemented by power electronic manufacturers. Accelerated damage tests implemented in the lab are used to determine the semiconductor lifetime with leverage stresses [70, 85]. The test results represent special operating conditions near or even exceeding the limits of the device under test (DUT). This method represents a practical estimation of the semiconductor's lifetime. There are two tests implemented in the power semiconductor accelerated damage tests, the power cycling (PC) test and the thermal cycling (TC) test [63, 86].

3.2.1 Power cycling test

In this test, a number of DUTs are tested and the estimated lifetime is calculated statistically where they experience cycles of their maximum and minimum currents and voltages until they fail [87,88]. This test provides a practical estimation of semiconductor lifetime however this test is costly as it requires lab equipment, technicians, and DUTs to be damaged for the test. An example of the PC test to analyse the substrate solder joints of power modules is given in [89].

3.2.2 Temperature cycling test

This test is performed by controlling the temperature of the semiconductor to evaluate the impact of changing ambient temperature on the semiconductor aiming the large area solder interconnection [86].

The test assesses the semiconductor reliability based on the number of thermal cycles before the device fails. As per IEC 60068-2-14, the minimum temperature cycles for IGBTs should be 100 and for diodes should be 25 before releasing the product [63]. By applying this test to the number of DUTs of the same model the estimated device temperature cycles to fail can be found [90]. Similar to the PC test, the TC test is costly because of the required special equipment, lab, staff, and number of DUTs.

3.2.3 Measuring semiconductor junction temperature

Junction temperature measurement is a technique used to analyse the impact of operation parameters on the power electronic junction temperature which can be used for reliability analyses or in design validation to ensure that the selected power module operates within the accepted junction temperature range in the circuit. Measuring the semiconductor junction temperature would be the direct way to estimate its lifetime. However, this technique involves challenges as the semiconductor junction is embedded inside the power module and measuring its temperature requires a complex arrangement of sensors and analysing devices so, accordingly, this technique involves a considerable high cost.

The semiconductor junction temperature can be measured using optical or physical methods. The optical method is implemented by an infrared camera or sensor while the physical method

is implemented by a thermocouple sensor where each method has advantages and disadvantages [91]. The infrared camera provides contactless measuring but it requires the power module to remove its case and the dielectric insulation besides for more accurate measurement, the bond wire and the die need to be painted for even infrared emissions across the region.

An example of using junction temperature measurement in reliability analysis is presented in [92] where a high-resolution infrared camera was used to analyse the effect of semiconductor junction temperature variation on the power module lifetime in the 2L-VSC circuit. This technique is presented for WTPC reliability analysis in [93] where measuring power semiconductor junction temperature is used to emulate the impact of wind speed on WTPC reliability.

The physical measurement method is implemented by an embedded temperature sensor which has great measurement resolution but it needs physical modification to the power module [91]. The thermocouple is the cheapest solution but its measurement accuracy is affected by heat dissipation due to its contact with the power module.

In both methods, the scaling-up of the measured temperature to reflect their values in real WTPC in the field is a challenging calculation as semiconductor junction temperature has a complex relationship with operating parameters and heat dissipation. The challenges of measuring power electronic junction temperature for reliability analysis can be summarised in:

- It is required to prepare a prototype that emulates the WTPC design and the semiconductor type.
- It is required to modify the power module packaging to allow access to the junction spot for measuring its temperature.
- Scaling the lab-measured junction temperature to the field operating parameters may impact the accuracy as the semiconductor power loss and its thermal parameters vary in a complex relationship.
- It is difficult to separate the junction temperature measurement of the transistor from the adjacent diode in the same power module as they are close to each other and demonstrate temperature cross-talk which may impact the accuracy of the results.

This method provides junction temperature values related to a practical WTPC operating compared to modelling however the cost and the parameter adaptation or scaling to the actual parameters are the most challenging in this technique. The best practice for measuring semiconductor junction temperature would be using it as a validation method for the junction temperature estimation by calculation or simulation.

3.3 Reliability analysis based on modelling

WTPC semiconductor junction temperature modelling is used to estimate the semiconductor lifetime and therefore in the WTPC reliability analysis. The WTPC reliability analysis is based on obtaining the semiconductor junction temperature during wind turbine loading related to wind turbine operation. The semiconductor junction temperature results from the generated

heat inside the semiconductor due to power loss and is affected by heat dissipation through the power module case and heatsink. The semiconductor power loss is produced by the semiconductor current and the semiconductor's internal parameters including internal resistance, saturation voltage, and switching energy. Therefore, semiconductor junction temperature modelling has to consider both the wind turbine loading and the semiconductor's internal parameters. The wind turbine load is driven primarily by the wind speed but it is also affected by the wind turbine's mechanical dynamics, the generator's electrical characteristics, and the control system.

The WTPC semiconductor parameters are not fixed and are affected by the operating voltage, frequency and temperature. Therefore it is important to consider the variation of the semiconductor parameters during the modelled wind turbine operation. Therefore, all the mentioned parameters impact the WTPC power loss and therefore the WTPC semiconductors' junction temperature. An overview of wind turbine modelling for WTPC reliability analysis is shown in figure 3.1 where the blocks represent submodels of wind turbine subsystems required for the WTPC reliability analyses. The modelling procedure provides a lower cost compared to lab tests or measurements however the accuracy of modelling results is highly influenced by the modelling details and assumptions considered by the researcher. The following sections describe the techniques that have been used by previous works in modelling each wind turbine subsystem for the WTPC reliability analysis.

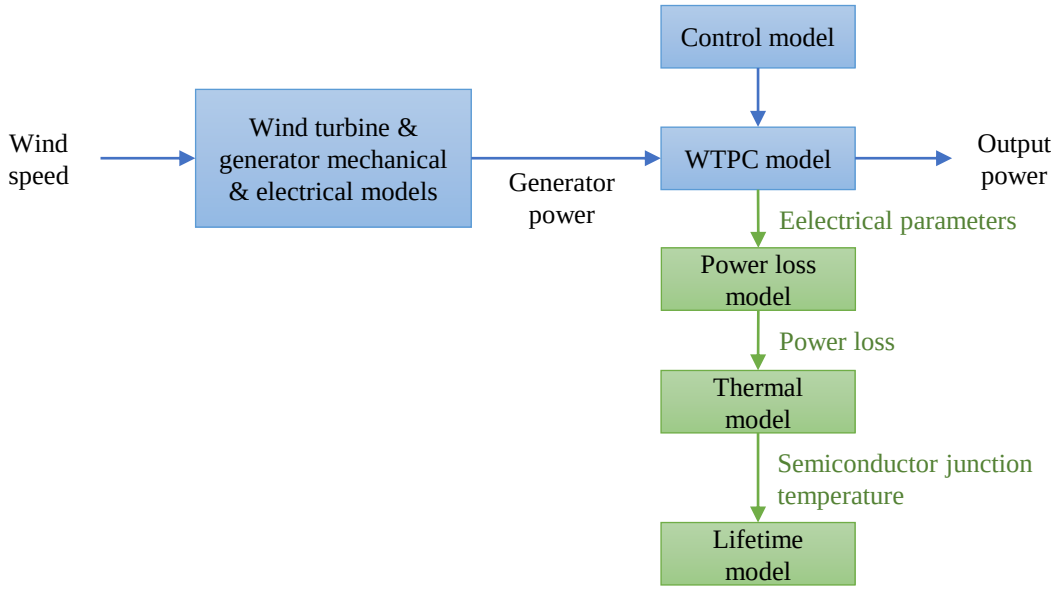

Figure 3.1: General procedure of modelling of semiconductor thermal loading for WTPC reliability analysis

3.3.1 Modelling wind speed

Wind speed is the input parameter to the wind turbine model. The modelled wind turbine should represent the current technology which is the variable-speed wind turbine. In this technology, the wind turbine output power has a cubic relation with wind speed between cut-in and rated

wind speeds. Therefore, undersampled wind speed measurements would have a bad impact on the model results accuracy. Smith et al. in [94] showed that a sampling rate lower than 0.25 Hz impacts the thermal analysis of the WTPC semiconductors. Constant wind speeds have been used in WTPC reliability analysis mainly with approaches based on mathematical calculations, like in [52]. This technique neglects the consideration of wind turbine mechanical and thermal dynamics during the changes in wind speed. The actual wind speed varies with time in a complex relation therefore assuming constant wind speed seems to be an unrealistic assumption.

3.3.2 Modelling wind turbine operating parameters

The wind turbine operating model is responsible for providing the WTPC operating voltage, current, and frequency which are necessary to calculate the WTPC semiconductor power loss. The techniques used in modelling the wind turbine operating parameters are mathematical calculation and model simulation. The mathematical calculation usually considers the steady state operation of the wind turbine based on constant wind speed input. The simulation can consider the wind turbine dynamics when the modelled input is variable wind speed. The simulation provides better details of the WTPC loading and therefore more details of its semiconductor power loss which is essential in calculating semiconductor junction temperature.

3.3.3 Modelling semiconductor power loss

The WTPC semiconductor power loss is important in calculating their junction temperatures which are essential for the WTPC lifetime estimation. The published articles in this field used several techniques in calculating or estimating the semiconductor power loss. Power electronics in switching applications like power converters produce power loss of two types: conduction power loss and switching power loss. The conduction power loss is produced by the interaction of the semiconductor current and semiconductor internal resistance and voltage drop. The conduction power loss occurs while the semiconductor status is on. The other power loss is the switching power loss which happens every time the semiconductor changes its status between on and off. The semiconductor switching power loss is produced by the interaction between semiconductor switching energy and switching frequency. The published articles presented techniques to calculate or estimate semiconductor power loss for WTPC reliability analyses. These techniques are mathematical calculation, lookup tables, and simulation.

Mathematical calculation of power loss

The mathematical calculation was used in [80] and [52] which used power loss equations for the diode and IGBT in the 2L-VSC as calculated by equations (3.1) and (3.2) respectively, where P_{loss} is the power loss for the diode (d) and IGBT (i), P_{cnd} is the conduction power loss, P_{sw} is the switching power loss, V_{F0} is the diode forward voltage, I is the converter current, M is the modulation factor, θ is the power factor angle, R_F and R_{CE} are the diode and IGBT forward resistance, f_{sw} is the switching frequency, E_{rec} is the diode recovery energy, V_{DC} is the converter dc voltage, V_{ref} and I_{ref} are the semiconductor datasheet reference voltage and current, E_{on} and E_{off} are the IGBT on and off switching energy.

$$\begin{aligned} P_{loss,d} =& P_{cd,d} + P_{sw,d} \\ =& V_{F0} I \left(\frac{1}{2\pi} \mp \frac{M}{8} \cos\theta \right) + R_f I^2 \left(\frac{1}{8} \pm \frac{M}{3\pi} \cos\theta \right) \\ &+ \frac{1}{\pi} f_{sw} E_{rec} \frac{V_{DC} I}{V_{ref,d} I_{ref,d}} \end{aligned} \tag{3.1}$$

$$\begin{aligned} P_{loss,i} =& P_{cd,i} + P_{i,sw} \\ =& V_{CE0} I \left(\frac{1}{2\pi} \pm \frac{M}{8} \cos\theta \right) + R_{CE} I^2 \left(\frac{1}{8} \pm \frac{M}{3\pi} \cos\theta \right) \\ &+ \frac{1}{\pi} f_{sw} (E_{on} + E_{off}) \frac{V_{DC} I}{V_{ref,i} I_{ref,i}} \end{aligned} \tag{3.2}$$

The equations are based on the steady-state operation meaning the results ignore the effects of the system dynamics. Furthermore, the semiconductors' internal parameters are affected by their junction temperature meaning the calculation has to use iterations to converge to the temperature value related to the operating parameters and heatsink temperature. The calculated power loss by equations (3.1) and (3.2) are for the 2L-VSC semiconductors, however, for other converter topologies like 3L-NPC or three-level active neutral point clamped (3L-ANPC), the power loss equations are more complex and include approximations [95] which make them unsuitable for WTPC reliability analyses.

Lookup tables

A similar technique to obtain semiconductor power loss is to use a lookup table that contains pre-calculated semiconductor power loss according to a range of operating parameters provided by the semiconductor manufacturer as in [96] and [97]. This can be more accurate than the approximated equations however this technique still involves small approximations due to quantizations of the input parameters required for the lookup tables.

Simulation

Simulation of the WTPC model can provide the semiconductor power loss based on the semiconductor model and the converter operating parameters. MATLAB with Simulink and PLECS are examples of the available software that can be used in WTPC reliability analysis as in [77]. The accuracy of simulation results relies on modelling details like the effect of junction temperature on semiconductor parameters and accurate WTPC loading considering system dynamics.

3.3.4 Modelling semiconductor junction temperature

Semiconductor junction temperature can be calculated mathematically considering semiconductor power loss and heat dissipation. Also, it can be simulated by modelling the semiconductor's internal and operational parameters. Both techniques are discussed in the following paragraphs:

Mathematical modelling

Mathematical modelling of semiconductor junction temperature can be used by solving the thermal equivalent circuit of the semiconductor power loss as a heat source and heat dissipation through thermal impedances of the semiconductor layers, power module case, and the attached heatsink as in equation (3.3) where $T_{j,Dev}$ is the device (IGBT or diode) power loss, $P_{loss,Dev}$ is the device power loss, $R_{th,Dev}$ is the device thermal impedance, $R_{th,Hs}$ is the heatsink thermal impedance, and T_a is the ambient temperature.

$$T_{j,Dev} = P_{loss,Dev}(R_{th,Dev} + R_{th,Hs}) + T_a \tag{3.3}$$

$$\tag{3.4}$$

Like in power loss mathematical modelling, the mathematical modelling of semiconductor junction temperature is valid for steady-state values. This technique when used in WTPC reliability analysis misses the dynamics of the system which has an impact on the semiconductor's estimated lifetime, particularly under high dynamic loading. Therefore, a more thorough approach is needed in analysing WTPC lifetime considering realistic wind turbine operation.

Simulation modelling

Semiconductor junction temperature can be obtained by thermal modelling the semiconductor internal layers, power module case, and heatsink. Software like MATLAB Simulink can be used in this technique by using the existing Thermal modelling toolbox. Unlike mathematical formulas, this technique can consider thermal dynamics by representing the thermal storage properties of the modelled parts. An equivalent thermal circuit is modelled where the current source represents semiconductor power loss, resistances represent thermal impedances, capacitors represent thermal storage, and the voltage source represents ambient or coolant temperature.

Thermal storage can be modelled as capacitors connected either parallel to thermal resistors or as paths to circuit ground depending on whether the Foster or Cauer equivalent circuit is used. Both circuits provide the same results however semiconductor datasheets usually provide the thermal parameter for use with the Cauer model [98]. While to use them in a Foster equivalent circuit those values need to be converted. Foster and Cauer thermal equivalent circuits used for modelling semiconductor junction temperature are shown in figures 3.3 and 3.2 respectively where $R_{th,Dev,Cau}$ and $R_{th,Hs,Cau}$, and $C_{th,Dev,Cau}$ and $C_{th,Hs,Cau}$ are Cauer's thermal resistors and capacitors of the device and heatsink respectively. $R_{th,Dev,Fos}$ and $R_{th,Hs,Fos}$, and $C_{th,Dev,Fos}$ and $C_{th,Hs,Fos}$ are Foster's thermal resistors and capacitors of the device and heatsink respectively.

For the thermal model to provide accurate estimations of the semiconductor junction temperature therefore, it has to consider the heat cross-talk between the semiconductors within the power module, IGBTs and diodes, and heat cross-talks among power modules attached to the same heatsink.

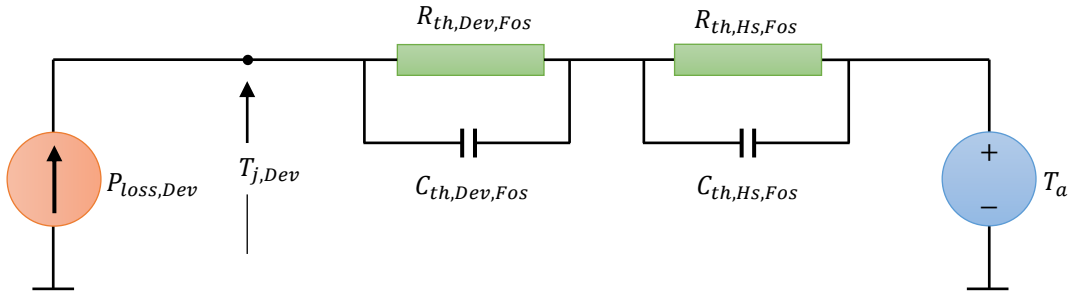

Figure 3.2: Foster thermal equivalent circuit of semiconductor junction temperature

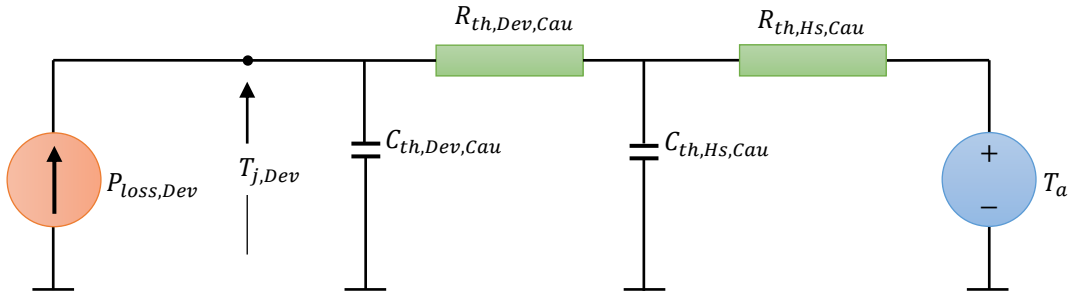

Figure 3.3: Cauer thermal equivalent circuit of semiconductor junction temperature

3.3.5 Modelling WTPC lifetime

Lifetime models are used as end-of-life estimations for power electronics. Empirical lifetime models were usually used in semiconductor lifetime estimation. They were constructed based on a large field failure database and a large number of accelerated damage tests [86]. Empirical lifetime models estimate the semiconductor lifetime by estimating the number of their thermal cycles to failure (N_f). The WTPC lifetime is then estimated by considering the lifetimes of its individual semiconductors, transistors and diodes. Different lifetime models have been developed based on the collected field data and accelerated damage tests. The following sections present the empirical lifetime models available for the power semiconductors and applied in WTPC reliability analysis.

Coffin-Manson model

The earliest empirical model used in semiconductor lifetime estimation was based on the Coffin-Manson law [99]. The Coffin-Manson model considers the thermal cycling of the semiconductor junction temperature as these changes produce cyclic thermo-mechanical stress causing accumulated damage to the semiconductor structure. The semiconductor lifetime is expressed by

the number of cycles to failure, N_f. Those cycles are assumed to be reduced by increasing the temperature changes, ΔT ($\Delta T = T_{max} - T_{min}$) where T_{max} and T_{min} are the semiconductor maximum and minimum junction temperatures respectively. The model equation is shown in equation (3.5) where a and b are empirical constants determined from the results of accelerated damage tests.

$$N_f = a.(\Delta T)^{-b} \tag{3.5}$$

Coffin-Manson Arrhenius model

In the 1990s, the LESIT project tested a large number of power semiconductor failure data for reliability analysis. After several tests, the semiconductor lifetime was found to be affected by the average junction temperature as well as junction temperature variation. While the estimated lifetime by the Coffin-Manson model is based on the variation of the junction temperature (ΔT), there was a need to include the average junction temperature as well. The term added to the Coffin-Manson law was by combining the Arrhenius equation which states that the lifetime of activated energy devices is exponentially proportional to their temperature [63]. The empirical model became known as the Coffin-Manson Arrhenius model. The model formula is shown in equation (3.6) where T_m is the mean semiconductor junction temperature in Kelvin, E_a is the activation energy, and K_B is the Boltzmann constant.

$$N_f = a(\Delta T)^{-b} e^{(\frac{E_a}{T_m K_B})} \tag{3.6}$$

The Coffin-Manson Arrhenius model is accepted by industry. However, the industry sought a more thorough lifetime model for the power module packages to include a more recent large reliability database of power semiconductors which led to the introduction of the CIPS08 model [82].

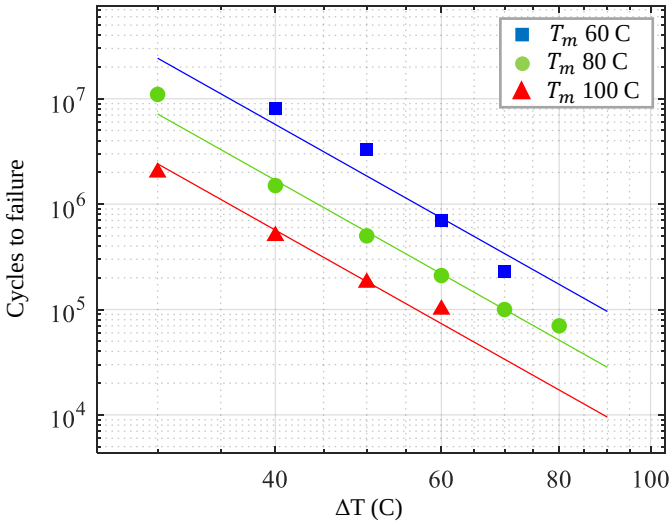

Figure 3.4: LESIT project failure data [100]

CIPS08 model

The Coffin-Manson Arrhenius equation was produced based on the failure data from lab tests of the LESIT project [100]. However, due to the limited available technology at that time, the LESIT project data did not categorise the failure data as related to different causes of failure. For example, some semiconductors' failures were due to the bond-wire lift-off while others' failures were due to solder fatigue. This approach impacted the produced lifetime model's accuracy as it combined all the failure mechanisms in one empirical lifetime model. When the technology improved, the semiconductor manufacturers became able to analyse semiconductor failures due to a variety of causes of failure individually therefore lifetime estimation parameters related to each failure mechanism could be identified and included in the lifetime model. The model presented by Bayerer from Infineon company is an extended empirical lifetime model known as the Bayerer model [101].

This model has been accepted in this field as it considers more impacts on the semiconductor lifetime than the Coffin-Manson model does, which results in more details about the failure mechanism. CIPS08 model considers parameters like the number of bond wires, the current per bond wire, maximum and cyclic range of junction temperature, operating voltage, and heating time. The Bayerer model is expressed by equation (3.7) where K and α_1 to α_6 are the semiconductor lifetime empirical constants and T_{jmax} is the semiconductor maximum junction temperature in Celsius, t_{on} is the semiconductor heating time, I is the current, V_B is the blocking voltage of the chip, and D_{bond} is bond wire diameter. The challenge of using the Bayerer model is the required parameters which usually are not easy to obtain from the power electronic module manufacturer.

$$N_f = K(\Delta T_j)^{\alpha_1} e^{\alpha_2/(T_{jmax}+273)} t_{on}^{\alpha_3} I^{\alpha_4} V_B^{\alpha_5} D_{bond}^{\alpha_6} \tag{3.7}$$

3.4 Gaps in the current WTPC reliability analysis techniques

3.4.1 Estimating WTPC base on constant wind speeds

This technique has been used in published articles like in [52, 80, 97] It is based on estimating WTPC lifetimes with respect to several constant wind speeds ranging from wind turbine cut-in to cut-out wind speeds. The overall WTPC lifetime is calculated based on the probability of each tested wind speed occurring during the year according to the Weibull distribution of annual wind speeds as shown in figure 3.5 where U is wind speed and PDF is the probability density function. The WTPC semiconductor power loss and junction temperature are either calculated mathematically or simulated with respect to selected constant wind speeds. This technique misses the impact of changing wind speeds which develop interaction with the wind turbine mechanical and thermal dynamics affecting the WTPC loading. Furthermore, when this technique uses mathematical calculations for semiconductor power loss and junction temperature, the accuracy will be even less since the changes in semiconductor internal parameters due to temperature increase are not considered. While using lookup tables, like in [97], is relatively more accurate than mathematical calculation, the simulation can provide the best estimation of

semiconductor junction temperature. However, ignoring the wind speed dynamics still restricts the accuracy of this technique. The best practice of this technique is in providing details about loading differences of semiconductors within the WTPC circuit like the junction temperature difference between the IGBT and diode with respect to constant wind speeds.

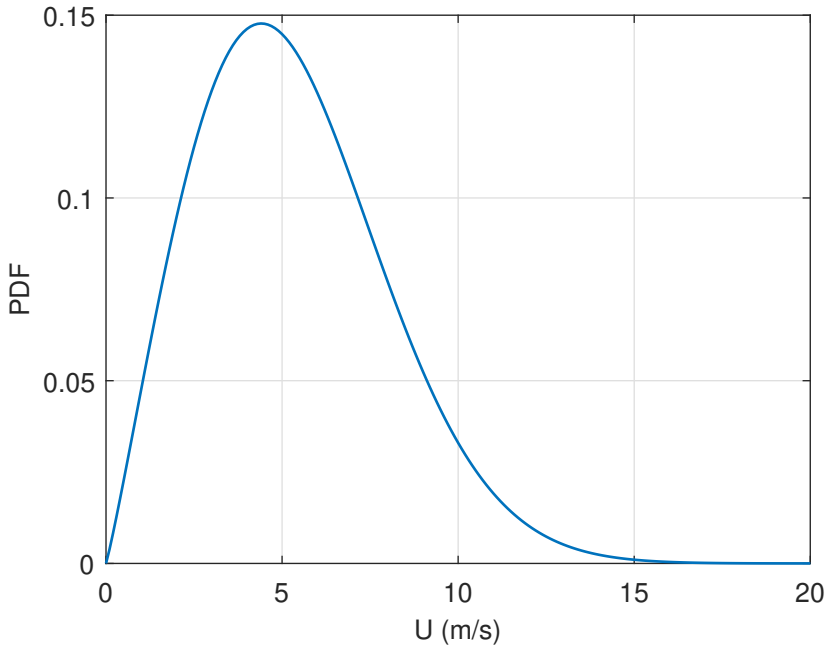

Figure 3.5: Weibull distribution of 6 m/s annual average wind speed and 2.1 shape parameter

3.4.2 Estimating WTPC based on variable wind speed

Compared to assessing the WTPC reliability based on constant wind speeds, published articles like [53,77] used variable wind speed profiles to estimate WTPC lifetime, providing more realistic results. However, the results' accuracy will also be impacted if this method involves assumptions like averaging operating parameters. The method also required testing a good number of variable wind profiles covering the range of wind speed and turbulence intensities otherwise the results would not represent the actual situation in the field.

3.4.3 Impact of turbulence intensity on WTPC lifetime

Most of the published articles related to WTPC reliability with respect to operating conditions were based on analysing the impact of wind speed on WTPC lifetime. The real wind speed keeps changing in a complex phenomenon which affects the wind turbine operating and therefore the WTPC loading. The impact of wind speed dynamics known as wind turbulence intensity on WTPC lifetime has not been discussed thoroughly by the published articles where some of them suggested opposing conclusions as reviewed in section 2.5.2. The WTPC reliability analyses should consider the impact of wind turbulence intensity which requires testing enough variable wind speed profiles and using statistical analysis since wind turbulence intensity is based on statistical measures of wind speed changes.

3.4.4 Impact of wind turbine technology on WTPC lifetime

The effect of wind turbine technology like the generator type, generator speed, and converter topology on WTPC lifetime has been discussed in published articles like in [41, 54, 80]. The reliability analyses were based on comparisons between two systems to identify the impact of the specified different technology on WTPC lifetime. However, the comparisons should consider fairness by utilising identical systems to compare with one difference for evaluating its impact otherwise, comparison results would work for specific examples rather than lead to general conclusions. Also, the reliability assessment will have better results when it is based on variable wind speed input to reflect the practical operation of wind turbines.

3.4.5 Models validation

The lifetime models are very sensitive to the semiconductor junction temperature due to the exponential relationship. Therefore, modelling wind turbines for WTPC reliability analysis requires validation to ensure that the simulated junction temperature concerning input wind speed is within accepted accuracy. The validation can proceed by comparing the model's result with lab measurements which involve cost and complexity or with another trusted model such as ones provided by the power electronic manufacturer.

3.4.6 Necessity to seek high accuracy in WTPC reliability analysis

The widely used lifetime models, Coffin-Manson Arrhenius and Bayerer, in WTPC reliability analysis, show that semiconductor cycles to failure are exponentially related to the mean and range of variation of semiconductor junction temperature. Therefore, approximations used in the calculation or simulation will greatly impact the accuracy of lifetime results.

3.5 The proposed method

The Reliability assessment of WTPCs used several techniques as discussed in previous sections. The discussed techniques all neglect some elements of importance to wind turbine operation and could not provide results based on the realistic operation of the wind turbine. The methods estimated WTPC lifetime either based on non-realistic constant wind speeds or based on one or a few samples of variable wind speed profiles for a short time of wind turbine operation.

The wind turbine has a considerably large inertia in its mechanical system and a high thermal latency produced by the cooling heatsink attached to WTPC semiconductors. These factors have to be considered to obtain realistic simulation results of the semiconductor junction temperature. Furthermore, wind speed varies in a very complex pattern where a few samples of variable wind speed can not cover the range of wind speeds and turbulence intensities that an actual wind turbine faces during its operation.

The estimated WTPC lifetime should not be generalised based on simulating wind turbine operation for seconds or a few minutes. On the other side, lifetime empirical models used in the WTPC reliability analysis have an exponential relationship with the semiconductor junction temperature which makes the estimated lifetime accuracy critical for any small deviation of the

measured or simulated junction temperature. Therefore, it is important to validate the junction temperature values before applying them to the WTPC reliability analysis.

In this research, a WTPC reliability assessment method is presented reflecting the realistic operation of the wind turbine by applying a variety of field-measured variable wind speed profiles to the WTPC reliability model and taking account of the statistical variability of results. The model simulates wind turbine operation for an appropriate time to collect useful temperature data considering the required time for the mechanical and thermal systems balance before collecting the semiconductor junction temperature data for the lifetime estimation. The variable wind speed profiles used are 1 Hz sampling rate which provides acceptable results. Furthermore, the modelled wind turbine is validated for its performance and temperature results to ensure the accuracy of the reliability analysis.

3.5.1 The model

The method is based on modelling a wind turbine to analyse the impact of wind speed on the WTPC loading. The model has to consider the wind turbine mechanical system as its dynamics affect the power transformed from the wind to the generator. The electrical system modelling is required to provide the WTPC voltage, current, and frequency related to wind speed. The thermal modelling analyses the junction temperature considering the dynamics of the converter heatsink and cooling method as the semiconductor lifetime relies on its junction temperature.

The information and assumptions used by this research model are based on the product datasheet parameters which is trustworthy information the manufacturer publishes. The manufacturer model should have considered the product datasheet as well besides validating their model before publishing it on their official website. The similarity of both models is about considering the power module information from its datasheet.

The model produces a validated junction temperature based on validating wind turbine operating parameters by comparing the simulated values with expected values by calculations. Also, the semiconductor junction temperatures are validated by comparing them with simulated junction temperatures by the power module manufacturer tool related to specific operating parameters. Although there can be a risk of using one model to validate another model, the manufacturer tool, SemiSel, is a reliable benchmark in estimating semiconductor junction temperature according to operating parameters. This tool is used in designing power converters with the selected power module to ensure safe junction temperature.

3.5.2 Lifetime estimation procedure

The reliability analysis in this method is based on estimating WTPC lifetime during the operation of the modelled wind turbine with an input of variable wind speed profiles. The simulation outputs are the junction temperature time series of the WTPC semiconductors. The thermal cycles are analysed and counted to calculate the damage that occurred in the WTPC semiconductors during the time of the variable wind speed profile. The mean time to failure (MTTF) is estimated considering the calculated damage and time. Further details of lifetime estimation are discussed in Chapter 4.

3.5.3 Reliability impact of operating conditions

The method analyses the impacts of wind turbine operating conditions including wind speed and turbulence intensity. The method simulates WTPC lifetimes concerning a large number of variable wind speed profiles and then uses statistical tools to analyse their impact on WTPC lifetime. The selected wind speed profiles are field-recorded wind speeds sampled at an accepted rate to emulate actual wind turbine operation. The selected wind speed profiles cover the range of wind turbine operating wind speeds and turbulence intensities as available in the records.

3.5.4 Reliability impact of WTPC design

The method analyses the impact of the WTPC design on its reliability by comparing the WTPC lifetimes of the most widely deployed converter topologies, two-level and three-level, in wind turbines. The method also analyses the impact of the wind turbine control system on WTPC reliability by comparing WTPC lifetime while controlled by the two known control systems, field-oriented control and direct torque control.

The following chapter presents the detailed wind turbine modelling and the model validation procedure. The model eliminates approximations as the simulation is based on the instantaneous values of the system variable parameters.

Chapter 4

Reliability modelling of WTPC

4.1 Introduction

The WTPC lifetime is highly impacted by the lifetime of its semiconductors where their thermal loading is the key factor of their lifetime estimation [40]. It is costly and difficult to measure the semiconductor junction temperature during the variable loads that result from the nature of wind turbine operation. Therefore, the simulation of a wind turbine model is chosen for the research as it provides flexibility and lower costs. Wind turbine modelling can provide detailed information about the WTPC loading and its semiconductor junction temperature during a variety of operating conditions. Furthermore, modelling is a cost-effective method to analyse different effects on the WTPC lifetime like changing the converter design or the wind turbine control system. It also provides relatively fast results in testing a large number of VWSPs to analyse the impact of different operational conditions on WTPC lifetime. In this research, modelling a wind turbine equipped with the widely deployed WTPC design for reliability analyses provides the required information to answer the first research question "How can the reliability of existing wind turbine two-level voltage source converters be better understood?"

In this research, the WTPC lifetime estimation is based on its semiconductors' lifetime as they are the dominant factor in WTPC lifetime [102]. The Coffin-Manson Arrhenius model is used to estimate WTPC semiconductors' lifetime. However, the lifetime estimation accuracy is highly affected by the accuracy of the semiconductor junction temperature which is the key challenge in WTPC reliability modelling. Therefore, in this research, the WTPC reliability modelling considers three important guidelines to assure the accuracy of the results.

1. The model minimises the use of approximations including averaging of operating parameters like currents, voltages, power loss, etc.

2. The input wind speed data used in the simulation are field-measured so the wind turbine simulation reflects practical operational parameters.

3. The reliability model passes a validation procedure to ensure simulation accuracy. That includes model performance parameters like rotating speed, torque, voltages, and currents. The validation also assesses the simulated semiconductor junction temperature accuracy as it is an essential parameter in semiconductor lifetime estimation.

The block diagram of the wind turbine model in the proposed method is presented in figure 4.1 where the details of each block are described in the corresponding section in this chapter.

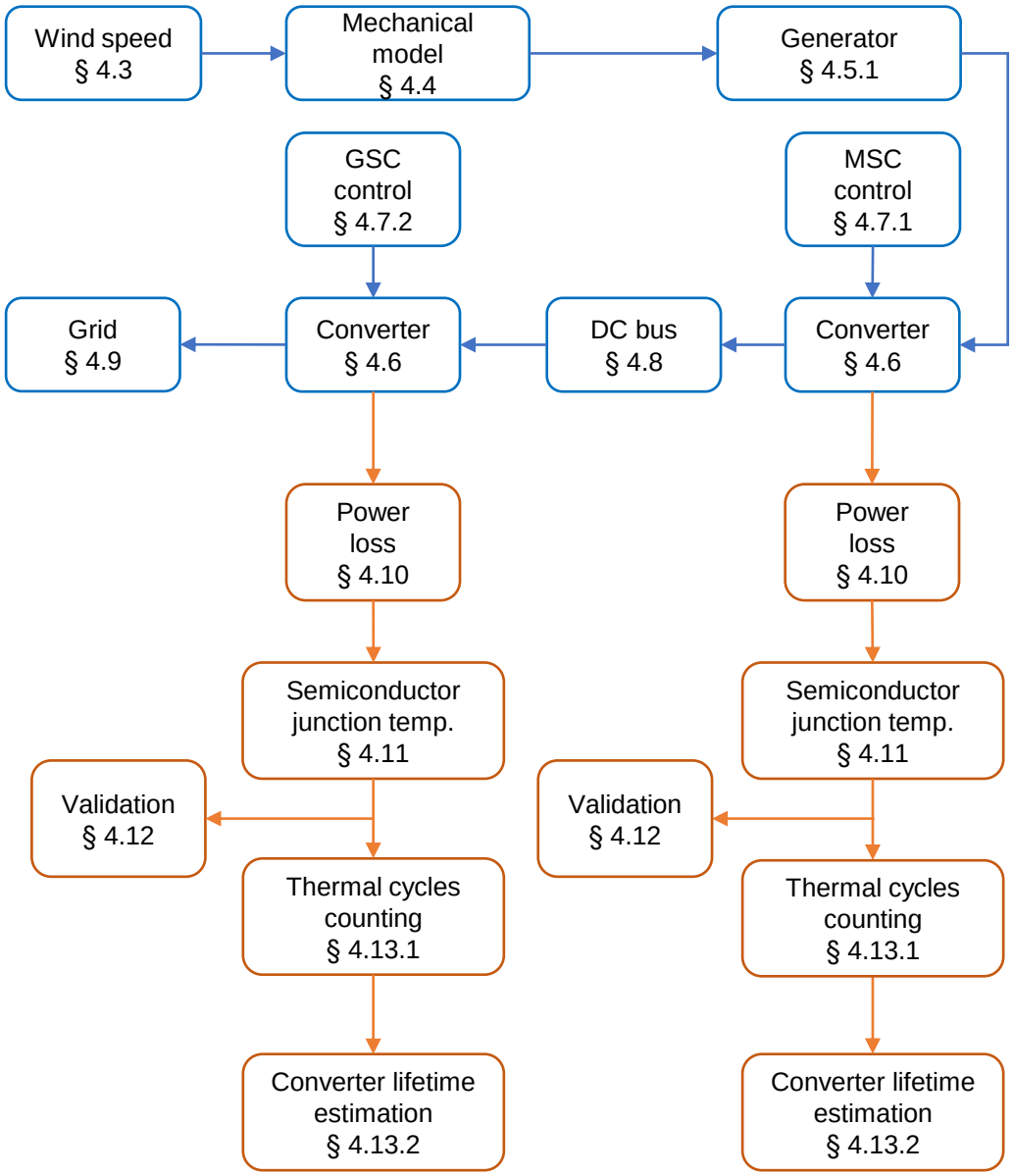

Figure 4.1: WTPC reliability modelling

4.1.1 Modelling software

MATLAB and Simulink are the modelling and simulation software used in this research. MATLAB offers a range of modelling and analysis toolboxes for modelling the mechanical, electrical, and thermal submodels in the wind turbine reliability model. MATLAB also provides the statistical functions and the signal processing tools needed for the reliability analysis in this research.

The wind turbine mechanical submodel is modelled by MATLAB Simscape Mechanical toolbox, the PMSG and converter circuit are modelled by MATLAB Simscape Specialized Power Systems toolbox, the semiconductor junction temperature is modelled by MATLAB Simscape Thermal toolbox, the lifetime model used RainFlow algorithm is from MATLAB Signal Processing toolbox, and the statistical functions used in the lifetime analysis are from MATLAB Statistical and Machine Learning toolbox.

4.2 Wind turbine model

In this research, the reliability analysis of WTPC is based on analysing the thermal stress of the converter's semiconductors during the wind turbine operation. An example of a wind turbine is modelled containing the affecting parts on the WTPC loading and its semiconductors' junction temperature. The model simulates WTPC operating parameters like current, voltage, frequency, control, and switching. All these parameters affect the WTPC loading and its semiconductors' junction temperature.

Information on multi-megawatt wind turbine (8 MW and above) designs and operating parameters is limited due to industry confidentiality in this field. However, parameters for modelling a smaller wind turbine were available like in [23]. The 2 MW PMSG-based wind turbine is selected for the reliability model in this research because it is based on the currently deployed generator type, PMSG, it is direct drive as current wind turbines, and its rated voltage is 690 V which is the same voltage as many deployed WTPC [25]. The rated power is lower than the currently being installed wind turbines however this does not affect the reliability analysis as the WTPC usually contains parallel converters for higher-power wind turbines which means that the same WTPC of a 2 MW wind turbine can be used in 6 MW or 8 MW by increasing the paralleled converters.

The wind turbine model is divided into three main submodels. The mechanical submodel contains the rotor, the coupling shaft, and the generator's mechanical parameters. The electrical submodel contains the generator's electrical parameters, the power converters, the control system, and the grid. The lifetime submodel contains the converter power loss, semiconductor junction temperatures, and lifetime estimation. The model overview is shown in figure 4.2 where ω_t is the rotor angular speed, I_m is the PMSG current, τ_{ref} is the reference turbine torque, T_j is the semiconductor junction temperature, MPPT is the maximum power point tracking, and V_g and I_g are the grid voltage and current respectively. The details of submodels are explained in the following sections of this chapter.

4.3 Wind speed

The wind speed is the fuel of the wind turbine on which operating parameters and output power rely. In wind turbine reliability models, the wind speed variable (U) in m/s is used as input for the model. The model either simulates constant wind speed operation where U is represented by a constant value, or it simulates variable wind speed operation where U is represented by a timeseries of sampled variable wind speed running for a defined time called variable wind speed

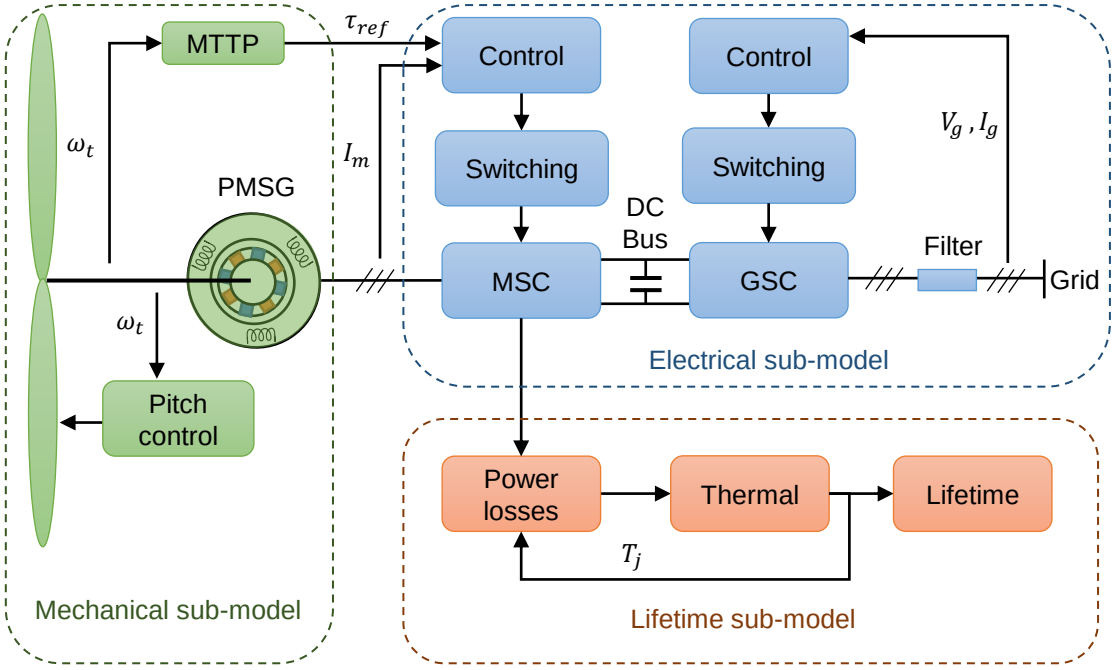

Figure 4.2: wind turbine model overview

profile denoted in this thesis by (VWSP).

The constant wind speed simulations are used to examine the proper operation of the model by comparing the steady-state operating parameters from the simulation with the expected values obtained by calculations. The variable wind speed tests are used for the reliability analyses of the WTPC as they emulate the actual wind turbine operation in the field where WTPC loading varies according to the exposed variable wind speed. The available wind speed data are categorized as low-frequency sampled wind speed and high-frequency sampled wind speed.

4.3.1 Low-frequency sampled wind speed data

Supervisory Control and Data Acquisition (SCADA) is used in wind turbines for collecting and recording operational parameters, alarms, and signals [103]. The wind speeds and directions are part of the environmental data stored by the wind turbine SCADA system [104]. The SCADA controller collects wind speed samples, calculates their average and standard deviations periodically usually every 10 or 5 minutes and stores them in wind turbine SCADA records [105]. The SCADA records contain wind speed information for a long time, a year or more. However, the recorded data is at low frequency, every 10 minutes, 5 minutes, or 1 minute like in some recent systems. The SCADA wind speed information frequency is too low for the WTPC reliability simulation [94] however it can be used in estimating the wind characteristics for the specific site to describe its average wind speed and turbulence intensity.

4.3.2 1-Hertz wind speed time series

The sampling frequency of wind speed is important for the converter reliability analysis. The lifetime of the WTPC semiconductors is overestimated when the wind speed sampling frequency

is lower than 0.25 Hz [75]. The 1 Hz sampled wind speed provides an accepted sampling resolution for tracing the semiconductor junction temperature variation. All the VWSPs used in this research for the WTPC reliability analyses are field-recorded wind speeds sampled at 1 Hz each 10 minutes long containing 600 wind speed measurements. A ten-minute duration is chosen to be similar to the average durations used in SCADA wind speed records. This similarity can be utilized in future research to compare the reliability results with the SCADA records. The source of VWSPs is a year-long data obtained from Catapult ORE at Blyth, UK. Figure 4.3 shows an example of VWSP represented 10 minutes of wind speed data recorded in June 2^{nd}, 2018.

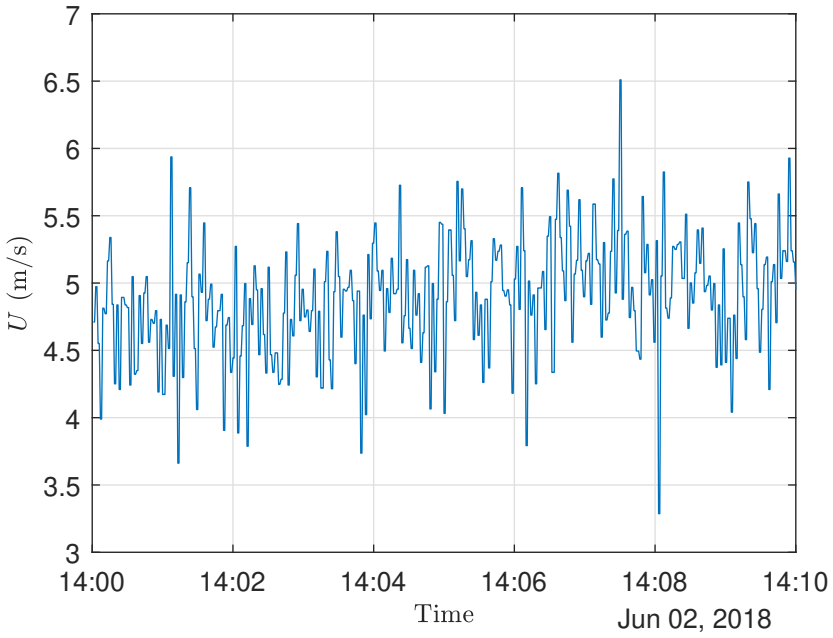

Figure 4.3: 10 minutes WSTS recorded at 1Hz sample rate

4.4 Wind turbine mechanical submodel

The wind turbine system dynamics affect the generator responses to wind speed variation which reflects on the generated power and therefore the WTPC loading and its lifetime [51]. Therefore, mechanical modelling is required in the WTPC reliability analysis. The selected wind turbine for reliability modelling is a direct-drive variable-speed pitch-controlled equipped with PMSG. The mechanical submodel simulates the system dynamics of the wind turbine rotor, coupling shaft, and the PMSG concerning the applied wind speed and the opposite electromagnetic torque developed in the PMSG.

4.4.1 Wind turbine rotor model

The blowing wind carries kinetic energy expressed by the power equation in (4.1) [106] where P_{air} is the power carried by the moving wind exposed to the wind turbine in Watt, ρ_{air} is the air density in kg/m^3, A_t is the wind turbine swept area in m^2, and U is the wind speed in m/s.

The wind turbine rotor can extract part of wind energy and convert it into mechanical energy as in equation (4.3) where C_p is the wind turbine power coefficient.

$$P_{air} = \frac{1}{2}\rho_{air} A_t U^3 \tag{4.1}$$

$$P_t = C_p P_{air} \tag{4.2}$$

$$= C_p \frac{1}{2}\rho_{air} A_t U^3 \tag{4.3}$$

The wind turbine rotor is modelled using the Wind Turbine model from MATLAB Simscape renewables library. The model inputs are wind speed (U) in m/s, blade pitch angle (β) in degree, and rotor speed (ω_t) in pu while its output is the rotor's developed torque (τ_t) in pu.

4.4.2 Two-mass model

The modelled wind turbine mechanical system is a direct drive where the wind turbine rotor is directly coupled with the generator by a coupling shaft without a gearbox. The mechanical modelling of this configuration is represented by a two-mass mechanical system constructed by the turbine rotor inertia (J_t), the generator inertia (J_m), the shaft spring stiffness (K_{sh}), and the shaft damping (D_{sh}). The developed torque in the wind turbine rotor is transferred to the generator by the coupling shaft. The developed torque at the generator end (τ_m) is expressed by the two-mass mathematical model expressed by equation (4.4) [107] where ω_m and ω_t are the angular speeds of the generator and turbine rotor respectively θ_m and θ_t are angles of generator and turbine rotor respectively.

$$\dot{\tau_m} = (\omega_t - \omega_m)D_{sh} + (\theta_t - \theta_m)K_{sh} \tag{4.4}$$

The generator induces voltage and current passes into the converter circuit. According to Lenz's law, the generator current develops an electromagnetic torque (τ_{em}) in a direction opposite to the rotating direction. Figure 4.4 shows the overview of the mechanical modelling of a direct drive with a pitch-controlled wind turbine. The mechanical submodel is constructed using the Simulink wind turbine model which is part of the Simscape Electrical toolbox. The Simulink wind turbine model produces wind turbine torque based on the U, β, and ω_m. The modelled wind turbine mechanical parameters are listed in table 4.1 and the model block diagram in Simulink is shown in figure 4.5.

4.4.3 Pitch control

The variable speed wind turbine utilises its blades' angle of attack to protect the wind turbine speed from overspeed. The wind turbine blades' attacking angle is usually positioned to develop maximum torque against the blowing wind. However, when the wind turbine rotor reaches its rated rotating speed and the wind speed goes even higher, the pitch control activates and reduces the blades' attacking angle to reduce the developed torque. This technique protects the wind turbine from damage by exceeding the rotating speed over the rated rotating speed. The result

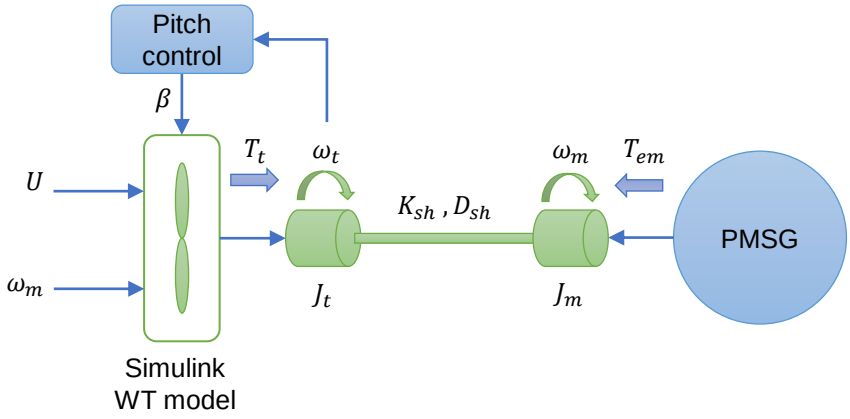

Figure 4.4: Mechanical modelling of pitch-controlled direct-drive wind turbine

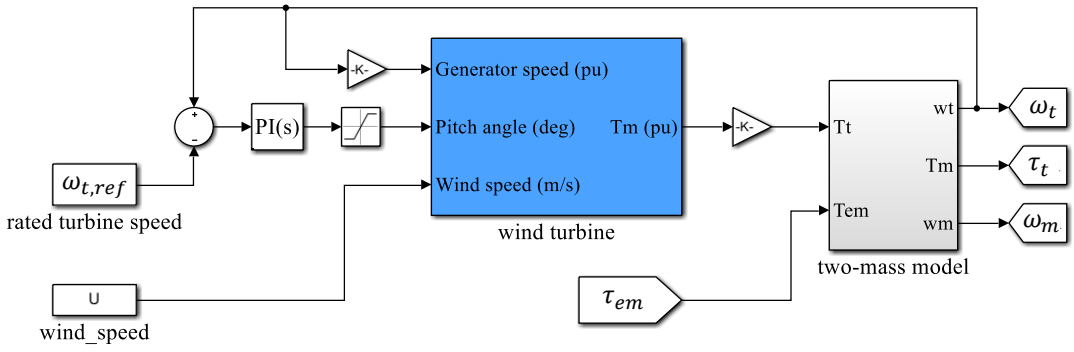

Figure 4.5: Wind turbine mechanical model by MATLAB Simulink

of this control is that the wind turbine will stay at its rated rotating speed and power even if the wind speed goes higher than the rated wind speed. The pitch control has to be modelled in the reliability model as it affects the WTPC loading when the input of variable wind speeds moves higher than the rated wind speed.

The modelled pitch control is designed according to [24]. It consists of a comparison between the actual rotor speed (ω_t) and the reference value ($\omega_{t_{ref}}$) which is set to the rated rotating speed. The error signal is then applied to a proportional-integral controller (PI) which sends the blade angle to the Simulink wind turbine model as previously shown in figure 4.5

4.4.4 Maximum Power Point Tracking

In variable-speed wind turbines, MPPT is utilised to extract the maximum power from the wind by controlling the rotor speed according to wind speed to keep the tip speed ratio (TSR) at the optimum value (TRS_{opt}) which is calculated by equation (4.5) for the rated wind speed and rated rotating speed. The MPPT operates as a speed control for the wind turbine rotor to keep optimum TSR by setting the reference torque according to equation (4.6) [24].

Table 4.1: Wind turbine mechanical parameters

Parameter	Symbol	Value
Rotor raduis	R	42 m
Rated power	$P_{t,rated}$	2 MW
Cut-in wind speed	U_{in}	4 m/s
Rated wind speed	U_{rated}	12 m/s
Cut-out wind speed	U_{out}	25 m/s
Power coefficient (maximum)	$C_{p,max}$	0.341
Rotor rotating speed (rated)	$\omega_{t,rated}$	0.75 rad/s
Generator inertia	J_m	200 (kg.m^2)
Rotor inertia	J_t	2.92 $\times 10^6$ (kg.m^2)
Shaft spring stiffness	K_{sh}	40 $\times 10^6$ N.m/rad
Shaft damping	D_{sh}	6.72 $\times 10^6$ J.s/rad

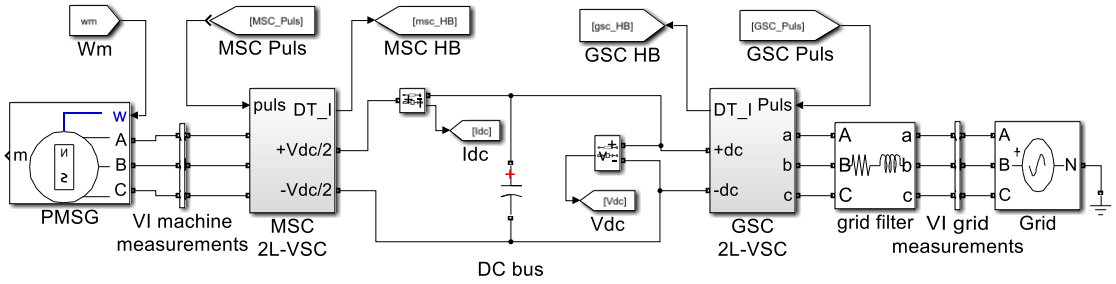

Figure 4.6: Simulink model of wind turbine electrical system

$$TSR_{opt} = \frac{\omega_{t,rated} R}{U_{rated}} \tag{4.5}$$

$$\tau_t = \frac{1}{2} \rho_{air} \pi \frac{R^5}{TSR_{opt}^3} C_{p,max} \omega_t^2 \tag{4.6}$$

4.5 Wind turbine electrical submodel

The wind turbine's electrical system is modelled to emulate the energy flow from the generator to the grid as in the actual wind turbine. Modelling the electrical system is needed to obtain the required electrical parameters for WTPC power loss calculation. The wind turbine electrical submodel includes the generator, the WTPC, the control system, and the connected grid. Figure 4.6 shows the electrical subsystem block diagram modelled in Simulink. The details of these blocks are explained in the following subsections.

4.5.1 Wind turbine generator

The wind turbine generator type selected for the WTPC reliability analysis is PMSG. Modelling the PMSG is based on the Simulink Permanent Magnet Synchronous Machine (PMSM) block

Table 4.2: Wind turbine PMSG parameters

Parameter	symbol	Value
Line voltage (rated)	$V_{m,rated}$	690 V
Active power (rated)	$P_{m,rated}$	2,000 kW
Apparent power (rated)	$S_{m,rated}$	2,241.9 kVAR
Rotating speed (rated)	$\omega_{m,rated}$	0.75 rad/s
Torque (rated)	$\tau_{m,rated}$	848,826 Nm
Number of poles pairs	P_p	26
Flux linkage (RMS)	$\Phi_{m,RMS}$	6.503 Wb
Stator winding resistance	R_s	2.34 mΩ
Stator winding inductance	L_s	1.573 mH

from MATLAB Simscape Specialized Power Systems toolbox [108]. This model can operate either as a motor or as a generator as in the wind turbine model. The modelled PMSG is a 2 MW nonsalient pole PMSM with parameters based on the example of a wind turbine generator in [23]. The modelled machine parameters are listed in table 4.2.

4.6 Power converter model

The main part of the WTPC reliability model is the power converter where two converters are modelled for MSC and GSC in the AC-DC-AC configuration used in wind turbines equipped with PMSG. Both converters are modelled to achieve two tasks. First, to simulate the proper operation of the wind turbine by delivering the right values of voltages, currents, and power to emulate the actual wind turbine operation. Second, to extract their semiconductors' operational parameters for the power loss calculation required for the thermal model and lifetime estimation.

Power converters vary in their design however addressing the first research question "understanding the reliability of currently and widely used WTPC". The selected converter design for both MSC and GSC is the three-phase 2L-VSC as equipped in the currently operating wind turbines like Seimens Gamesa SWT-7.0/SG 8.0, MHI Vestas V164-8.0, and Enercon E126-7.58 [47]. Both MSC and GSC models are assumed to be identical as they operate at the same voltage and power however each has its dedicated control to perform the required function. MSC is expected to extract the maximum power from the wind turbine generator, PMSG, rectify it, and inject it to the DC bus while GSC is expected to regulate the DC bus voltage and invert the DC power to AC to deliver it to the grid.

The WTPC's converters, MSC and GSC, are assumed to be operating in the normal operation mode of balanced phases and in no-fault conditions. Accordingly, the converter semiconductor switches are operating symmetrically and their operational parameters are equal so the simulation of one half-bridge arm in each converter reflects the operation of the rest of the converter switches. The converter circuit is built based on individual power modules for clearer reliability analysis of the semiconductors' thermal stresses rather than modelling a prefabricated power stack. The 2L-VSC circuit includes six power modules. The selected power module is SKM800GA176D manufactured by SEMIKRON company and specified for wind power application [17].

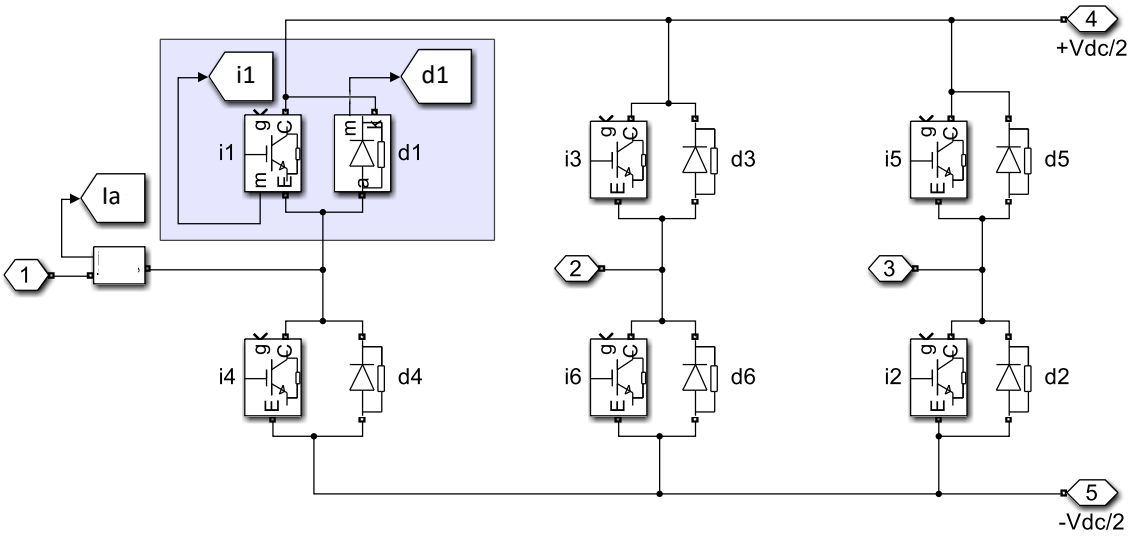

Figure 4.7: Simulink model of 2L-VSC power converter

Table 4.3: Power module SKM800GA176D parameters

Parameter	symbol	value
Blocking voltage	V_{CES}	1,700 V
Nominal IGBT current	I_{Cnom}	600 A
Nominal diode current	I_F	600 A
Terminal ac current	I_{tRMS}	500 A
Saturated CE voltage	$V_{CE0\ typical}$	1.0 V
IGBT CE on resistance	$R_{CE\ typical}$	1.7 mΩ
Diode on resistance	R_F	0.83 mΩ

The power module contains one IGBT and one reverse parallel freewheeling diode. The module can operate on up to 1,700 V making it suitable for selected PMSG rated voltage. The parameters details of SKM800GA176D are shown in table 4.3 and the full parameters are shown in its datasheet in Appendix B [17]. The rated power of the modelled converter circuit based on the SKM800AG176D power module is limited to 250 kW due to the operating temperature limitation. Therefore, eight parallel converters are assumed to be installed in the 2 MW wind turbine. In the simulation model, the generator current is divided by eight to achieve the right current value for the modelled converter circuit. Parallel converters are widely used in multi-megawatt wind turbines to share the generator power [29, 109]. Figure 4.7 shows the Simulink model of the converter circuit where terminals 1, 2, and 3 are the three-phase connections, i1 and d1 are the IGBT and diode of the power module SKM800GA176D, m_{i1} and m_{d1} are their measurement ports respectively, I_a is the phase current measurement port, terminals 4 and 5 are the DC bus connections.

4.7 WTPC control

The operation of the WTPC is controlled by the converter controller aiming for a stable wind turbine operation and energy delivery to the grid. The converter controller affects the wind turbine's operating speed, torque and ultimately its output power. Depending on the wind turbine generator type, different converter control system design is applied like control systems used with PMSG, DFIG, or IG. The current control loop is selected for controlling MSC and GSC as it is preferred in grid-connected wind turbines for accepted harmonics level [110]. As MSC and GSC have different functions, a dedicated control is modelled for each one.

4.7.1 Control of MSC

The MSC control implements the field-oriented control (FOC) strategy in the modelled wind turbine. This control strategy is used with DFIG and PMSG wind turbines for its performance and smooth operation of the generator due to low torque ripple [111]. The lower ripple operation results in better efficiency and less stress on the wind turbine's mechanical and electrical parts which reflects on their reliability.

FOC is based on decoupling the generator current (I_m) into two components, direct current (I_{md}) and quadrant current (I_{mq}). The Park transformation is used to decouple I_m where its electrical vector angle (θ_e) is calculated by multiplying the generator number of pole pairs (P_p) with the mechanical shaft angle θ_m obtained from the rotor encoder. The direct component is related to the machine flux while the quadrant component is related to the machine torque. By controlling each component individually the desired torque and flux can be achieved.

For PMSG, the flux is supplied by the permanent magnets therefore, there is no need to induce flux by the machine current and accordingly $I_{dm,ref}$ is set to zero. This controlling scheme is called zero direct current (ZDC) which achieves maximum torque per ampere (MTPA) in the generator [23]. The $I_{dm,ref}$ is compared with I_{dm} and the error signal is fed into the PI controller for the direct voltage component (V_{dm}).

On the other hand, the quadrant current component reference (I_{qref}) is calculated for the reference torque ($T_{m,ref}$) which is calculated by the maximum power point tracking (MPPT) to achieve the highest possible output power. The reference torque is converted into $I_{qm,ref}$ and compared with I_{qm}. The error quadrant current is fed into the PI controller for the quadrant voltage component (V_{qm}).

The direct and quadrant voltage components include coupling components which are required to be removed. This is achieved by multiplying the PMSG current components with the machine impedance components and adding these results to both voltage components as shown in figure 4.8. The reference voltage components, direct ($V_{dm,ref}$) and quadrant ($V_{qm,ref}$) are obtained and fed into the inverse Park transformer to generate the three-phase reference voltage which feeds into the SVM for the converter IGBTs pulses.

The parameters of PI controllers are calculated according to Absolute Value Optimum and Symmetric Optimum criteria [112]. This method involves calculating the time delay in the control loop to determine PI proportional and integral parameters, k_p and k_i respectively as shown in equations (4.7) to (4.10) where t_{dq} is the inner control loop time delay, R_m and L_m

are the machine winding resistance and inductance, t_s is the simulation sampling time, and t_Σ is the total delay in the control loop.

$$t_{dq} = \frac{Lm}{Rm} \tag{4.7}$$

$$t_\Sigma = 2t_s + t_{qd} \tag{4.8}$$

$$k_p = \frac{L_m}{2t_\Sigma} \tag{4.9}$$

$$k_i = \frac{k_p}{t_{dq}} \tag{4.10}$$

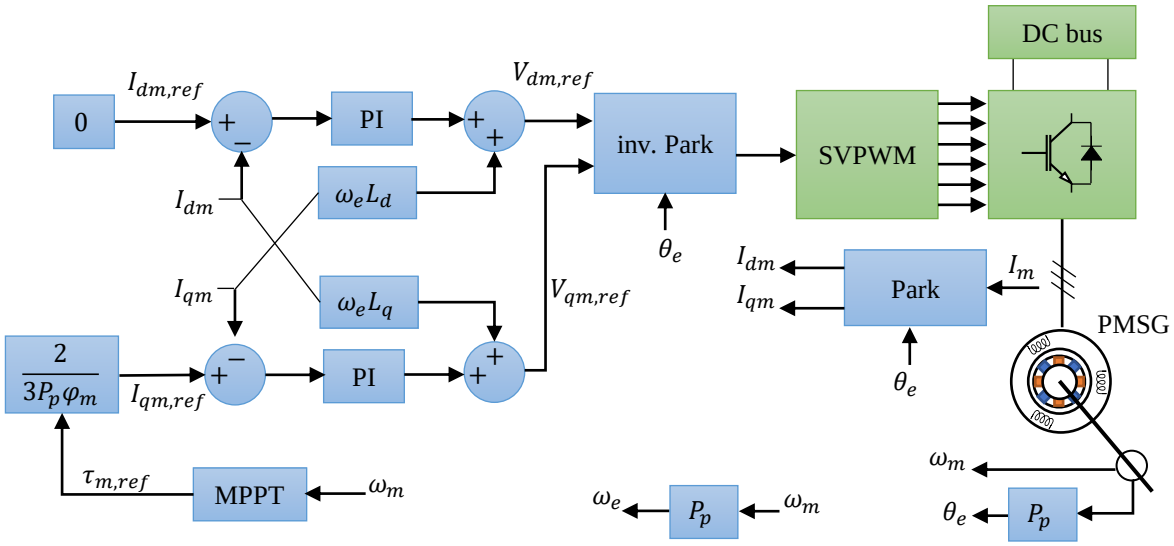

Figure 4.8: MSC control block diagram

4.7.2 Control of GSC

In the modelled wind turbine, the GSC regulates the DC bus voltage and controls the reactive power exported to the grid [23]. The control strategy used is voltage-oriented control (VOC) which is developed based on the FOC. The VOC is a vector decoupling control where in the grid-connected inverter circuits, the reference direct current controls the DC voltage and the reference quadrant current controls the reactive power.

The measured DC bus voltage is subtracted from the DC reference voltage ($V_{DC,ref}$) and fed into the PI controller to obtain the direct current reference ($I_{dg,ref}$) which is subtracted by grid direct current (I_{dg}) and send to the direct voltage PI controller. On the other hand, the reference grid quadrant current component ($I_{qg,ref}$) is calculated based on the reactive power reference (Q_{ref}). The grid quadrant current (i_{qg}) is compared with the $I_{qg,ref}$ and fed into the quadrant voltage component PI controller. The reference of direct and quadrant grid voltage componentes ($V_{dg,ref}$) and ($V_{qg,ref}$) are obtained after the cancellation of coupling terms and adding the grid voltage components. The Inverse Park transformation converts the direct and quadrant voltage components into the three-phase voltage which is modulated by the SVM. The

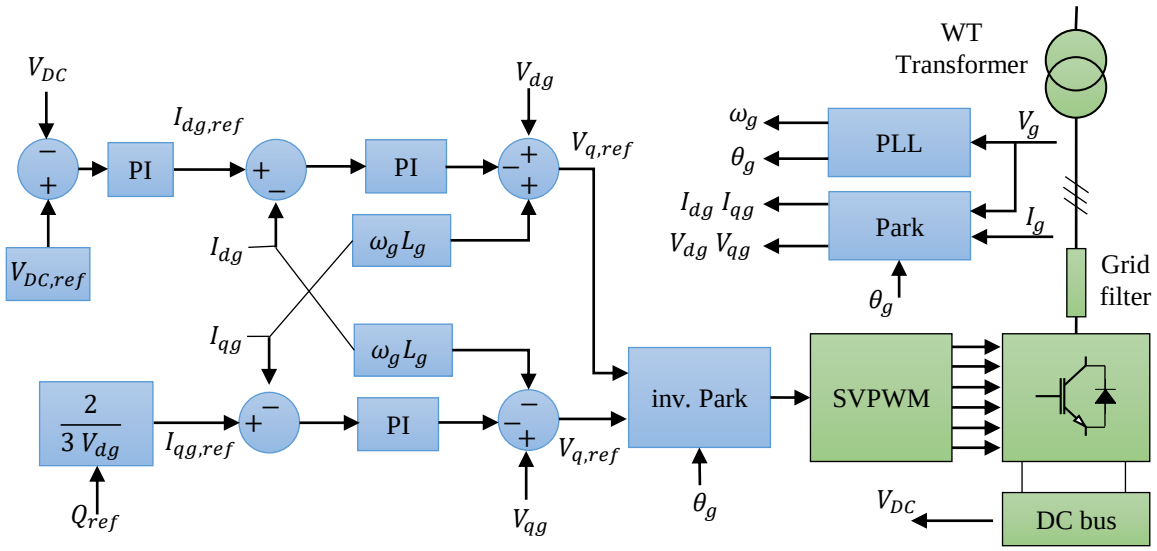

Figure 4.9: GSC control block diagram

SVM pulses are sent to the GSC IGBTs to perform the switching.

Figure 4.9 shows the GSC control system block diagram where I_g is the grid current, ω_g and is the grid voltage angular frequency, θ_g is the grid load angle, and L_g is the grid filter inductance. The design of the modelled GSC control system is based on [113].

4.7.3 Converter switching module

The SVM is used as a switching method for both MSC and GSC. The SVM is usually used with three-phase converters for the benefit of lower DC voltage requirement than the sinewave PWM [114]. Although the SVM output voltage waveform looks distorted sinewave due to the added third harmonic, the generated current is sinusoidal and that is because the added harmonics are cancelling each other among the three phases' voltages [115]. The modelled wind turbine uses the Simulink PWM generator block which provides the SVM pulse method option. The outputs of the switching model are connected to the IGBTs of the modelled converters, MSC and GSC.

4.8 DC Bus

In the back-to-back power converter configuration, the DC bus links both converters, MSC and GSC, and provides an energy path between them. The DC bus voltage has to be higher than the peak-to-peak value of the AC sinewave voltage in the voltage source converter when the modulation type is sinewave PWM (SPWM). The minimum DC bus voltage has to be higher than the peak-to-peak value of the inverter output. However, if the converter modulation type is SVM, then the minimum DC bus voltage will be reduced by 15% [114]. Therefore, SVM is the preferred modulation type due to the efficient utilisation of the DC voltage. The DC bus voltage is required to stay regulated during load variations for the proper operation of both converters, MSC and GSC. A capacitor bank is connected to the DC bus to minimize the voltage ripple

generated by the switching operation of both converters. The DC bus capacitor value is selected at 53.49mF based on WTPC parameters shown in [23] of a similar wind turbine model.

4.9 Grid

The grid is modelled as a three-phase voltage source. The line voltage (V_g) is set to 690 V which is identical to the rated voltage of the wind turbine PMSG. The grid frequency (f_g) is set to 50 Hz as in most world countries. The grid filter is modelled as an inductor having an impedance equal to 0.2 pu [23]. Equations 4.11 and 4.12 are used to calculate grid filter inductance (L_g).

$$Z_{base} = \frac{V_g^2}{P_{m,rated}} \tag{4.11}$$

$$L_g = \frac{0.2}{2\pi f_g} Z_{base} \tag{4.12}$$

4.10 WTPC power loss

Converter semiconductors' lifetime is highly impacted by their junction temperature which relies on their power loss and the heatsink thermal characteristics. Modelling the semiconductors' power loss is essential in WTPC reliability analysis as it is the source of the heat in the semiconductor junction. Two types of power loss are produced by the semiconductor when operating as a switch like in WTPC, the switching power loss (P_{sw}) and conduction power loss (P_{cn}). The switching power loss occurs when the semiconductor changes its status between on and off, while the conduction power loss develops when the semiconductor status is on. Equations (3.1) and (3.2) describe the power loss of the diode and IGBT respectively including switching and conduction power loss terms.

The semiconductor power loss is influenced by its internal parameters like internal resistance, saturated voltage, and switching energy. The semiconductor's internal parameters are affected by temperature, voltage, and current according to the manufacturer datasheet [17]. Therefore, their values are required to be updated with the related affecting parameters during the simulation. Figure 4.10 shows the modelling of the diode power losses where $P_{cn,d}$ and $P_{sw,d}$ are the conduction and switching power losses, $T_{j,d}$ is the diode junction temperature, I_d is the diode current, E_{rr} is the reverse recovery energy, V_{d0} is the diode threshold voltage, and R_d is the diode on status internal resistance. Similarly, the IGBT power loss is modelled.

4.11 Semiconductors thermal model

It is difficult to measure the semiconductor's junction temperature and it is complex to calculate it during the variable load of the WTPC. Therefore, thermal modelling is used to determine it by a thermal equivalent circuit. The semiconductor power loss is modelled as a current source and the thermal impedances of the heatsink and semiconductors are modelled as resistors and capacitors. The junction temperature is obtained as the measured voltage of the current source. Thermal impedances, (Z_{th}), include thermal resistances, (R_{th}), and thermal storage, (C_{th}),

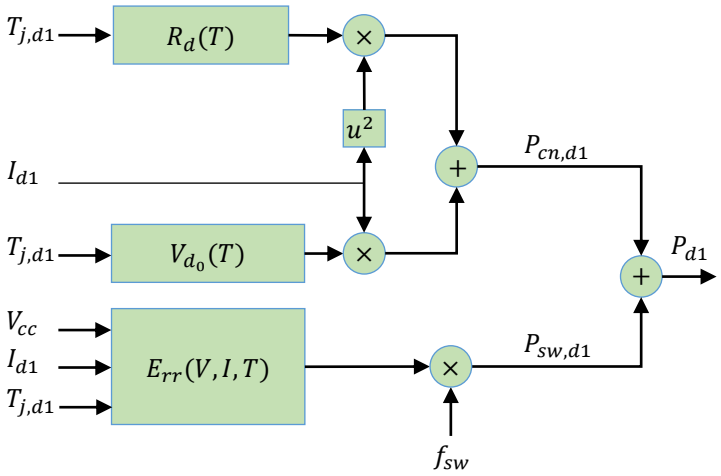

Figure 4.10: Power losses modelling of the diode in WTPC circuit

are obtained from the semiconductor datasheet and the heatsink parameters. The thermal equivalent circuit is modelled using the Foster model as it is widely used in similar analyses [49]. MATLAB Simscape Thermal Model toolbox [116] components are used in modelling the converter equivalent thermal circuit.

Assuming normal wind turbine operation conditions, the converter phases are balanced and the converter upper arm and lower arm in each half-bridge are operating symmetrically, then, only one arm of each converter is needed to be modelled. The thermal equivalent circuit of the 2L-VSC half-bridge upper arm with the attached heatsink is shown in figure 4.12 where $Z_{th,i}$ and $Z_{th,d}$ are the IGBT and the diode thermal impedances, $Z_{th,M}$ is the thermal impedance of the power electronic module, $Z_{th,Hs}$ is the thermal impedance of the heatsink, $T_{j,i}$ and $T_{j,d}$ are the IGBT and diode junction temperatures, and T_{ct} is the heatsink coolant temperature.

The wind turbine model extracts the converter's IGBT and diode junction temperature as time series values saved in MATLAB file (mat file). The junction temperature of the IGBT and diode oscillates oppositely at the PMSG frequency. As the IGBT junction temperature increases the diode junction temperature drops and that is due to the loading principle of the boost converter operation of the MSC.

In AC-DC-AC converter configuration, the MSC operates as an active rectifier while the GSC operates as an inverter. Therefore, the diode is loaded higher than the IGBT in MSC while the IGBT is loaded higher than the diode in GSC. Figures 4.13 and 4.14 present the thermal cycling of IGBT and diode in MSC and GSC respectively at the rated wind turbine power, at 12 m/s wind speed. Although in this case, both MSC and GSC operate at the same voltage and current approximately (ignoring the power losses) the MSC's diode shows a higher temperature than GSC's IGBT. The reason for that is the diode has a smaller contact area at the substrate in the power module chip compared to the IGBT as shown in figure 2.4. Therefore, the diode has a higher thermal impedance than the IGBT making the diode junction temperature will be higher for a similar current.

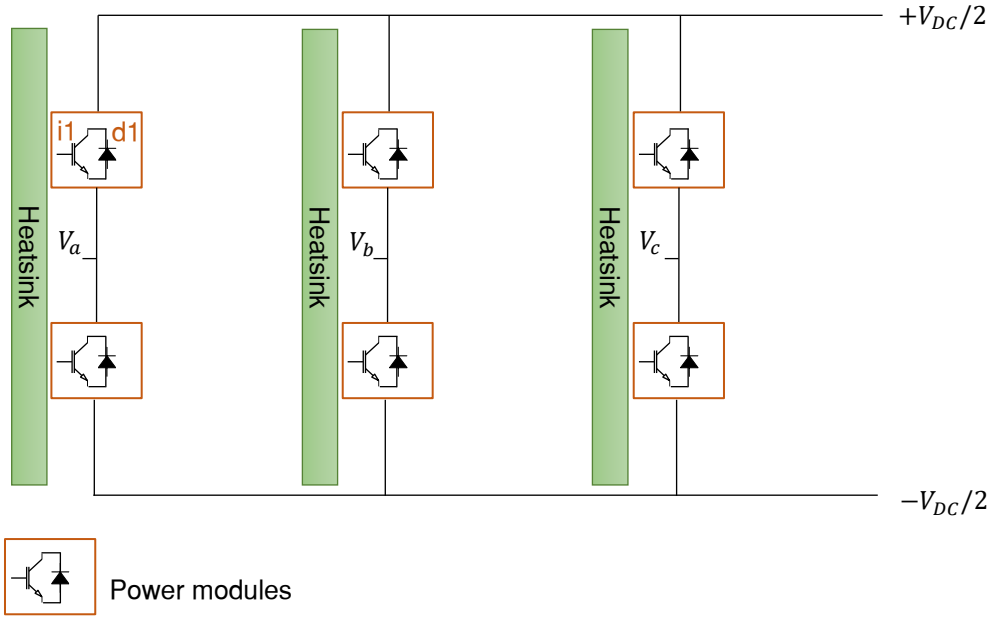

Figure 4.11: Schematic diagram of the modelled 2L-VSC with the heatsink configuration

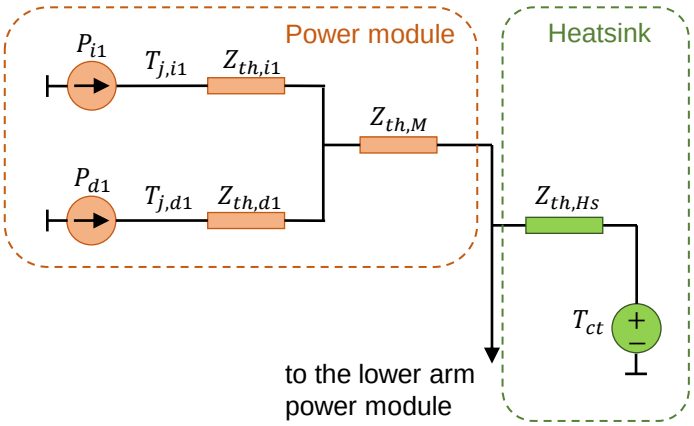

Figure 4.12: thermal equivalent circuit

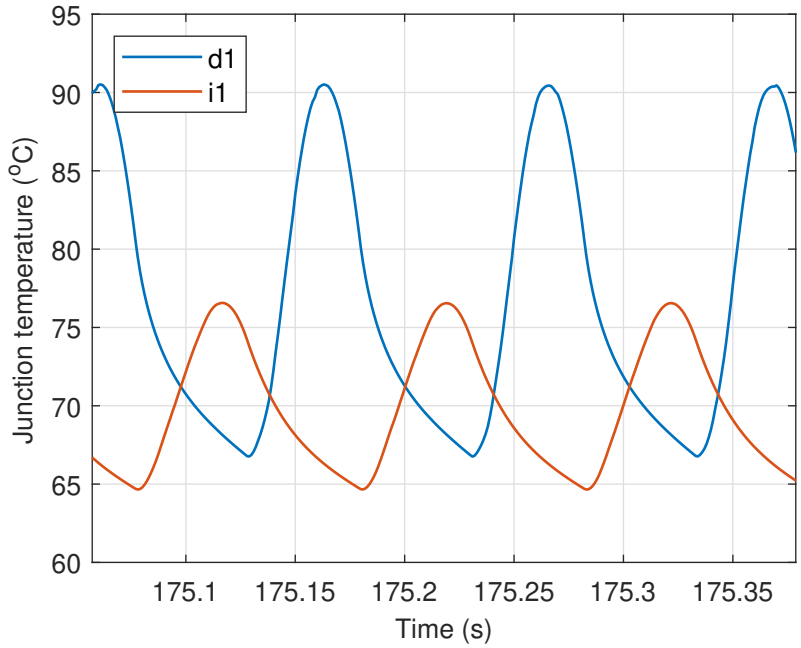

Figure 4.13: Simulated junction temperatures of IGBT and diode in MSC with rated wind speed (12 m/s) constant input

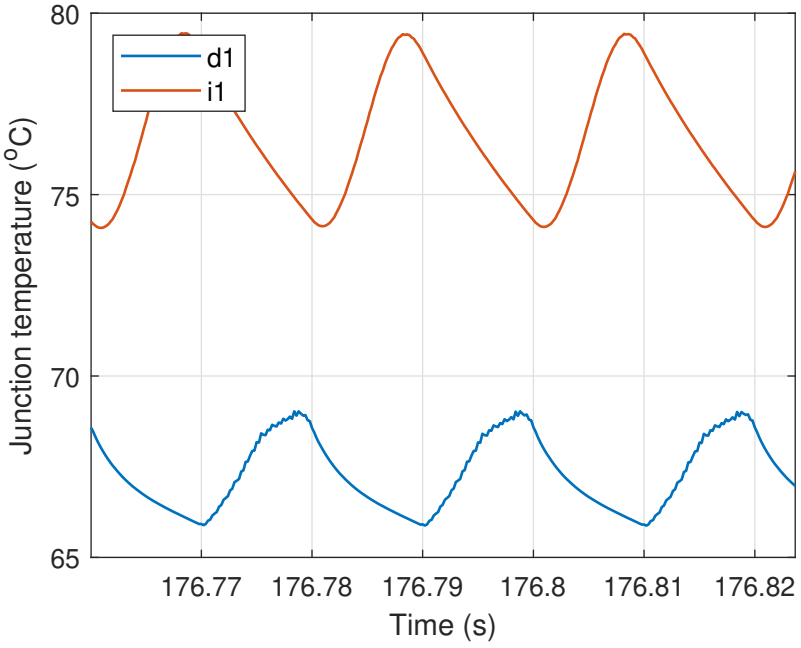

Figure 4.14: Simulated junction temperatures of IGBT and diode in GSC with rated wind speed (12 m/s) constant input

4.12 Model validation

The purpose of the wind turbine model is to simulate the junction temperature of the WTPC semiconductors related to the wind speed input. It is important to validate the model simulation to ensure the proper simulation of the wind turbine reliability model and that the accuracy of the results is valid for WTPC lifetime estimation. The validation of the entire model is achieved by comparing the model's simulated parameters with the expected values related to the input wind speed. The model validation is an important step before using the model in reliability analyses to ensure accurate lifetime results. The procedure of validation is based on comparing the research model simulation results with expected results obtained either by calculation or by simulating a trusted model like the one provided by the power electronic manufacturer as discussed in section 3.4.5.

The validation process is done for the mechanical, electrical, and thermal submodels. The simulated junction temperature accuracy is impacted by these submodels which will result in inaccurate WTPC lifetime estimation. Due to the complexity of calculating the operating parameters of the wind turbine during the variable load related to the variable wind speed input, a series of constant wind speeds are used for the validation process. A stair function containing steps of constant wind speeds is used as input to the model and the operating parameters are obtained and compared with the expected values related to each wind speed. The expected values of the model operation are calculated for constant wind speeds covering the range from the cut-in wind speed (4 m/s) to 14 m/s which is higher than the rated wind speed (12 m/s) of the modelled wind turbine.

The stair function of wind speed is shown in figure 4.15. The first step of 4 m/s is given 200 s considering the wind turbine starting-up time and thermal balance then each step represents an increase of 2 m/s given 100 s for wind turbine response and thermal balance until the stair function ends at 14 m/s. The comparison between simulated values and calculated values is evaluated by calculating the relative difference (Δ_{Rel}) for each tested wind speed by equation (4.13).

$$\Delta_{Rel} = \frac{\text{value by calculation} - \text{value by simulation}}{\text{value by calculation}} \times 100\% \tag{4.13}$$

4.12.1 Validation of model mechanical parameters

The validation of the simulated mechanical parameters is achieved by comparing simulated values and calculated values. The wind turbine model is input with a constant wind speed step function as shown in figure 4.15. The simulation results of wind turbine developed torque (τ_t) related to input wind speed and wind turbine generator rotating speed (ω_t) are shown in figure 4.16.

The first 200 seconds represent the starting up of the modelled wind turbine where its torque and speed are building up to their steady values corresponding to 4 m/s wind speed. The wind speed values from 6 m/s to 12 m/s show an increase in wind turbine torque and speed while the step wind speed to 14 m/s does not affect both wind turbine torque and speed as the pitch control keeps the rotating speed at the rated value corresponding to (12 m/s) wind speed. Since

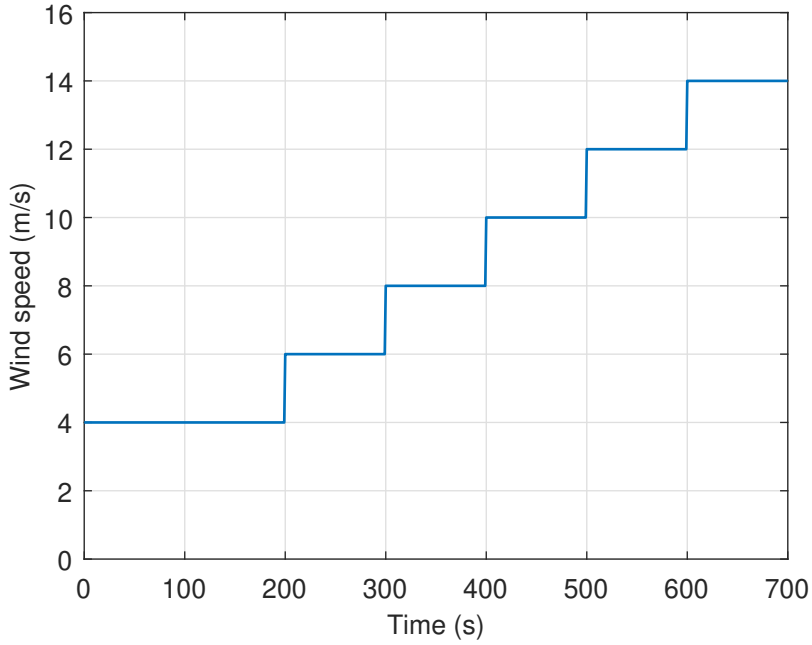

Figure 4.15: Constant wind speed stair function

the wind turbine is controlled by MPPT, which keeps optimum TSR, the expected rotating speed is proportional to wind speed. Also, since wind turbine power is proportional to wind speed cubic, the torque will be proportional to the wind speed square. These relationships are expressed by equations (4.14) and (4.15) to calculate the expected ω_t and τ_t respectively.

The comparisons between simulation and calculation results are shown in table 4.4 which show that there is a very small difference between the simulated and calculated values of both torque and rotating speed.

$$\omega_t = \omega_{t,rated} \frac{U}{U_{rated}} \tag{4.14}$$

$$\tau_t = \tau_{t,rated} (\frac{U}{U_{rated}})^2 \tag{4.15}$$

Table 4.4: Wind turbine mechanical parameters with constant wind speeds input

U (m/s)	ω_t (rad/s)			τ_t (kNm)		
	Calculated	Simulated	Δ_{Rel} (%)	Calculated	Simulated	Δ_{Rel} (%)
4	0.785	0.785	9.0×10^{-3}	94.3	94.3	4.9×10^{-2}
6	1.781	1.781	-3.6×10^{-4}	212	212	-2.2×10^{-2}
8	1.571	1.571	-6.5×10^{-4}	377	377	-2.4×10^{-3}
10	1.964	1.964	-6.8×10^{-4}	589	589	-6.9×10^{-3}
12	2.356	2.356	1.0×10^{-4}	849	849	5.9×10^{-3}
14	2.356	2.356	-2.7×10^{-2}	849	849	-4.8×10^{-2}

(a) Wind turbine torque vs constant wind speeds

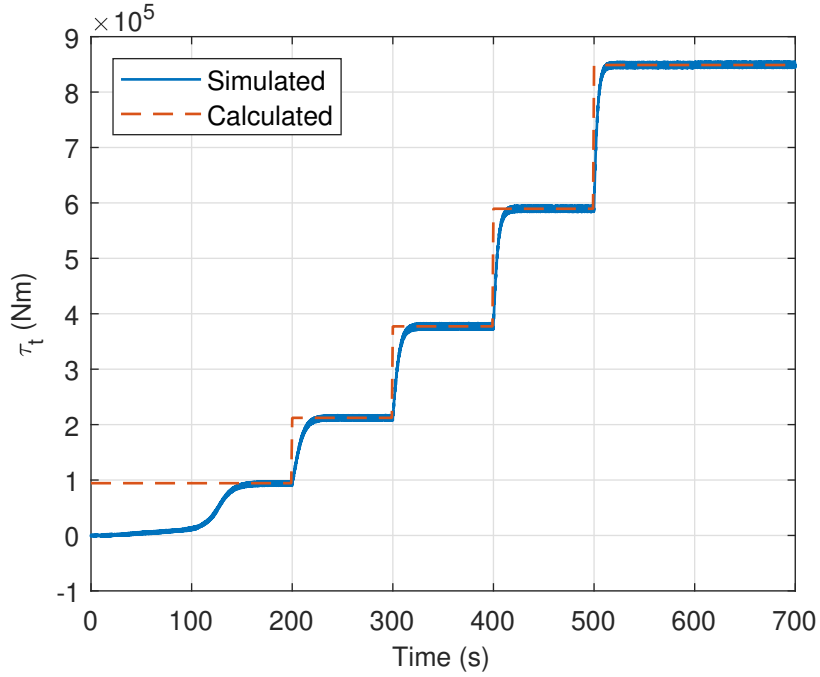

(b) Wind turbine speed vs constant wind speeds

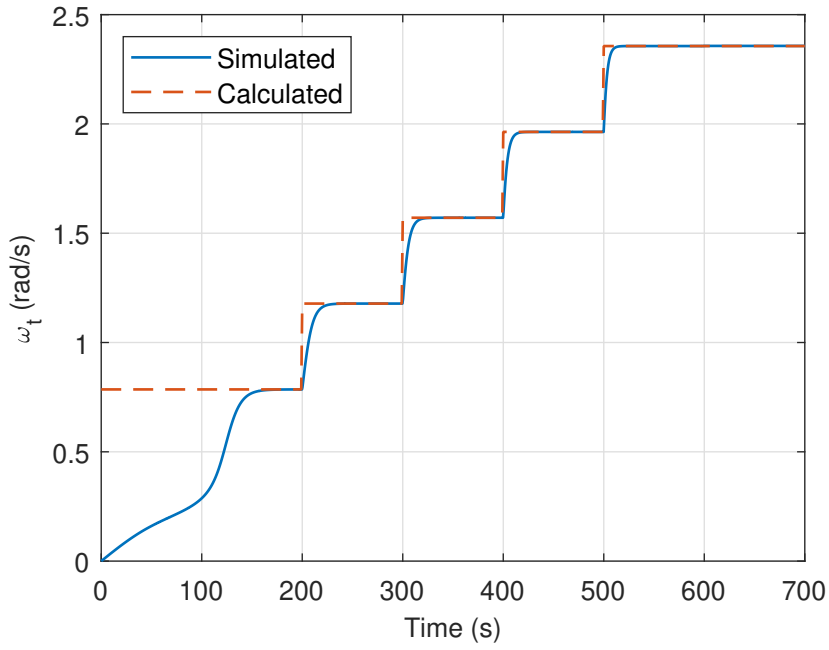

Figure 4.16: Turbine torque (a) and speed (b) related to input wind speed

4.12.2 Validation of model electrical parameters

The electrical parameters of the wind turbine model are validated by comparing their values from the simulation with expected values by calculation related to the input wind speeds. Constant wind speeds from 4 m/s to 14 m/s in 2 m/s steps as shown in figure 4.15 were used to perform the comparison. The validated electrical parameters are PMSG current and power, DC bus

voltage and current, and grid active and reactive output power.

Validation of wind turbine generator parameters

The wind turbine generator converts the mechanical power of the wind turbine rotor to electrical power fed into the WTPC as a three-phase current. The validation of the simulated generator's electrical parameters is crucial as they influence the WTPC loading and therefore its lifetime. The expected values of the generator current (I_m) and power (P_m) are calculated and compared with the values obtained from the model simulation. Figure 4.17 shows I_m and P_m related to input constant wind speeds. The expected P_m and I_m are approximately calculated by equations (4.16) and (4.17) respectively where V_m is the generator voltage. The approximation is due to neglecting the generator power loss and assuming a unity power factor respectively. The comparison between calculated and simulated parameters is shown in table 4.5.

$$P_m \approx P_t \tag{4.16}$$

$$I_m \approx \frac{P_m}{\sqrt{3}V_m} \tag{4.17}$$

Table 4.5: PMSG parameters validation with constant wind speeds input

U (m/s)	I_m (A)			P_m (kW)		
	Calculated	Simulated	Δ_{Rel} (%)	Calculated	Simulated	Δ_{Rel} (%)
4	185.9	185.8	6.7×10^{-2}	74.1	72.1	2.6
6	418.4	417.9	1.0×10^{-1}	250	247.9	0.9
8	743.8	743.7	4.8×10^{-3}	592.6	590.4	0.4
10	1162.1	1162.7	-4.8×10^{-2}	1,157	1,146	1.0
12	1673.5	1673.4	2.7×10^{-3}	2,000	1,965	1.8
14	1673.5	1674.1	-3.7×10^{-2}	2,000	1,966	1.7

Validation of DC bus parameters

The DC bus transfers the wind turbine generator power from the MSC to the GSC. The DC bus voltage is controlled by the GSC which should be fixed during the wind turbine operation as discussed in 4.7.2. Therefore, the changes in wind speed should not affect the DC bus voltage while the DC bus current is related to the generator power which is affected by the input wind speed. Since the wind turbine power is proportional to U^3 in the variable wind speed range, and the DC bus voltage is constant, the DC bus current will be proportional to U^3. Figure 4.18 shows the DC bus current and voltage for steps of constant wind speeds from 4m/s to 14 m/s in 2 m/s steps as shown in figure 4.15. The DC bus voltage shows a fixed value of 1,150 V. The expected value of the I_{DC} is approximately calculated by equation (4.18) neglecting MSC power loss.

$$I_{DC} \approx \frac{P_m}{V_{DC}} \tag{4.18}$$

(a) Generator current vs constant wind speeds

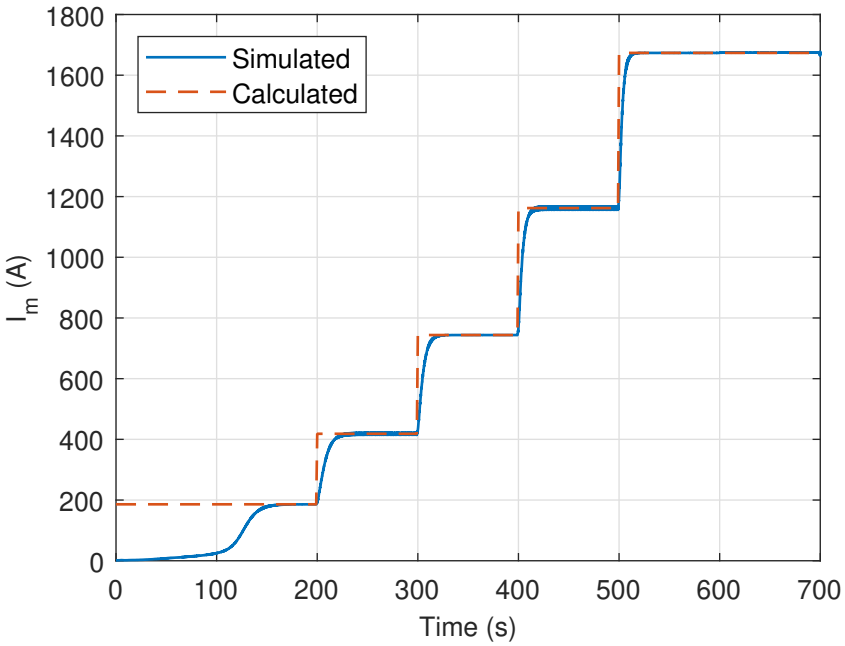

(b) Generator power vs constant wind speeds

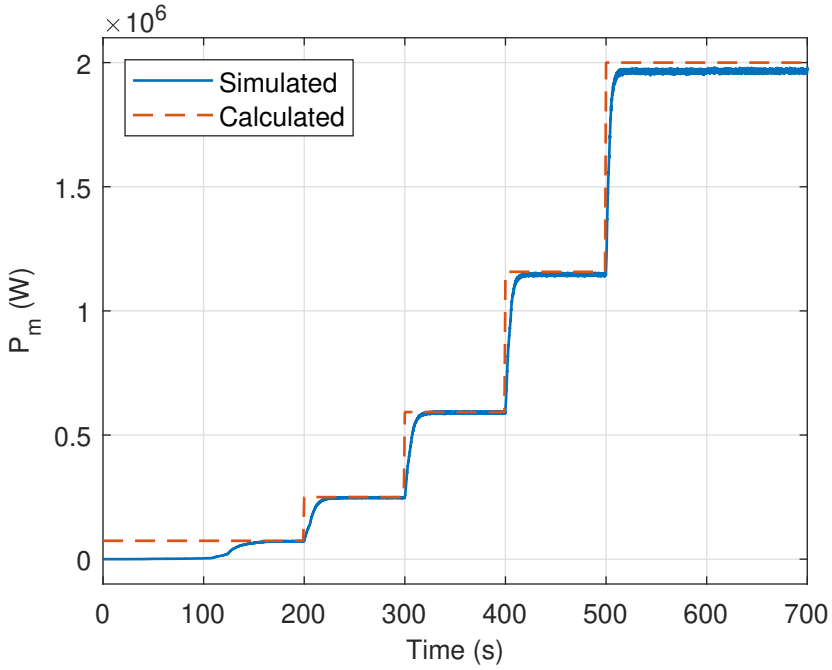

Figure 4.17: Wind turbine generator current (a) and power (b) in constant wind speed test

(a) DC bus current vs constant wind speeds

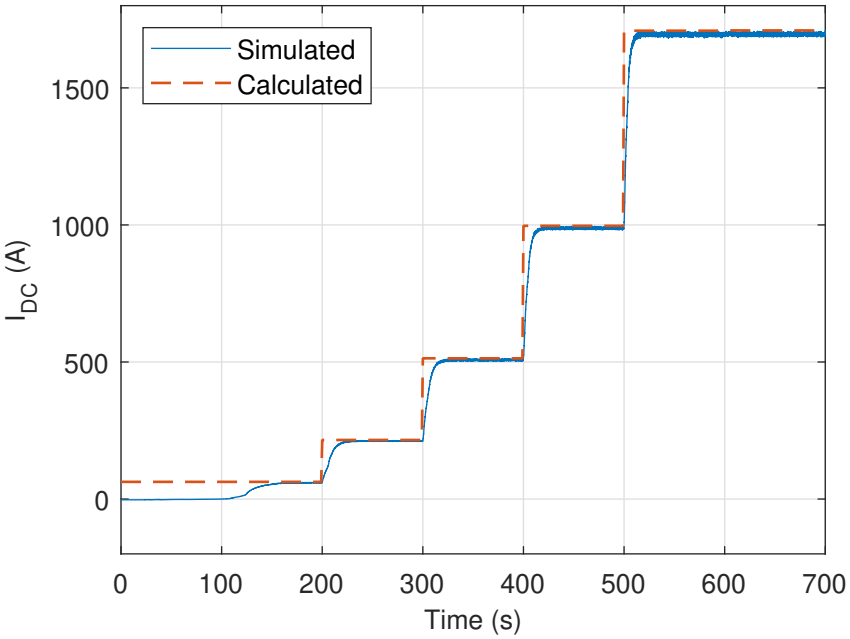

(b) DC bus voltage vs constant wind speeds

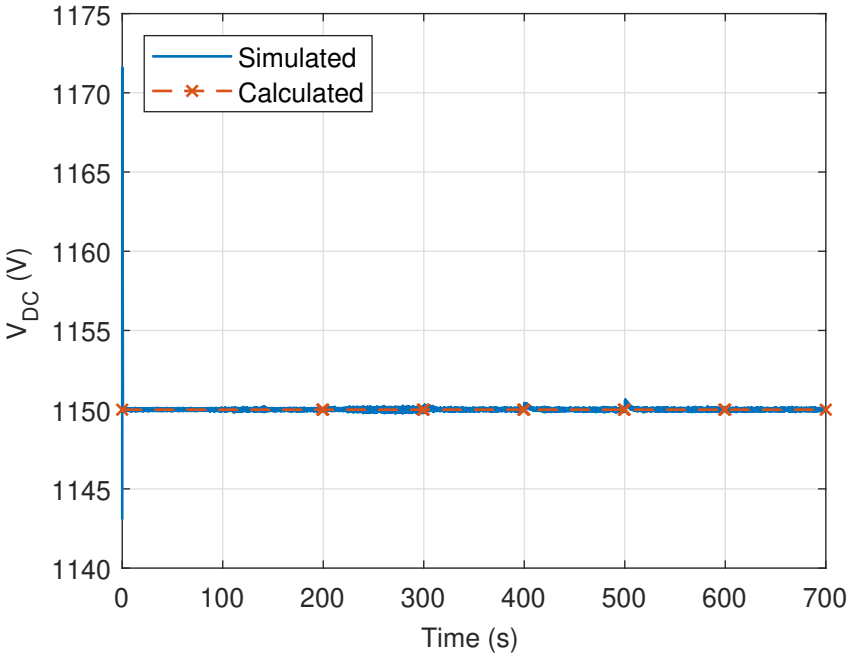

Figure 4.18: DC bus current (a) and voltage (b) in constant wind speed test

Validation of wind turbine output parameters

In the wind turbine reliability model, the output power is supplied to the modelled grid through the GSC. The validation of the supplied power is important as it is related to the GSC loading and can be considered as an indication that the overall model is operating properly where the output power should show a valid relationship to the input wind speed like in actual wind

Table 4.6: DC bus current validation

U (m/s)	$I_{DC,cal}$ (A)	$I_{DC,sim}$ (A)	Δ_{Rel} (%)
4	$6.27\times10^{+1}$	$5.98\times10^{+1}$	4.7
6	$2.16\times10^{+2}$	$2.12\times10^{+2}$	1.8
8	$5.13\times10^{+2}$	$5.08\times10^{+2}$	1.2
10	$9.97\times10^{+2}$	$9.88\times10^{+2}$	0.9
12	$1.71\times10^{+3}$	$1.70\times10^{+3}$	0.8
14	$1.71\times10^{+3}$	$1.70\times10^{+3}$	0.8

turbines. The input wind speed is steps of constant wind speeds from 4 m/s to 14 m/s as shown in figure 4.15 while the simulated output active and reactive power are related to the input wind speeds are shown in figure 4.19. The GSC control set the reactive power reference value to zero for a unity power factor, however, a small and ineffective negative reactive power appeared at high wind speed due to the need for controller fine-tuning.

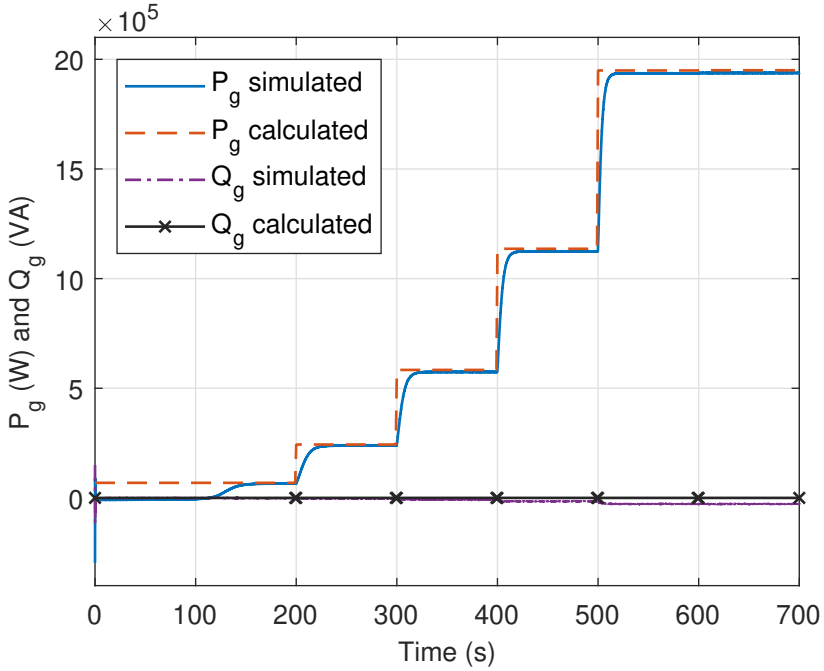

Figure 4.19: Grid active and reactive power during constant wind speed test

4.12.3 Validation of semiconductor junction temperatures

The validity of the simulated junction temperature is important for the reliability analysis of the WTPC since the semiconductor's lifetime is affected exponentially by its junction temperature. Therefore, the simulated junction temperatures are validated before using them in the reliability analysis. The thermal validation is achieved by comparing the model's simulated semiconductor junction temperature with the results of the semiconductor manufacturer simulation tool for the same operating parameters. The power module manufacturer, SEMIKRON, provides the simulation tool, SemiSel [117] for determining junction temperature related to converter design

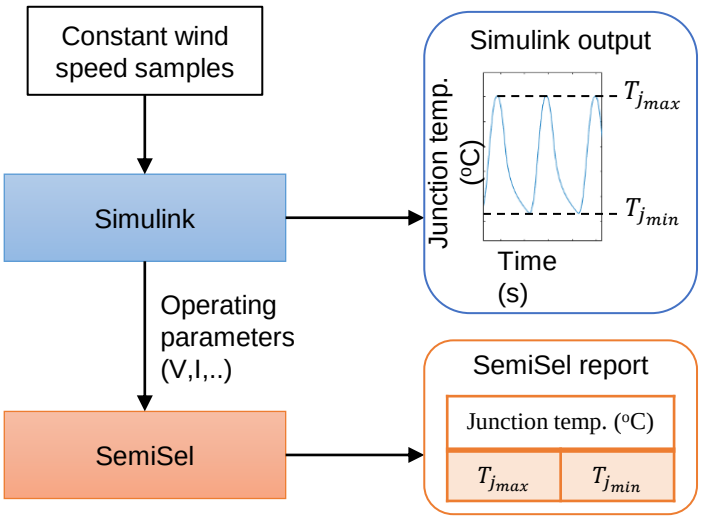

Figure 4.20: Validation process

and loading parameters.

SemiSel tool

SemiSel is a software tool provided by the power electronics manufacturer SEMIKRON to test the operating temperature limits of their power modules. SemiSel offers a variety of standard converter circuits to start with and then the operating parameters are required to be entered on the tool interface. For the 2L-VSC circuit, these parameters are DC voltage, phase current, phase frequency, switching frequency, power factor, and modulation type. Next, the tool lists selectable power modules that fit the circuit and the entered operating parameters. The following step is to enter the heatsink details which include the cooling method, liquid or air, the heatsink configuration, and the thermal impedances. After entering all the required details, SemiSel presents the output report which shows the circuit semiconductors' maximum and minimum junction temperatures, power module case and heatsink temperatures, and semiconductors' power losses. SemiSel report results are related to fixed operating parameters and therefore to compare those results with the Simulink wind turbine model, the model needs to run constant wind speed simulation for fixed output results. The validation process is shown in figure 4.20.

Results comparison procedure

The comparisons between Simulink results and SemiSel results are accomplished for nine constant wind speeds representing the variable speed range of the modelled wind turbine from 4 m/s to 12 m/s in 1 m/s steps. The results are shown in table 4.7 and table 4.8 for the converter IGBT and diode respectively. The relative differences between SemiSel and Simulink results are calculated by equation (4.19) for maximum and minimum junction temperature for each tested wind speed. The root mean square error (RMSE) is used to evaluate the relative differences between the SemiSel and Simulink results for each semiconductor's maximum and minimum

Table 4.7: Junction temperature of i1

	$T_{j_{max},i1}$ (°C)			$T_{j_{min},i1}$(°C)		
U (m/s)	Simulink	SemiSel	Δ_{Rel} (%)	Simulink	SemiSel	Δ_{Rel} (%)
4	44.82	44.62	-4.5 $\times 10^{-1}$	42.37	42.22	-3.5 $\times 10^{-1}$
5	47.18	47.01	-3.6 $\times 10^{-1}$	43.67	43.56	-2.5 $\times 10^{-1}$
6	49.97	49.82	-3.1 $\times 10^{-1}$	45.32	45.21	-2.3 $\times 10^{-1}$
7	53.20	53.09	-2.0 $\times 10^{-1}$	47.35	47.31	-7.8 $\times 10^{-2}$
8	56.87	56.77	-1.7 $\times 10^{-1}$	49.80	49.79	-1.8 $\times 10^{-2}$
9	61.03	60.99	-6.0 $\times 10^{-2}$	52.71	52.73	3.8 $\times 10^{-2}$
10	65.68	65.73	7.0 $\times 10^{-2}$	56.12	56.24	2.1 $\times 10^{-2}$
11	70.87	70.81	-8.6 $\times 10^{-2}$	60.08	60.12	6.0 $\times 10^{-2}$
12	76.60	76.60	2.4 $\times 10^{-3}$	64.65	64.72	1.1 $\times 10^{-1}$
	$RMSE_{T_{jmax,i1}}$ = 2.4 $\times 10^{-3}$ °C			$RMSE_{T_{jmin,i1}}$ = 1.8 $\times 10^{-3}$ °C		

Table 4.8: Junction temperature of d1

	$T_{j_{max},d1}$(°C)			$T_{j_{min},d1}$(°C)		
U (m/s)	Simulink	SemiSel	Δ_{Rel} (%)	Simulink	SemiSel	Δ_{Rel} (%)
4	45.89	45.49	-8.8 $\times 10^{-1}$	42.42	42.28	-3.3 $\times 10^{-1}$
5	48.62	48.32	-6.1 $\times 10^{-1}$	43.79	43.66	-2.9 $\times 10^{-1}$
6	51.93	51.67	-5.0 $\times 10^{-1}$	45.53	45.40	-2.8 $\times 10^{-1}$
7	55.92	55.79	-2.3 $\times 10^{-1}$	47.68	47.63	-1.1 $\times 10^{-1}$
8	60.69	60.69	-5.0 $\times 10^{-3}$	50.30	50.27	-5.7 $\times 10^{-2}$
9	66.35	66.43	1.2 $\times 10^{-1}$	53.44	53.44	4.4 $\times 10^{-3}$
10	73.07	73.31	3.3 $\times 10^{-1}$	57.16	57.27	1.9 $\times 10^{-1}$
11	81.06	81.21	1.8 $\times 10^{-1}$	61.56	61.59	5.1 $\times 10^{-2}$
12	90.57	90.66	9.7 $\times 10^{-2}$	66.74	66.81	1.1 $\times 10^{-1}$
	$RMSE_{T_{jmax,d1}}$ = 4.3 $\times 10^{-3}$ °C			$RMSE_{T_{jmin,d1}}$ = 1.9 $\times 10^{-3}$ °C		

junction temperatures as in equation (4.20). The evaluation of the results differences between Simulink and SemiSel Simulations are shown in tables 4.7 and 4.8 for the converter IGBT and diode.

$$\Delta_{Rel} = \frac{T_{jSS} - T_{jSL}}{T_{jSS}} \times 100\% \tag{4.19}$$

$$RMSE_{Tj} = \sqrt{\frac{\sum_{i=1}^{k} (\Delta_{Rel})^2}{k}} \tag{4.20}$$

4.13 Lifetime estimation

The WTPC reliability analysis is based on analysing the semiconductors' lifetime of the power converters, MSC and GSC as they highly influence the converter failure rate and are considered the main cause of failures in WTPC according to the field failure data [40].

4.13.1 Thermal cycles counting

The wind turbine model simulation provides temperature-time variation trends of the WTPC semiconductors junction temperature as shown in figures 4.13 and 4.14. These trends contain cyclic variations of temperature which are causing damage to the semiconductor. To estimate the semiconductor lifetime related to input VWSP, the accumulated damage in WTPC semiconductors during the run time needs to be calculated. This damage is the summation of the smaller damages that occurred due to every thermal cycle. It is essential to count and identify each thermal cycle from the simulation output related to the VWSP input. The Rainflow algorithm [118] is used in analysing the simulation output trends for thermal cycle counting and identifying the junction temperature values, T_m and ΔT. The Rainflow algorithm is one of the counting methods used in semiconductor fatigue and failure analyses [119]. Rainflow algorithm is provided by the MATLAB signal processing toolbox.

4.13.2 Lifetime estimation

The damage per each thermal cycle is obtained using the Coffin-Manson Arrhenius formula considering the semiconductor's junction temperatures, T_m and ΔT as in equation (3.6). This equation can be rewritten as a function of cycle's mean $T_m, cycle$ and cycle's range ΔT_{cycle} as in equation (4.21). Since N_f represents the thermal cycles to failure, then the damage developed by one thermal cycle ($D_{f,cycle}$) is the inverse of N_f calculated by equation (4.22). The accumulated semiconductor damage to failure that occurred due to a VWSP ($D_{f,VWSP}$) for the VWSP time $t_{VWSP}$is the summation of the damages caused by all thermal cycles that occurred in the VWSP time calculated by the equation (4.23) where n is the number of total thermal cycles that occurred during t_{VWSP}.

$$N_f(T_m, \Delta T) = a(\Delta T)^{-n} e^{(\frac{E_a}{T_m K_B})} \tag{4.21}$$

$$D_{f,cycle} = \frac{1}{N_f(T_{m,cycle}, \Delta T_{cycle})} \tag{4.22}$$

$$D_{f,VWSP} = \sum_{i=1}^{n} D_{f,cycle} \tag{4.23}$$

By definition, the failure rate, λ, is the amount of damage per time which can be expressed by equation (4.24) for the VWSP. Accordingly, the semiconductor's estimated lifetime (MTTF) can be calculated for the IGBT ($MTTF_i$) and diode ($MTTF_d$) as in equations (4.25) and (4.26) respectively.

$$\lambda = \frac{D_{f,WSP}}{t_{WSP}} \tag{4.24}$$

$$MTTF_i = \frac{t_{WSP}}{D_{f,WSP,i}} \tag{4.25}$$

$$MTTF_d = \frac{t_{WSP}}{D_{f,WSP,d}} \tag{4.26}$$

The WTPC consist of two power converters, MSC and GSC, each is considered as a system that contains stressed parts. The failure rate of each MSC and GSC is the summation of their parts' failure rates as expressed in equations (4.27) and (4.28) respectively where λ_{MSC} and λ_{GSC} are the MSC and GSC failure rates, λ_i and λ_d are the IGBT and diode failure rates, s_i and s_d are the number of IGBTs and the number of diodes in MSC and GSC. MSC and GSC estimated lifetimes ($MTTF_{MSC}$) and ($MTTF_{GSC}$) are calculated by equations (4.29) and (4.30) respectively. The WTPC lifetime is estimated considering MSC and GSC lifetimes as in equation (4.31).

$$\lambda_{MSC} = s_{i,MSC} \cdot \lambda_{i,MSC} + s_{d,MSC} \cdot \lambda_{d,MSC} \tag{4.27}$$

$$\lambda_{GSC} = s_{i,GSC} \cdot \lambda_i + s_{d,GSC} \cdot \lambda_{d,GSC} \tag{4.28}$$

$$MTTF_{MSC} = \frac{1}{\lambda_{MSC}} \tag{4.29}$$

$$MTTF_{GSC} = \frac{1}{\lambda_{GSC}} \tag{4.30}$$

$$MTTF_{WTPC} = \left(\frac{1}{MTTF_{MSC}} + \frac{1}{MTTF_{GSC}} \right)^{-1} \tag{4.31}$$

4.14 Chapter summary

This chapter presented the wind turbine model to be used for the WTPC reliability analyses. The model considers the widely used WTPC topology, 2L-VSC, to provide the reliability analyses required to address the first research question "How can the reliability of existing wind turbine two-level voltage source converters be better understood?" The model selected the PMSG direct-drive wind turbine to adapt the current wind turbine technology. The model considers mechanical, electrical and control, and thermal submodeles as they impact the WTPC loading and its lifetime. The lifetime estimation used the Coffin-Manson Arrhenius formula as recommended by the manufacturer of the modelled semiconductor power module.

The reliability analyses of WTPC in this thesis are based on three main considerations to ensure accepted reliability results. First, the WTPC reliability analysis is based on field-measured wind speeds with an accepted sampling rate to emulate the actual loading of WTPC. Second, the reliability analyses avoid approximations of the performance and thermal parameters related to wind turbine operation as approximations have a huge impact on WTPC reliability analyses accuracy as discussed in 3.4.6 Third, The model passed a validation procedure testing the accuracy of its performance and thermal parameters before utilising it in WTPC reliability analyses. The validation of the simulated junction temperature showed very low differences compared to the simulation results (RMSE in terms of 10^{-3} °C) using the semiconductor manufacturer simulation tool.

The proven accuracy of the WTPC reliability model of the widely used WTPC topology, 2L-VSC, allows extending this model to other WTPC technologies including the 3L-NPC topology and direct torque control (DTC) WTPCs since these are also available in the field of wind energy conversion. Comparing the WTPC lifetime of different models provides information about the

impact of converter design on WTPC reliability including the interactions with operational parameters like average wind speed and turbulence intensity. The following chapter presents a wind turbine model with DTC and another wind turbine model with medium voltage 3L-NPC WTPC.

Chapter 5

Extending WTPC reliability models

5.1 Introduction

In the previous chapter, the reliability model of a wind turbine is implemented with the widely deployed converter topology used in WTPC, 2L-VSC. Recently, the industry has adopted different control systems for wind turbines. FOC and DTC have been used with IG, DFIG and PMSG wind turbines. While assessing the impact of converter design on WTPC reliability, it is worth evaluating the impact of the control system on the WTPC lifetime. The wind turbine model of the previous chapter is modified to use DTC rather than FOC to analyse the impact of WTPC's control strategy on its reliability.

On the other hand, the wind turbine industry has extended the WTPC design to adapt to the increasing size and power of wind turbines mainly for offshore wind farms. With power ratings of 7 MW and higher, wind turbine manufacturers introduced MV wind turbines where the rated generator voltage is above 1kV to avoid the very high current of LV generators and to reduce the size of the cables and transformers [32]. Accordingly, higher voltage WTPCs were needed for the MV wind turbines. The WTPC design and the utilised power electronics have thus been affected. The wind turbine industry selected the 3L-NPC topology converter which provides higher voltage operation capability over the widely popular 2L-VSC converter in LV wind turbines.

Both wind turbine models, with DTC and with 3L-NPC WTPC, are presented in this chapter including their validation procedure for use in WTPC reliability and lifetime analysis.

5.2 DTC model

5.2.1 Introduction to direct torque control

DTC was first presented in 1986 by Takahashi and Noguchi [120] for induction machine speed control. The control system drives the machine by energising the right coil at the right time to achieve the maximum output torque and power. The selection of the right coil to energize is based on estimating the instantaneous torque and rotor magnetic field.

The classical version of this control strategy provides good performance and simplicity as shown in figure 5.1 [121] where τ_e and ϕ_s are the motor estimated torque and flux. The classical

DTC does not need high computational power as needed with FOC where triangular functions need to be calculated at the sampling frequency for the stationary frame transformation [122]. However, the classical DTC has the drawback of changing the output frequency rapidly, producing high torque and flux ripple and unbalanced switching power loss in the converter semiconductors [123].

An updated version of this control strategy based on fixed switching frequency was introduced with space vector modulation (SVM) called DTC-SVM scheme with closed-loop flux control [124]. DTC-SVM adds more complexity to the classic DTC as shown in the block diagram in figure 5.2. The DTC provides good performance, simplicity, and robustness in controlling motors and generators [121]. Both DTC and FOC are used in wind energy and they proved their performances in the field. However, each has advantages and drawbacks in performance and requirements. A brief comparison between FOC and DTC is shown in table 5.1.

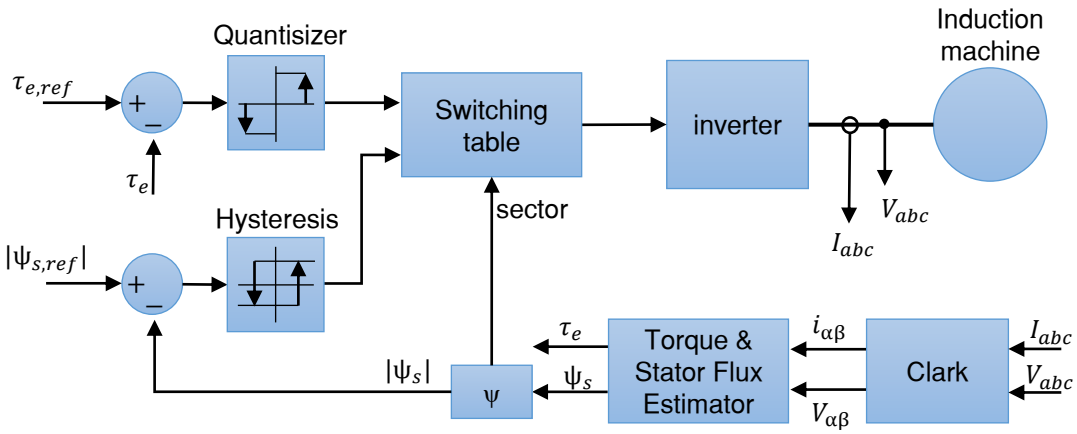

Figure 5.1: Classical DTC block diagram

Table 5.1: Comparison between FOC and DTC [125]

	FOC	DTC
Reference frame transformation	Required	Not required
Stator current control	No	Yes
Parameters required	Windings' inductance and resistance	Windings' resistance
PWM scheme	SVM, hysteresis band, or carrier based	Hysteries band
Sensitive to machine parameters variations	Sensitive	Not sensitive
Control scheme	Complex	Simple

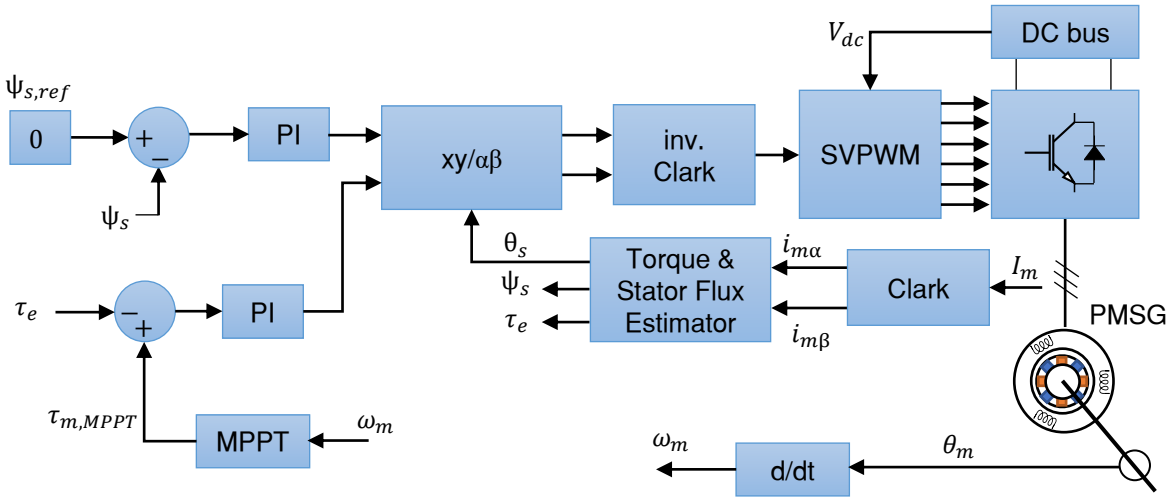

Figure 5.2: DTC-SVM control strategy block diagram

5.2.2 Wind turbine model with direct torque control

To analyse the WTPC reliability impact related to the WTPC control system, the wind turbine model of chapter 4 is slightly changed by adding DTC in a switchable WTPC control system so the model can operate with FOC or DTC. The new model is named 'DTC model' to distinguish it from the original model of chapter 4. DTC model kept the mechanical and thermal submodels unchanged but modified the electrical submodel by replacing the GSC with a DC source since the WTPC lifetime is influenced mainly by the MSC lifetime [75, 126]. Figure 5.3 shows the DTC model overview including the switchable control, FOC and DTC. The model simulates the junction temperature of the MSC semiconductors twice, one time with FOC and the other with DTC. The same wind speed input is used with both control strategies for comparison of the results. Following this procedure, the reliability results of both control strategies will not be affected by using different models.

5.3 DTC model validation

A crucial step before utilising the wind turbine model in WTPC reliability analyses is to pass the model validation. The DTC model is validated by a similar procedure used with the 2L-VSC model which considers checking the proper operation of the model subsystems by assessing the accuracy of the simulated parameters. Constant wind speeds are used for the validation procedure represented by a stair function (from 4 m/s to 14 m/s) wind speed input with time for the model to settle to a steady state before the next step change. The model validation procedure includes assessing mechanical, electrical, and thermal simulated parameters since these affect the WTPC reliability analyses.

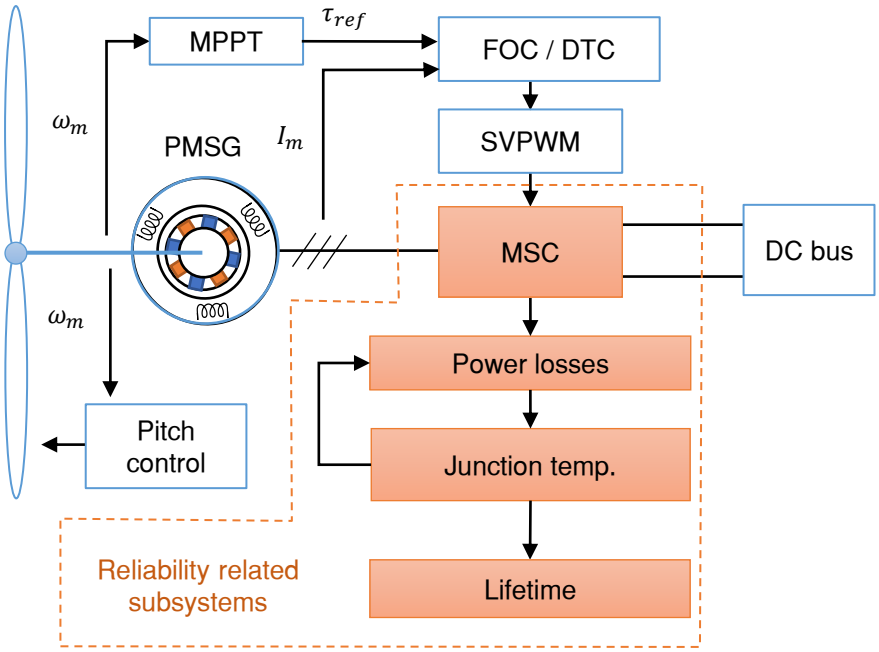

Figure 5.3: DTC model block diagram

5.3.1 Validation of the mechanical parameters in the DTC model

The validation of the mechanical simulated parameters is achieved by comparing them with the expected calculated values. The wind turbine model is input with the constant wind speed stair function shown in Chapter 4 in figure 4.15. The simulation results of the wind turbine developed torque (τ_t) and turbine rotating speed (ω_t) related to the input wind speed (U) are shown in figure 5.4.

The first 200 seconds of the simulation time represent the initialising of the modelled wind turbine where its torque and speed are building up to their steady values corresponding to the 4 m/s wind speed input. Later, the wind speed input increases to 14 m/s in steps of 2 m/s every 100 s. Until 12 m/s wind speed input, the simulation shows an increase in wind turbine torque and speed according to the input wind speed changes with response delay due to wind turbine inertia. The step wind speed to 14 m/s does not affect wind turbine torque and speed as the pitch control keeps the rotating speed at the rated value (2.36 rad/s) related to 12 m/s wind speed. The validation of mechanical parameters is achieved by comparing the parameters' simulated values with the expected calculated values. Table 5.2 lists these values for the tested wind speeds. The relative difference values (Δ_{Rel}) are calculated by equation (4.13)

5.3.2 Validation of the electrical parameters in the DTC model

Similar to the mechanical parameters validation procedure, the electrical simulated parameters are validated using the same input of constant wind speeds (4 m/s to 14 m/s). The simulated electrical parameters are compared with the expected values obtained by calculations related to the input wind speeds in the following paragraphs.

(a) Torque and wind speed

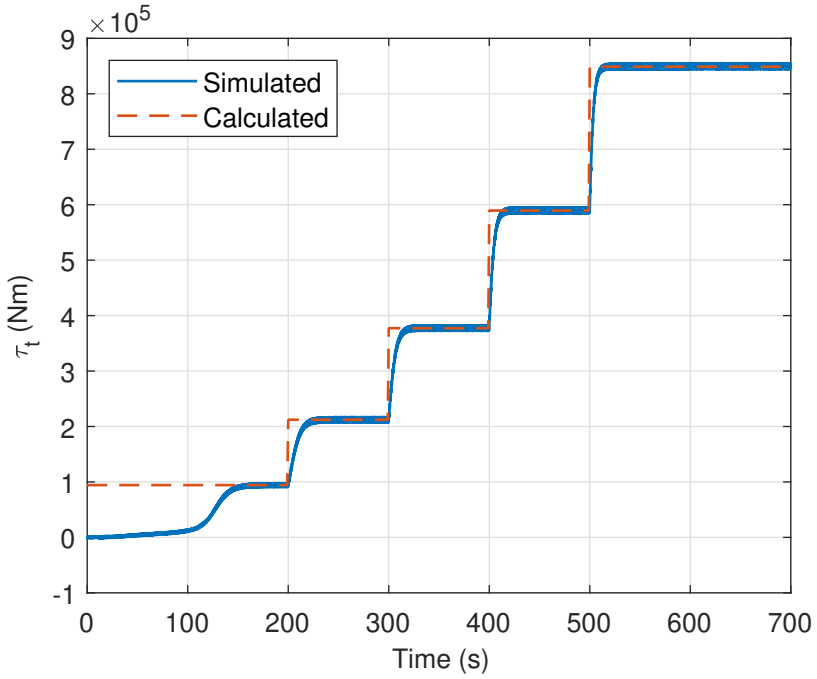

(b) Rotational speed and wind speed

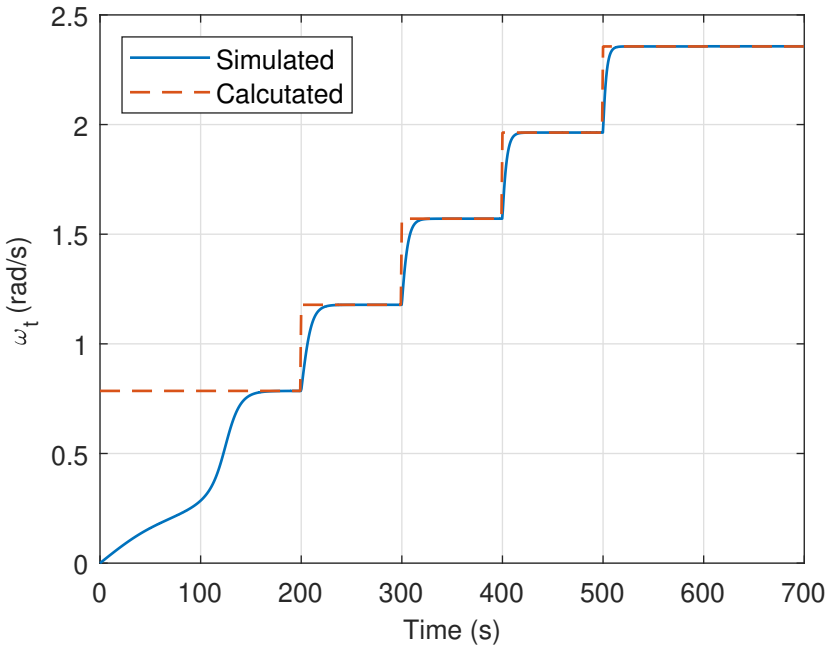

Figure 5.4: Wind turbine (a) torque and (b) speed with input wind steps in DTC model

Validation of wind turbine generator parameters

The validation of the simulated generator's electrical parameters is crucial as they impact the WTPC loading and therefore its lifetime. The wind turbine generator converts the mechanical power of the wind turbine rotor to electrical power fed into WTPC in the form of a three-phase current. The expected values of the generator current (I_m) and power (P_m) are calculated by

equations (4.17) and (4.16) respectively. The simulated values are obtained from the model simulation by applying the constant wind speeds. The simulation outputs of (I_m) and (P_m) are shown in figure 5.5. Comparisons between simulated and calculated values are listed in table 5.3.

Validation of DC bus parameters in DTC model

The DC bus transfers the wind turbine generator power from the MSC to the GSC. However, in the DTC model, the GSC is substituted with a DC source so the DC bus voltage is fixed and does not need to be validated. Therefore, only the DC bus current is validated with respect to input wind speed. Figure 5.6 shows the DC bus current (I_{DC}) for steps of constant wind speeds from 4 m/s to 14 m/s where it shows increasing steps according to input wind speed except for 14 m/s wind speed as the pitch control keeps the rated output power even when wind speed increase further. The simulated I_{DC} is compared with the expected value related to input wind speed for the validation. The expected I_{DC} is calculated by equation (5.1). Table 5.4 lists the calculated $I_{DC,cal}$ and simulated $I_{DC,sim}$ currents and the relative difference between them.

$$I_{DC,cal} \approx \frac{P_{m,sim}}{V_{DC}} \tag{5.1}$$

5.3.3 Validation of semiconductor junction temperatures

Validation of the simulated junction temperature is essential before using the model for reliability analysis. Similar to the validation procedure used with the LV model in section 4.12.3, the comparison between SemiSel and Simulink results of the semiconductor junction temperature for constant wind speeds is implemented. The tested wind speeds were from 4 m/s to 12 m/s to cover the variable wind speed range of the modelled wind turbine. Tables 5.5 and 5.6 list both simulation results for the IGBT and diode of the converter circuit respectively. The temperature difference between SemiSel and Simulink simulation is lower than 1% and the RMSE for maximum and minimum junction temperatures are 3.9×10^{-03} and 2.4×10^{-03} for the IGBT and 6.3×10^{-03} and 5.5×10^{-03} for the diode. Therefore, the model provides an acceptable accuracy level to be used in the WTPC reliability analysis.

Table 5.2: DTC model mechanical parameters with constant wind speeds input

U (m/s)	ω_t (rad/s)			τ_t (kNm)		
	Calculated	Simulated	Δ_{Rel} (%)	Calculated	Simulated	Δ_{Rel} (%)
4	0.79	0.79	1.08×10^{-2}	94.3	94.3	5.00×10^{-2}
6	1.18	1.18	3.09×10^{-4}	212	212	-6.70×10^{-3}
8	1.57	1.57	3.25×10^{-4}	377	377	1.26×10^{-2}
10	1.96	1.96	2.90×10^{-4}	589	589	2.70×10^{-3}
12	2.36	2.36	2.74×10^{-4}	849	849	-1.49×10^{-4}
14	2.36	2.36	-2.67×10^{-2}	849	849	-5.37×10^{-2}

(a) PMSG current

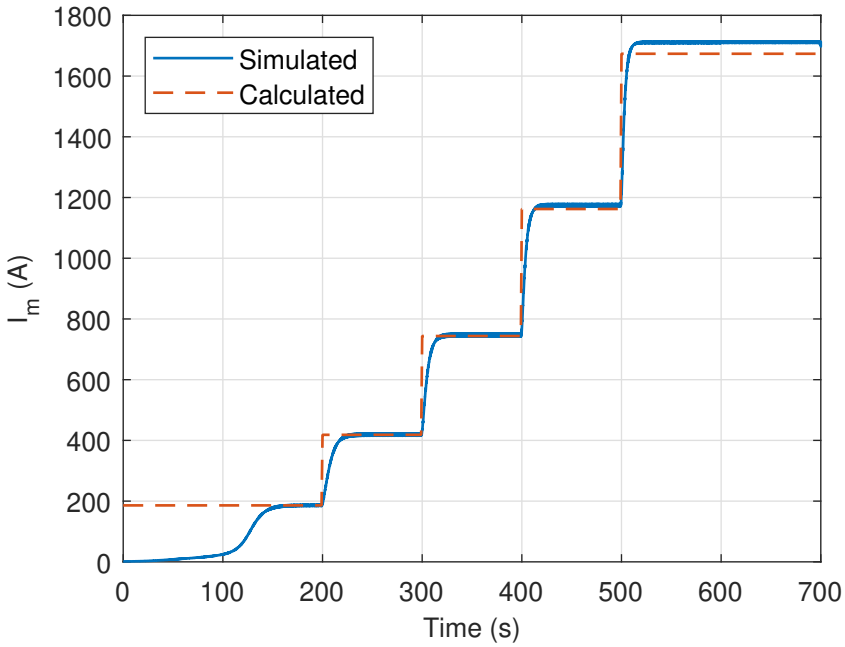

(b) PMSG power

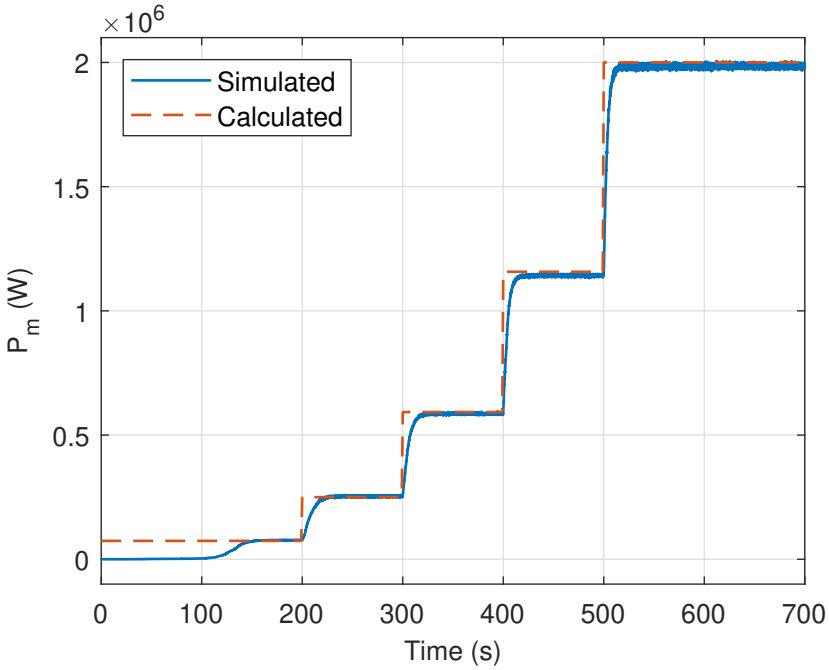

Figure 5.5: PMSG (a) current and (b) power during input wind steps in DTC model

5.4 Wind turbine with 3L-NPC power converter

Addressing the second research question "How can the reliability of more complex converter topologies in wind turbine applications be estimated from knowledge of 2L-VSC systems?", this research extends the reliability analyses to include the more complex higher voltage 3L-VPC WTPC. This approach provides a better understanding of the possible reliability improvement

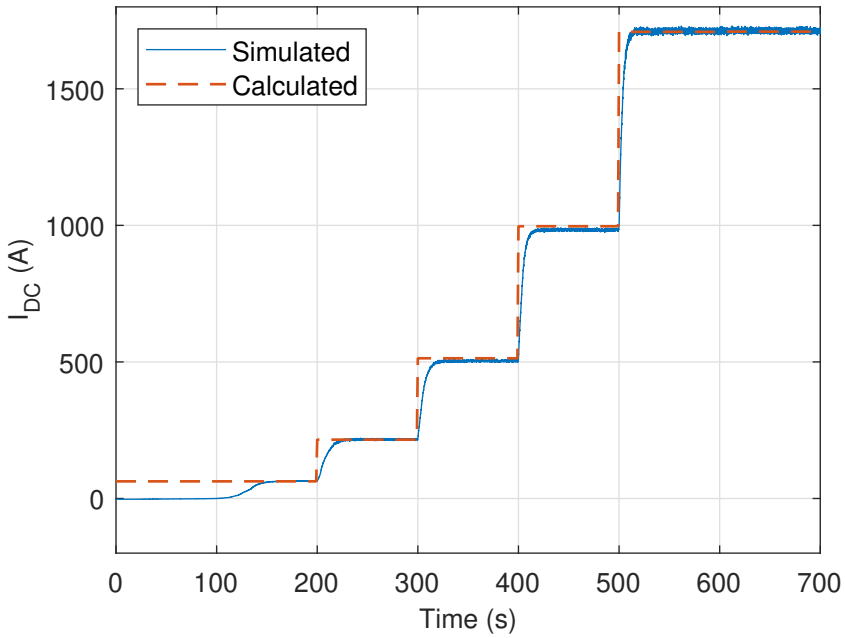

Figure 5.6: DC bus current with input wind steps for DTC model

in future wind turbines. It also provides information about the reliability of WTPC affected by the interactions between operating conditions and converter design.

Some wind turbine manufacturers introduced MV wind turbines replacing the well-known LV technology. These manufacturers claim the advantage of increasing the wind turbine operating voltage to reduce the rated current which reflects on the size of the cables and the grid

Table 5.3: DTC model PMSG parameters with constant wind speeds input

U (m/s)	I_m (A)			P_m (kW)		
	Calculated	Simulated	Δ_{Rel} (%)	Calculated	Simulated	Δ_{Rel} (%)
4	185.9	186.0	-5.1×10^{-2}	74.1	77.1	4.1
6	418.4	419.0	1.6×10^{-1}	250	253.4	-1.4
8	743.8	746.9	-4.2×10^{-1}	592.6	585.7	1.2
10	1162.1	1174.2	1.0×10^{-2}	1157.4	1141.7	1.3
12	1673.5	1710.8	2.2×10^{-2}	2000	1983.9	0.8

Table 5.4: DC bus current validation

U (m/s)	I_{DC} (A)		
	Calculated	Simulated	Δ_{Rel} (%)
4	$6.7\times10^{+1}$	$6.4\times10^{+1}$	4.9
6	$2.2\times10^{+2}$	$2.2\times10^{+2}$	1.9
8	$5.1\times10^{+2}$	$5.0\times10^{+2}$	1.2
10	$9.9\times10^{+2}$	$9.8\times10^{+2}$	0.9
12	$1.7\times10^{+3}$	$1.7\times10^{+3}$	0.8
14	$1.7\times10^{+3}$	$1.7\times10^{+3}$	0.8

transformer. Moreover, MV wind turbine manufacturers claimed a rapid improvement in the WTPC reliability compared to LV wind turbines [36]. Examples of MV wind turbines are Samsung S7.0-171 [127] and GE HaliadeX [33] where both deploy ABB PCS6000 converter which is a 3L-NPC topology constructed using IGCT semiconductors [32].

5.4.1 3L-NPC model description

To proceed with the reliability analyses of 3L-NPC WTPC in wind turbines, modelling an example of an MV wind turbine is required for WTPC reliability analysis. Because of the limited information about the IGCTs used in the 3L-NPC WTPCs, mainly their lifetime empirical parameters which are required for the lifetime estimation. Therefore, this research models the 3L-NPC WTPC with IGBT power modules rather than IGCTs. The model also uses the same power module used in the 2L-VSC model described in Chapter 4. This approach provides a fair comparison between 2L-VSC and 3L-NPC excluding effects produced by using different power modules. Furthermore, the 3L-NPC model has the same rated power, mechanical, and control

Table 5.5: Junction temperature of i1 in DTC model

	$T_{j,i1,max}(^oC)$			$T_{j,i1,min}(^oC)$		
U (m/s)	SemiSel	Simulink	Δ_{Rel} (%)	SemiSel	Simulink	Δ_{Rel} (%)
4	43.4	43.6	-4.9×10^{-1}	41.7	41.8	-4.2×10^{-1}
5	45.7	45.4	6.1×10^{-1}	42.6	42.8	-4.7×10^{-1}
6	47.3	47.5	-3.1×10^{-1}	43.9	44.0	-2.5×10^{-1}
7	49.5	49.8	-6.9×10^{-1}	45.5	45.5	1.7×10^{-2}
8	52.4	52.5	-2.1×10^{-1}	47.3	47.3	-1.3×10^{-1}
9	55.4	55.6	-2.9×10^{-1}	49.4	49.5	-1.5×10^{-1}
10	59.0	59.0	-7.3×10^{-2}	52.0	52.0	8.3×10^{-2}
11	62.7	62.9	-2.0×10^{-1}	54.9	55.0	8.8×10^{-2}
12	67.1	67.2	-1.2×10^{-1}	58.3	58.3	3.7×10^{-2}
	RMSE = 3.9×10^{-3} °C			RMSE = 2.4×10^{-3} °C		

Table 5.6: Junction temperature of d1 in DTC model

	$T_{j,d1,max}(^oC)$			$T_{j,d1,min}(^oC)$		
U (m/s)	SemiSel	Simulink	Δ_{Rel} (%)	SemiSel	Simulink	Δ_{Rel} (%)
4	44.1	44.6	-1.3	41.7	41.9	-4.2×10^{-1}
5	46.4	46.7	-6.4×10^{-1}	42.8	42.9	-3.1×10^{-1}
6	48.9	49.2	-5.9×10^{-1}	44.1	44.2	-2.8×10^{-1}
7	51.7	52.1	-8.8×10^{-1}	45.1	45.8	-1.5×10^{-2}
8	55.5	55.6	-2.1×10^{-1}	47.7	47.7	-4.9×10^{-5}
9	59.6	59.7	-1.9×10^{-1}	49.9	50.0	-1.8×10^{-3}
10	64.7	64.6	1.8×10^{-1}	52.8	52.8	6.6×10^{-4}
11	70.4	70.2	2.2×10^{-1}	56.0	56.0	3.0×10^{-4}
12	77.3	76.9	5.3×10^{-1}	59.8	59.7	8.6×10^{-4}
	RMSE = 6.3 $\times10^{-3}$ °C			RMSE = 5.5×10^{-3} °C		

parameters used in the 2L-VSC model presented in Chapter 4. This made a direct reliability comparison possible. The 3L-NPC wind turbine model includes submodels of mechanical, electrical and control, and thermal subsystems similar to the 2L-VSC wind turbine model. The following sections describe the 3L-NPC wind turbine model subsystems in detail.

5.4.2 3L-NPC model mechanical subsystem

The 3L-NPC wind turbine model is a direct-drive 2MW PMSG wind turbine. It models the wind turbine rotor, coupling shaft, and generator as a two-mass mechanical system considering parts inertias, stiffness and damping constants. The mechanical parameters and modelling of the 3L-NPC model are similar to the mechanical subsystem of the 2L-VSC model explained in section 4.4.

5.4.3 3L-NPC model electrical and control subsystem

The 3L-NPC model electrical subsystem varies from the 2L-VSC model by the converter circuit design and operating voltages. The overview of the electrical modelling by Simulink is shown in figure 5.7. The control of MSC and GSC are FOC and VOC respectively which are similar to control schemes used in the 2L-VSC model discussed in section 4.7. The following paragraphs explain the details of the 3L-NPC model electrical parts, PMSG, DC bus and grid.

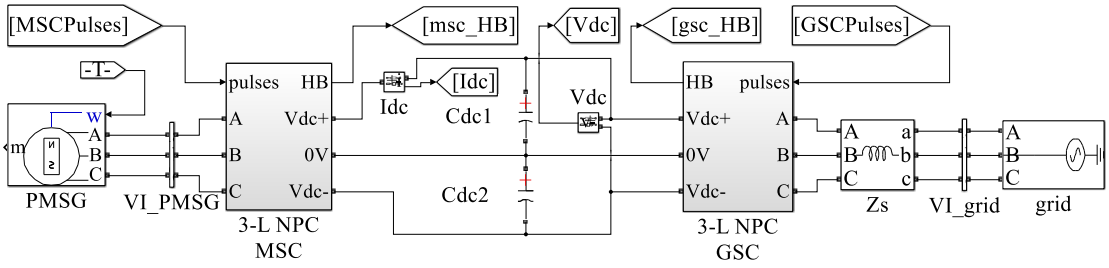

Figure 5.7: Electrical modelling of 3L-NPC WTPC using Simulink

Modelling 3L-NPC wind turbine generator

The 3L-NPC wind turbine model utilises the PMSG with parameters similar to the 2L-VSC model PMSG except its rated voltage which is set to 1,380 V equalling twice the 2L-VSC model generator's rated voltage. The 3L-NPC model implements the Simulink PMSM model from the Simscape Specialized Power System toolbox. The generator parameters are listed in table 5.7.

DC bus model

The DC bus provides an energy path between MSC and GSC as explained in section 4.8. The DC bus voltage is required to be regulated during load variations for the proper operation of

MSC and GSC. In the 3L-NPC topology, the DC bus has three lines, $+V_{DC}$, $-V_{DC}$ and neutral ($V0$). A capacitor bank is connected to the DC bus to minimize the voltage ripple generated by the switching operation of both converters. The selected DC bus capacitor value is calculated by equation (5.2) [128] where C_{DC} is the DC bus capacitor, S is the PMSG apparent power (2.24 MW), and ΔV_{DC} is the allowed change in DC bus voltage which is set to 2% of the DC bus voltage (V_{DC}). The calculated C_{DC} is $\geq 33.7\ mF$ and the selected value is 40 mF.

$$C_{DC} \geq \frac{S}{4\pi f_g V_{DC} \Delta V_{DC}} \tag{5.2}$$

Grid model

The wind turbine output power is assumed to be fed into the grid. The grid is modelled as a three-phase voltage source. The line voltage ($V_{g,3L-NPC}$) is set to 1,380 V which is equal to the rated voltage of the wind turbine generator. The grid frequency (f_g) is set to 50 Hz as in most of world countries. The grid filter is modelled as an inductor having an impedance equal to 0.2 pu [23]. Equations (4.11) and (4.12) in section 4.9 are used to calculate grid filter inductance ($L_{g,3L-NPC}$).

5.4.4 Modelling 3L-NPC WTPC

The 3L-NPC model's WTPC implements back-to-back AC-DC-AC WTPC. It includes two converters, MSC and GSC, and the DC bus. The converters are three-phase 3L-NPC topology connected back to back by the three-lines DC bus. Each converter (similar to the 2L-VSC model) is assembled by individual power modules containing IGBT and freewheel diode as shown in figure 5.8. The selected power module SMK800GD176D is the same power module used in the 2L-VSC model. In the 3L-NPC topology, the applied voltage on the semiconductor is half of the converter operating voltage [128] which is an advantage of moving towards 3L-NPC topology. Therefore, the 3L-NPC model WTPC is set to operate on 1,380 V AC and 2300 V DC which are twice the 2L-VSC model operating voltages.

The 3L-NPC rated current is the same as the 2L-VSC model's rated current since both use the same power module. However, the 3L-NPC rated voltage is twice the 2L-VSC rated voltage

Table 5.7: PMSG parameters of 3L-NPC wind turbine model

Parameter	symbol	Value
Line voltage (rated)	$V_{m,rated}$	1,380 V
Active power (rated)	$P_{m,rated}$	2,000 kW
Apparent power (rated)	$S_{m,rated}$	2,242 kVAR
Rotating speed (rated)	$\omega_{m,rated}$	0.75 rad/s
Torque (rated)	$T_{m,rated}$	848,826 Nm
Number of poles pairs	P_p	26 pole pairs
Flux linkage (RMS)	$\Phi_{m,RMS}$	13 Wb
Stator winding resistance	R_s	2.34 mΩ
Stator winding inductance	L_s	1.573 mH

therefore 3L-NPC rated power will be 500 kW, twice the rated power of 2L-VSC (250 kW). Accordingly, 4 parallel 3L-NPC are required for the 2 MW wind turbine instead of 8 parallel converters used in the 2L-VSC model.

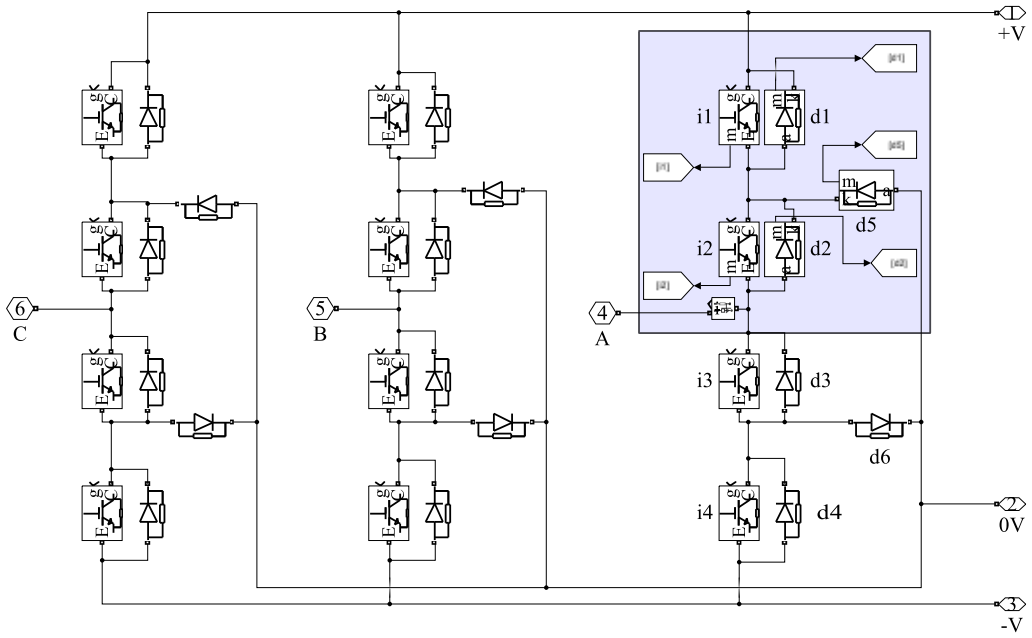

Figure 5.8: Simulink model of the 3L-NPC MSC

5.4.5 Power loss model

The power loss simulation procedure is similar to the one used in the 2L-VSC model explained in section 4.10.However, in 3L-NPC, each half-bridge in the converter contains 10 semiconductors, 5 in each arm instead of 2 semiconductors in each 2L-VSC arm. Also, assuming normal operation conditions, the generator phases are balanced therefore simulating the power losses of one converter arm represent the rest of the converter arms. Semiconductors' power losses are used to simulate their junction temperatures by the thermal model.

5.4.6 Semiconductor junction temperatures in the 3L-NPC model

The junction temperatures of the 3L-NPC semiconductors are obtained by thermal modelling of the converter circuit. Assuming the wind turbine operates in normal conditions with balanced three-phase currents then simulated junction temperatures of one converter arm's semiconductors reflect junction temperatures of all converter semiconductors. The WTPC cooling is based on liquid-cooled heatsinks. Each converter, MSC and GSC, uses three individual heatsinks each for each converter leg as shown in figure 5.9. The 3L-NPC half bridge leg consists of two arms, upper and lower, where each one has three power modules containing two IGBTs, i1 and i2, and three diodes d1, d2, and d5. The heatsink coolant is 1:1 water glycerine mixture of 40°C temperature controlled. The thermal model of the 3L-NPC WTPC is shown in Figure 5.10 where P_i is the IGBT power loss, P_d is the diode power loss, T_j is semiconductor junction temperature, $Z_{th,i}$

and $Z_{th,d}$ are IGBT and diode thermal impedances, $Z_{th,M}$ is power module thermal impedance, $Z_{th,Hs}$ is heatsink thermal impedance, and T_{ct} is coolant temperature.

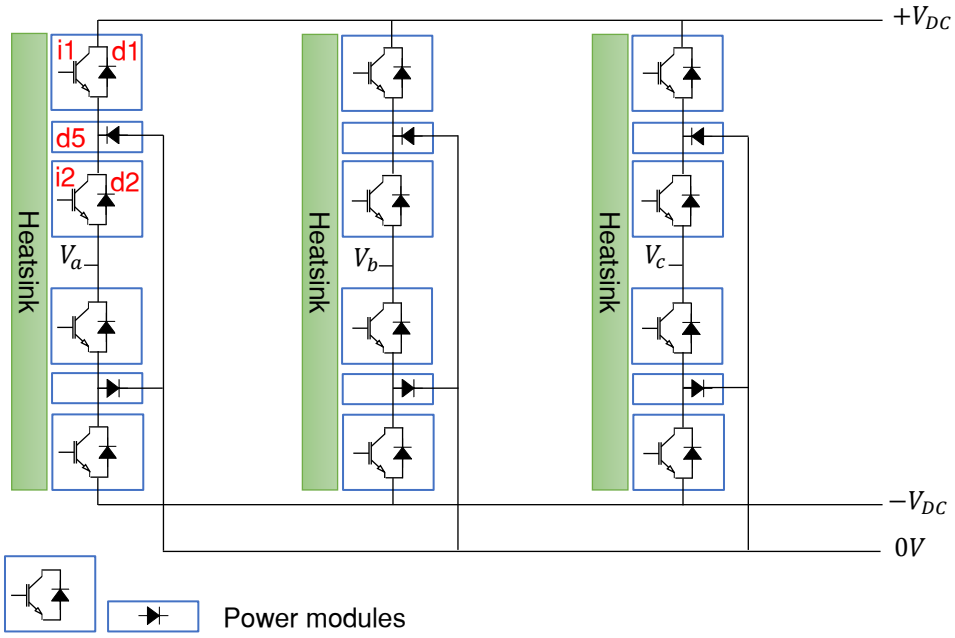

Figure 5.9: Schematic diagram of three-phase 3L-NPC with heatsink configuration

5.5 Validation process of 3L-NPC model

Similar to the 2L-VSC model, the 3L-NPC wind turbine model passes into the validation process to ensure that simulation results are within the accepted accuracy. The validation procedure of the 3L-NPC model operational parameters is achieved by using the stair function of constant wind speeds with time as an input to the model. The stair function starts with the cut-in wind speed (4 m/s) for 200 s to allow the model mechanical and thermal dynamics to reach their steady-state values then it increases at 2 m/s every 100 s until it reaches 14 m/s which is above the rated wind speed to confirm that pitch system limits the rotor speed at its rated value. The wind speed stair function used in the model validation is shown in figure 4.15 in section 4.12. The model validation covers the wind turbine mechanical and electrical operating parameters besides the WTPC semiconductors' junction temperatures.

5.5.1 Validation of mechanical parameters

The validation of the simulated mechanical parameters is achieved by comparing the simulated values with the calculated values. The wind turbine model is input with constant wind speed stair function shown in figure 4.15 in Chapter 4. The simulation results of the wind turbine developed torque (τ_t) and turbine rotating speed (ω_t) related to the input wind speeds are shown in figure (5.11). The first 200 s represent the starting up of the modelled wind turbine where its torque and speed are building up to their steady values corresponding to 4 m/s wind speed. The wind speed values from 6 m/s to 12 m/s show an increase in wind turbine torque

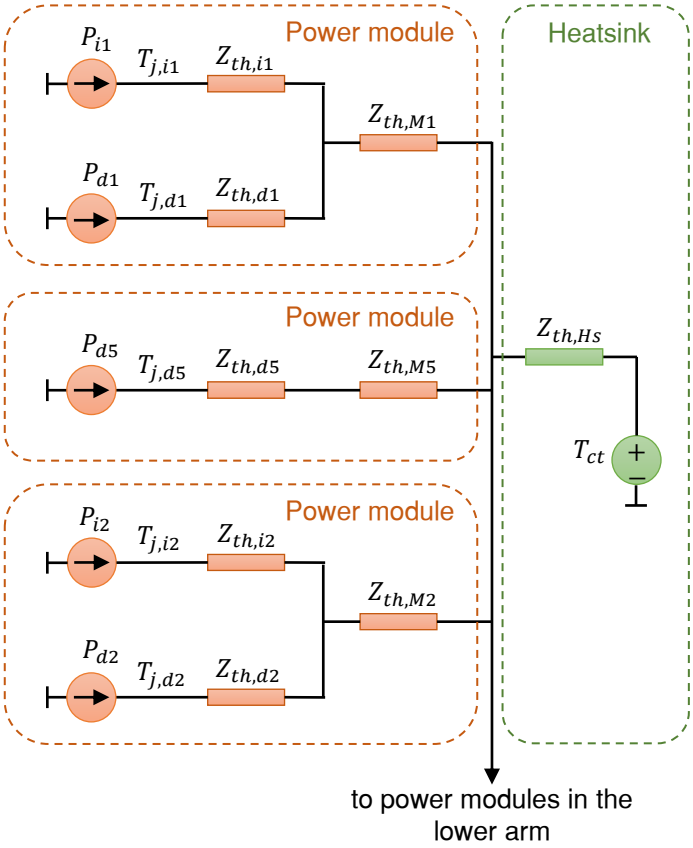

Figure 5.10: Thermal equivalent circuit of the modelled 3L-NPC WTPC

and speed while the step wind speed to 14 m/s does not affect both wind turbine torque and speed because the pitch control keeps the rotating speed at the rated value (2.36 rad/s) which is corresponding to the rated wind speed (12 m/s).

Table 5.8: 3L-NPC model mechanical parameters with constant wind speeds input

U (m/s)	ω_t (rad/s)			τ_t (kNm)		
	Calculated	Simulated	Δ_{Rel} (%)	Calculated	Simulated	Δ_{Rel} (%)
4	0.79	0.79	1.0×10^{-2}	94.3	94.1	1.7×10^{-1}
6	1.78	1.78	-1.2×10^{-4}	212	212	-1.4×10^{-3}
8	1.57	1.57	-3.0×10^{-4}	377	377	-3.4×10^{-2}
10	1.96	1.96	-2.4×10^{-4}	589	589	-4.3×10^{-2}
12	2.36	2.36	-2.0×10^{-4}	849	849	-1.6×10^{-2}
14	2.36	2.36	-2.7×10^{-2}	849	849	-7.0×10^{-2}

5.5.2 Validation of electrical parameters

The electrical parameters of the wind turbine model are validated by comparing their values from the simulation with expected values by calculation related to the input wind speeds. Constant wind speeds from 4 m/s to 14 m/s in 2 m/s steps as shown in figure 4.15 are used to perform

(a) Turbine torque and wind speed

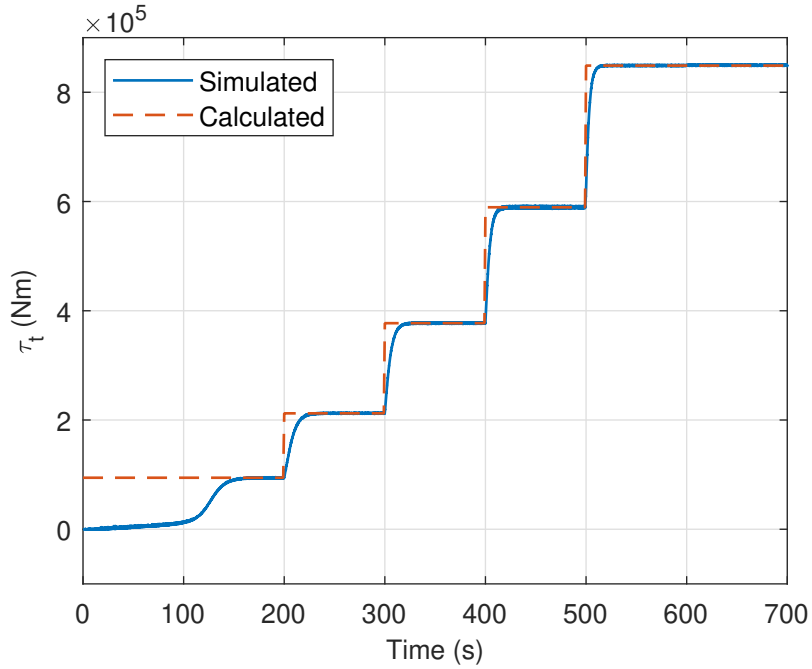

(b) Turbine speed and wind speed

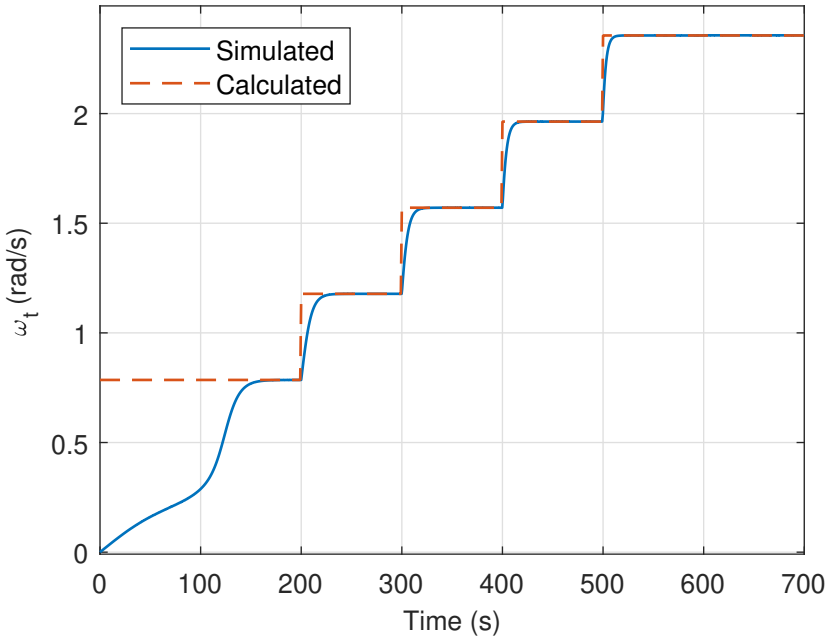

Figure 5.11: Wind turbine (a) torque and (b) speed with input wind steps of 3L-NPC model

the validation which covers electrical parameters of the PMSG, DC bus, and grid.

Validation of wind turbine PMSG parameters

The wind turbine generator converts the mechanical power of the wind turbine rotor to electrical power fed into WTPC as a three-phase current. The validation of the simulated generator's electrical parameters is crucial as they influence the WTPC loading and therefore its lifetime.

The expected values of the generator current (I_m) and power (P_m) are calculated and compared with the values obtained from the model simulation. The simulation results are shown in figure 5.12 and table 5.9 where the relative differences (Δ_{Rel}) between calculated and simulated values are very small.

(a) PMSG current and wind speed

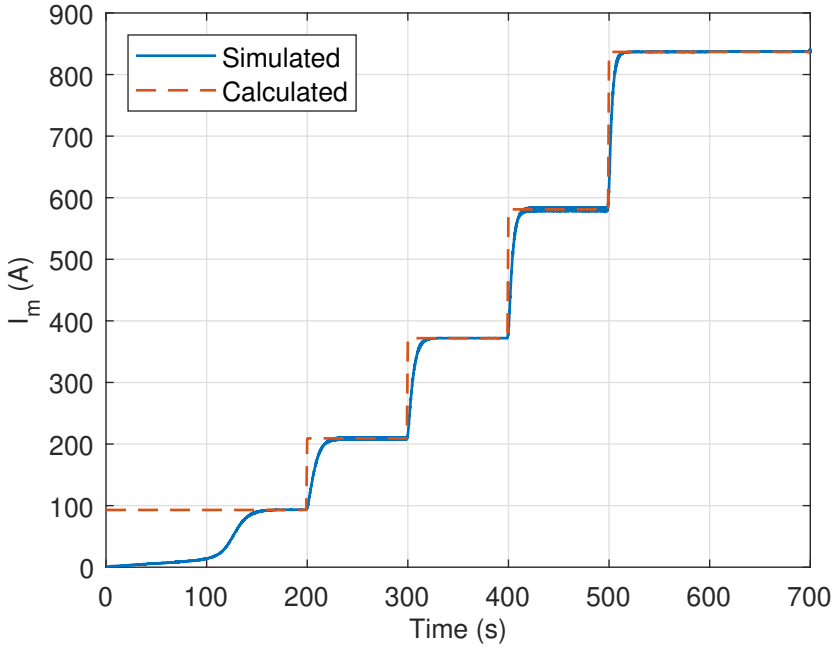

(b) PMSG power and wind speed

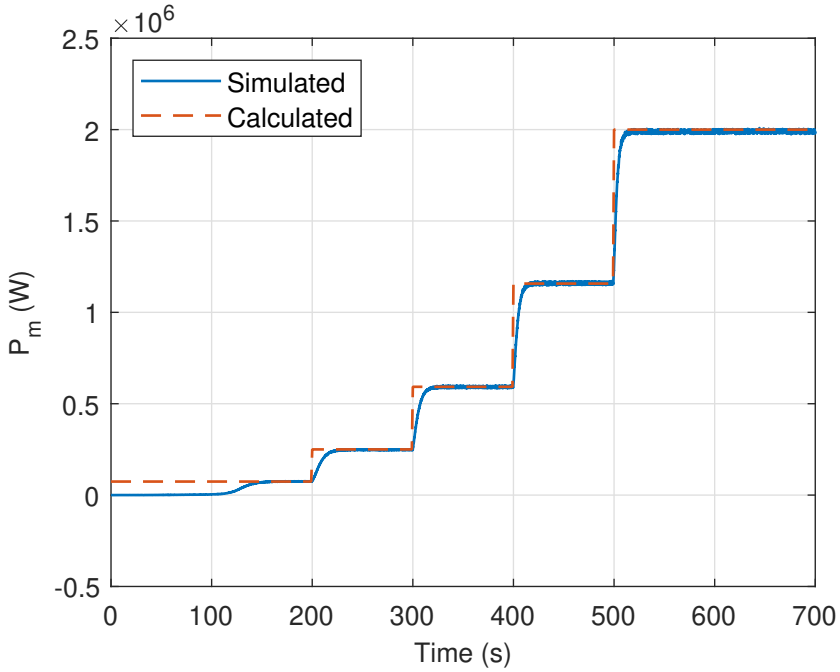

Figure 5.12: PMSG (a) current and (b) power with input wind steps for 3L-NPC model

Validation of DC bus parameters

The DC bus transfers the wind turbine generator power from the MSC to the GSC. Its voltage is controlled by the GSC as discussed in section 4.7.2. The DC bus voltage is required to stay constant during the variable wind turbine loading for MSC and GSC proper operating. Therefore, the changes in wind speed should not affect the DC bus voltage while the DC bus current (I_{DC}) is related to the PMSG power which is influenced by the input wind speed. Since the wind turbine power is in a cubic relationship with the wind speed and the DC bus voltage is constant, the DC bus current shows a cubic relationship with the wind speed. Figure 5.13 shows the DC bus current and voltage for steps of constant wind speeds from 4 m/s to 14 m/s. The DC bus voltage shows a fixed value at 2,300 V while I_{DC} changes concerning the input wind speed. Table 5.10 lists the calculated ($I_{DC,cal}$) and simulated ($I_{DC,sim}$) values where the relative differences (Δ_{Rel}) between them showing low differences.

Validation of wind turbine output parameters

In the wind turbine reliability model, the output power is supplied to the modelled grid through the GSC. The validation of the supplied power is important as it is related to the GSC loading and can be considered as an indication that the overall model is operating properly where the output power should show a valid relationship to the input wind speed like in actual wind turbines. The simulated wind turbine output parameters, the grid active power (P_g), and grid reactive power (Q_g) related to the input wind speeds are shown in figure 5.14. The input wind speed is steps of constant wind speeds from 4 m/s to 14 m/s. Q_g is kept minimum by GSC control as shown in section 4.7.2 to obtain a unity power factor. The validation of wind turbine exported active power is done by comparing output power with input power considering reasonable efficiency. The validation of wind turbine reactive power is done by calculating the power factor which should have an approximate unity value. Table 5.11 lists the simulated P_g, P_m, and the efficiency (Eff) for constant wind speeds besides simulated Q_g and power factor (PF). The efficiency of the wind turbine electrical system shows a reasonable value as in [129–131] while PF is very close to unity.

Table 5.9: PMSG parameter validation with constant wind speeds input for 3L-NPC model

U (m/s)	I_m (A)			P_m (kW)		
	Calculated	Simulated	Δ_{Rel} (%)	Calculated	Simulated	Δ_{Rel} (%)
4	93.0	93.3	-3.7×10^{-1}	74.1	74.7	-8.6×10^{-1}
6	209	209	2.2×10^{-2}	250	248	7.0×10^{-1}
8	372	372	-3.5×10^{-2}	593	592	6.6×10^{-2}
10	581	581	-5.3×10^{-2}	1,157	1,159	-1.5×10^{-1}
12	837	837	-5.1×10^{-3}	2,000	1,989	5.7×10^{-1}
14	837	837	-7.5×10^{-2}	2,000	1,990	5.0×10^{-1}

(a) DC bus current and wind Speed

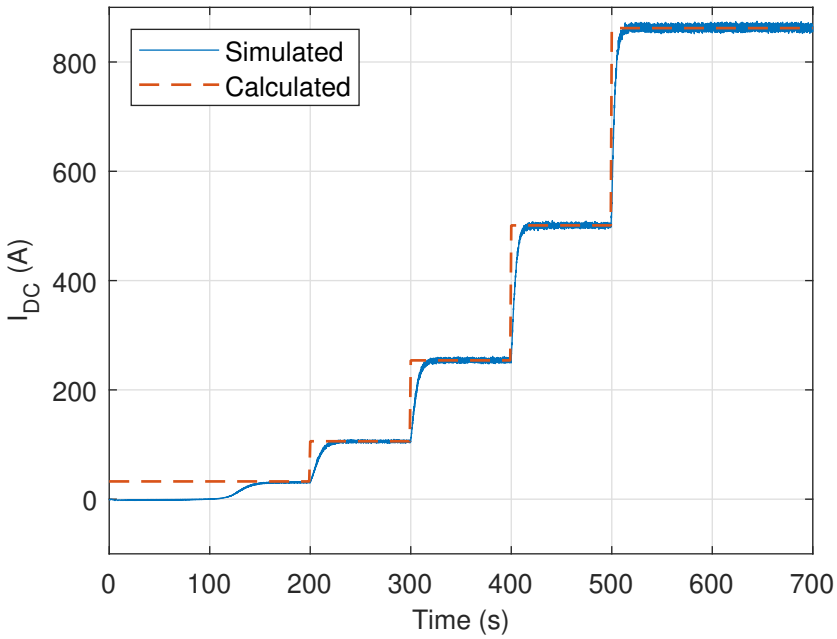

(b) DC bus voltage and wind speed

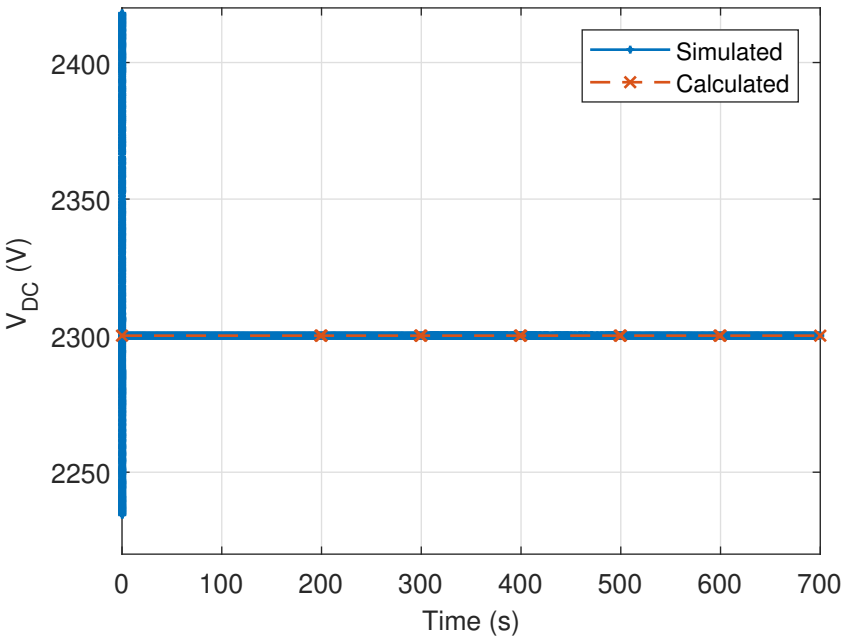

Figure 5.13: DC bus (a) current and (b) voltage with input wind steps for 3L-NPC model

5.5.3 Validation of semiconductors' junction temperature

The validation of 3L-NPC semiconductors' junction temperatures is similar to the procedure of validation of the 2L-VSC semiconductors' junction temperatures in section 4.12.3.However, the one half-bridge in the 3L-NPC converter contains six power modules, three in each arm containing five semiconductors. The validation is done by comparing the junction temperature

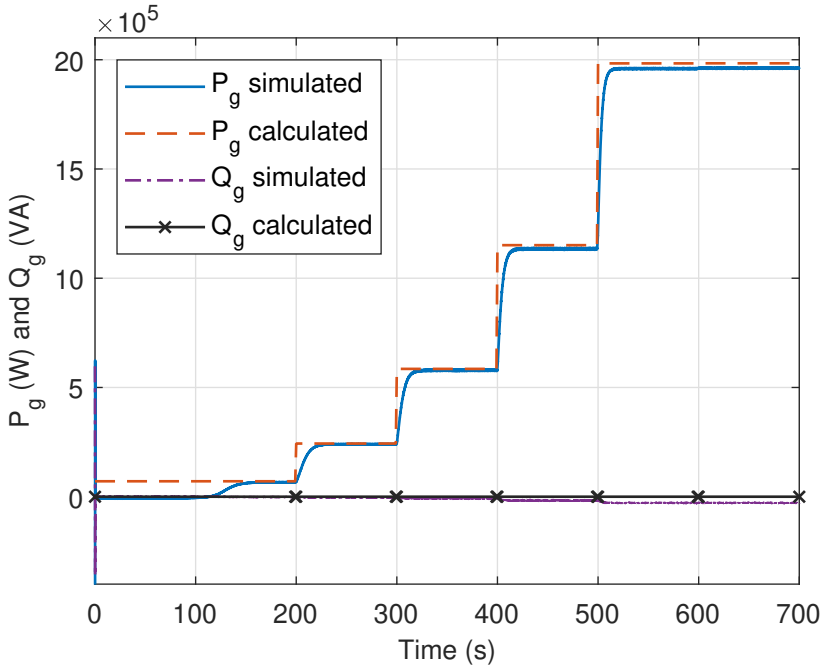

Figure 5.14: Grid exported power with input wind steps for 3L-NPC model

of one arm's semiconductors, i1, d1, i2, d2, and d5. Constant wind speeds are used to obtain maximum and minimum junction temperatures for these semiconductors. On the other side, SemiSel is set to simulate 3L-NPC topology and fed with operating parameters related to the constant wind speeds. The maximum and minimum junction temperatures obtained from the SemiSel report and Simulink are compared. The relative differences are calculated for each wind speed and each semiconductor. The RMSE is calculated for all tested wind speeds of each

Table 5.10: DC bus current validation

U (m/s)	$I_{DC,cal}$ (A)	$I_{DC,sim}$ (A)	Δ_{Rel} (%)
4	$3.25\times10^{+1}$	$3.07\times10^{+1}$	5.3
6	$1.08\times10^{+2}$	$1.06\times10^{+2}$	1.9
8	$2.57\times10^{+2}$	$2.54\times10^{+2}$	1.2
10	$5.04\times10^{+2}$	$5.01\times10^{+2}$	0.7
12	$8.65\times10^{+2}$	$8.62\times10^{+2}$	0.3
14	$8.65\times10^{+2}$	$8.62\times10^{+2}$	0.3

Table 5.11: Wind turbine output parameter validation

U (m/s)	$P_{g,sim}$ (kW)	$P_{m,sim}$ (kW)	Eff (%)	$Q_{g,sim}$ (kVA)	PF
4	66.4	74.7	88.9	-1.65	0.99
6	241	248	96.9	-3.53	0.99
8	578	592	97.7	-8.55	0.99
10	1135	1,157	97.9	-16.8	0.99
12	1,960	1,989	98.5	-28.2	0.99
14	1,961	1,990	98.6	-28.2	0.99

semiconductor. Table 5.12 lists the validation results of the 3L-NPC WTPC model. The relative difference (Δ_{Rel}) is calculated by equation (4.19) in section 4.12.3.

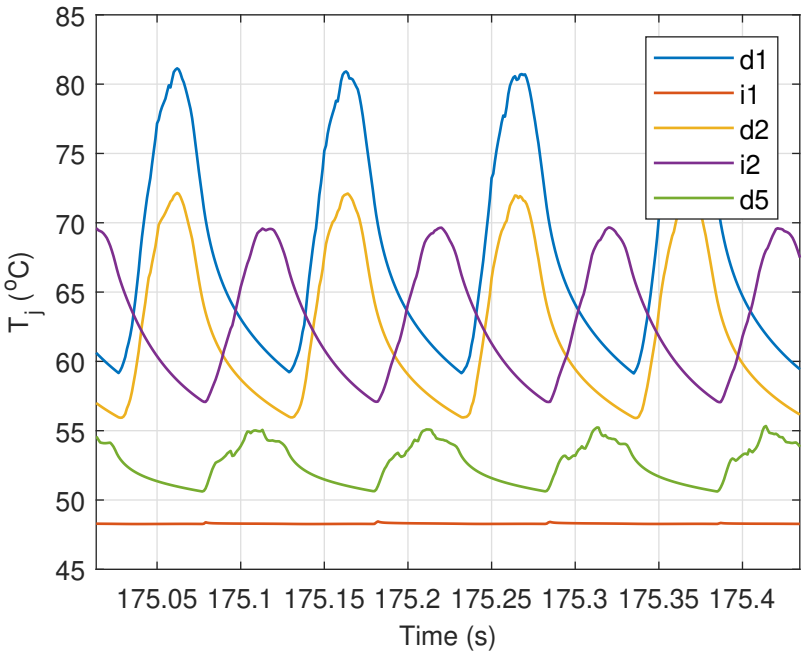

Figure 5.15: MSC's semiconductor junction temperatures at 12 m/s input wind speed of 3L-NPC WTPC

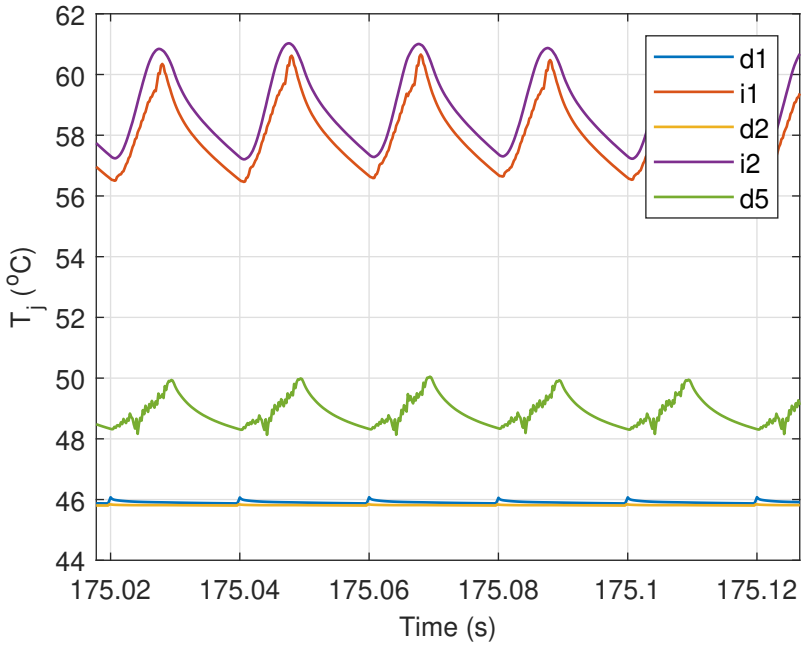

Figure 5.16: GSC's semiconductor junction temperatures at 12 m/s input wind speed of 3L-NPC WTPC

5.5.4 Lifetime estimation of the 3L-NPC WTPC

The WTPC lifetime estimation in the 3L-NPC wind turbine model is calculated for the WTPC semiconductors and for the converter as a whole. The simulation of the WTPC semiconductors' thermal loading as shown in figure 5.15 and figure 5.16 is used to obtain the mean (T_m) and variation (ΔT) in their junction temperature. Each thermal cycle develops an amount of damage in the semiconductor which is calculated according to the Coffin-Manson Arrhenius equation (3.6). Assuming the wind turbine operates at a balanced load with no-fault conditions, then the converter arms operate symmetrically and produce similar operating parameters (voltage, currents, and power losses). Therefore, estimating the lifetime of one converter arm by thermal loading simulation is used to estimate the lifetime of the rest of the converter arms. The three-phase 3L-NPC converter circuit has six arms, each containing five semiconductors (i1, d1, i2, d2, and d5). Therefore, the converter failure rate $\lambda_{cnv,3L-NPC}$ is the sum of the failure rates of all semiconductors in its circuit calculated by equation (5.3) where λ_{i1} to λ_{d5} are the failure rates of the corresponding semiconductors i1 to d5 respectively. Accordingly, the converter lifetime $MTTF_{cnv,3L-NPC}$ is calculated by equation (5.4) where $MTTF_{i1}$ to $MTTF_{d5}$ are the MTTF of the corresponding semiconductors i1 to d5 respectively.

$$\lambda_{cnv,3L-NPC} = 6 \times (\lambda_{i1} + \lambda_{d1} + \lambda_{i2} + \lambda_{d2} + \lambda_{d5}) \tag{5.3}$$

$$MTTF_{cnv,3L-NPC} = \frac{1}{6}\left(\frac{1}{MTTF_{i1}} + \frac{1}{MTTF_{d1}} + \frac{1}{MTTF_{i2}} + \frac{1}{MTTF_{d2}} + \frac{1}{MTTF_{d5}}\right)^{-1} \tag{5.4}$$

5.6 Chapter summary

In this chapter, the reliability modelling of WTPC has been extended to two models for analysing the impact of changing the WTPC design on its reliability. The selected changes in WTPC design are control strategy and converter topology. The first modified wind turbine model used the DTC scheme rather than the FOC scheme used originally. This model will be used in the

Table 5.12: Junction temperature comparison between SemiSel and Simulink for d1

U (m/s)	$T_{jmax,d1}$(°C)			$T_{jmin,d1}$(°C)		
	SemiSel	Simulink	Δ_{Rel} (%)	SemiSel	Simulink	Δ_{Rel} (%)
4	42.69	43.28	-1.4	40.94	41.13	-0.5
5	44.34	44.73	-0.9	41.59	41.76	-0.4
6	46.11	46.56	-1.0	42.41	42.59	-0.4
7	48.33	48.87	-1.1	43.44	43.66	-0.5
8	51.20	51.68	-0.9	44.80	44.98	-0.4
9	54.63	55.12	-0.9	46.45	46.59	-0.3
10	58.67	59.28	-1.0	48.41	48.59	-0.4
11	63.76	64.26	-0.8	50.88	51.00	-0.3
12	69.63	70.35	-1.0	53.73	53.94	-0.4
	RMSE = 1.1×10^{-2} °C			RMSE = 4.2×10^{-3} °C		

analyses of the reliability impacts on the WTPC due to modifying the control system in section 6.3. The parameters of the FOC model are kept the same in the DTC model for comparison while the change was only in the control system scheme. The DTC model validated the performance parameters and junction temperature of the WTPC semiconductors to ensure the simulation results' accuracy.

The second modified wind turbine model extended the WTPC operating voltage to the MV and utilised a higher voltage 3L-NPC topology rather than the LV 2L-VSC topology used in the original model. In this model, most of the LV model parameters were kept the same for reliability comparison except the operating voltage which is required to be in the range of MV voltage ($\geq 1000V$). The 3L-NPC model was validated for its performance parameters and its semiconductors' junction temperatures to ensure the simulation results' accuracy. This model will be used to analyse the impact of moving toward higher level higher voltage converters on the reliability of WTPC. Chapter 6 will utilize the three wind turbine models, 2L-VSC model, DTC model, and 3L-NPC model in comparative WTPC reliability analyses. The analysis will allow assessment of the impact of operating conditions on each of these models to determine the significance of converter design on the WTPC's reliability.

Table 5.13: RMSE of 3L-NPC semiconductors junction temperature differences between SemiSel and Simulink

Semiconductor	RMSE of T_{jmax} (°C)	RMSE of T_{jmin} (°C)
i1	1.1×10^{-3}	4.4×10^{-3}
d1	1.1×10^{-2}	4.2×10^{-3}
i2	7.5×10^{-3}	3.3×10^{-3}
d2	8.3×10^{-3}	3.1×10^{-3}
d5	1.9×10^{-2}	3.5×10^{-3}

Chapter 6

Results, analyses, and discussion

6.1 Introduction

The reliability analysis of WTPC in this research is based on estimating WTPC lifetime concerning wind turbine operating parameters. The WTPC lifetime estimation is based on the semiconductor's junction temperature cycling according to the Coffin-Manson Arrhenius equation.

Three modelled wind turbines for WTPC reliability analyses are utilised in this chapter to address research questions. The 2L-VSC model constructed in Chapter 4 is used to analyse the reliability of the widely deployed WTPC. Reliability analysis of the 2L-VSC model is utilised to address the first research question "How can the reliability of existing wind turbine two-level voltage source converters be better understood?". The DTC model constructed in section 5.2 is used to analyse the control system change on the WTPC reliability. The 3L-NPC model constructed in section 5.4 is used to analyse the reliability of a more complex topology WTPC. Reliability analysis of the 3L-NPC model is utilised to address the second research question "How can the reliability of more complex converter topologies in wind turbine applications be estimated from knowledge of 2L-VSC systems?"

To consider the practical operation of wind turbines, the wind speed data used in the reliability analysis is selected from field-measured wind speeds of one year covering a variety of speeds and turbulence intensities. The conclusions of the reliability analysis are based on simulating WTPC lifetime at hundreds of variable wind speed profiles (VWSP) since utilising a few VWSPs may not be enough to emulate the actual wind turbine operation.

In this research, the WTPC reliability analysis does not intend to predict the WTPC lifetime of a specific wind turbine in the field. Instead, it analyses the factors that impact the reliability of the WTPC including the operating conditions, converter design and control technique. The wind turbines in the field may use different converter parameters or controls which affect their estimated lifetimes. For example, wind turbines may deploy prefabricated stack converters or use techniques like controlled load-sharing among the parallel converters for reliability optimisation as in [29] which improves WTPC lifetime. However, the analyses performed in this thesis demonstrate that the proposed approach could be applied to different WTPC topologies and control techniques and, as such, could be applied to more novel or complex WTPC systems.

6.2 Reliability analysis of 2L-VSC WTPC

In this section, the reliability analysis of 2L-VSC WTPC simulates the impact of wind turbine operating conditions on the WTPC lifetime. The wind turbine model presented in Chapter 4 is utilised for this analysis.

6.2.1 Analysing WTPC's semiconductors lifetime

The WTPC has two converters, MSC and GSC, and each includes IGBTs and diodes. It is useful to understand how each part is loaded during the operation of the wind turbine. This information helps identify the failure influencing part and parts that can be ignored from further reliability analyses. The understanding of the WTPC loading is based on estimating the WTPC lifetime during constant wind speed input. This simulation does not intend to assess the reliability of WTPC during the actual operation of the wind turbine but to show how WTPC's converters, MSC and GSC, and their semiconductors are affected by wind turbine loading. In this simulation, the lifetimes of WTPC's IGBTs and diodes are estimated based on their junction temperature during a range of constant wind speeds used as input to the reliability model. The selected wind speeds ranged from the wind turbine cut-in wind speed (4 m/s) to its rated wind speed (12 m/s) with a 1 m/s increase in each simulation, assuming higher wind speeds will have a similar impact as the rated wind speed due to the speed regulation by the wind turbine blades' pitch control. Each test is conducted with a constant wind speed for 184 s to allow system dynamics to reach their steady-state values then junction temperatures of IGBT and diode are recorded for 16 s to obtain their mean (T_m) and variation (ΔT) values for the lifetime estimation equation (4.21).

The simulation results of WTPC semiconductors of both MSC and GSC are listed in table 6.1 and the visual presentation is shown in bar diagram figure 6.1. The simulation results show that the lifetimes of IGBT and diode are impacted by wind speed differently where the MSC's diode was the most affected semiconductor in the WTPC. The GSC's semiconductors' loading is considerably lower than MSC's semiconductors therefore they achieve higher lifetimes.

Table 6.1: MTTF of MSC and GSC semiconductors of WTPC at constant wind speeds with 2L-VSC model

U (m/s)	$MTTF_{i1,MSC}$(hr)	$MTTF_{d1,MSC}$(hr)	$MTTF_{i1,GSC}$(hr)	$MTTF_{d1,GSC}$(hr)
4	$9.73\times10^{+9}$	$1.23\times10^{+9}$	$1.65\times10^{+15}$	$1.37\times10^{+14}$
5	$1.16\times10^{+9}$	$1.71\times10^{+9}$	$4.32\times10^{+13}$	$4.22\times10^{+12}$
6	$2.13\times10^{+8}$	$3.20\times10^{+7}$	$2.27\times10^{+12}$	$5.99\times10^{+11}$
7	$5.04\times10^{+7}$	$6.88\times10^{+6}$	$1.75\times10^{+11}$	$1.06\times10^{+11}$
8	$1.50\times10^{+7}$	$1.67\times10^{+6}$	$1.57\times10^{+10}$	$2.03\times10^{+10}$
9	$5.00\times10^{+6}$	$4.16\times10^{+5}$	$1.88\times10^{+9}$	$4.76\times10^{+9}$
10	$1.87\times10^{+6}$	$1.10\times10^{+5}$	$2.28\times10^{+8}$	$1.04\times10^{+9}$
11	$7.71\times10^{+5}$	$2.94\times10^{+4}$	$2.92\times10^{+7}$	$2.52\times10^{+8}$
12	$3.41\times10^{+5}$	$7.81\times10^{+3}$	$4.05\times10^{+6}$	$5.52\times10^{+7}$

(a) MSC semiconductors

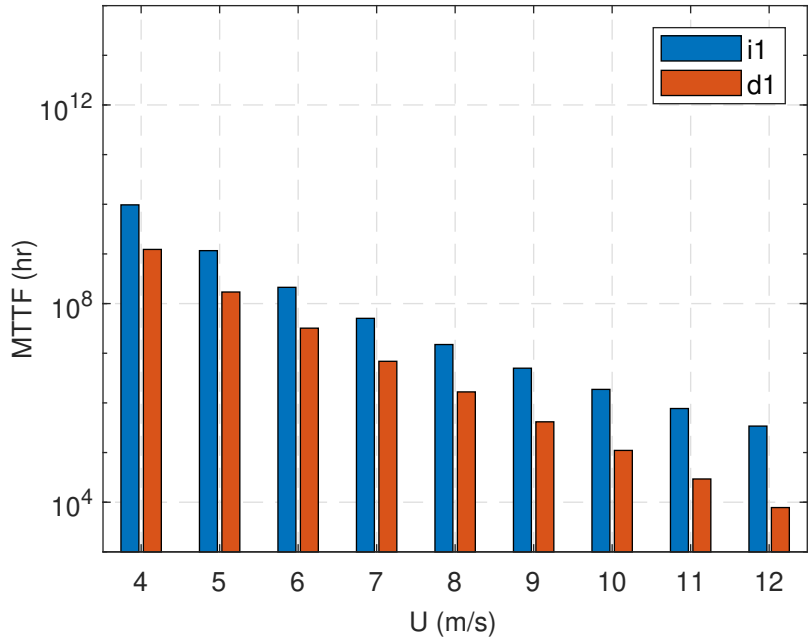

(b) GSC semiconductors

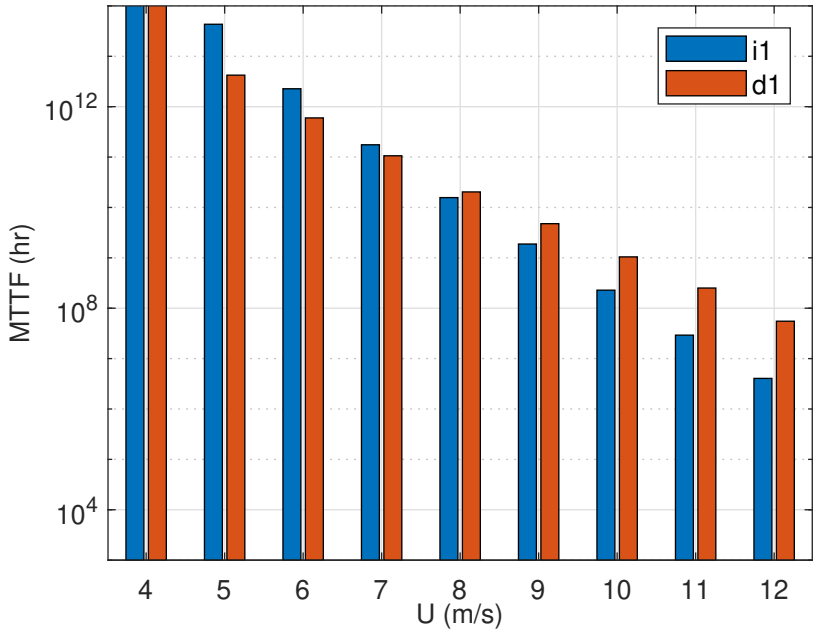

Figure 6.1: Lifetimes of IGBT and diode in MSC (a) and GSC (b) of WTPC at constant wind speeds with 2L-VSC model

6.2.2 Considering MSC for the WTPC reliability analysis

Based on the estimated lifetimes of IGBT and diode, the MSC and GSC lifetimes are calculated. Accordingly, WTPC lifetime is calculated considering both MSC and GSC failure rates as expressed in equation (6.1) where λ_{WTPC}, λ_{MSC}, and λ_{GSC} are failure rates of WTPC, MSC, and GSC respectively and $MTTF_{WTPC}$, $MTTF_{MSC}$, and $MTTF_{GSC}$ are mean times to fail-

ure of WTPC, MSC, and GSC respectively. The constant wind speeds simulation shows that MSC semiconductors are thermally loaded higher than GSC semiconductors at the same wind speed. Accordingly, the estimated lifetime of GSC is higher than the MSC's lifetime as shown in table 6.2 and in figure 6.2. The big difference between $MTTF_{MSC}$ and $MTTF_{GSC}$ made $MTTF_{WTPC}$ influenced by the $MTTF_{MSC}$. The lifetime results in table 6.2 and in figure 6.2 show that $MTTF_{WTPC}$ is nearly equals $MTTF_{MSC}$. Therefore, reliability analysis of WTPC can rely on MSC lifetime analysis only and GSC can be replaced by a DC source for model simplicity and to reduce simulation time. This conclusion aligns with published articles about WTPC reliability like in [75, 132] which indicates the validity of this analysis.

$$\begin{aligned} \lambda_{WTPC} &= \lambda_{MSC} + \lambda_{GSC} \\ MTTF_{WTPC} &= \left(\frac{1}{MTTF_{MSC}} + \frac{1}{MTTF_{GSC}} \right)^{-1} \end{aligned} \tag{6.1}$$

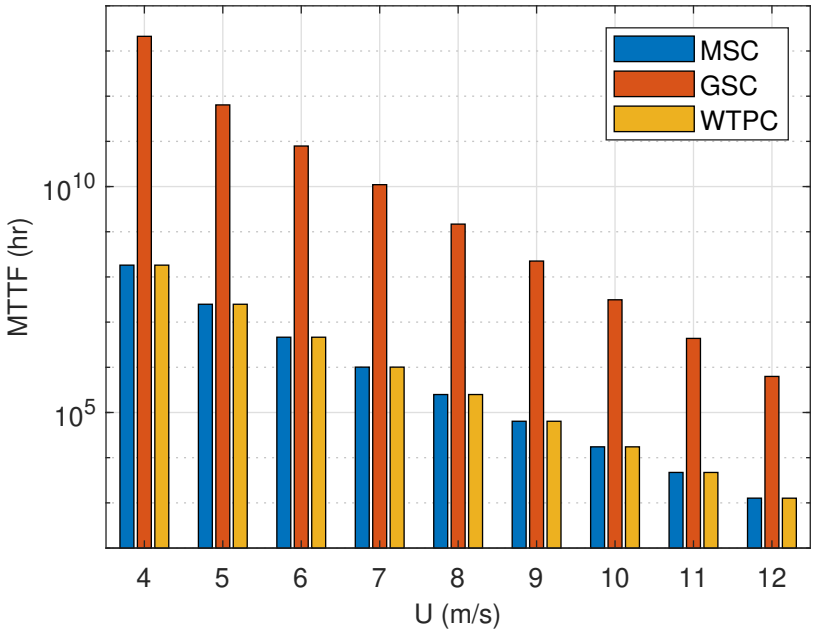

Figure 6.2: Lifetimes of MSC, GSC, and WTPC at constant wind speeds in 2L-VSC model

6.2.3 Impact of variable wind speed on WTPC lifetime

The previous test analysed the effect of constant wind speed on WTPC semiconductor lifetime to demonstrate the impact of wind turbine loading on converter semiconductors. However, WTPC lifetime estimation should be analysed based on the impact of variable wind speed to reflect the actual wind turbine operation. Therefore in this test, the WTPC lifetime is assessed concerning the realistic operating wind conditions by applying field-recorded variable wind speed profiles (VWSPs). The VWSPs are selected so that their average wind speeds ($\overline{U}$) cover the modelled wind turbine operating range of wind speeds from 4 m/s to 25 m/s and also cover a range of

turbulence intensity from 5% to 30%. Based on the availability of wind speed data and the required range, 230 VWSPs were selected for this test. The simulated semiconductors junction temperature of each VWSP is used to estimate WTPC lifetime. The results are 230 WTPC lifetime estimations ($MTTF_{WTPC}$) related to the 230 VWSP are shown in the scatter diagram in figure 6.3.

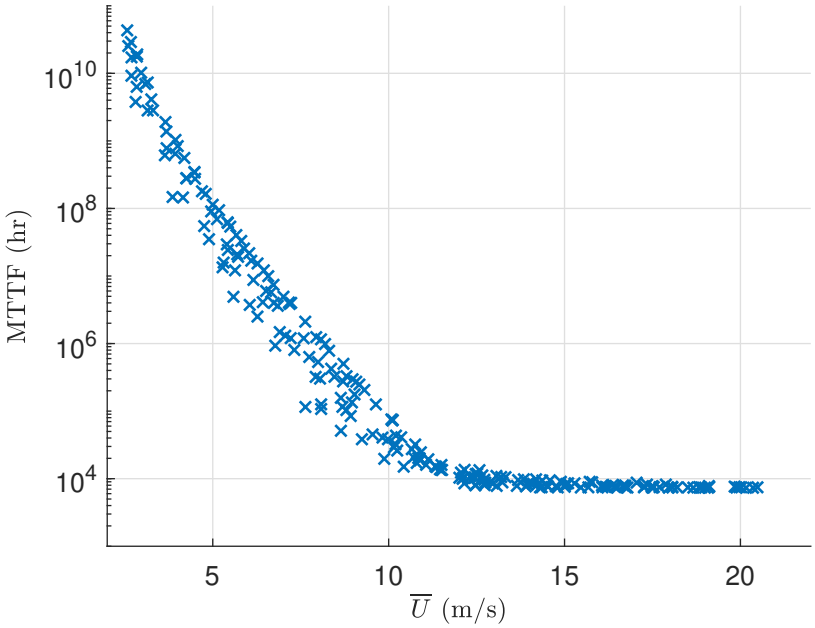

Figure 6.3: WTPC lifetimes related to 230 VWSPs in 2L-VSC model

Results discussion

To analyse the impact of WVSP's average wind speed, the test results are presented in a scatter diagram in figure 6.3. The WVSPs' average wind speeds affect the WTPC lifetime on a logarithmic scale. As average wind speed increases the WTPC lifetime decreases until the average wind speed reaches the rated wind speed (12 m/s) of the modelled wind turbine where the wind turbine speed control implemented by the pitch control operates and keeps the rotating speed

Table 6.2: Lifetime of MSC, GSC, and WTPC at constant wind speeds

U (m/s)	$MTTF_{MSC}$(hr)	$MTTF_{GSC}$(hr)	$MTTF_{wtpc}$(hr)
4	$1.82\times10^{+8}$	$2.11\times10^{+13}$	$1.82\times10^{+8}$
5	$2.49\times10^{+7}$	$6.41\times10^{+11}$	$2.49\times10^{+7}$
6	$4.63\times10^{+6}$	$7.89\times10^{+10}$	$4.63\times10^{+6}$
7	$1.01\times10^{+6}$	$1.10\times10^{+10}$	$1.01\times10^{+6}$
8	$2.50\times10^{+5}$	$1.48\times10^{+9}$	$2.50\times10^{+5}$
9	$6.40\times10^{+4}$	$2.25\times10^{+8}$	$6.40\times10^{+4}$
10	$1.74\times10^{+4}$	$3.12\times10^{+7}$	$1.74\times10^{+4}$
11	$4.71\times10^{+3}$	$4.36\times10^{+6}$	$4.71\times10^{+3}$
12	$1.27\times10^{+3}$	$6.28\times10^{+5}$	$1.27\times10^{+3}$

regulated at its rated value. Therefore, when the wind speed increases above the rated wind speed the WTPC loading will not be affected and accordingly the WTPC lifetime approaches a fixed value that appears as a horizontal line in the lifetime scatter diagram in figure 6.3. The scatter diagram also shows a spread of points that demonstrates that WTPC lifetime varies even when VWSPs have similar average wind speeds. This indicates that the wind speed fluctuations within the VWSP produce different impacts even when they have the same average wind speed. To consider the wind speed fluctuation within the VWSP, the wind turbulence intensity (TI) needed to be considered as it expresses the wind speed changes within the VWSP. The 230 VWSPs have a range of turbulence intensities from 5.6% to 30.5%. The scatter diagram can be reproduced with categorised lifetime results according to the VWSPs' turbulence intensities, $TI \leq 20\%$ and $TI > 20\%$ as shown in figure 6.4. The turbulence intensity categorised scatted diagram shows that lower turbulence VWSPs ($TI \leq 20\%$) achieved higher WTPC lifetime than higher turbulence VWSPs ($TI > 20\%$). However, there are overlaps among lifetime results which require further analysis to confirm the impact of wind turbulence intensity on WTPC lifetime which will be discussed in the following analysis.

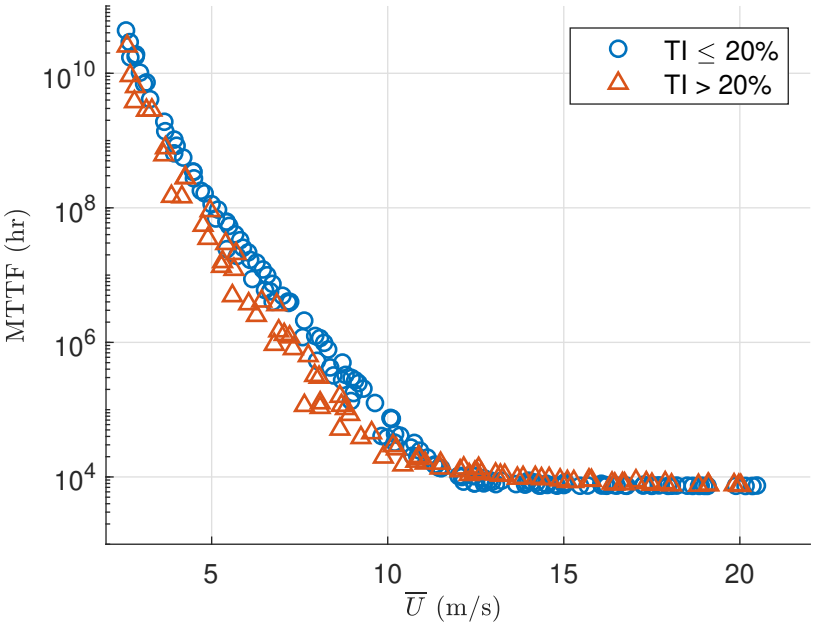

Figure 6.4: Effect of VWSP's turbulence intensity on WTPC lifetime in 2L-VSC model

6.2.4 Impact of wind turbulence intensity on WTPC lifetime

To analyse the impact of VWSPs' turbulence intensities on the WTPC lifetime without interfering with the effect of average wind speed, four groups of VWSPs are selected for this analysis where the average wind speed of all VWSPs is 6 m/s so the impact of average wind speed is minimised. Each group has a selected n number of VWSPs of a defined turbulence intensity so the lifetime can be analysed based on the variation of turbulence intensity among the four groups. The simulation results of each VWSP are used to calculate the corresponding logarithmic of WTPC lifetime ($\log(MTTF_{WTPC})$). The results are visually presented by a histogram diagram

in figure 6.5 which shows that the WTPC lifetimes of each group are accumulated together. However, whilst the distributions vary with turbulence intensity, there is no clear separation between the groups' results mainly between adjacent groups. To analyse that, the distribution type of the results must be identified to apply the proper statistical tools. The Anderson-Darling test (AD test) is a statistical tool used to test whether or not the data is normally distributed [133]. Applying the results of each group to the AD test shows that they are normally distributed. Therefore, the results of each group can be represented by a normal distribution curve of the same mean and standard deviation of the results. The mean (μ) and standard deviation (σ) of $\ln(MTTF_{WTPC})$ are calculated by equations (6.2) and (6.3) respectively. The μ and σ of the turbulence intensity groups are shown in table 6.3. Accordingly, four distribution curves are shown in figure 6.6 representing the four turbulence intensity groups of VWSPs.

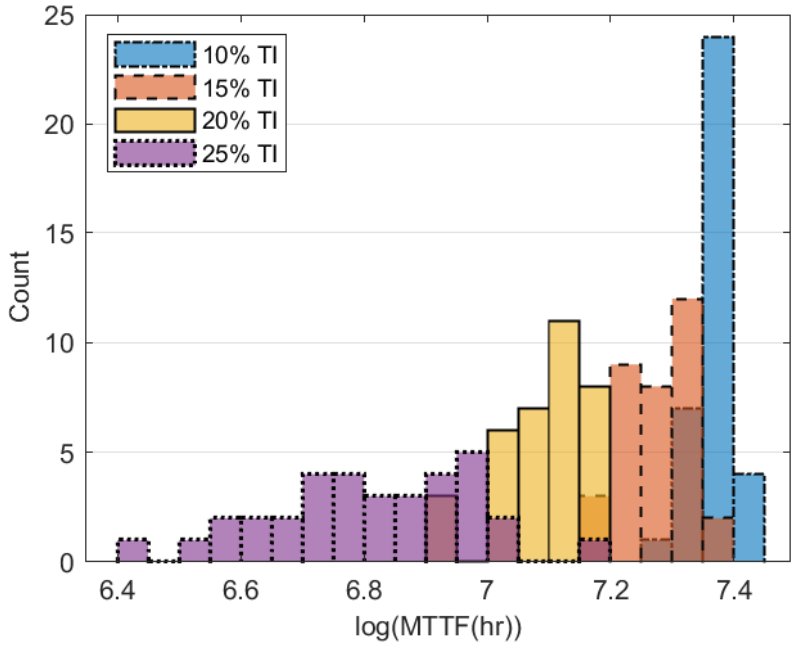

Figure 6.5: Histogram of WTPC lifetimes related to 4 turbulence intensities groups of VWSPs with 2L-VSC model

Results discussion

The four groups' lifetime results show that the lifetime mean of each group decreases as the group turbulence intensity increases. Furthermore, the lifetime standard deviation of each group increases as the group turbulence intensity increases. This can be seen clearly in figure 6.6 as the lifetime distribution is wider when the group's turbulence intensity is higher. This analysis concludes that lower turbulence intensity wind causes longer and more predictable WTPC lifetime while high turbulence wind causes shorter and more difficult to predict WTPC lifetime.

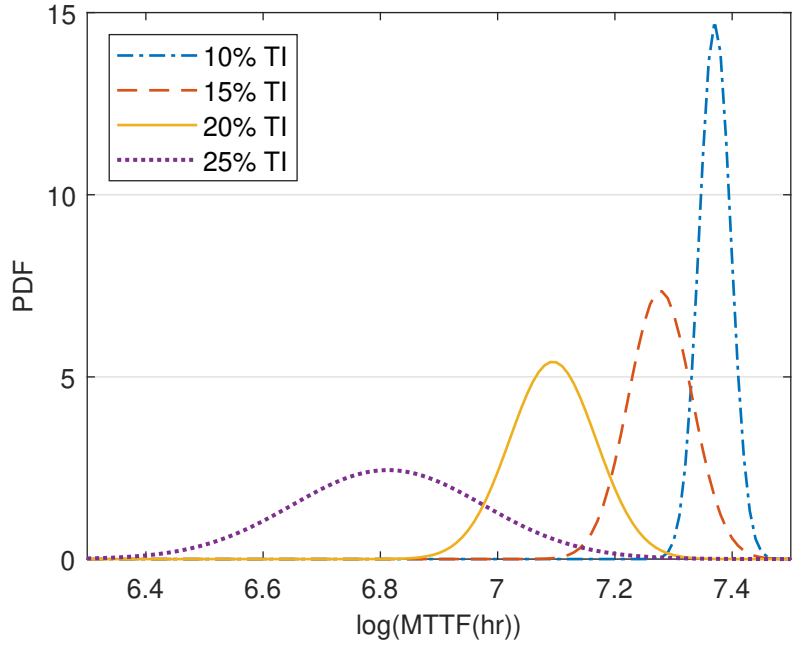

Figure 6.6: Fitting curves of WTPC lifetimes of four VWSP groups with 2L-VSC model

Table 6.3: WTPC lifetimes' mean and standard deviation of four groups of VWSPs

VWSP			$\log(MTTF_{WTPC}(hr))$	
$\overline{U}$(m/s)	TI(%)	n	μ	σ
6 ± 0.05	10 ± 0.5	36	7.37	0.027
6 ± 0.05	15 ± 0.5	34	7.28	0.054
6 ± 0.05	20 ± 0.5	35	7.10	0.074
6 ± 0.05	25 ± 0.5	34	6.81	0.163

$$\mu = \frac{\sum_{i=1}^{i=n} \ln\left(MTTF_{pc_i}\right)}{n} \tag{6.2}$$

$$\sigma = \sqrt{\frac{\sum_{i=1}^{n} \left(\ln\left(MTTF_{pc_i}\right) - \mu\right)^2}{n}} \tag{6.3}$$

6.2.5 Significance of turbulence intensity impact

The previous test showed that turbulence intensity impacted the WTPC lifetime at one average wind speed (6 m/s) while this test analyses the significance of turbulence intensity impact on WTPC lifetime covering the range of wind turbine's operating wind speeds. To do this, 10 groups of VWSPs are applied to the wind turbine model containing 2 turbulence intensities (10% and 20%) each including 5 average wind speeds (4 m/s, 6 m/s, 8 m/s, 10 m/s and 12 m/s). The simulation results are used to calculate the logarithmic value of $MTTF_{WTPC}$ for each tested VWSP. For each group, the average and standard deviation of the logarithmic $MTTF_{WTPC}$

are calculated by equations (6.2) and (6.3) respectively. To test the significance of the WTPC lifetime difference caused by 10% and 20% TIs for the same average wind speed, the statistical confidence interval (CI) value is used. CI is calculated for the defined confidence level (z) by equation (6.4). The value of z is set to 1.96 for the confidence level of 95% which is widely accepted in scientific research. The results of the tested 10 groups of VWSPs are listed in table 6.4 where n is the number of VWSPs in each group. The significant difference in WTPC lifetime between 10% and 20% TIs for the same average wind speed is indicated by their CIs as their values should not overlap. To illustrate this, the error bar diagram is used as presented in figure 6.7. The CIs of VWSPs of average wind speeds from 4 m/s to 10 m/s show that 10% TI VWSPs produce higher WTPC lifetime than 20% TI VWSPs with a clear separation between their CIs. However, just below 12 m/s, the 10% and 20% TI WTPC lifetime intersect and the 20% TI VWSPs produce a higher WTPC lifetime than 10% TI VWSPs. The reason can be that wind turbine pitch control impacts high TI wind more than low TI which results in more regulated 20% TI VWSPs than 10% TI VWSPs. The test proves that wind turbulence intensity has a significant impact on the WTPC lifetime for most of the wind turbine operating wind speed. This test is applied to the 2L-VSC wind turbine model and in the following sections, the test will be applied to models of different control and different converter topology.

$$CI = \mu \pm z\frac{\sigma}{\sqrt{n}} \tag{6.4}$$

Table 6.4: Confidence intervals of WTPC lifetimes related to VWSP groups with 2L-VSC model

VWSP			$\ln(MTTF_{WTPC}(hr))$
$\overline{U}$ (m/s)	TI (%)	n	CI
4	10	34	8.96 ± 0.014
6		36	7.37 ± 0.009
8		36	6.07 ± 0.012
10		34	4.87 ± 0.011
12		32	4.03 ± 0.005
4	20	36	8.76 ± 0.026
6		36	7.09 ± 0.027
8		36	5.69 ± 0.025
10		35	4.54 ± 0.016
12		22	4.12 ± 0.010

6.3 Reliability analysis of 2L-VSC WTPC with DTC

The WTPC reliability analyses in the previous section demonstrated the impact of wind conditions on WTPC lifetime for the widely known converter IGBT-based, 2L-VSC topology controlled by FOC drive. WTPC manufacturers, like Hitachi ABB, utilised DTC for their WTPCs like the LV 2L-VSC ACS880 [134]. The reliability analysis in this research considers changing the control system to analyse the impact of the control strategy on WTPC lifetime. This section

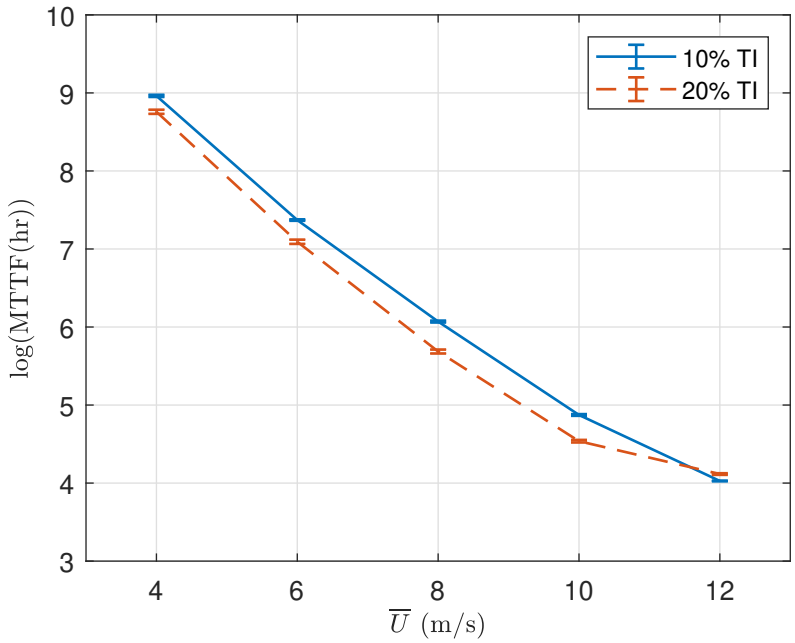

Figure 6.7: WTPC lifetime error bars related to two TI groups of VWSPs with 2L-VSC model

analyses how the WTPC reliability responds to DTC by applying constant and variable wind speeds to the DTC model which has been developed and validated in section 5.2.

6.3.1 WTPC semiconductors loading with DTC

In this simulation, constant wind speeds are applied to the DTC model to understand how the WTPC semiconductors are affected by wind speed. The WTPC's IGBT ($i1$) and diode ($d1$) lifetimes are estimated according to their junction temperature cycling by applying the Coffin-Manson Arrhenius equation (4.21). The constant wind speeds are selected ranging from wind turbine cut-in wind speed (4 m/s) to rated wind speed (12 m/s) at 1 m/s increase in each test. The lifetime estimations of $i1$ and $d1$ based on simulation results are shown in table 6.5 and their visual presentation is shown in figure 6.8.

Results discussion

The simulation results showed that WTPC semiconductors' lifetimes are reduced as wind speed increases which is expected because increasing wind speed increases the WTPC load. However, the diode showed a lower lifetime than the IGBT which can be explained as it is subjected to higher thermal loading due to the fact that most of the rectifier current passes in the diode rather than the IGBT. This test conclusion is similar to the 2L-VSC with FOC conclusion and the comparison between both models results will be discussed in section 6.4.

6.3.2 Impact of Variable wind speed on WTPC lifetime driven by DTC

The WTPC semiconductor loading analysis with constant wind speeds shows that the WTPC lifetime is impacted by increasing wind speed. However, the WTPC reliability analyses based on

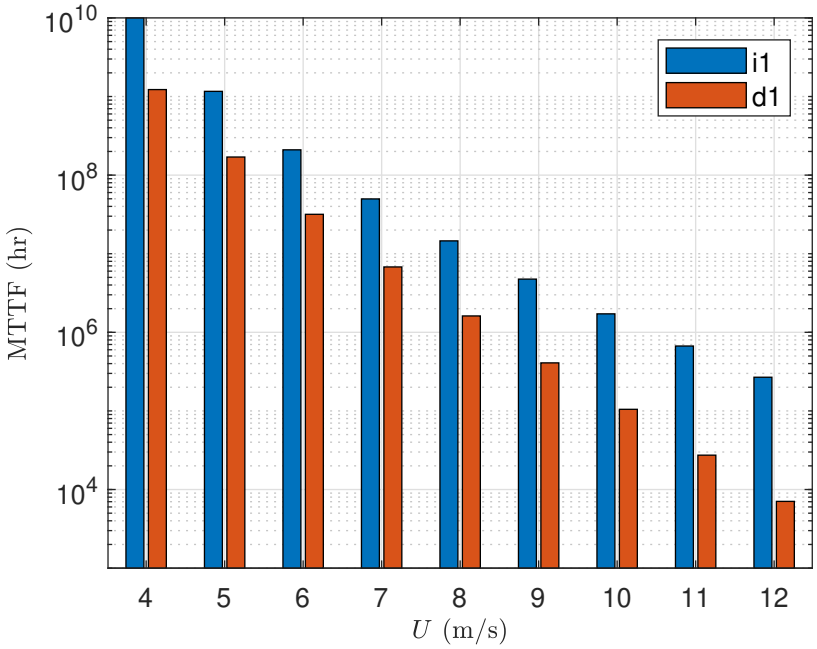

Figure 6.8: Lifetimes of WTPC IGBT and diode at constant wind speeds with 2L-VSC DTC model

realistic wind turbine operation utilise the field-recorded variable wind speed. This analysis uses a set of VWSPs to analyse the effect of the operating wind conditions on the WTPC lifetime. The VWSPs are selected to cover the modelled wind turbine operating wind speed. The same VWSPs used with the 2L-VSC model, in section 6.2.3, are used for the DTC model simulation to provide consistency and allow direct comparison between the two control systems models of the DTC and FOC.

6.3.3 Impact of average wind speed on WTPC lifetime driven

In this simulation, 230 VWSPs are input to the DTC model described in section 5.2. The selected 230 VWSPs are the same as those used with the 2L-VSC model controlled by FOC. They are recorded wind speed data from the field at 1Hz sampling frequency. Each VWSP is 10

Table 6.5: Lifetimes of WTPC at constant wind speeds with 2L-VSC DTC model

U (m/s)	$MTTF_{i1,MSC}$(hr)	$MTTF_{d1,MSC}$(hr)	$MTTF_{WTPC}$(hr)
4	$1.00\times10^{+10}$	$1.23\times10^{+9}$	$1.82\times10^{+8}$
5	$1.16\times10^{+9}$	$1.70\times10^{+8}$	$2.47\times10^{+7}$
6	$2.10\times10^{+8}$	$3.17\times10^{+7}$	$4.59\times10^{+6}$
7	$5.00\times10^{+7}$	$6.79\times10^{+6}$	$9.96\times10^{+5}$
8	$1.46\times10^{+7}$	$1.62\times10^{+6}$	$2.42\times10^{+5}$
9	$4.75\times10^{+6}$	$4.09\times10^{+5}$	$6.27\times10^{+4}$
10	$1.72\times10^{+6}$	$1.05\times10^{+5}$	$1.65\times10^{+4}$
11	$6.69\times10^{+5}$	$2.74\times10^{+4}$	$4.38\times10^{+3}$
12	$2.68\times10^{+5}$	$7.06\times10^{+3}$	$1.15\times10^{+3}$

minutes long containing 600 wind speed data. They are obtained from one year of recorded data varying in their average wind speed ($\overline{U}$) and turbulence intensity (TI) to cover a wide range of wind characteristics.

The simulations of the 230 VWSPs provide 230 WTPC lifetime results. The WTPC lifetimes are estimated based on the simulations of semiconductors' junction temperatures as explained in section 4.13. The WTPC lifetimes are demonstrated by the scatter diagram in figure 6.9. The results show a relation between the logarithm of WTPC's lifetimes and VWSPs' average wind speed ($\overline{U}$).

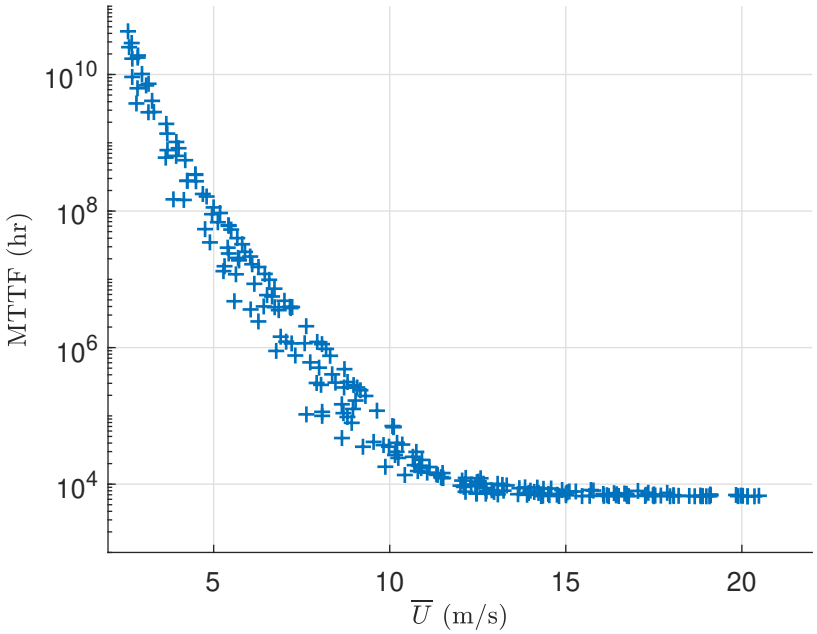

Figure 6.9: WTPC lifetimes related to 230 VWSPs with 2L-VSC DTC model

Results discussion

As average wind speed increases, the WTPC lifetime decreases until the average wind speed reaches the rated wind speed of the modelled wind turbine (12 m/s). At this speed, the wind turbine speed control implemented by the pitch control operates and keeps the rotational speed regulated at its rated value. Therefore, when the wind speed increases above the rated wind speed the WTPC loading will not be affected and therefore the WTPC lifetime approaches a fixed value that appears as a horizontal line in the lifetime scatter diagram in figure 6.9. The scatter diagram also shows that WTPC lifetime varies even with similar VWSP average wind speeds indicating that VWSPs with the same average wind speed can produce different WTPC lifetimes and that is due to varying wind speeds within the VWSP in similar results appeared with previous tests of 2L-VSC with FOC. Similarly, wind turbulence intensity is considered to analyse these differences in WTPC lifetimes. The turbulence intensity of the 230 VWSPs used in the simulation ranges from 5.6% to 30.5%. The scatter diagram is represented with VWSP categorised according to their TI, $\leq$ 20% and $>$ 20%. The scatter in figure 6.10 shows that lower turbulence VWSPs (TI $\leq$ 20%) achieved higher WTPC lifetime than higher turbulence

VWSPs. However, there are overlaps among lifetime results which require further analysis to illustrate the impact of turbulence intensity on WTPC lifetime.

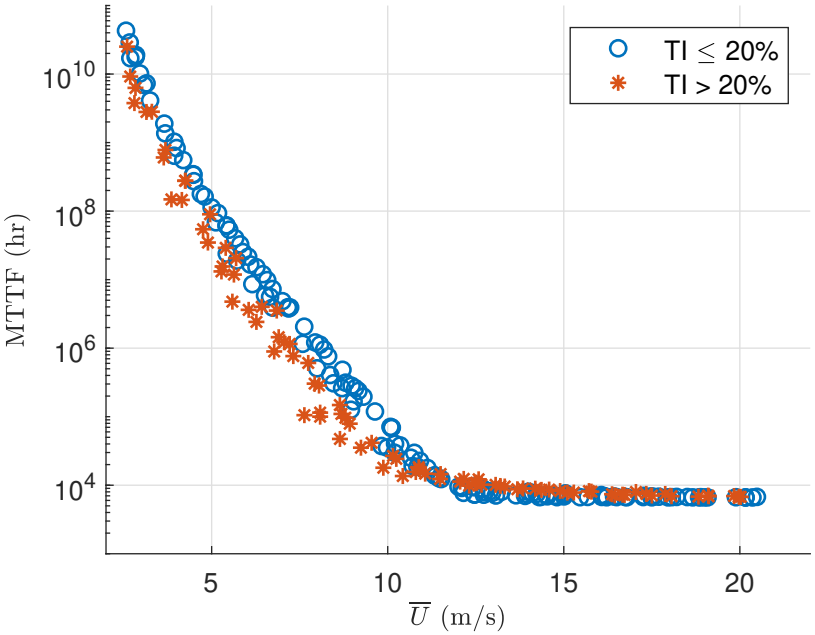

Figure 6.10: Effect of VWSP turbulence intensity on WTPC lifetime with 2L-VSC DTC model

6.3.4 Impact of wind turbulence intensity on WTPC lifetime

In this simulation, the wind turbine model is input with four groups of VWSPs having the same average wind speed (6 m/s) to eliminate its impact on the WTPC lifetime but each group has a defined range of VWSP turbulence intensity. The selected four groups of VWSPs have turbulence intensities of 10%, 15%, 20%, and 25%. Each group contains n number of VWSPs applied to the wind turbine model for simulating WTPC lifetimes related to each VWSP. The logarithmic values of the estimated WTPC's lifetimes are obtained for all results and presented by histogram shown in figure 6.5. The mean (μ) and standard deviation (σ) of the each group's results ($\log(MTTF_{WTPC})$ are calculated by equations (6.2) and (6.3) respectively. The groups' mean and standard deviation are listed in table 6.6.

Table 6.6: WTPC lifetime μ and σ of the four TI groups speed simulated with DTC model

VWSP			$\log(MTTF_{WTPC}(hr))$	
$\overline{U}$(m/s)	TI(%)	n	μ	σ
6 ± 0.05	10 ± 0.5	36	7.37	0.027
6 ± 0.05	15 ± 0.5	34	7.27	0.055
6 ± 0.05	20 ± 0.5	35	7.09	0.074
6 ± 0.05	25 ± 0.5	34	6.80	0.166

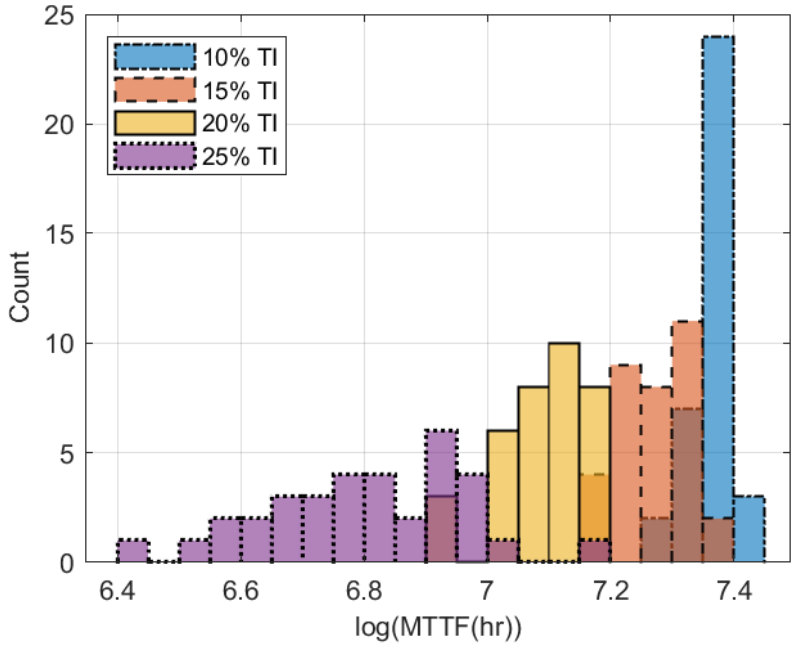

Figure 6.11: Histogram of WTPC lifetimes related to 4 turbulence intensity groups of VWSPs with 2L-VSC DTC model

Results discussion

The histogram of the four groups of VWSPs in figure 6.11 shows that the lifetime results of each VWSP group are distinct which indicates that VWSPs impacted the WTPC lifetime differently according to their turbulence intensities. However, the histogram does not show a clear separation between the four groups' results. To evaluate the differences among the four groups' results according to their turbulence intensities, it is required to analyse the distribution of the results. Again, the Anderson-Darling test was applied to the results of each group and showed that they were all normally distributed. Therefore, each group's results can be represented by a normal distribution fitting curve. The fitting curve of each group is defined by the mean(μ) and standard deviation (σ) of the results calculated by equations (6.2) and (6.3) respectively. Table 6.6 lists the four groups of VWSPs where $\overline{U}$ is the VWSPs average wind speed range, TI is the VWSPs turbulence intensity range, n is the number of VWSPs in each group, and μ and σ are the mean and standard deviation of the logarithmic of WTPC lifetimes respectively. The results from the table 6.6, μ and σ, are used to generate the distribution fitting cures for the four turbulence intensity groups as shown in figure 6.12. The fitting curves show that the lowest TI group (10%) develops the longest WTPC lifetime ($\mu = 7.37$) with a narrow distribution curve ($\sigma = 0.027$) while the highest TI group (25%) develops the shortest WTPC lifetime ($\mu = 6.8$) with the widest distribution curve ($\sigma = 0.166$). Accordingly, this confirms the earlier finding for 2L-VSC FOC that high turbulence intensity wind reduces the WTPC lifetime and makes it difficult to predict compared to the low turbulence intensity wind.

6.3.5 Significance of turbulence intensity impact on WTPC lifetime with DTC

The previous analysis shows that wind turbulence intensity impacted the WTPC's lifetime for one selected average wind speed (6 m/s), however, this simulation shows the significant impact of turbulence intensity over the range of wind turbine operating wind speed. Ten groups of VWSPs are applied to the DTC model for WTPC lifetime estimation. The groups represented 2 turbulence intensities, 10% and 20%, and 5 wind speeds which cover the wind turbine variable wind speed range, 4 m/s, 6 m/s, 8 m/s, 10 m/s, and 12 m/s. The simulation results are used to calculate the logarithmic of WTPC lifetime for each VWSP. To evaluate the significance of the WTPC's lifetime differences between 10% and 20% groups, the statistical confidence interval (CI) technique is used. CI is calculated for the defined confidence level (z) by equation (6.4). Setting z equal to 1.96 for a confidence level of 95% which is widely accepted in scientific research. Table 6.7 lists the results of the tested 10 groups of VWSPs. The significant difference in WTPC lifetime between 10% and 20% TIs for the same average wind speed is indicated by their CIs as their values should not overlap. To illustrate this, the error bar diagram is used as shown in figure 6.13. The CIs of VWSPs of average wind speeds from 4 m/s to 10 m/s show that 10% TI VWSPs produce higher WTPC lifetime than 20% TI. The CI's error bars of 10% TI and 20% TI show a clear separation. However, the two groups intersect around the rated wind speed (12 m/s) and higher lifetime produced by the 20% TI than 10% TI VWSPs in a similar phenomenon appeared in the 2L-VSC with FOC. The reason of that is wind turbine pitch control regulates the rotating speed more effectively at higher turbulence intensity (20%) which reflects in more WTPC lifetime compared to 10% TI. The test proves that wind TI has a significant impact on the WTPC lifetime controlled by DTC for most of the wind turbine operating wind speeds in a similar conclusion for the WTPC controlled by FOC as shown in section 6.2.5.

Table 6.7: Confidence intervals of WTPC lifetimes groups for DTC model

VWSP			$\log(MTTF_{WTPC}(hr))$
$\overline{U}$ (m/s)	TI (%)	n	CI
4	10	34	8.96 ± 0.014
6		36	7.37 ± 0.009
8		36	6.06 ± 0.012
10		34	4.85 ± 0.011
12		32	3.99 ± 0.005
4	20	36	8.76 ± 0.026
6		36	7.09 ± 0.027
8		36	5.67 ± 0.026
10		35	4.50 ± 0.017
12		22	4.07 ± 0.010

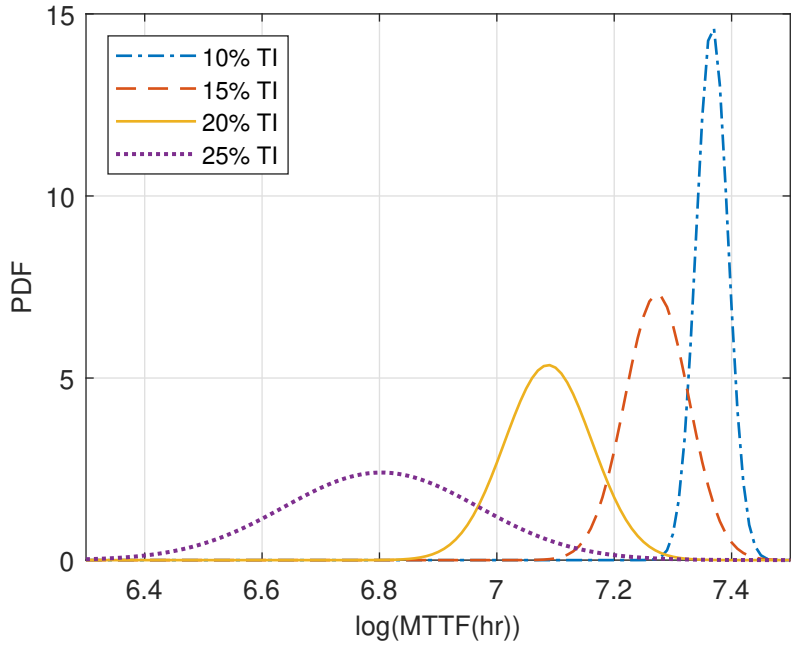

Figure 6.12: Distribution fitting curves of TI groups for 2L-VSC DTC model

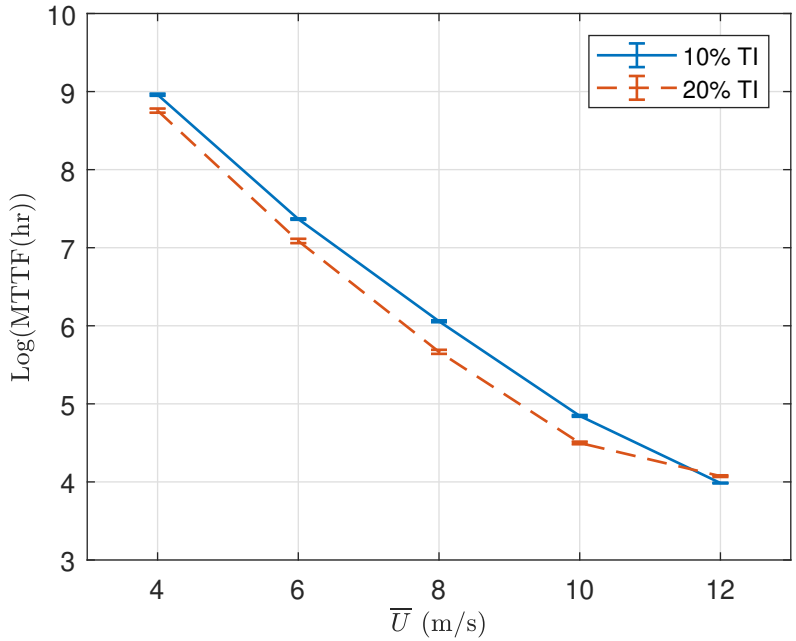

Figure 6.13: Error bars represent MSC's lifetime CI for 10% and 20% TIs VWSPs with 2L-VSC DTC model

6.4 Reliability comparison between DTC and FOC

The reliability analysis of the two models, 2L-VSC controlled by FOC and 2L-VSC controlled by DTC, revealed the impact of average wind speed and turbulence intensity on the WTPC lifetime. However, the WTPC reliability differences between the two control systems must be highlighted to analyse the impact of using the control system on the WTPC lifetime. The relia-

bility comparison considers the operation condition to demonstrate the interaction of WTPC's control, wind speed, and turbulence intensity on WTPC's lifetime.

6.4.1 Reliability comparison based on constant wind speeds

Although the WTPC lifetime simulations based on constant wind speeds do not reflect the practical operation of a wind turbine, they can show how the thermal stress in the WTPC semiconductors is affected by the control strategy at different wind speeds. In this analysis, the wind turbine model simulation runs for 200 seconds with a constant wind speed input. The junction temperature output of the first 164 seconds is neglected to allow the semiconductors and their heatsink to reach their balance temperatures. The simulation output of the following 36 seconds is recorded for the lifetime analysis. This test is implemented for wind speeds of the wind turbine variable wind speed range, from 4 m/s to 12 m/s, as for higher wind speeds the blade pitch control keeps the rotating speed at its rated value. For each simulated wind speed, the lifetime of the WTPC IGBT and diode are estimated for both FOC and DTC models. To evaluate the effect of the wind turbine control system on the WTPC reliability, the lifetime ratio (LTR) is introduced. LTR is defined as the ratio of the modified system lifetime to the original system lifetime. In this section, LTR_{DTC} is the lifetime ratio of WTPC driven by DTC to the lifetime of WTPC driven by FOC. The LTR of $i1$ and $d1$ for 2L-VSC DTC model is calculated by equations (6.5) and (6.6) respectively. The results of the WTPC's IGBT and diode lifetimes are shown in table 6.8. The WTPC lifetime is calculated for both DTC and FOC wind turbine models considering their IGBT and diode failure rates as in equation (4.31). Table 6.5 shows the LTR_{DTC} related to constant wind speeds. Figure 6.14 shows the LTR_{i1}, LTR_{d1}, and LTR_{MSC} for constant wind speeds.

$$LTR_{DTC,i1} = \frac{MTTF_{i1,DTC}}{MTTF_{i1,FOC}} \tag{6.5}$$

$$LTR_{DTC,d1} = \frac{MTTF_{d1,DTC}}{MTTF_{d1,FOC}} \tag{6.6}$$

$$LTR_{DTC} = \frac{MTTF_{WTPC,DTC}}{MTTF_{WTPC,FOC}} \tag{6.7}$$

Table 6.8: Lifetime of WTPC semiconductors driven by FOC and DTC at constant wind speeds

U (m/s)	$MTTF_{i1}$(hr)		$LTR_{DTC,i1}$	$MTTF_{d1}$(hr)		$LTR_{DTC,d1}$
	DTC	FOC		DTC	FOC	
4	$1.00\times10^{+10}$	$9.73\times10^{+9}$	1.03	$1.23\times10^{+9}$	$1.23\times10^{+9}$	0.99
6	$2.10\times10^{+8}$	$2.13\times10^{+8}$	0.99	$3.17\times10^{+7}$	$3.20\times10^{+8}$	0.99
8	$1.64\times10^{+7}$	$1.50\times10^{+7}$	0.97	$1.62\times10^{+6}$	$1.67\times10^{+6}$	0.97
10	$1.72\times10^{+6}$	$1.87\times10^{+6}$	0.92	$1.05\times10^{+5}$	$1.10\times10^{+5}$	0.95
12	$2.68\times10^{+5}$	$3.41\times10^{+5}$	0.79	$7.06\times10^{+3}$	$7.81\times10^{+3}$	0.91

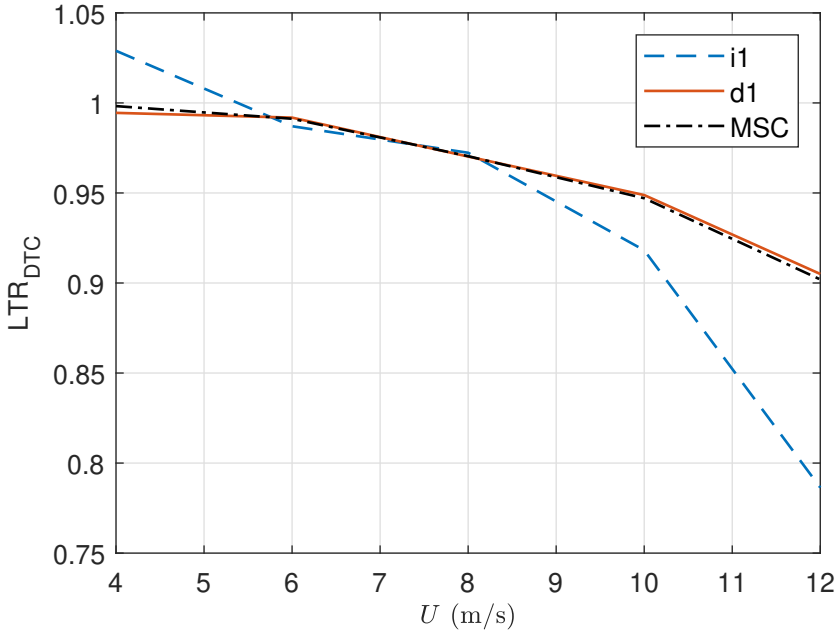

Figure 6.14: Lifetime ratio of DTC 2L-VSC to FOC 2L-VSC at constant wind speeds

Results discussion

This simulation shows that MSC's IGBT and diode lifetimes are affected by the control system differently with increasing wind speed. At cut-in wind speed (4 m/s) both LTR_{i1} and LTR_{d1} were around 1.00 which means that the control system does not affect their lifetimes. However, as wind speed increases LTR_{i1} drops significantly to 0.79 and LTR_{d1} drops to 0.91 at rated wind speed (12 m/s) which means that IGBT and diode have a shorter lifetime at higher wind speed when controlled by DTC. Accordingly, LTR_{MSC} drops as well following the $LTRd1$ to 0.9 at rated wind speed. This is because MSC's lifetime is influenced by the diode lifetime since the diode's failure rate is larger than the IGBT failure rate. This test shows MSC's lifetime is affected by the interaction between wind speed and the control system. However, more realistic results can be concluded based on the variable wind speed test.

6.4.2 Reliability comparison based on variable wind speed

The previous analysis shows how MSC's IGBT and diode are loaded differently due to using different control systems with constant wind speed tests. However, for realistic results, the

Table 6.9: Lifetime of WTPC driven by FOC and DTC at constant wind speeds

U (m/s)	$MTTF_{MSC,DTC}$(hr)	$MTTF_{MSC,FOC}$(hr)	LTR_{DTC}
4	$1.82\times10^{+8}$	$1.82\times10^{+8}$	1.00
6	$4.59\times10^{+6}$	$4.63\times10^{+6}$	0.99
8	$2.42\times10^{+5}$	$2.50\times10^{+5}$	0.97
10	$1.65\times10^{+4}$	$1.74\times10^{+4}$	0.95
12	$1.15\times10^{+3}$	$1.27\times10^{+3}$	0.90

comparison between two wind turbines varies in their control systems, one with FOC and the other with DTC would be based on the variable wind speed test. In this test, 229 VWSPs are used as input for both models, FOC and DTC. The VWSPs are selected from a year-long field measured wind speeds at 1 Hz sampling frequency. Each VWSP is 10 minutes long containing 600 wind speed measurements. The simulation results of both models, DTC and FOC, provide two MSC lifetime values for each VWSP.

To compare the lifetime results of DTC and FOC, LTR_{DTC} is calculated for each VWSP. The LTR_{DTC} results are illustrated against the VWSP average wind speeds ($\overline{U}$) in a scatter diagram shown in figure 6.15. The trend of the MSC lifetime points in figure 6.15 is similar to the constant wind speed results shown in figure 6.14. At wind turbine cut-in wind speed the LTR_{DTC} is around 1.00 but it drops to 0.90 at rated wind speed (12 m/s). For wind speeds above 12 m/s, LTR_{DTC} stops decreasing and stays around 0.9 because the pitch control regulates the rotating speed when the wind speed is higher than the rated value.

The LTR_{DTC} points in figure 6.15 vary for the same average wind speed and this is because VWSPs may have the same $\overline{U}$ but they have different TI. To analyse that, a new scatted diagram is generated highlighting two groups of the LTR_{DTC} based on the VWSPs TI, $\leq 10\%$ and $> 25\%$. The scatter diagram is shown in figure 6.16 where the high TI VWSPs show lower LTR_{DTC} bellow rated wind speed and slightly higher LTR_{DTC} above rated wind speed. This indicates that the lifetime of DTC WTPC is more affected by wind turbulence intensity than FOC WTPC. This simulation showed that the wind turbine control system has an impact on the WTPC mainly at higher wind speeds or with higher turbulence intensities.

The WTPC lifetime reduction showed in this research was limited to 90% however, larger wind turbines, higher WTPC's rated power, or different control parameters can produce different lifetime ratios. An example of that is shown in [135] where a similar WTPC reliability comparison between FOC and DTC showed that the lifetime ratio reaches 85% at rated wind speed. However, the paper modelled different power WTPC. Therefore, it is worth considering the WTPC control system when analysing the WTPC reliability.

6.5 Reliability Analysis of 3L-NPC WTPC

The WTPC reliability analysis of the more complex 3L-NPC WTPC is part of this research to answer the second research question "How can the reliability of more complex converter topologies in wind turbine applications be estimated from knowledge of 2L-VSC systems?" Here, the analysis and modelling approach that has been demonstrated for 2L-VSC WTPCs can be applied with confidence to another converter type. Reliability analysis of 3L-NPC WTPC provides a further step toward understanding WTPC reliability. It also provides a reliability comparison between the two converter topologies, 2L-VSC and 3L-NPC, in wind turbine applications. This comparison can be utilised for cost analysis and in deciding which topology is better to install at a particular site depending on the wind characteristics of that specific site. The MV model presented in section 5.4 is utilised for the WTPC reliability analysis in this section.

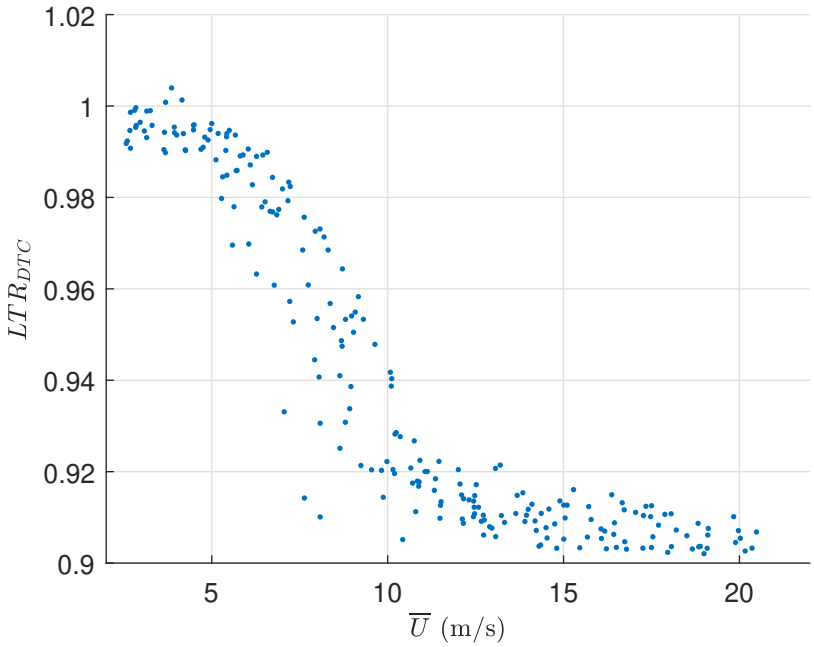

Figure 6.15: WTPC lifetime ratio of DTC 2L-VSC to FOC 2L-VSC vs average wind speed

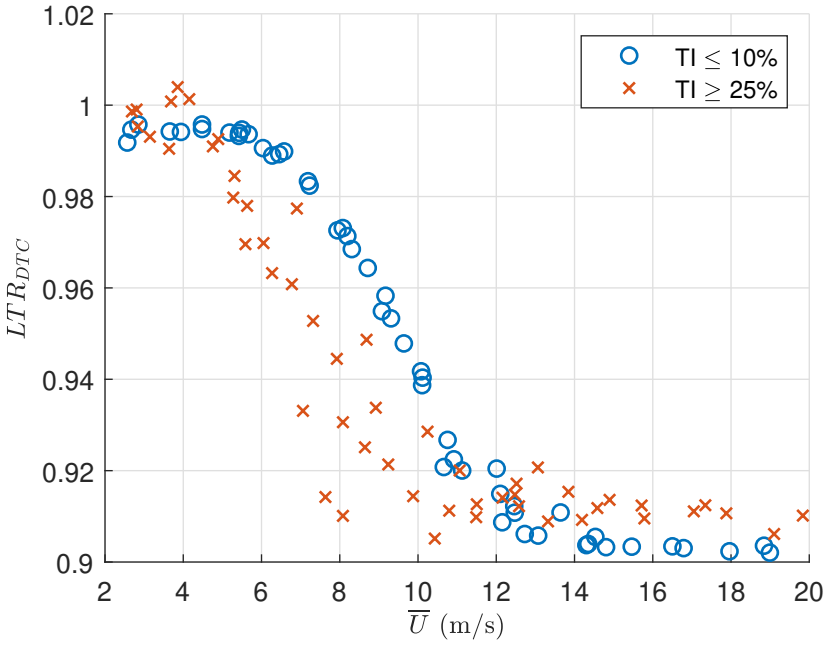

Figure 6.16: Effect of turbulence intensity on LTR_{DTC}

6.5.1 Analysing WTPC's semiconductors lifetime with constant wind speeds

The WTPC semiconductor loading can be analysed by applying constant wind speeds to the wind turbine model. The 3L-NPC converter has five semiconductors in each converter arm: i1, d1, i2, d2, and d5 as shown in figure 5.9. During the operation of the wind turbine, the WTPC semiconductors withstand increase and fluctuation in their junction temperature as shown in figure 5.15 and figure 5.16 for MSC and GSC semiconductors respectively.

To analyse the WTPC semiconductors loading, a range of constant wind speeds covering the wind turbine's variable speed range, from 4 m/s to 12 m/s, are used in the simulation. The simulation results of WTPC semiconductors' junction temperatures are used to estimate their lifetimes by applying the Coffin-Manson Arrhenius equation. This analysis is applied to MSC and GSC to analyse their influence on the WTPC lifetime. The lifetimes of MSC and GSC are calculated considering their semiconductors' lifetimes by equations (6.8) and (6.9) respectively. The semiconductors' estimated lifetimes are listed in tables 6.10 and 6.11 for MSC and GSC respectively while the bar diagrams in figure 6.17 present them visually.

$$MTTF_{MSC} = \frac{1}{6}\left(\frac{1}{MTTF_{i1,MSC}} + \frac{1}{MTTF_{d1,MSC}} + \frac{1}{MTTF_{i2,MSC}} + \frac{1}{MTTF_{d2,MSC}} + \frac{1}{MTTF_{d5,MSC}}\right)^{-1} \tag{6.8}$$

$$MTTF_{GSC} = \frac{1}{6}\left(\frac{1}{MTTF_{i1,GSC}} + \frac{1}{MTTF_{d1,GSC}} + \frac{1}{MTTF_{i2,GSC}} + \frac{1}{MTTF_{d2,GSC}} + \frac{1}{MTTF_{d5,GSC}}\right)^{-1} \tag{6.9}$$

Table 6.10: Semiconductors' MTTF of 3L-NPC MSC at constant wind speeds

	MTTF (hr)				
U (m/s)	i1	d1	i2	d2	d5
4	inf	$4.87\times10^{+9}$	$2.48\times10^{+9}$	$2.81\times10^{+12}$	$1.46\times10^{+10}$
5	inf	$6.85\times10^{+8}$	$3.49\times10^{+8}$	$1.11\times10^{+11}$	$2.35\times10^{+9}$
6	inf	$1.20\times10^{+8}$	$6.85\times10^{+7}$	$7.71\times10^{+9}$	$5.53\times10^{+8}$
7	inf	$2.35\times10^{+7}$	$1.79\times10^{+7}$	$8.21\times10^{+8}$	$1.70\times10^{+8}$
8	inf	$5.14\times10^{+6}$	$6.39\times10^{+6}$	$1.09\times10^{+8}$	$8.25\times10^{+7}$
9	inf	$1.13\times10^{+6}$	$2.63\times10^{+6}$	$1.66\times10^{+7}$	$6.57\times10^{+7}$
10	inf	$2.65\times10^{+5}$	$1.15\times10^{+6}$	$2.86\times10^{+6}$	$6.53\times10^{+7}$
11	inf	$6.23\times10^{+4}$	$6.02\times10^{+5}$	$5.54\times10^{+5}$	$7.73\times10^{+7}$
12	inf	$1.48\times10^{+4}$	$3.69\times10^{+5}$	$1.11\times10^{+5}$	$1.16\times10^{+8}$

Results discussion

Analysing the WTPC semiconductors against constant wind speeds shows how their lifetimes are affected by wind speed. Unlike the 2L-VSC where both IGBT and diode have nearly a linear relationship between wind speed and the logarithmic MTTF, the 3L-NPC WTPC semiconductors show different lifetime impacts with increasing wind speed. The logarithmic values of MTTF of d1 and d2 decrease nearly linearly as wind speed increases because their current is related to the converter load. Both i2 and d5 show nonlinear relationships between their logarithmic lifetimes and wind speed. On the other hand, GSC semiconductors show linear relationships between their logarithmic MTTF and wind speed. However, only i1, i2, and d5 appeared in the lifetime

diagram shown in figure 6.18 for wind speeds 8 m/s and higher as the rest of the semiconductors have very large number lifetimes denoted by 'inf' in table 6.11 and shown as long bars in figure 6.18. This simulation shows that 3L-NPC semiconductors' lifetimes were impacted differently by increasing wind speed compared to the 2L-VSC semiconductors. This is because 3L-NPC semiconductors do not share the converter load equally or at a fixed ratio due to the converter operation principle.

6.5.2 Considering MSC for WTPC reliability analysis

The WTPC lifetime is calculated considering the lifetimes of both MSC and GSC by equation (5.4). Table 6.12 lists the lifetimes of MSC, GSC, and WTPC related to constant wind speeds from 4 m/s to 12 m/s. Because MSC shows considerably lower lifetimes than GSC, it impacted the WTPC lifetime more than GSC. This can be seen from the results in table 6.12 and figure 6.18 where the WTPC lifetimes are approximately equal to MSC lifetimes.

$$MTTF_{WTPC} = \left(\frac{1}{MTTF_{MSC}} + \frac{1}{MTTF_{GSC}} \right)^{-1} \tag{6.10}$$

Table 6.11: Semiconductors' MTTF of 3L-NPC GSC at constant wind speeds

	MTTF (hr)				
U (m/s)	i1	d1	i2	d2	d5
4	inf	inf	inf	inf	inf
5	inf	inf	inf	inf	inf
6	inf	inf	inf	inf	inf
7	inf	inf	inf	inf	inf
8	$2.34\times10^{+11}$	inf	$2.25\times10^{+11}$	inf	inf
9	$2.67\times10^{+10}$	inf	$2.65\times10^{+10}$	inf	$2.25\times10^{+12}$
10	$3.54\times10^{+9}$	inf	$3.25\times10^{+9}$	inf	$1.11\times10^{+11}$
11	$4.72\times10^{+8}$	inf	$3.73\times10^{+8}$	inf	$1.96\times10^{+10}$
12	$8.76\times10^{+7}$	inf	$5.82\times10^{+7}$	inf	$4.40\times10^{+9}$

Table 6.12: MTTFs of MSC, GSC, and WTPC of 3L-NPC topology at constant wind speeds

	MTTF (hr)		
U (m/s)	MSC	GSC	WTPC
4	$2.46\times10^{+8}$	inf	$2.46\times10^{+8}$
5	$3.50\times10^{+7}$	inf	$3.50\times10^{+7}$
6	$6.69\times10^{+6}$	inf	$6.69\times10^{+6}$
7	$1.58\times10^{+6}$	inf	$1.58\times10^{+6}$
8	$4.48\times10^{+5}$	$1.91\times10^{+10}$	$4.48\times10^{+5}$
9	$1.24\times10^{+5}$	$2.20\times10^{+9}$	$1.24\times10^{+5}$
10	$3.32\times10^{+4}$	$2.78\times10^{+8}$	$3.32\times10^{+4}$
11	$8.53\times10^{+3}$	$3.44\times10^{+7}$	$8.53\times10^{+3}$
12	$2.10\times10^{+3}$	$3.78\times10^{+6}$	$2.10\times10^{+3}$

(a) MSC semiconductors

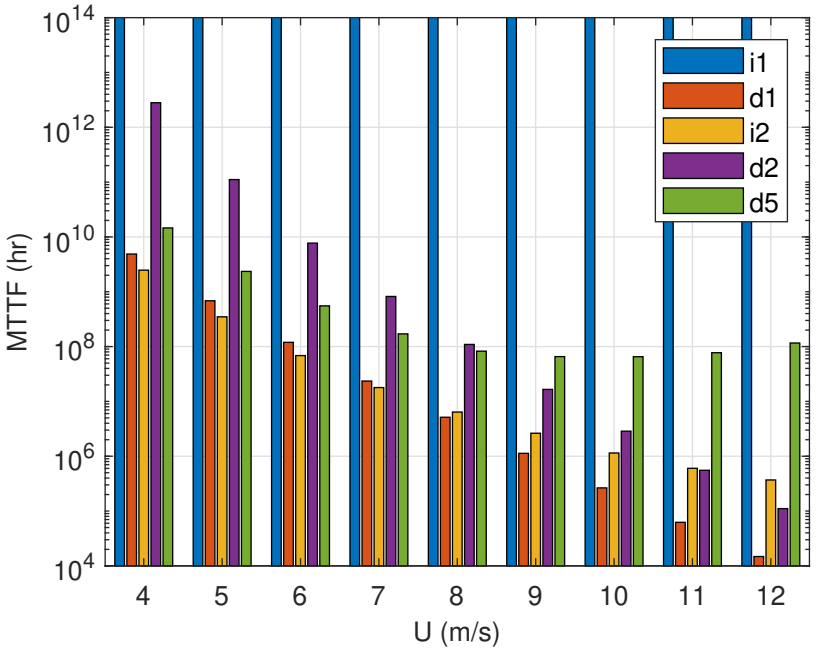

(b) GSC semiconductors

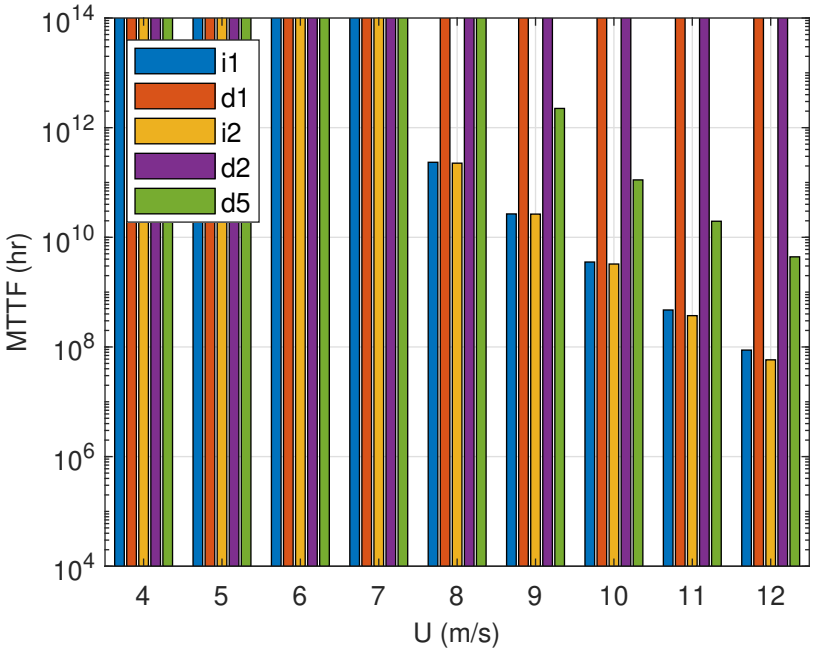

Figure 6.17: Lifetimes of IGBTs and diodes in 3L-NPC MSC (a) and 3L-NPC GSC (b) at constant wind speeds

6.5.3 Impact of variable wind speed on WTPC lifetime

WTPC lifetime estimation based on variable wind speed reflects the realistic operation of the wind turbine. In this simulation, the set of 230 VWSPs is used to analyse the impact of average wind speed on the WTPC lifetime. This set contains the same VWSPs used with 2L-VSC in section 6.2. The VWSPs are field-measured wind speeds measured at a 1 Hz sampling rate. Each

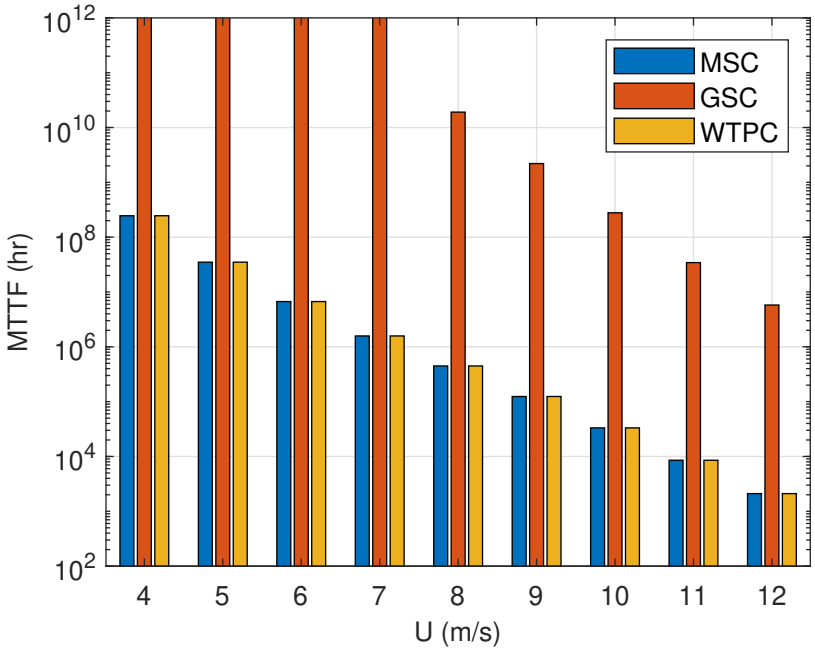

Figure 6.18: Lifetimes of MSC, GSC, and WTPC in 3L-NPC model with constant wind speeds

VWSP is 10 minutes in duration containing 600 wind speed data points. The simulation of the 3L-NPC model provides the WTPC semiconductors' junction temperature cycles which are used to estimate their lifetimes. The WTPC lifetime is estimated considering the lifetimes of all the semiconductors in the circuit. The logarithmic values of the WTPC lifetimes $MTT_{WTPC,3L}$ are calculated and presented in a scatter diagram against VWSP average wind speed $\overline{U}$ as shown in figure 6.19.

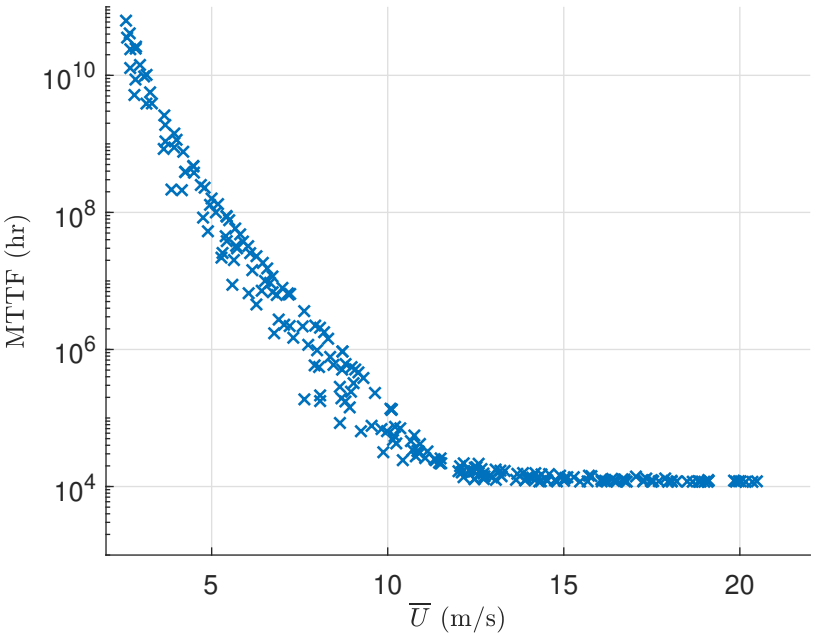

Figure 6.19: WTPC lifetime with variable wind speed with 3L-NPC model

Results discussion

The results show that as the average wind speed increases the WTPC lifetime decreases in a nearly linear relationship until the average wind speed reaches the wind turbine's rated wind speed (12 m/s) where the logarithm of $MTTF_{WTPC,3L}$ does not decrease further and that is because the pitch control keeps the wind turbine rotating speed regulated when wind speed goes higher than the rated value (12 m/s). The results show a variation in $MTTF_{WTPC,3L}$ for the same $\overline{U}$ and that is because VWSPs vary in their wind speed fluctuations even when they have the same $\overline{U}$. Wind speed fluctuations within the VWSP are expressed by the turbulence intensity of the VWSP. The 230 VWSPs used in the previous simulation cover a range of average wind speeds (4 m/s to 25 m/s) and turbulence intensities (5% to 30%).

To analyse the impact of VWSP turbulence intensity, the results of the previous simulation shown in figure 6.19 are split into two groups, $\leq$ 20% and $>$ 20% and represented in a new scatter diagram shown in figure 6.20. The visual inspection of the results shows that VWSPs with higher TI have shorter lifetimes than the VWSPs with lower TI. This indicates that VWSP TI has an impact on WTPC lifetime. To analyse this impact, further simulations are applied. The next section analyses the impact of VWSP turbulence intensity on $MTTF_{WTPC,3L}$.

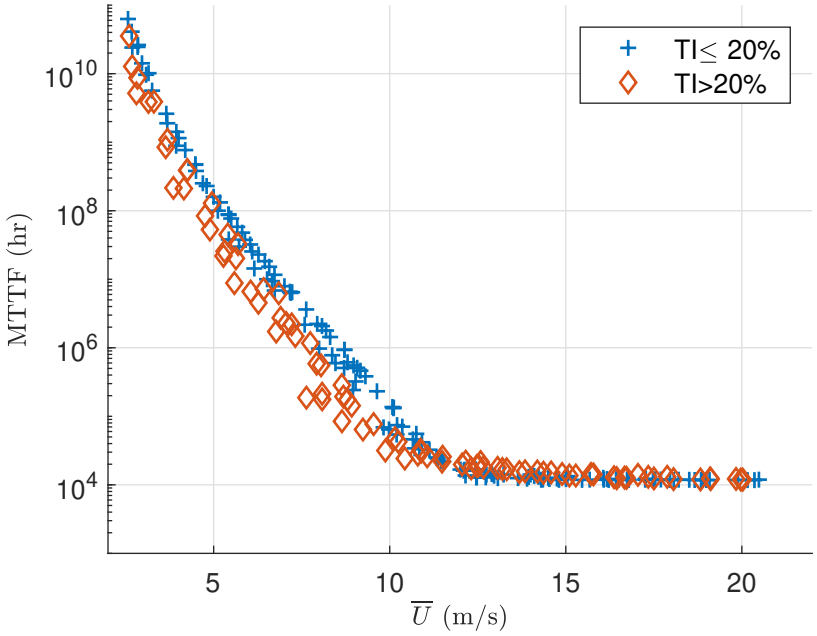

Figure 6.20: Effect of VWSP turbulence intensity on WTPC lifetime with 3L-NPC model

6.5.4 Impact of wind turbulence intensity on WTPC lifetime

To analyse the impact of VWSPs' turbulence intensities on the WTPC lifetime without interfering with the effect of average wind speed, four groups of VWSPs are selected for this analysis where the average wind speed of all VWSPs is 6 m/s so the impact of average wind speed is minimised. Each group has a selected n number of VWSPs of a defined turbulence intensity so the lifetime can be analysed based on the variation of turbulence intensity among the four

groups. The simulation results of each VWSP are used to calculate the corresponding logarithm of WTPC lifetime ($\ln(MTTF_{WTPC})$). The results are visually presented by a histogram diagram in figure 6.21 which shows that the WTPC lifetimes of each group are accumulated together however there is no clear separation among the groups' results. The distribution type of the results is required to be identified to apply the proper statistical tools. Similar to the analysis of 2L-VSC, the AD test is applied to test whether or not the data is normally distributed. The AD test shows that the results of each group are normally distributed. Therefore, a normal distribution curve can represent the distribution of each group having the same mean and standard deviation of the results. The mean (μ) and standard deviation (σ) of $\ln(MTTF_{WTPC})$ are calculated by equations (6.2) and (6.3) respectively. The μ and σ of the turbulence intensity groups are shown in table 6.13. Accordingly, four distribution curves are shown in figure 6.22 representing the four turbulence intensity groups of VWSPs.

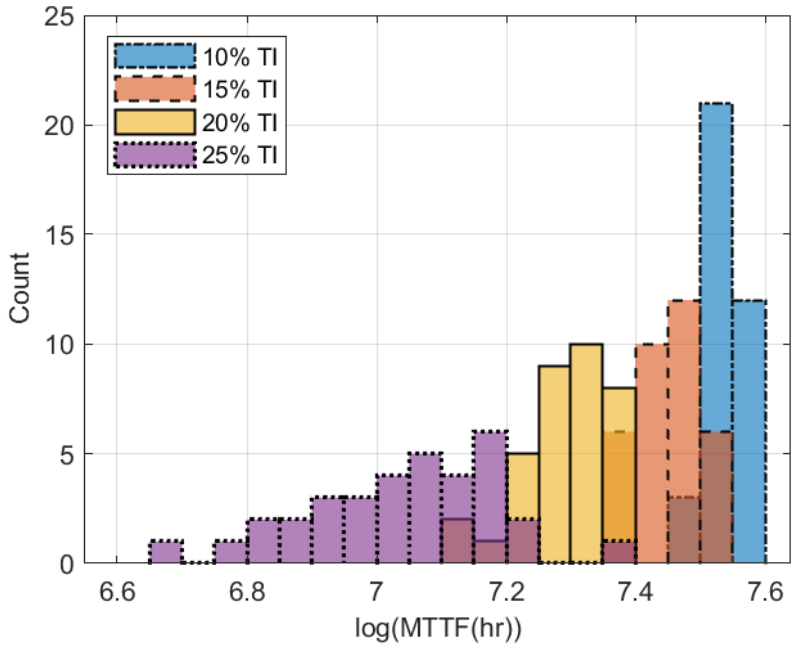

Figure 6.21: Histogram of WTPC lifetimes related to 4 turbulence intensity groups of VWSPs with 3L-NPC model

Table 6.13: Average and standard deviation of four turbulence intensity groups lifetimes with 3L-NPC model

VWSP			$\log(MTTF_{WTPC}(hr))$	
$\overline{U}$(m/s)	TI(%)	n	μ	σ
6 ± 0.05	10 ± 0.5	36	7.54	0.025
6 ± 0.05	15 ± 0.5	34	7.46	0.048
6 ± 0.05	20 ± 0.5	35	7.29	0.064
6 ± 0.05	25 ± 0.5	34	7.04	0.147

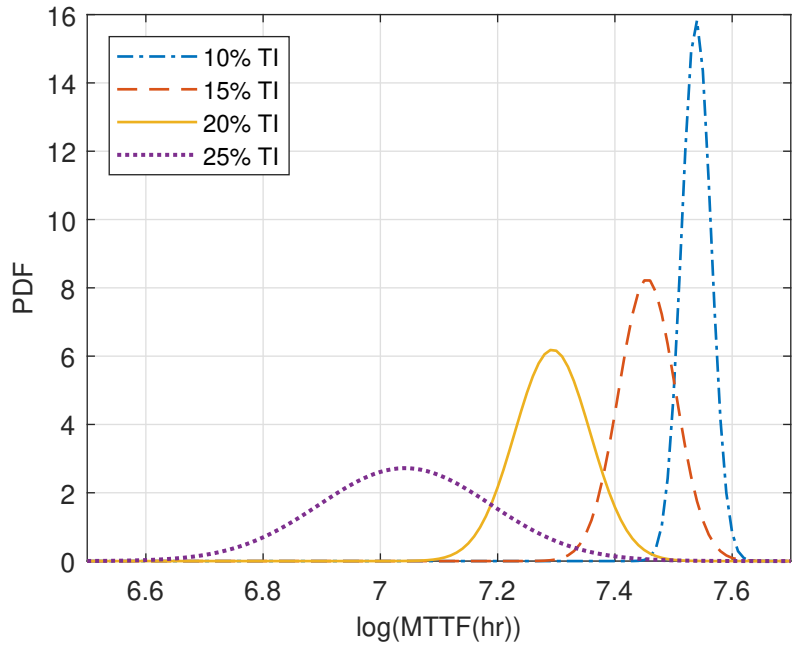

Figure 6.22: Distribution fitting curves of TI groups with 3L-NPC model

Results discussion

The four groups' lifetime results show that the lifetime mean of each group decreases as the group turbulence intensity increases. Furthermore, the lifetime standard deviation of each group increases as the group turbulence intensity increases. This can be seen clearly in figure 6.22 as the lifetime distribution is wider when the group's turbulence intensity is higher. This analysis concluded that lower turbulence intensity wind causes longer and more predictable WTPC lifetime while high turbulence wind causes shorter and more difficult to predict WTPC lifetime.

6.5.5 Significant impact of turbulence intensity on WTPC lifetime

The previous analysis showed that wind turbulence intensity impacts the WTPC's lifetime for one average wind speed (6 m/s). However, this analysis shows the significance of turbulence intensity impact on WTPC lifetime for wind speeds covering the wind turbine's variable wind speed range. Ten groups of VWSPs are used to simulate WTPC lifetime where they cover 2 turbulence intensities of 10% and 20% with 5 average wind speeds, 4 m/s, 6 m/s, 8 m/s, 10 m/s, and 12 m/s. The VWSPs are selected from a year-long field-measured wind speed data sampled at 1 Hz. Each VWSP is 10 minutes in duration containing 600 wind speed data points. The number of VWSPs in each group (n) is selected based on the availability to satisfy the required $\overline{U}$ and TI. The model simulation outputs were used to calculate the logarithm of $MTTF_{WTPC,3L}$ corresponding to each VWSP. The $\ln(MTTF_{WTPC,3L})$ values of each group appeared to have a normal distribution after testing them by AD test. The mean and standard deviation of $\ln(MTTF_{WTPC,3L})$ are calculated for each group by equations (6.2) and (6.3) respectively.

To check the statistical significance difference between 10% and 20% groups' WTPC lifetimes, the statistical confidence interval (CI) method is used. CI is calculated for the defined confidence

level (z) by equation (6.4). As in previous tests, the value of z is set to 1.96 for a confidence level of 95% as this value is widely accepted in scientific research. Table 6.14 lists the CIs of the tested 10 groups of VWSPs. The significant difference in WTPC lifetime between 10% and 20% turbulence intensities for the same average wind speed is indicated by their CIs as their values should not overlap. To illustrate this visually, the error bar diagram is used as shown in figure 6.23.

Table 6.14: Confidence intervals of TI groups with 3L-NPC model

VWSP			$\log(MTTF_{WTPC}(hr))$
$\overline{U}$ (m/s)	TI (%)	n	CI
4	10	34	9.10 ± 0.014
6		36	7.54 ± 0.008
8		36	6.32 ± 0.011
10		34	5.13 ± 0.012
12		32	4.23 ± 0.005
4	20	36	8.90 ± 0.026
6		35	7.29 ± 0.021
8		36	5.95 ± 0.027
10		35	4.75 ± 0.017
12		22	4.32 ± 0.010

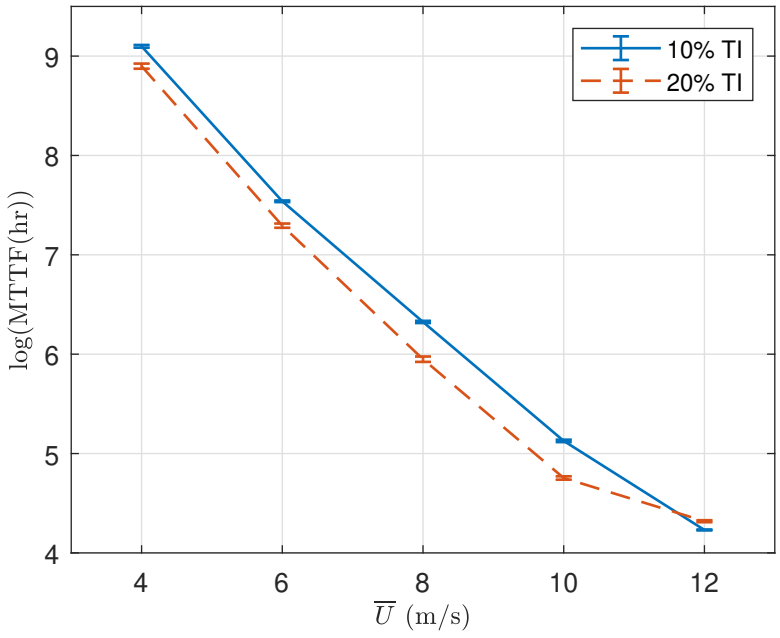

Figure 6.23: WTPC's lifetime error bars for two turbulence intensity groups with 3L-NPC model

Results discussion

The CIs of VWSPs of average wind speeds from 4 m/s to 10 m/s show that 10% TI VWSPs produce higher WTPC lifetime than 20% TI VWSPs with a clear separation between their CIs'

error bars. However, just below 12 m/s, the 10% and 20% TI WTPC lifetime intersect and the 20% TI VWSPs produce a higher WTPC lifetime than 10% TI VWSPs. That is because wind turbine pitch control impacts high TI wind more than low TI which results in more regulated 20% TI VWSPs than 10% TI VWSPs. This analysis proves that wind turbulence intensity has a significant impact on the WTPC lifetime of 3L-NPC topology in a similar conclusion for the 2L-VSC WTPC as has been shown in section 6.2.5. This analysis concludes that wind turbulence intensity reduces the WTPC lifetime by a significant difference for most operating wind speeds. However, the impact of turbulence intensity on WTPC lifetime appears during the long run of wind turbines since its impact has a statistical effect.

6.6 Reliability comparison between 2L-VSC and 3L-NPC

The reliability analyses of 2L-VSC and 3L-NPC WTPC discussed in sections 6.2 and 6.5 show that the WTPC lifetimes of both topologies have been impacted by wind speed and turbulence intensity. However, analysing the WTPC reliability differences between both topologies is worthwhile as it provides information to help decide which topology is more reliable for the selected wind farm site.

For example, a particular site's wind profile might result in a clear separation between the estimated lifetimes of different converter topologies or control whilst another site's wind conditions might suggest there is little difference in lifetime between converter topologies. The comparison uses the lifetime results of the constant wind speeds analysis and variable wind speeds analysis of both simulated topologies, 2L-VSC and 3L-NPC. To evaluate the comparison between 3L-NPC and 2L-VSC WTPC, the lifetime ratio for the 3L-NPC topology (LTR_{3L}) is calculated. LTR_{3L} is defined as the ratio of 3L-NPC WTPC lifetime divided by 2L-VSC WTPC lifetime as shown in equation (6.11). The failure rate of the WTPC is the failure rate of the one converter multiplied by the number of the parallel converters in the WTPC as shown in equation (6.12) where λ is the failure rate and s is the number of parallel converters.

The WTPC reliability models of 2L-VSC and 3L-NPC constructed in sections 4.6 and 5.4.4 respectively are utilised for this analysis. Both models are based on the same PMSG and same rotor size which ensure fairness of comparison. However, the 3L-NPC model contains 4 parallel converters in its WTPC while the 2L-VSC model contains 8 parallel converters in its WTPC. Considering the number of parallel converters in each WTPC model, the LTR_{3L} is calculated by equation (6.13) and used to evaluate the lifetime ratio at constant wind speeds and variable wind speeds lifetime analyses. These figures are selected to allow a demonstration of the method and could be adapted to reflect the structure of a specific wind turbine type, just as the exact converter configuration or control strategy could be adapted.

$$LTR_{3L} = \frac{Lifetime\ of\ 3L-NPC\ WTPC}{Lifetime\ of\ 2L-VSC\ WTPC} \tag{6.11}$$

$$= \frac{\lambda_{2L-VSC}\ s_{2L-VSC}}{\lambda_{3L-NPC}\ s_{3L-NPC}} \tag{6.12}$$

$$= \frac{MTTF_{3L-NPC}/s_{3L-NPC}}{MTTF_{2L-VSC}/s_{2L-VSC}} \tag{6.13}$$

6.6.1 WTPC lifetime analysis at constant wind speeds

This comparison shows how constant wind speed impacts WTPC's lifetime in the two converter topologies, 2L-VSC and 3L-NPC. The results of constant wind speed simulations performed for both topologies in sections 6.2.1 and 6.5.1 are used in this comparison and the related LTR_{3L} is calculated for each wind speed. Table 6.15 lists the estimated WTPC lifetimes of both topologies and the LTR_{3L}.

Table 6.15: Lifetimes of 2L-VSC and 3L-NPC WTPCs and their lifetime ratio at constant wind speeds

U (m/s)	$MTTF_{WTPC,2L-VSC}$ (hr)	$MTTF_{WTPC,3L-NPC}$ (hr)	LTR_{3L}
4	$1.82\times10^{+8}$	$2.46\times10^{+8}$	2.7
5	$2.49\times10^{+7}$	$3.50\times10^{+7}$	2.8
6	$4.63\times10^{+6}$	$6.69\times10^{+6}$	2.9
7	$1.01\times10^{+6}$	$1.58\times10^{+6}$	3.1
8	$2.50\times10^{+5}$	$4.48\times10^{+5}$	3.6
9	$6.40\times10^{+4}$	$1.24\times10^{+5}$	3.9
10	$1.74\times10^{+4}$	$3.32\times10^{+4}$	3.8
11	$4.71\times10^{+3}$	$8.53\times10^{+3}$	3.6
12	$1.27\times10^{+3}$	$2.10\times10^{+3}$	3.3

Results discussion

The calculated LTR_{3L} in table 6.15 varies as wind speed changes. The visual presentation of LTR_{3L} against constant wind speed is shown in figure 6.24. LTR_{3L} started with 2.7 at cut-in wind speed (4 m/s) then it reaches 3.9 at 9 m/s before drop to 3.3 at rated wind speed (12 m/s). This analysis shows that 3L-NPC WTPC has a longer lifetime than 2L-VSC WTPC with a minimum lifetime ratio equal to 2.7 and as wind speed increases the ratio improves. However, the certainty with which one can select the most reliable WTPC topology and control depends on the specific site wind speed profile. In some cases, there might be little distinction between designs whilst in others there might be clear differences.

For example, figure 6.25 indicates that analysis of a site with a significant proportion of wind between 8m/s and 11m/s is likely to suggest that a 3L-NPC converter provides significant reliability benefits over the 2L-VSC, with good confidence. WTPC lifetime analysis based on constant wind speed simulation ignores the interaction between wind speed changes and wind turbine dynamics. Therefore, a realistic lifetime ratio would be based on WTPC lifetime simulation with variable wind speed input as presented in the following analysis.

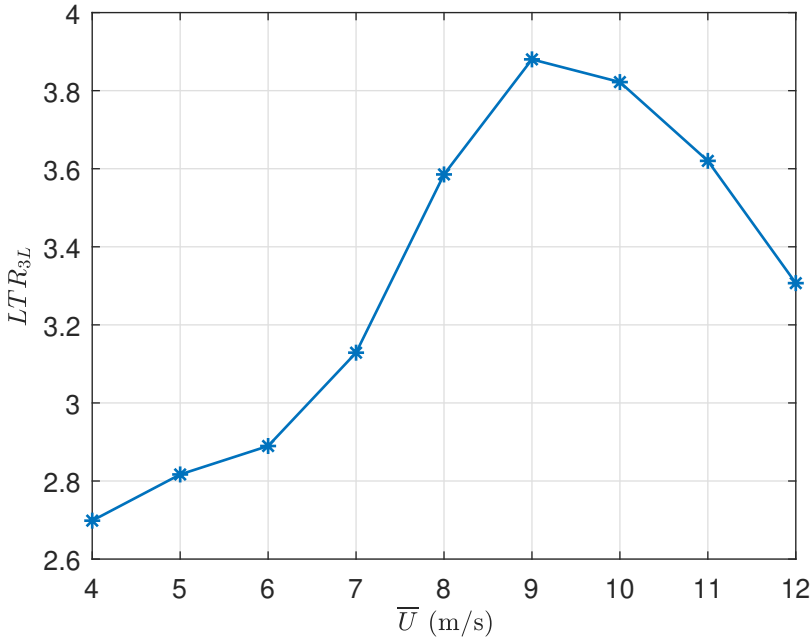

Figure 6.24: Lifetime ratio of 3L-NPC to 2L-VSC at constant wind speeds

6.6.2 Lifetime ratio based on variable wind speed

To consider the effects of wind speed fluctuations and the wind turbine dynamics, the variable wind speed test would produce more realistic results. The WTPC lifetime results of variable wind speed tests in sections 6.2.3 and 6.5.3 which were based on testing 230 VWSPs are used in this analysis. The results of 2L-VSC WTPC and 3L-NPC WTPC shown in figures 6.3 and 6.19 respectively show a similar trend of the WTPC's lifetime against VWSPs' average wind speed however their values vary in both topologies. To evaluate the differences, LTR_{3L} is calculated for the tested 230 VWSPs resulting in 230 LTR_{3L} as presented against their average wind speeds in the scatter diagram shown in figure 6.25.

Results discussion

Figure 6.25 shows LTR_{3L} varies with increasing average wind speed in a similar trend to LTR_{3L} obtained by constant wind speed simulation. However, there are fluctuations of LTR_{3L} at average wind speeds below the rated wind speed (12 m/s). The reason can be that wind speed is fluctuating within the VWSP developing different turbulence intensities. To analyse this effect, two groups of LTR_{3L} are selected based on their VWSPs' turbulence intensities, $TI \leq 10\%$ and $TI \geq 25\%$.

The two groups of LTR_{3L}s are represented in a scatter diagram shown in figure 6.26 which indicates that VWSP turbulence intensity also affects the LTR_{3L}. The $\leq 10\% TI$ group constructed a clear curve that peaks around 3.7 and decays to settle at 3.2 while the $\geq 25\% TI$ shows a noisy trend that raises and decays earlier to settle at 3.2 For average wind speeds above the rated wind speed (12 m/s) the LTR_{3L}s approach fixed value around 3.2 because wind turbine speed is regulated by pitch control above the rated wind speed.

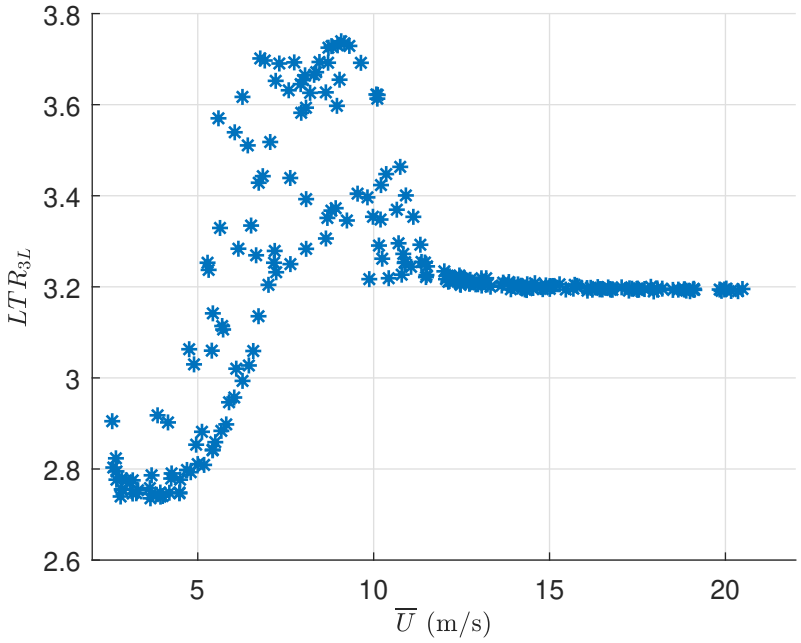

Figure 6.25: Lifetime ratio points corresponding to 230 VWSPs vs their average wind speeds

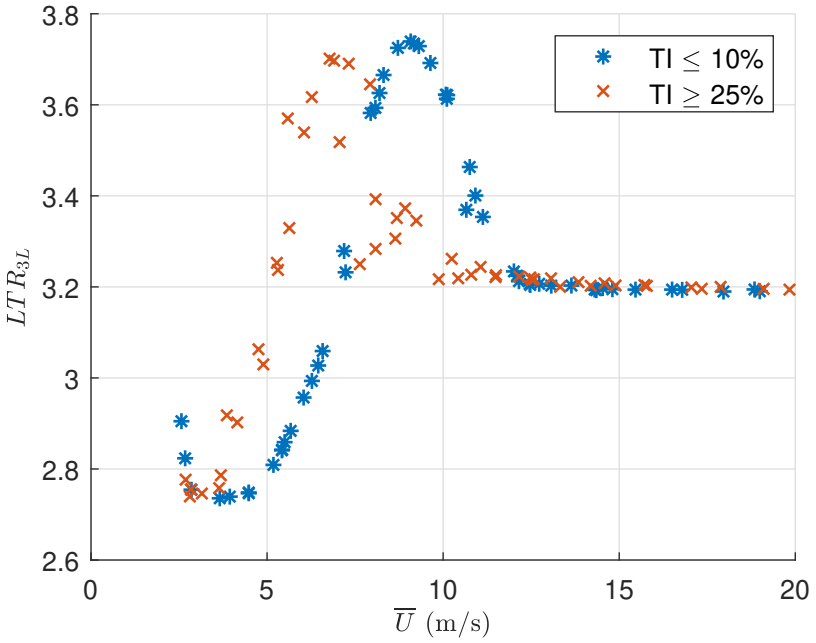

Figure 6.26: Effect of VWSPs' turbulence intensities on LTR_{3L}

This indicates that wind speed and turbulence intensity affect the lifetime ratio when comparing 2L-VSC and 3L-NPC topologies for WTPC reliability. Moreover, the trend of LTR_{3L} shown against average wind speed can vary based on power converter parameters including rated power as in [132] where LTR_{3L} trend was more skew settled on 4.0 at rated wind speed as shown in figure 6.27. Therefore, for specific wind turbines, the lifetime ratio would be re-analysed considering the wind turbine dynamics, WTPCs details, and wind characteristics of the proposed

wind farm site.

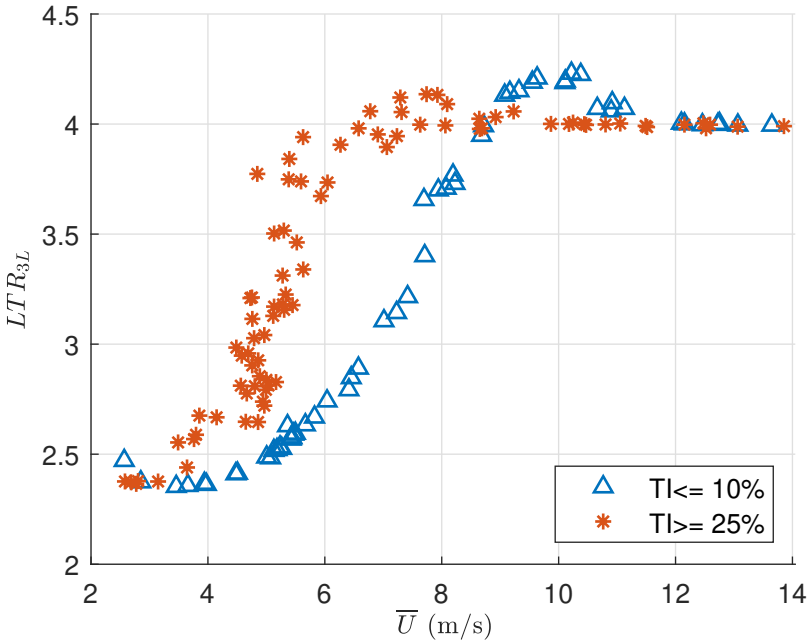

Figure 6.27: Lifeime ratio of different rated power WTPC for two turbulence intensities from [132]

6.7 Reliability Comparison

In this section, the lifetimes of the three modelled wind turbines are tested with the same VWSPs to analyse the impact on their lifetimes. The selected VWSPs cover a range of wind turbine operating wind speeds. Figure 6.28 presents the simulated lifetimes of the three modelled wind turbines using the same input of VSWPs. The visual inspection shows that the lifetimes of 2L-VSC with FOC appeared slightly higher than 2L-VSC with DTC mainly after rated wind speed (12 m/s) however a more detailed comparison with evaluation between them is presented in section 6.4. Also, the visual inspection of figure 6.28 suggests that the lifetimes achieved by 3L-NPC are higher than the lifetimes achieved by 2L-VSC with FOC over the range of VWSPs average wind speeds. More detailed comparisons with evaluation between them are presented in section 6.6.

6.8 Reliability analysis of future WTPC

Within the last two decades, WTPC has developed its design and semiconductor technology to adapt to the increasing wind turbine power and different generator types. Wind energy development is directed toward increasing the wind turbine size for higher output power. Therefore, WTPC is expected to continue developing and adapting to future wind turbine parameters. Increasing the rated voltage is the preferred option for high power wind turbines so the WTPC topology, semiconductor, or both may change.

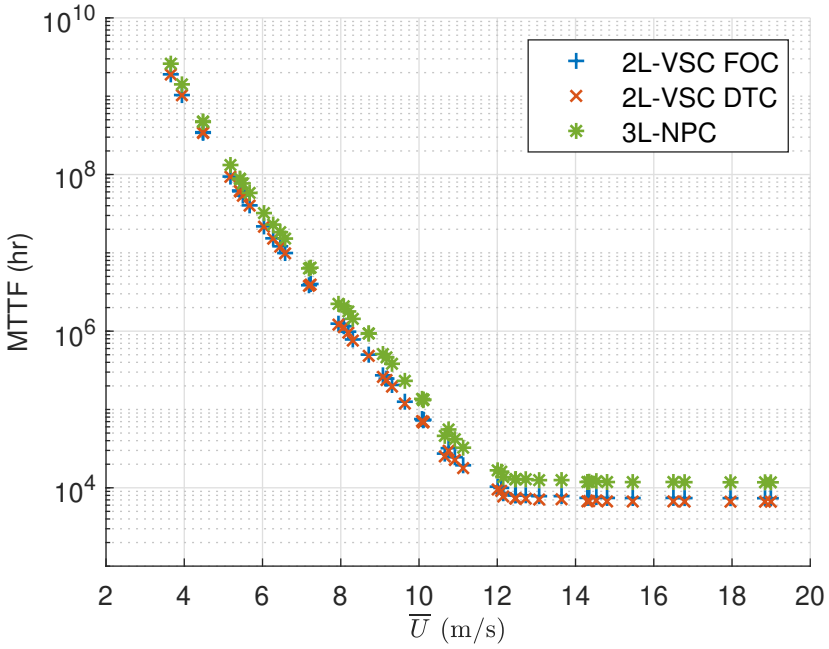

Figure 6.28: Lifetimes of three WTPC designs, 2L-VSC FOC, 2L-VSC DTC, and 3L-NPC, with VWSPs

The WTPC reliability analysis used with 2L-VSC FOC and DTC and with 3L-NPC has followed one method as presented in figure 4.1. Addressing the third research question "How can the reliability of future wind turbine power converters be estimated? " this section describes how to use this method with future WTPC considering its different design, semiconductor, or wind turbine mechanical details.

6.8.1 Effect of changing wind turbine mechanical details on WTPC reliability analysis

Current higher than 10 MW wind turbines are variable speed direct-drive machines equipped with PMSG. With this configuration, modelling the mechanical subsystem for future wind turbines will be similar to this research considering the change of the parameters related to its mechanical details. For wind turbines with different configurations, like with a gearbox, the mechanical subsystem of the reliability model has to be modified accordingly. The modelled mechanical subsystem is important to emulate the actual wind turbine since wind turbine dynamics affect the WTPC loading by wind speeds and turbulence.

6.8.2 Effect of changing converter topologies on WTPC reliability analysis

The method discussed in this thesis analysed two converter topologies, 2L-VSC and 3L-NPC. For different converter topologies, the WTPC model has to amend the modelled power converter accordingly, for example, modelling three-level active neutral point clamped (3L-ANPC) or modular multilevel converter (MMC). This modification may affect the semiconductor's applied voltage, current, and switching frequency which will affect the semiconductors' power loss

simulation. Therefore, the power loss will need to be amended according to the future converter circuit. However, the overall model and analysis structure remains the same.

6.8.3 Effect of changing semiconductor technology on WTPC reliability analysis

The reliability analysis of WTPC in this research is based on power converters constructed with individual IGBT power modules. This provides clarity of WTPC's semiconductors loading and comparisons based on control strategy and converter topology. The current market WTPCs are based on IGBT and IGCT however other semiconductors can be seen in WTPCs in future like SiC MOSFET and GaN. Therefore, the wind turbine model would consider amending the the semiconductor's power loss block according to its characteristics if required besides amending the parameters affecting switching and conduction power loss. The thermal block may need to change if the new semiconductor has different internal layers affecting the heat dissipation.

Future WTPC semiconductors may have different lifetime empirical constants which will result in different numbers of thermal cycles to failure. Also, the semiconductor manufacturer may recommend different lifetime models like the Bayerer model instead of the Cofin-Manson Arrhenius model used in this research. These two amendments will be implemented in the wind turbine mode if needed. However, the reset of the model and the overall method remain the same. The required changes to the current method for reliability analysis of future WTPC are summarised in table 6.16.

Table 6.16: Required modifications in method's models for future WTPC reliability analysis

Changes in future wind turbine	Method's model or subsystem				
	Mechanical	Power converter	Power loss	Thermal	Lifetime
Power train	x				
Converter topology		x	x		
Power module				x	
Semiconductor technology			x		x

6.8.4 The method's analyses

The WTPC reliability analysis against wind speed and turbulence intensity used in this thesis will be valid for use with the future WTPC as it delivers the relationship between wind characteristics and WTPC lifetime based on simulating a large number of VWSPs. It is important to emulate the actual wind for the WTPC lifetime simulation by input field-measured wind speeds

sampled at an accepted rate ($> 0.25\ Hz$) [94]. Also, it is important to validate the wind turbine model before using it in the WTPC reliability analyses.

The method's analyses are:

- Simulate VWSPs to analyse the impact of average wind speed on WTPC lifetime
- Simulate VWSPs of the same average wind speed but represent different turbulence intestines to analyse their impact on WTPC lifetime.
- Simulate VWSPs of different average wind speeds and different turbulence intensities to assess the impact of turbulence intensities on the wind turbine operating win speed.
- Using statistical tools to assess the significance of turbulence intensity impact on WTPC lifetime.

Whatever the system is being modelled, this overarching framework remains the same and provides the means of analysis to enable WTPC lifetime estimation.

6.9 Chapter summary

In this chapter reliability analyses and comparisons of WTPC have been shown in three cases, the widely deployed 2L-VSC with FOC and DTC drives, and the 3L-NPC topology. The analyses proved that average wind speed has a direct impact on WTPC lifetime due to the relationship between wind speed and WTPC loading. The relation between wind speed and logarithm of WTPC's MTTF drops nearly linearly until the rated wind speed then it keeps a fixed value due to the effect of wind turbine speed control.

The reliability analysis in this chapter related to wind turbulence intensity showed an important impact on the WTPC lifetime, however, this impact appeared during the long run on the wind turbine due to its stochastic nature. The analyses showed a significant difference between 10% and 20% turbulence intensities VWSP at 95% confidence level for the 2L-VSC with FOC and DTC and for the 3L-NPC WTPCs.

The comparison between FOC and DTC drivers used with 2L-VSC shows that IGBT and diode lifetimes were more impacted by wind speed with DTC vs FOC. At low wind speeds, the impact was negligible however as wind speed increases the DTC WTPC lifetime reduces affected by converter IGBT and diode. At rated wind speed, the IGBT lifetime reduces to 79% and the diode lifetime reduces to 91% making the WTPC lifetime reduce to 90%. The WTPC semiconductors' lifetimes would reduce to different levels based on the WTPC parameters including its rated power.

The reliability comparison between 2L-VSC and 3L-NPC topologies used in WTPC shows that 3L-NPC WTPC achieves a longer lifetime than 2L-VSC when used with the same wind turbine. The lifetime ratio changes between 2.4 and 3.7 depending on wind speed and turbulence intensity. The WTPC lifetime comparisons between two controls or topologies can be utilised for the best WTPC technology for specific wind turbine sites. For example, if most of the wind speeds of a specific site are between 8 m/s and 10 m/s with low turbulence intensity, then it will

be expected that 3L-NPC WTPC will achieve a lifetime 3.5 times the 2L-VSC WTPC lifetime as shown in figure 6.26.

This WTPC reliability analysis method can be applied for future WTPC considering changing related simulation models and parameters to emulate the analysed WTPC. The method will continue to use a large number of VWSPs covering the wind turbine operating wind speeds and the proposed site wind turbulence intensities. The statistical approach for WTPC lifetime related to wind characteristics is essential since wind is a complex phenomenon and WTPC lifetime estimation is stochastic.

Chapter 7

Conclusions

In this thesis, the reliability of WTPCs was analysed using a new method. A wind turbine is modelled for WTPC reliability analysis where its operating parameters and semiconductor junction temperatures are validated for this task in section 4.6. The WTPC reliability analysis is based on simulating its lifetimes corresponding to hundreds of VWSPs with particular characteristics and then using statistical tools to examine the impact of wind speed and turbulence intensity on WTPC lifetime. The proposed method is demonstrated for two converter topologies (2L-VSC and 3L-NPC) and under two control regimes (DTC and FOC), demonstrating its flexibility for application to various and future WTPCs.

7.1 Conclusion

Addressing the first research question, the reliability analysis was first applied to the widely deployed 2L-VSC WTPC in section 6.2.3 In line with previous research, this research found that average wind speed has a direct impact on WTPC lifetime due to the direct relationship between wind speed and wind turbine loading, thus validating the proposed approach.

As a contribution to this field, this research has analysed the relationship between wind turbulence and WTPC lifetime in section 6.2.4. This research found that WTPC lifetimes related to a group of VWSPs having the same average wind speeds and same turbulence intensity are normally distributed. As the VWSP group's turbulence intensity increases, the mean of WTPC lifetimes decreases and their standard deviation increases. Therefore, wind turbulence not only harms the WTPC lifetime but also makes it difficult to predict with certainty. Furthermore, the thesis has proved a significant difference, at a 95% confidence level, in WTPC lifetimes when different turbulence intensities VWSPs are applied to the wind turbine. It is worthwhile to consider this conclusion when planning maintenance for wind farms with high-turbulence wind.

Addressing the second research question, the reliability analyses are extended to examine the impact of changing WTPC control to DTC and topology to 3L-NPC. Two wind turbine and WTPC models are constructed and validated for WTPC reliability analyses: 2L-VSC with DTC and 3L-NPC with FOC in sections 5.2 and 5.4.4 respectively. The research found that the impacts of average wind speed and turbulence intensity on WTPC lifetime in the two extended models have similar effects as in the original 2L-VSC model. Accordingly, the research concluded

that the effects of average wind speed and turbulence intensity on WTPC lifetime are linked to WTPC loading regardless of its design and control, albeit with different magnitude effects. However, the research found that WTPC lifetimes estimated from the same VWSPs in the three models show differences which demonstrate that WTPC converter lifetime is not only affected by wind conditions but also by the interactions between wind conditions and WTPC topology and operation.

By changing the WTPC control to DTC instead of FOC, the WTPC lifetime was more impacted by increasing wind speeds. Both controls, FOC and DTC, showed equal WTPC lifetimes around the cut-in wind speed (4 m/s) but as wind speed increases, the WTPC with DTC drops its lifetime to 90% of WTPC with FOC by rated wind speed (12 m/s). The drop in WTPC lifetime was caused by lifetime drops of its IGBTs to 79% and its diodes to 91% of their lifetimes under FOC. VWSPs of high turbulence intensities shifted the point at which estimated lifetime drops to a lower average wind speeds however the maximum drop in WTPC lifetime stays around 90% as shown in section 6.4.

The WTPC lifetime comparison based on its topology shows that changing the WTPC topology to 3L-NPC instead of 2L-VSC increased its lifetime across all mean wind speeds and turbulence intensities. The increase in the lifetime interacts with average wind speed and turbulence intensity. At cut-in wind speed (4 m/s), the 3L-NPC WTPC lifetime was around 2.7 times the lifetime of the 2L-VSC WTPC. As wind speed increases, the ratio becomes 3.9 times that of the 2L-VSC WTPC at 9 m/s wind speed. It then drops to 3.3 at the rated wind speed (12 m/s) and stays fixed until the cut-out wind speed (25 m/s). However, the ratio trend is shifted toward lower average wind speeds with high turbulence intensity VWSPs ($\geq$ 25%) as shown in section 6.6. The lifetime ratios between FOC and DTC and between 2L-VSC and 3L-NPC WTPCs are affected by the WTPC's parameters therefore it is necessary to perform this analysis on individual cases for reliability comparison however the core approach remains unchanged.

Addressing the third research question, the reliability of the future WTPC can be analysed using this method of simulating a large number of WTPC lifetimes based on field-measured VWSPs and using statistical analyses to understand the reliability impacts of future WTPC. Minor changes in model details for future wind turbines and their WTPCs are required as discussed in section 6.8 however this does not change the overall methodology or analysis.

7.2 Future work

The method presented in this thesis was successfully applied to two converter topologies and two control strategies used in wind turbines. The method is based on WTPC lifetime simulations related to hundreds of VWSPs therefore it requires computer resources for the time-consuming simulations. For example, the simulation of 2L-VSC WTPC lifetime related to one 10-minute VWSP requires an average of 25 minutes with a computer equipped with an Intel Core i5 processor and 8 GB RAM using Simulink 2022a. While simulating 3L-NPC WTPC related to one 10-minute VWSP required 55 minutes using the same computer. Therefore, parallel computing performed in this research was necessary for eliminating the required time for estimating

WTPC lifetimes corresponding to hundreds of VWSPs. Future work may improve this method's performance to reduce its need for high computational and time resources.

Also, future work can be done by amending the method's WTPC and wind turbine models to perform reliability analyses on future WTPCs considering new technologies in wind energy such as grid-forming wind turbines or WTPCs constructed using new and advanced semiconductors. This method provides a strong base for reliability analysis and lifetime estimation of future wind turbines, as well as potential retrospective application to existing wind farms to understand differences in reliability at different sites.

Ideas for future work can be developed based on the method presented in this research such as extending the reliability comparison to include the modular multilevel converter (MMC) in wind turbine applications. In such an example, the reliability analysis needs to consider changes in converter design which affects power loss calculation but the rest of this research method will be applicable.

Another proposed project is to analyse the WTPC reliability used in promising grid-forming wind energy, where the WTPC is controlled to support the grid frequency by implementing a different control system than the current grid-following wind energy. In this case, only the model's control system needs to be modified for the WTPC reliability analyses and the rest of the method remains the same.

The third proposed research is to develop this research method to analyse the reliability of WTPC based on IGCT semiconductors like the PCS6000 converter used with the HaliadeX wind turbine. The reliability analyses would use this research method however, the semiconductor details and its control will need to be modelled according to the information obtained from the WTPC manufacturer. The rest of the model and reliability analysis will stay the same.

Comparing the reliability of different WTPC topologies or control systems related to the realistic operation conditions helps in identifying the most reliable technology for the selected location based on its average wind speed and turbulence intensity. This will reflect on the overall wind turbine reliability and the related maintenance cost which impacts the cost of produced energy.

Bibliography

[1] Alois Schaffarczyk. *Understanding Wind Power Technology: Theory, Deployment and Optimisation.* A John Wiley and Sons Ltd. Publication, 2014.

[2] Inemesit Ukpanah. UK's Wind Power: A Gust of Growth in the Renewable Energy Sector, 2024.

[3] World Nuclair Association. Carbon Dioxide Emissions From Electricity, 2024.

[4] United Nations Economic Commission for Europe (UNECE). Carbon Neutrality in the UNECE Region: Integrated Life-cycle Assessment of Electricity Sources. Technical report, United Nations Economic Commission for Europe, Geneva, 2022.

[5] Sadie Cox, Laura Beshilas, and Eliza Hotchkiss. Renewable Energy to Support Energy Security. *Resilient Energy Platform*, pages 2–4, 2019.

[6] Małgorzata Wiatros-Motyka, Dave Jones, Hannah Broadbent, Nicolas Fulghum, Chelsea Bruce-Lockhart, Reynaldo Dizon, Phil Macdonald, Charles Moore, Alison Candlin, Uni Lee, Libby Copsey, Sam Hawkins, Matt Ewen, Bryony Worthington, Harry Benham, Michele Trueman, Muyi Yang, Aditya Lolla, Achmed Shahram Edianto, Paweł Czyżak, Sarah Brown, Chris Rosslowe, Richard Black, and Marion Bachelet. Global Electricity Review 2023. Technical Report April, EMBER, 2023.

[7] GWEC. GWEC Global Wind Report. *Global Wind Energy Council*, page 75, 2021.

[8] Qiuwei Wu and Yuanzhang Sun. *Modeling and Modern Control of Wind Power.* IEEE-PRESS WILEY, 2017.

[9] Olimpo Anaya-Lara, Nick Jenkins, Janaka Ekanayake, and Phill Cartwright. *Wind Energy Generation Modelling and Control.* A John Wiley and Sons Ltd. Publication, 2016.

[10] Venkata Yaramasu and Bin Wu. *Model Predictive Control of Wind Energy Conversion Systems.* IEEE-PRESS WILEY, 2016.

[11] Amirnaser Yazdani and Reza Iravani. *Voltage-Sourced Converters in Power Systems Modeling Control and Applications.* A John Wiley and Sons Ltd. Publication, 2018.

[12] Venkata Narasimha Rao Yaramasu. *Predictive Control of Mutilevel Converters for Megawatt Wind Energy Conversion Systems.* PhD thesis, Ryerson University, 2014.

[13] Frede Blaabjerg. *Control of Power Electronic Converters and Systems*, volume 1. Elsevier Scince & Technology, 2018.

[14] Eric Monmasson. *Power Electronic Converters PWM Strategies and Current Control Techniques*, volume 11. A John Wiley and Sons Ltd. Publication, 2018.

[15] Herbert L. Hess, Noor A. Abdul Melek, and Eduard Muljadi. Power converter for wind turbine application. In *Proceedings of the IEEE Power Engineering Society Transmission and Distribution Conference*, volume 2, pages 1275–1276, 2000.

[16] Frede Blaabjerg, Yongheng Yang, Ke Ma, and Xiongfei Wang. Power electronics - the key technology for renewable energy system integration. In *2015 International Conference on Renewable Energy Research and Applications (ICRERA)*, pages 1618–1626, 2015.

[17] Semikron Danfoss. SKM800GA176D IGBT Module.

[18] HITACHI ABB. Power Semiconductors Product Catalogue 2021. Technical report, HITACHI ABB, 2021.

[19] Semikron Danfoss. SKiiP 1013 GB172-2DWV3.

[20] Frede Blaabjerg, Marco Liserre, and Ke Ma. Power electronics converters for wind turbine systems. *IEEE Transactions on Industry Applications*, 48(2):708–719, 2012.

[21] Tim D. Strous, Henk Polinder, and Jan A. Ferreira. Brushless doubly-fed induction machines for wind turbines: Developments and research challenges. *IET Electric Power Applications*, 11(6):991–1000, 2017.

[22] Bhavna Jain, Shailendra Jain, and R. K. Nema. Control strategies of grid interfaced wind energy conversion system: An overview. *Renewable and Sustainable Energy Reviews*, 47:983–996, 2015.

[23] Bin Wu, Yongqiang Lang, Navid Zargari, and Samir Kouro. *Power Conversion and Control of Wind Energy System*, volume 148. A JOHN WILEY & SONS, INC., PUBLICATION, 2011.

[24] Gonzalo Abad, Jesús López, Miguel A. Rodríguez, Luis Marroyo, and Grzegorz Iwanski. *Doubly Fed Induction Machine Modeling and Control for Wind Energy*. A John Wiley and Sons Ltd. Publication, 2011.

[25] Xu Yang, Dean Patterson, and Jerry Hudgins. Permanent magnet generator design and control for large wind turbines. In *PEMWA 2012 - 2012 IEEE Power Electronics and Machines in Wind Applications*, pages 1–5. IEEE, 2012.

[26] Clifford Choe Wei Chang, Tan Jian Ding, Tan Jian Ping, Kang Chia Chao, and Mohammad Arif Sobhan Bhuiyan. Getting more from the wind: Recent advancements and challenges in generators development for wind turbines. *Sustainable Energy Technologies and Assessments*, 53(PC):102731, 2022.

[27] Xiaokang Peng, Zicheng Liu, and Dong Jiang. A review of multiphase energy conversion in wind power generation. *Renewable and Sustainable Energy Reviews*, 147(May):111172, 2021.

[28] Zhou Honglin, Wu Xiaotian, Dai Tongzhen, and Xiao Wenjing. Control of parallel-connected grid-side converters of a wind turbine with real-Time ethernet. In *Proceedings IECON 2017 - 43rd Annual Conference of the IEEE Industrial Electronics Society*, volume 2017-Janua, pages 2413–2418, 2017.

[29] Jens Birk and Björn Andresen. Parallel-connected converters for optimizing efficiency, reliability and grid harmonics in a wind turbine. *Gamesa Wind Engineering*, pages 4–10, 2007.

[30] The International Electrotechnical Commission. IEC TS 62749, 2020.

[31] Victor R. F. B. de Souza, Luciano S. Barros, and Flavio B. Costa. Performance Comparison of 2L-VSC, 3L-NPC, and 3L-MMC Converter Topologies for Interfacing Grid-Connected Systems. *Sociedade Brasileira Automatica*, 2021.

[32] Xuchao Hu and Zhang Lin. Application of PCS6000 in full-power wind turbines. In *Conference Proceedings - 2012 IEEE 7th International Power Electronics and Motion Control Conference - ECCE Asia, IPEMC 2012*, volume 2, pages 790–795. IEEE, 2012.

[33] GE. Haliade-X offshore wind turbine, 2021.

[34] Amina Bensalah, Georges Barakat, and Yacine Amara. Electrical Generators for Large Wind Turbine: Trends and Challenges. *Energies*, 15(18), 2022.

[35] Pedro Catalán, Yanbo Wang, Joseba Arza, and Zhe Chen. A Comprehensive Overview of Power Converter Applied in High-Power Wind Turbine: Key Challenges and Potential Solutions. *IEEE Transactions on Power Electronics*, 38(5):6169–6195, 2023.

[36] Sandeep Bala, Jiuping Pan, Debrup Das, Oscar Apeldoorn, and Stephan Ebner. Lowering failure rates and improving serviceability in offshore wind conversion-collection systems. In *PEMWA 2012 - 2012 IEEE Power Electronics and Machines in Wind Applications*, volume 1, pages 1–7. IEEE, 2012.

[37] Roger R Hill, Jennifer a Stinebaugh, Daniel Briand, Allan S Benjamin, and James Linsday. Wind Turbine Reliability: A Database and Analysis Approach. Technical Report February, Sandia National Laboratories, 2008.

[38] Mohamed F. El-Naggar, Ahmed Sayed Abdelhamid, Mostafa A. Elshahed, and Mohamed El-Shimy Mahmoud Bekhet. Ranking Subassemblies of Wind Energy Conversion Systems concerning Their Impact on the Overall Reliability. *IEEE Access*, 9:53754–53768, 2021.

[39] Elsayed A Elsayed. *Reliability Engineering*. A John Wiley and Sons Ltd. Publication, second edi edition, 2012.

[40] F. Spinato, P. J. Tavner, G. J.W. Van Bussel, and E. Koutoulakos. Reliability of wind turbine subassemblies. *IET Renewable Power Generation*, 3(4):387–401, 2009.

[41] Amin Sadeghfam, Sajjad Tohidi, and Mehdi Abapour. Reliability comparison of different power electronic converters for grid-connected PMSG wind turbines. *International Transactions on Electrical Energy Systems*, 27(9):1–11, 2017.

[42] James Carroll, Alasdair McDonald, and David McMillan. Failure rate, repair time and unscheduled O& M cost analysis of offshore wind turbines. *Wind Energy*, 19(6):1107–1119, 2016.

[43] Mohamed F. El-Naggar, Ahmed Sayed Abdelhamid, Mostafa A. Elshahed, and Mohamed El Shimy Mahmoud Bekhet. Dynamic Reliability and Availability Allocation of Wind Turbine Subassemblies Through Importance Measures. *IEEE Access*, 10(July):99445–99459, 2022.

[44] Huai Wang, Frede Blaabjerg, Ke Ma, and Rui Wu. Design for Reliability in Power Electronics in Renewable Energy Systems - Status and Future. In *4th International Conference on Power Engineering, Energy and Electrical Drives*, pages 1846–1851, 2014.

[45] Sanjay Jaiswal and G. L. Pahuja. Effect of reliability of wind power converters in productivity of wind turbine. In *India International Conference on Power Electronics, IICPE*, volume 2015-May, pages 1–6. IEEE, 2015.

[46] Michael Wilkinson, Ben Hendriks, Fabio Spinato, Keir Harman, Eugenio Gomez, Horacio Bulacio, Jordi Roca, Peter Tavner, Yanhui Feng, and Hui Long. Methodology and results of the reliawind reliability field study. *European Wind Energy Conference and Exhibition 2010, EWEC 2010*, 3(November 2016):1984–2004, 2010.

[47] Katharina Fischer, Karoline Pelka, Arne Bartschat, Bernd Tegtmeier, Diego Coronado, Christian Broer, and Jan Wenske. Reliability of power converters in wind turbines: Exploratory analysis of failure and operating data from a worldwide turbine fleet. *IEEE Transactions on Power Electronics*, 34(7):6332–6344, 2019.

[48] Cuong Dao, Behzad Kazemtabrizi, and Christopher Crabtree. Wind turbine reliability data review and impacts on levelised cost of energy. *Wind Energy*, 22(12):1848–1871, 2019.

[49] Andrea Isidoril, Fabio Mario Rossi, Frede Blaabjerg, and Ke Ma. Thermal loading and reliability of 10-MW multilevel wind power converter at different wind roughness classes. *IEEE Transactions on Industry Applications*, 50(1):484–494, 2014.

[50] Sai Xue, Quan Zhou, Jian Li, Chenmeng Xiang, and Shi Chen. Reliability evaluation for the DC-link capacitor considering mission profiles in wind power converter. In *ICHVE 2016 - 2016 IEEE International Conference on High Voltage Engineering and Application*. IEEE, 2016.

[51] Christopher Smith. *Holistic Physics-of-Failure Approach to Wind Turbine Power Converter Reliability*. PhD thesis, Durham Universityt, 2018.

[52] Kaigui Xie, Zefu Jiang, and Wenyuan Li. Effect of wind speed on wind turbine power converter reliability. *IEEE Transactions on Energy Conversion*, 27(1):96–104, 2012.

[53] Hui Li, Haiting Ji, Yang Li, Shengquan Liu, Dong Yang, Xing Qin, and Li Ran. Reliability evaluation model of wind power converter system considering variable wind profiles. In *2014 IEEE Energy Conversion Congress and Exposition, ECCE 2014*, pages 3051–3058. IEEE, 2014.

[54] James Carroll, Alasdair McDonald, and David McMillan. Reliability Comparison of Wind Turbines With DFIG and PMG Drive Trains. *IEEE Transactions on Energy Conversion*, 30(2):663–670, 2015.

[55] Zhimin Yang and Yi Chai. A survey of fault diagnosis for onshore grid-connected converter in wind energy conversion systems. *Renewable and Sustainable Energy Reviews*, 66:345–359, 2016.

[56] Arsim Ahmedi, Mike Barnes, Victor Levi, Jesus Carmona Sanchez, Chong Ng, and Paul Mckeever. Modelling of Wind Turbine Operation for Enhanced Power Electronics Reliability. *IEEE Transactions on Energy Conversion*, 37(3):1764–1776, 2022.

[57] Jinping Liang, Ke Zhang, Ahmed Al-Durra, S. M. Muyeen, and Daming Zhou. A state-of-the-art review on wind power converter fault diagnosis. *Energy Reports*, 8:5341–5369, 2022.

[58] Huai Wang and Frede Blaabjerg. Reliability of capacitors for DC-link applications in power electronic converters - An overview. *IEEE Transactions on Industry Applications*, 50(5):3569–3578, 2014.

[59] Karim Abdennadher, Pascal Venet, Gérard Rojat, Jean Marie Rétif, and Christophe Rosset. A real-time predictive-maintenance system of aluminum electrolytic capacitors used in uninterrupted power supplies. *IEEE Transactions on Industry Applications*, 46(4):1644–1652, 2010.

[60] Gustavo Malagoni Buiatti, Juan A. Martín-Ramos, Acácio M.R. Amaral, Piotr Dworakowski, and Antonio J.M. Cardoso. Condition monitoring of metallized polypropylene film capacitors in railway power trains. *IEEE Transactions on Instrumentation and Measurement*, 58(10):3796–3805, 2009.

[61] Mohammed Khorshed Alam and Faisal H. Khan. Reliability analysis and performance degradation of a Boost converter. In *2013 IEEE Energy Conversion Congress and Exposition, ECCE 2013*, pages 5592–5597. IEEE, 2013.

[62] Vinod Kumar Khanna. *Power Device Evolution and the Advent of IGBT*, pages 1–33. Wiley-IEEE Press, 2003.

[63] Arendt Wintrich, Ulrich Nicoai, Tobias Reimann, and Werner Tursky. *Application Manual Power Semiconductors*. ISLE Verlag, 2nd revise edition, 2015.

[64] Shuaichen Ye, Dao Zhou, Xiaoxian Yao, and Frede Blaabjerg. Component-Level Reliability Assessment of a Direct-Drive PMSG Wind Power Converter Considering Two Terms of Thermal Cycles and the Parameter Sensitivity Analysis. *IEEE Transactions on Power Electronics*, 36(9):10037–10050, 2021.

[65] Borong Hu, Sylvia Konaklieva, Nadia Kourra, Mark A. Williams, Li Ran, and Wei Lai. Long-Term Reliability Evaluation of Power Modules with Low Amplitude Thermomechanical Stresses and Initial Defects. *IEEE Journal of Emerging and Selected Topics in Power Electronics*, 9(1):602–615, 2021.

[66] C. Busca, R. Teodorescu, F. Blaabjerg, S. Munk-Nielsen, L. Helle, T. Abeyasekera, and P. Rodriguez. An overview of the reliability prediction related aspects of high power IGBTs in wind power applications. *Microelectronics Reliability*, 51(9-11):1903–1907, 2011.

[67] Mauro Ciappa. Selected failure mechanisms of modern power modules. *Microelectronics Reliability*, 42(4-5):653–667, 2002.

[68] O Schilling, M Schäfer, K Mainka, M Thoben, and F Sauerland. Power cycling testing and FE modelling focussed on Al wire bond fatigue in high power IGBT modules. *Microelectronics Reliability*, 52(9-10):2347–2352, 2012.

[69] Hanwen Ren, Siyang Zhao, Jian Mu, Wei Wang, Zhiyun Han, Zhihui Li, Qingmin Li, Jian Wang, and Yiming Liu. Research on the Electro-Thermal Properties of IGBT Modules Under Different Bond Wire Failure Modes. *IEEE Transactions on Electron Devices*, 71(7):4259–4266, 2024.

[70] R. Amro, J. Lutz, and A. Lindemann. Power cycling with high temperature swing of discrete components based on different technologies. *PESC Record - IEEE Annual Power Electronics Specialists Conference*, 4:2593–2598, 2004.

[71] Pushpa Rajaguru, Tim Tilford, Chris Bailey, and Stoyan Stoyanov. Damage Mechanics-Based Failure Prediction of Wirebond in Power Electronic Module. *IEEE Access*, 12(December 2023):25215–25227, 2024.

[72] Tien Anh Nguyen, Stephane Lefebvre, Pierre Yves Joubert, Denis Labrousse, and Serge Bontemps. Estimating current distributions in power semiconductor dies under aging conditions: Bond wire liftoff and aluminum reconstruction. *IEEE Transactions on Components, Packaging and Manufacturing Technology*, 5(4):483–495, 2015.

[73] Shengxue Tang, Dong Chen, Fang Yao, and Zhankai Li. Package Fatigue Failure Evolution of IGBT Modules. In *Proceedings of 2019 IEEE 3rd International Electrical and Energy Conference, CIEEC 2019*, pages 1240–1245, 2019.

[74] Wei Lai, Minyou Chen, Li Ran, Olayiwola Alatise, Shengyou Xu, and Philip Mawby. Low Δtj Stress Cycle Effect in IGBT Power Module Die-Attach Lifetime Modeling. *IEEE Transactions on Power Electronics*, 31(9):6575–6585, 2016.

[75] Christopher J. Smith, Christopher J. Crabtree, and Peter C. Matthews. Impact of wind conditions on thermal loading of PMSG wind turbine power converters. *IET Power Electronics*, 10(11):1268–1278, 2017.

[76] P. M. Anderson and Anjan Bose. Stability Simulation of Wind Turbine Systems. *IEEE Power Engineering Review*, PER-3(12):32–32, 1983.

[77] Elvira Baygildina, Pasi Peltoniemi, Olli Pyrhonen, Ke Ma, and Frede Blaabjerg. Thermal loading of wind power converter considering dynamics of wind speed. In *IECON Proceedings (Industrial Electronics Conference)*, pages 1362–1367, 2013.

[78] Björn Andresen and Jens Birk. A high power density converter system for the Gamesa G10x 4,5 MW wind turbine. In *2007 European Conference on Power Electronics and Applications, EPE*, pages 1–8, 2007.

[79] Marco Liserre, Roberto Cárdenas, Marta Molinas, and José Rodríguez. Overview of multi-MW wind turbines and wind parks. *IEEE Transactions on Industrial Electronics*, 58(4):1081–1095, 2011.

[80] Dao Zhou, Frede Blaabjerg, Toke Franke, Michael Tønnes, and Mogens Lau. Comparison of Wind Power Converter Reliability with Low-Speed and Medium-Speed Permanent-Magnet Synchronous Generators. *IEEE Transactions on Industrial Electronics*, 62(10):6575–6584, 2015.

[81] Udai Shipurkar, Emmanouil Lyrakis, Ke Ma, Henk Polinder, and Jan A. Ferreira. Lifetime Comparison of Power Semiconductors in Three-Level Converters for 10-MW Wind Turbine Systems. *IEEE Journal of Emerging and Selected Topics in Power Electronics*, 6(3):1366–1377, 2018.

[82] I. F. Kovačević, U. Drofenik, and J. W. Kolar. New physical model for lifetime estimation of power modules. In *2010 International Power Electronics Conference - ECCE Asia -, IPEC 2010*, pages 2106–2114, 2010.

[83] Markus Andresen, Ke Ma, Giampaolo Buticchi, Johannes Falck, Frede Blaabjerg, and Marco Liserre. Junction Temperature Control for More Reliable Power Electronics. *IEEE Transactions on Power Electronics*, 33(1):765–776, 2018.

[84] Karthik Desingu, Raghu Selvaraj, Thanga Raj Chelliah, Deepak Khare, and L. P. Joshi. Thermal Loading of Multi-Megawatt Medium-Voltage Power Converters Serving to Variable Speed Large Pumped Storage Units. In *Proceedings of 2018 IEEE International Conference on Power Electronics, Drives and Energy Systems, PEDES 2018*, pages 5–10. IEEE, 2018.

[85] Ui Min Choi, Frede Blaabjerg, and Søren Jørgensen. Power Cycling Test Methods for Reliability Assessment of Power Device Modules in Respect to Temperature Stress. *IEEE Transactions on Power Electronics*, 33(3):2531–2551, 2018.

[86] Ivana F. Kovačević-Badstuebner, Johann W. Kolar, and Uwe Schilling. Modelling for the lifetime prediction of power semiconductor modules. In *Reliability of Power Electronic Converter Systems*, chapter Chapter 5, pages 103–140. IET Publishing, 2016.

[87] C. Durand, M. Klingler, D. Coutellier, and H. Naceur. Power Cycling Reliability of Power Module: A Survey. *IEEE Transactions on Device and Materials Reliability*, 16(1):80–97, 2016.

[88] Ui-Min Choi, Frede Blaabjerg, and Søren Jørgensen. Power Cycling Test Methods for Reliability Assessment of Power Device Modules in Respect to Temperature Stress. *IEEE Transactions on Power Electronics*, 33(3):2531–2551, 2018.

[89] Thomas Hunger and Reinhold Bayerer. Extended Reliability of Substrate Solder Joints in Power Modules Keywords Modules with Lead Containing Substrate Solder and Copper Base Plate in Power Cycling. In *2009 13th European Conference on Power Electronics and Applications*, pages 1–8. IEEE, 2009.

[90] Yong Liu, S Irving, D Desbiens, Timwah Luk, N S How, YongSuk Kwon, and SangDo Lee. Impact of the die attach process on power & thermal cycling for a discrete style semiconductor package. In *EuroSimE 2005. Proceedings of the 6th International Conference on Thermal, Mechanial and Multi-Physics Simulation and Experiments in Micro-Electronics and Micro-Systems, 2005.*, pages 221–226, 2005.

[91] Mohamed Halick Mohamed Sathik, Josep Pou, Sundararajan Prasanth, Vivek Muthu, Rejeki Simanjorang, and Amit Kumar Gupta. Comparison of IGBT junction temperature measurement and estimation methods- A review. In *2017 Asian Conference on Energy, Power and Transportation Electrification, ACEPT 2017*, volume 2017-Decem, pages 1–8, 2017.

[92] Ui Min Choi, Frede Blaabjerg, and Søren Jørgensen. Study on Effect of Junction Temperature Swing Duration on Lifetime of Transfer Molded Power IGBT Modules. *IEEE Transactions on Power Electronics*, 32(8):6434–6443, 2017.

[93] Christopher J. Smith, Donatella Zappalá, Christopher J. Crabtree, Justo Lapiedra, and Brian Mulholland. Power converter junction temperature measurement using infra-red sensors. In *The Journal of Engineering*, volume 2019, pages 4452–4456, 2019.

[94] C. J. Smith, C. J. Crabtree, and P. C. Matthews. Evaluation of synthetic wind speed time series for reliability analysis of offshore wind farms. *European Wind Energy Association Annual Conference and Exhibition 2015, EWEA 2015 - Scientific Proceedings*, 2015.

[95] SEMIKRON. Application Note AN-11001 3L NPC & TNPC Topology. Technical report, SEMIKRON, 2015.

[96] Yi Zhang, Huai Wang, Zhongxu Wang, Yongheng Yang, and Frede Blaabjerg. The impact of mission profile models on the predicted lifetime of IGBT modules in the modular multilevel converter. In *Proceedings IECON 2017 - 43rd Annual Conference of the IEEE Industrial Electronics Society*, volume 2017-Janua, pages 7980–7985, 2017.

[97] Ke Ma, Marco Liserre, Frede Blaabjerg, and Tamas Kerekes. Thermal loading and lifetime estimation for power device considering mission profiles in wind power converter. *IEEE Transactions on Power Electronics*, 30(2):590–602, 2015.

[98] E. E. Kostandyan and K. Ma. Reliability estimation with uncertainties consideration for high power IGBTs in 2.3 MW wind turbine converter system. *Microelectronics Reliability*, 52:2403–2408, 2012.

[99] Magnar Hernes, Salvatore D'Arco, Antonios Antonopoulos, and Dimosthenis Peftitsis. Failure analysis and lifetime assessment of IGBT power modules at low temperature stress cycles. *IET Power Electronics*, 14(7):1271–1283, 2021.

[100] M. Held, P. Jacob, G. Nicoletti, P. Scacco, and M. H. Poech. Fast power cycling test for insulated gate bipolar transistor modules in traction application. *International Journal of Electronics*, 86(10):1193–1204, 1999.

[101] Reinhold Bayerer, Tobias Herrmann, Thomas Licht, Josef Lutz, and Marco Feller. Model for power cycling lifetime of IGBT modules – Various factors influencing lifetime. In *CIPS 2008 - 5th International Conference on Integrated Power Electronics Systems, Proceedings*, pages 37–42, 2008.

[102] Ke Ma, Marco Liserre, and Frede Blaabjerg. Lifetime estimation for the power semiconductors considering mission profiles in wind power converter. In *2013 IEEE Energy Conversion Congress and Exposition, ECCE 2013*, pages 2962–2971, 2013.

[103] J. F. Manwell and J. G. McGrowan. *Wind Energy Explained*. A JOHN WILEY & SONS, Ltd, PUBLICATION, 2009.

[104] Wei Qiao and Dingguo Lu. A Survey on Wind Turbine Condition Monitoring and Fault Diagnosis - Part II: Signals and Signal Processing Methods. *IEEE Transactions on Industrial Electronics*, 62(10):6546–6557, 2015.

[105] B Badrzadeh, M Bradt, N Castillo, R Janakiraman, R Kennedy, S Klein, T Smith, and L Vargas. Wind power plant SCADA and controls. In *2011 IEEE Power and Energy Society General Meeting*, pages 1–7, 2011.

[106] Israel Divan Lopes da Costa, Danilo Iglesias Brandao, Seleme Isaac Seleme, and Lenin Martins Ferreira Morais. Torque Control for PMSG-Based Wind-Power System Using Stationary abc-Reference Frame. *Energies*, 15(21), 2022.

[107] S S Rao. *Mechanical Vibrations*. Number v. 978, nos. 0-212813 in Mechanical Vibrations. Prentice Hall, 2011.

[108] The Mathworks Inc. Permanent Magnet Synchronous Machine.

[109] Remus Teodorescu, Marco Liserre, and Pedro Rodriguez. *Grid Converter Structures for Wind Turbine Systems*, pages 123–143. Wiley-IEEE Press, 2007.

[110] Adrian Timbus, Marco Liserre, Remus Teodorescu, Pedro Rodriguez, and Frede Blaabjerg. Evaluation of Current Controllers for Distributed Power Generation Systems. *IEEE Transactions on Power Electronics*, 24(3):654–664, 2009.

[111] Emil Levi. FOC: Field-Oriented Control. In *Power Electronics and Motor Drives*, chapter 24. Wilamowski, B. M., & Irwin, J. D. (Eds.), 2011.

[112] B Zigmund, A Terlizzi, X T Garcia, R Pavlanin, and L Salvatore. Experimental evaluation of PI tuning techniques for field oriented control of permanent magnet synchronous motors. *Advances in electrical and electronic engineering*, 5(3):114–119, 2006.

[113] M. Zarif and M. Monfared. Step-by-step design and tuning of VOC control loops for grid connected rectifiers. *International Journal of Electrical Power and Energy Systems*, 64:708–713, 2015.

[114] K Vinoth Kumar, Prawin Angel Michael, Joseph P John, and S Suresh Kumar. Simulation and Comparison of Spwm and Svpwm Control for Three Phase Inverter. *ARPN Journal of Engineering and Applied Sciences*, 5(7):61–74, 2010.

[115] Remus Teodorescu, Marco Liserre, and Pedro Rodrigues. *Grid Converters for Photovoltaic and Wind Power Systems.* A John Wiley and Sons Ltd. Publication, 2018.

[116] The Mathworks Inc. Semscape 5.0.

[117] SEMIKRON INTERNATIONAL GmbH. SemiSel, 2021.

[118] M Matsuichi and Tsutomu Endo. Fatigue of metals subjected to varying stress. In *Japan Soc. Mech. Engineering.*, 1968.

[119] Lakshmi Reddy GopiReddy, Leon M. Tolbert, Burak Ozpineci, and João O.P. Pinto. Rainflow Algorithm-Based Lifetime Estimation of Power Semiconductors in Utility Applications. *IEEE Transactions on Industry Applications*, 51(4):3368–3375, 2015.

[120] Isao Takahashi and Toshihiko Noguchi. A New Quick-Response and High-Efficiency Control Strategy of an Induction Motor. *IEEE Transactions on Industry Applications*, IA-22(5):820–827, 1986.

[121] Domenico Casadei, Francesco Profumo, Giovanni Serra, and Angelo Tani. FOC and DTC: Two viable schemes for induction motors torque control. *IEEE Transactions on Power Electronics*, 17(5):779–787, 2002.

[122] Xinyi Hua, Jianfei Yang, Huaren Wu, and Jian Liu. Direct torque control of a permanent magnet synchronous generator based on space vector modulation. In *2014 17th International Conference on Electrical Machines and Systems, ICEMS 2014*, pages 3520–3523. IEEE, 2014.

[123] Gonzalo Abad, Jesús López, Miguel A. Rodríguez, Luis Marroyo, and Grzegorz Iwanski. *Doubly Fed Induction Machine*. John Wiley & Sons Ltd, 2011.

[124] Giuseppe S. Buja and Marian P. Kazmierkowski. Direct torque control of PWM inverter-fed AC motors - A survey. *IEEE Transactions on Industrial Electronics*, 51(4):744–757, 2004.

[125] Bin Wu and Mehdi Narimani. *High-Power Converters and AC Drives*. IEEE-PRESS WILEY, 2016.

[126] Katharina Fischer, Thomas Stalin, Hans Ramberg, Jan Wenske, Göran Wetter, Robert Karlsson, and Torbjörn Thiringer. Field-experience based root-cause analysis of power-converter failure in wind turbines. *IEEE Transactions on Power Electronics*, 30(5):2481–2492, 2015.

[127] SAMSUNG HEAVY INDUSTRIES. Samsung Wind Energy Solutions. Technical report, SAMSUNG HEAVY INDUSTRIES, 2015.

[128] Emilio J. Bueno, Santiago Cóbreces, Francisco J. Rodríguez, Álvaro Hernádez, and Felipe Espinosa. Design of a back-to-back NPC converter interface for wind turbines with squirrel-cage induction generator. *IEEE Transactions on Energy Conversion*, 23(3):932–945, 2008.

[129] Jelena Loncarski, Hussain A. Hussain, and Alberto Bellini. Efficiency, Cost, and Volume Comparison of SiC-Based and IGBT-Based Full-Scale Converter in PMSG Wind Turbine. *Electronics (Switzerland)*, 12(2):1–14, 2023.

[130] Anders Grauers. Efficiency of three wind energy generator systems. *IEEE Transactions on Energy Conversion*, 11(3):650–655, 1996.

[131] A. Stabile, A. J. Marques Cardoso, and C. Boccaletti. Efficiency analysis of power converters for urban wind turbine applications. In *2010 IEEE International Conference on Sustainable Energy Technologies, ICSET 2010*, 2010.

[132] Sermed Alsaadi, Christopher J Crabtree, Peter C Matthews, and Mahmoud Shahbazi. Understanding wind turbine power converter reliability under realistic wind conditions. *IET Power Electronics*, n/a(n/a), 2024.

[133] T W Anderson and D A Darling. A Test of Goodness of Fit. *Journal of the American Statistical Association*, 49(268):765–769, dec 1954.

[134] ABB. Low Voltage Wind Converter. Technical report, ABB, 2018.

[135] Sermed A.B.R. Alsaadi, Peter C. Matthews, and Christopher J. Crabtree. Control Strategy Assessment for Wind Turbine Converter Reliability. In *IET Conference Proceedings*, volume 2022, pages 230–234, 2022.

Appendix A

Journal and Conference Papers

This appendix includes the journal and conference papers produced during the research project:

- Understanding wind turbine power converter reliability under realistic wind conditions
- Control Strategy Assessment for Wind Turbine Converter Reliability

Received: 6 September 2023 | Revised: 14 December 2023 | Accepted: 4 February 2024

IET Power Electronics

DOI: 10.1049/pel2.12670

The Institution of Engineering and Technology WILEY

ORIGINAL RESEARCH

Understanding wind turbine power converter reliability under realistic wind conditions

Sermed Alsaadi | **Christopher J. Crabtree** | **Peter C. Matthews** | **Mahmoud Shahbazi**

Department of Engineering, Durham University, Durham, United Kingdom of Great Britain and Northern Ireland

Correspondence
S. Alsaadi, Department of Engineering, Durham University, Durham, United Kingdom of Great Britain and Northern Ireland.
Email: sermed.a.alsaadi@durham.ac.uk

Funding information
UKRI EPSRC Prosperity Partnership in Offshore Wind, Grant/Award Number: EP/R0049/1

Abstract

The reliability of wind turbine power converters is crucial for analyzing wind energy project costs, and for estimating maintenance and downtime. The published literature in this field relies on evaluating the reliability effect of wind speed to estimate the converter lifetime. However, this paper demonstrates that wind turbulence intensity, which has not been widely considered in similar reliability analyses, shows a significant impact on converter lifetime. This paper uses 821 10-min wind speed time series sampled at 1 Hz on the two most commonly deployed wind turbine converter topologies: the two-level voltage source and the three-level neutral point clamped. Electromechanical and thermal modelling, combined with statistical analysis shows that mean wind speed and turbulence intensity both impact the lifetime of both converter topologies. However, the paper estimates that the three-level converter can operate 2.4 to 4.0 times longer than the two-level converter depending on the operating wind speed and turbulence intensity.

1 | INTRODUCTION

Wind turbine (WT) reliability impacts the cost of wind energy due to WT downtime and the cost of maintenance [1]. The reliability data of WT subassemblies show that the wind turbine power converter (WTPC) ranks as one of the highest failing parts in the system [2]. WTPC reliability analysis provides the device's end-of-life estimation which is important information required for the cost analysis of the new wind farms and the maintenance planning of the operational farms.

After frequent and costly failures of WTPC, a large group of researchers from academia and industry joined the investigations of the impacting factors and causes of failures [3]. The semiconductor thermal loading was found to be the main cause of failure in WTPC [4]. The differences in the thermal expansion coefficient of the semiconductor internal parts and the cycling junction temperature develop a cyclic thermomechanical stress that causes damage in the semiconductor [5]. Methods for estimating converter lifetime based on its semiconductor's thermal cycling are widely used by academia [6–8] and industry [9, 10]. Empirical lifetime models like Coffin–Manson Arrhenius [5] and Bayerer [11] estimate semiconductor lifetime based on junction temperature cycling.

Current state-of-the-art WTs have adopted the permanent magnet synchronous generator (PMSG). This generator type requires a full power back-to-back AC–DC–AC converter for energy conversion and control. Two converter topologies have been used with PMSG WTs: the two-level voltage-source converter (2L-VSC) and the three-level neutral point clamped converter (3L-NPC). The 3L-NPC provides higher operating voltage with reduced current which reduces the size of cables and transformer. However, it requires more semiconductors than 2L-VSC and needs more complex control and maintenance. 3L-NPC is the preferred topology with medium voltage (MV) applications like MV wind turbines while 2L-VSC is preferred with low voltage (LV) applications. Examples of LV WTs equipped with 2L-VSC include Siemens Gamesa SWT-7.0/SG-8.0, MHI Vestas V164-8.0 and Enercon E126-7.58 [3] While MV WTs equipped with 3L-NPC include GE Haliade-X [12] and Samsung S7.0.171 [13]. The published literature in this field focuses on the relationship between the operating wind speed and the reliability of WTPC where the reliability analyses show wind speed has a direct impact on the lifetime of the converter's semiconductors. The relationship between wind speed and WTPC reliability is widely discussed [6, 7, 14, 15].

Besides the average wind speed, WTPC reliability is also impacted by other wind parameters like gust frequency and turbulence intensity [14, 16]. Wind turbulence intensity (TI) is an important parameter that can be extracted from the wind speed data. The TI of a wind speed time series (WSTS) is expressed as the percentage value of the standard deviation of wind speed measurements (U_σ) divided by the WSTS average wind speed (U_{avg}) [17], as in Equation (1).

$$\text{TI} = \frac{U_\sigma}{U_{\text{avg}}} \cdot 100\% \tag{1}$$

A few published articles introduced the possibility of a relationship between TI and WTPC reliability. In [14], the impact of wind gust frequency on the semiconductors' lifetime in WTPC has been presented. The paper analyzed the impact of wind gust frequency on the reliability of the 2L-VSC WTPC by simulating the thermal loading of the converter semiconductors. The results showed that thermal loading increases at slower wind gust frequency. Accordingly, the paper concluded that lower turbulence sites would have a more damaging impact on the WTPC. The paper built that conclusion based on the results of simulations using synthetic constant and square wave wind speed time series. However, a simulation with field-measured wind speed data would have provided more realistic results of the impact of wind turbulence on WTPC lifetime.

In [7], The reliability interactions between wind roughness classes and the WTPC modulation method have been presented. The paper tested the lifetime of 3L-NPC WTPC using thermal loading simulation with different wind roughness classes. Based on the simulation results, the paper suggested that a certain type of converter pulse width modulation (PWM) achieves better converter reliability during high roughness class wind. Accordingly, the paper concluded that higher turbulence intensity wind has a negative reliability impact on the WTPC. However, the paper did not analyze nor evaluate the mentioned impact. This paper's conclusion conflicts with the findings of the previous paper.

In [18], the thermal loading of the WTPC semiconductors is assessed against the wind speed dynamics. The paper simulated the WTPC semiconductor junction temperature of a 1.5 MW WT while applying a 180 WSTS. The visual comparison between the WTPC semiconductors' simulated junction temperature and the wind speed trends showed that during the high-frequency wind speed changes, the semiconductors had lower thermal loading. The paper found that it is reasonable to assume that low-frequency turbulence winds produce a higher damage rate to the WTPC. However, the paper's conclusion was based on the results of only one 180-s WTST without demonstrating further analysis to evaluate the results.

The reviewed papers as well as other published papers on this subject assess WTPC reliability either based on constant wind speeds, synthetic wind samples, or a small number of WSTS. The practical loading of the WT is complex due to the nature of wind and, as such, is the WTPC reliability assessment. Therefore, WTPC reliability analysis has to consider a wide range of wind speeds and use statistical analysis to approach the expected lifetime. Furthermore, statistical analysis would be the best way to determine the impact of wind TI on WTPC lifetime since TI is a statistically calculated value based on the standard deviation of wind speed as in Equation (1).

This paper analyzes that relationship by applying field-measured wind speed data on the two most commonly deployed WTPC topologies in WTs, 2L-VSC and 3L-NPC. The paper uses the WTPC's semiconductor thermal loading to assess the WTPC lifetime and analyze the effects of wind conditions. Furthermore, the paper demonstrates the reliability comparison between both WTPC topologies for the same input wind to identify which converter shows better reliability for the particular tested wind characteristics.

2 | WTPC MODELLING AND RELIABILITY ANALYSIS

The reliability of a WTPC is highly influenced by the lifetime of its semiconductors where the thermal cycling of their junction temperature is considered the main cause of WTPC failure [8]. The semiconductor lifetime can be estimated by the Coffin–Manson Arrhenius model. This considers the range and average of their junction temperature cycles to calculate the accumulated damage and accordingly the estimated lifetime. Semiconductor junction temperature is a function of the semiconductor power losses which depend on the WTPC loading and thus the wind speed. The semiconductor junction temperature affects its internal parameters which impact its junction temperature in an iterating process. Junction temperature estimation of WTPC semiconductors during variable wind speed is complex and therefore system simulation is chosen to provide a suitable approach.

The two most widely deployed converters in WTs (2L-VSC and 3L-NPC) are modelled in two separate models for reliability analysis. Both models involve mechanical, electrical, and thermal subsystems to capture the system dynamics in the simulation results. Both models are based on 2 MW PMSG direct-drive variable-speed wind turbines. The overview of the wind turbine model is shown in Figure 1 where ω_m is the WT generator speed (rad/s), T_{ref} is the reference torque (Nm), I_m is the generator current (Ampere), FOC is the field-oriented control, and SVPWM is the space vector pulse width modulation. The shaded blocks in the diagram represent the reliability-related subsystems showing the corresponding sections of this section while the other blocks are modelled as required for the WT operation and control. The WT parameters and control design are based on [19] and shown in Table 1. MATLAB and Simulink are used in the modelling and simulating of both WT models, 2L-VSC and 3L-NPC. The following sections describe the modelling of the reliability-related subsystems as indicated in Figure 1.

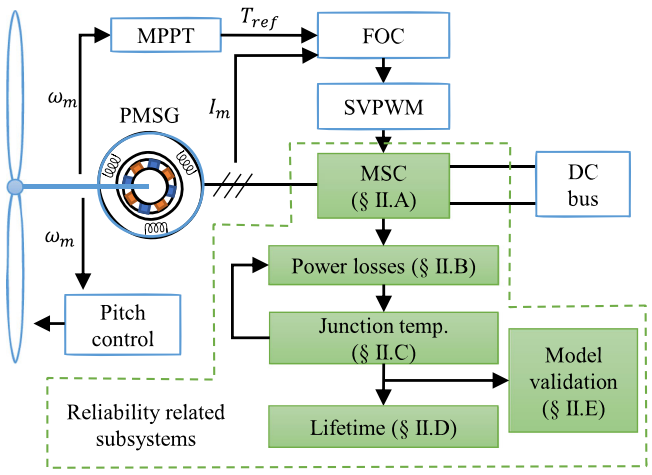

FIGURE 1 Wind turbine model overview.

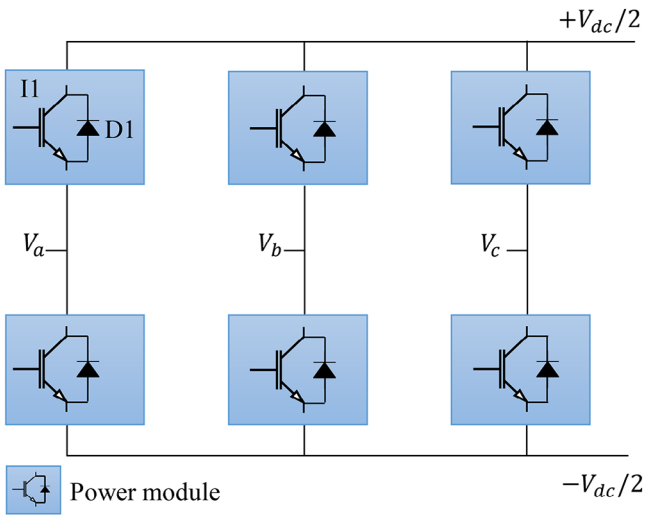

FIGURE 2 Schematic diagram of three-phase 2L-VSC.

TABLE 1 Wind turbine parameters.

Wind turbine type	Direct-drive variable speed
Cut-in wind speed (m/s)	4
Rated wind speed (m/s)	12
Cut-out wind speed (m/s)	25
Rotor diameter (m)	82
Power coefficient, $C_{p_{max}}$	0.34
Rotor moment of inertia (kg m^2)	2,920,000
Generator type	Three-phase PMSG
Generator rated power (kW)	2,000
Generator rated apparent power (kVA)	2,242
Generator number of pole pairs	26
Generator rated frequency (Hz)	9.75

2.1 | Converter system

A PMSG WT usually employs a fully rated power AC–DC–AC converter which consists of a machine-side converter (MSC) and a grid-side converter (GSC). The MSC is connected between the generator and the DC bus and is responsible for extracting the generator power. The GSC is connected between the DC bus and the grid transformer and is responsible for providing regulated DC voltage in the DC bus. The GSC shows a lower failure rate (higher lifetime) than the MSC because it operates at fixed grid frequency and voltage. Therefore, the WTPC system reliability is dominated by the MSC [14, 20]. The MSC lifetime is considered for the WTPC reliability analysis in this paper while the GSC is substituted with a DC supply to reduce model complexity and simulation time.

The two WT models, 2L-VSC and 3L-NPC, have the same WT mechanical subsystem and the same control and use the same input of WSTS for reliability analysis and comparison. However, they vary by the operating voltage as 3L-NPC is usually deployed in MV WTs (rated generator voltage is above 1 kV) while 2L-VSC is deployed in LV WTs, (rated generator voltage is below 1 kV). The following paragraphs describe the modelling of both converters.

2.1.1 | 2L-VSC

This converter model is constructed with six power modules each having an IGBT and a reverse parallel diode. Semikron's power module SKM800AG167D [21] is selected for this model due to its ratings and the specified application area by the manufacturer. Accordingly, the modelled converter's rated power is 335 kW. Therefore, six converters are required to operate in parallel to handle the generator's rated power (2 MW). Parallel converters are used in WTs to share the generator power. An example of this is the Siemens G10x 4.5 MW where six converters are placed in parallel [22]. The converter subsystem schematic diagram is shown in Figure 2 where I1 is IGBT1, D1 is diode1, $V_{a,b,c}$ are the AC three-phase voltages.

2.1.2 | 3L-NPC

This converter model is assembled with 18 power modules as shown in the schematic diagram in Figure 3. Similar to the 2L-VSC power module, SKM800AG167D is selected for the 3L-NPC model for the reliability comparison. The 3L-NPC operating voltage is twice the power module's rated voltage [4]. Therefore, the 3L-NPC rated voltage is twice the 2L-VSC rated voltage when both converters are constructed using the same power module. However, both converters will have the same current capacity which is equal to the power module's rated current and that makes the modelled 3L-NPC rated power 670 kW. Accordingly, only three parallel 3L-NPC are required to handle the generator's rated power (2 MW). The parameters of the 2L-VSC and 3L-NPC models are listed in Table 2.

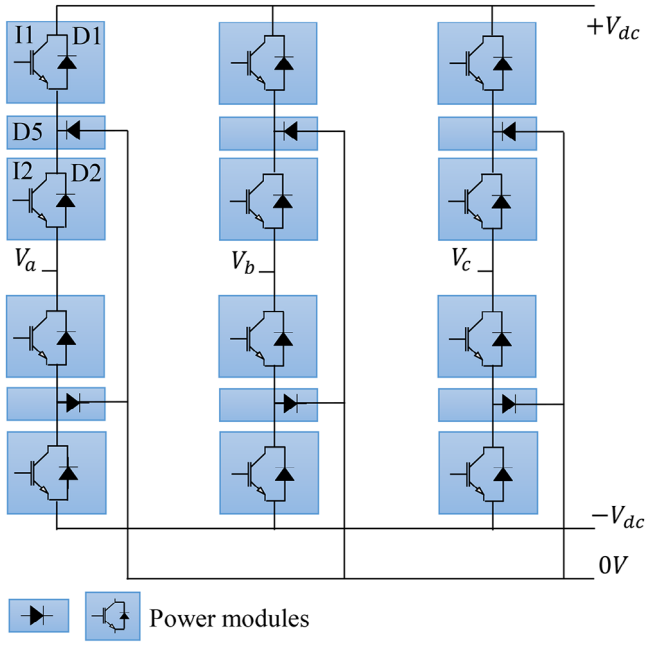

FIGURE 3 Schematic diagram of three-phase 3L-NPC.

TABLE 2 2L-VSC and 3L-NPC models parameters.

Converter topology	2L-VSC	3L-NPC
Rated power of one converter (kW)	335	670
Number of parallel converters in WT	6	3
Total rated power (kW)	2,000	2,000
Total number of IGBTs	36	36
Total number of diodes	36	54
DC bus voltage (V)	1150	2300
Generator line voltage (V)	230-690	460-1380
Power module	SKM800AG176D	
Heatsink cooling method	Liquid	
Coolant temperature (C)	40	
Generator frequency (Hz)	3.25–9.75	
Control strategy	FOC	
Switching frequency (Hz)	1900	

2.2 | Power losses

The converter semiconductors' lifetime is highly impacted by their junction temperature which varies as a function of their power losses and the heatsink thermal characteristics. Semiconductors' power loss modelling is essential in WTPC reliability analysis. Two types of power losses are produced by the semiconductor when operating as a switch as in a WTPC: the switching power losses (P_{sw}) and the conduction power losses (P_{cn}). The switching power losses occur when the semiconductor changes its status between on and off states while the conduction power loss develops when the semiconductor is on. Equations (2) to (4) describe the IGBT conduction, switching,

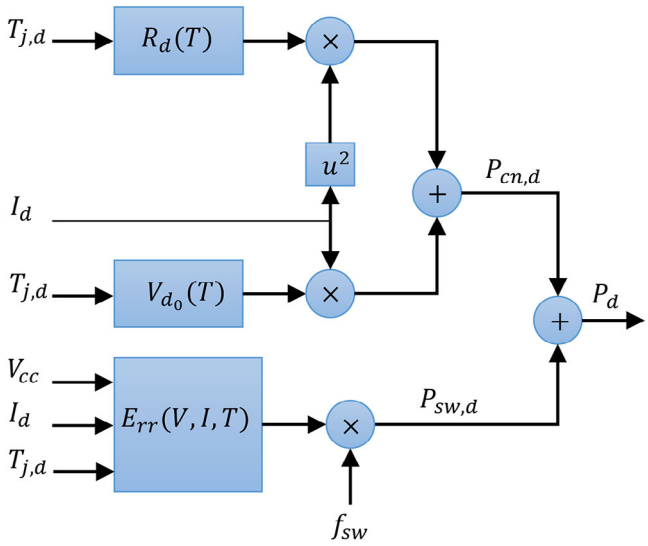

FIGURE 4 Diode power losses in power converter.

and total power losses respectively where V_{ce_0} is the collector–emitter threshold voltage, I_c is the IGBT current, R_{ce} is the IGBT conduction resistance, V_{cc} is semiconductor operating voltage, $P_{cn,i}$ is the IGBT conduction power loss, f_{sw} is converter switching frequency, E_{on} and E_{off} are the IGBT on and off energy, $P_{sw,i}$ is the IGBT switching power loss, and P_i is the IGBT power losses. Similarly, the diode power losses (P_d) are calculated based on the diode parameters.

$$P_{cn,i} = V_{ce_0} \cdot I_c + R_{ce} \cdot I_c^2 \tag{2}$$

$$P_{sw,i} = f_{sw} \cdot (E_{on} + E_{off}) \tag{3}$$

$$P_i = P_{cn,i} + P_{sw,i} \tag{4}$$

The semiconductor's internal parameters are affected by temperature, voltage, and current according to the manufacturer datasheet [21]. Therefore, their values are required to be updated with the related affecting parameters during the simulation. Figure 4 shows the modelling of the diode power losses where $P_{cn,d}$ and $P_{sw,d}$ are the conduction and switching power losses, $T_{j,d}$ is the diode junction temperature, I_d is the diode current, E_{rr} is the reverse recovery energy, V_{d_0} is the threshold voltage, and R_d is the diode on status internal resistance. Similarly, the IGBT power losses are modelled.

2.3 | Thermal modelling

It is difficult to measure the semiconductor's junction temperature and it is complex to calculate it during the variable load of the WTPC. Therefore, thermal modelling is used to determine it in this paper by using the thermal equivalent circuit. The semiconductor power loss is modelled as a current source and the junction temperature is the measured voltage. The thermal impedance, (Z_{th}), includes thermal resistance, (R_{th}), and thermal

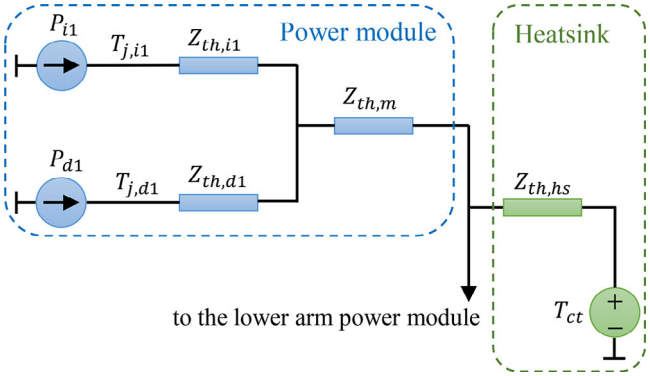

FIGURE 5 Thermal equivalent circuit of the half-bridge upper arm in 2L-VSC.

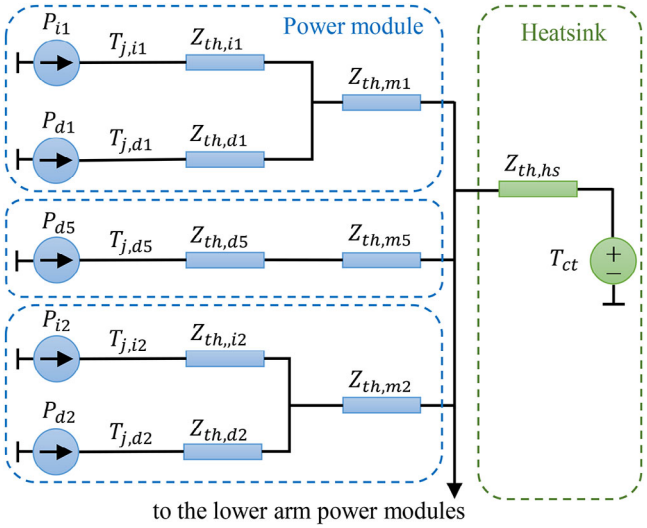

FIGURE 6 Thermal equivalent circuit of the half-bridge upper arm in 3L-NPC.

storage, (C_{th}), are obtained from the semiconductor datasheet and the heatsink parameters. The thermal equivalent circuit is modelled using the Foster model as it is widely used in similar analyses [7]. MATLAB Simscape Thermal Model toolbox [23] components are used in modelling the converter equivalent thermal circuit.

Assuming normal WT operation conditions, the converter phases are balanced and the converter upper arm and lower arm in each half-bridge are operating symmetrically, then only one arm of each converter topology is needed to be modelled. The thermal equivalent circuit of the 2L-VSC half-bridge upper arm with the attached heatsink is shown in Figure 5 while the 3L-NPC half-bridge upper arm with the attached heatsink is shown in Figure 6 where $Z_{\text{th,i}}$ and $Z_{\text{th,d}}$ are the IGBT and the diode thermal impedances, $Z_{\text{th,m}}$ is the thermal impedance of the power electronic module, $Z_{\text{th,hs}}$ is the thermal impedance of the heatsink, $T_{\text{j,i}}$ and $T_{\text{j,d}}$ are the IGBT and diode junction temperatures, and T_{ct} is the heatsink coolant temperature.

2.4 | WTPC lifetime

The WTPC lifetime is estimated based on the lifetimes of its semiconductors, IGBTs and diodes, where the Coffin–Manson Arrhenius lifetime model [5] is used for that as recommended by the power module manufacturer [9]. The lifetime model estimates the number of thermal cycles that the semiconductor can withstand before it will fail which is known as the cycles to failure (N_{f}) calculated for each thermal cycle as a function of the average and range of the junction temperature as in Equation (5) where T_{m} is the semiconductor average junction temperature, ΔT is the junction temperature cyclic range, K_{B} is the Boltzmann constant (1.381×10^{-23} J/K), E_{g} is the semiconductor activation energy (9.891×10^{-20} J), a and b are the model empirical constants, (2.025×10^{5}) and (5.039) respectively as they set by the semiconductor manufacturer data [9]. The WT model simulation provides the time trend of WTPC semiconductor junction temperature related to the WSTS input. The Rainflow algorithm [5] is used to extract the thermal cycles where each one contributes an amount of damage (D_{f}) to the semiconductor calculated by Equation (6). According to Miner's rule [24], the semiconductor accumulated damage (D_{ws}) that occurred during the WSTS time (t_{ws}) is the sum of damages of all thermal cycles of that time calculated as in Equation (7).

$$N_{\text{f}} = a \cdot (\Delta T)^{-b} \cdot e^{E_{\text{g}}/(K_{\text{B}} T_{\text{m}})} \tag{5}$$

$$D_{\text{f}} = \frac{1}{N_{\text{f}}} \tag{6}$$

$$D_{\text{ws}} = \sum_{t=0}^{t=t_{\text{ws}}} D_{\text{f}}(t) \tag{7}$$

Mean time to failure (MTTF) in hours is used to evaluate the lifetimes of the WTPC based on its IGBTs and diodes lifetime. The IGBT lifetime (MTTF_{i}) related to the tested WSTS is calculated as in Equation (8) where $D_{\text{ws,i}}$ is the IGBT accumulated damage and the diode lifetime (MTTF_{d}) is calculated as in Equation (9) where $D_{\text{ws,d}}$ is the diode accumulated damage. The WTPC is considered a system of stressed parts, IGBTs and diodes, where its rate of failure equals the sum of the pars rates of failure. The WTPC's lifetime (MTTF_{pc}) is calculated considering the lifetime of all the IGBTs and diodes in the converter circuit as in Equation (10) where s_{i} and s_{d} are the numbers of IGBTs and diodes in the converter circuit respectively.

$$\text{MTTF}_{i} = \frac{t_{\text{ws}}}{D_{\text{ws,i}}} \tag{8}$$

$$\text{MTTF}_{\text{d}} = \frac{t_{\text{ws}}}{D_{\text{ws,d}}} \tag{9}$$

$$\text{MTTF}_{\text{pc}} = \left(\frac{s_{\text{i}}}{\text{MTTF}_{\text{i}}} + \frac{s_{\text{d}}}{\text{MTTF}_{\text{d}}} \right)^{-1} \tag{10}$$

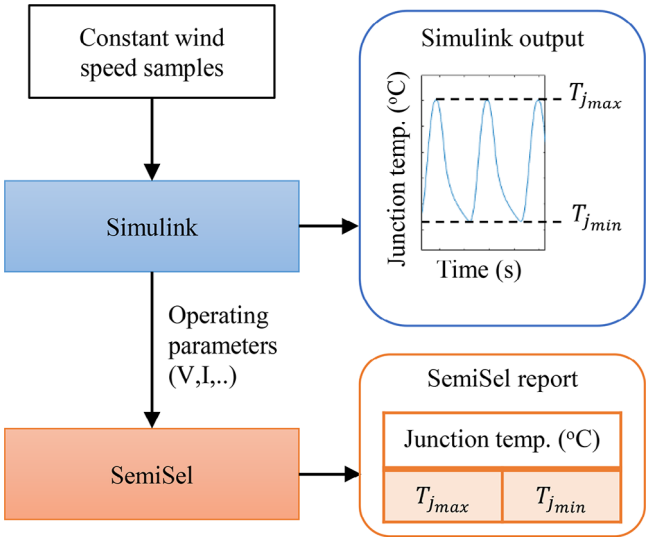

FIGURE 7 Simulation results validation procedure.

2.5 | Validation of simulation results

The precise result of semiconductor junction temperature is crucial for the WTPC lifetime estimation. Semiconductor lifetime is affected exponentially by the junction temperature mean (T_m) and range (ΔT) values as in Equation (5). The Simulink simulation model of the junction temperature is verified by comparing its results with the results of the manufacturer simulation tool, SemiSel [25]. SemiSel simulates the junction temperature of the converter semiconductors with fixed operating parameters (voltage, current, frequency, etc.). These fixed parameters can be extracted using constant wind speed simulation of the modelled WT. SemiSel's output report lists the minimum and maximum junction temperature, (T_{jmin}) and (T_{jmax}), which can be compared with the results of the Simulink model output. Simulink results comparison with SemiSel is used to determine the simulation accuracy. The procedure of the comparison between both results is shown in Figure 7. The results comparison is performed for nine constant wind speeds (4m/s, 5m/s,… 12m/s) which cover the WT's variable wind speed range. The results' accuracy is evaluated for each semiconductor by calculating the root mean square error (RMSE) of the results' relative differences (T_{jDif}) during all tested constant wind speeds. For each tested constant wind speed, T_{jDif} is calculated as in Equation (11) where T_{jSS} is the SemiSel simulation result and T_{jSL} is the Simulink simulation result. RMSE for each semiconductor is calculated as in Equation (12) for all the tested wind speeds where T_{jRSME} is the RMSE of the simulation results and k is the number of simulated constant wind speeds.

$$T_{jDif} = \frac{T_{jSS} - T_{jSL}}{T_{jSS}} \tag{11}$$

$$T_{jRSME} = \sqrt{\frac{\sum_{i=1}^{k} T_{jDif}^2}{k}} \tag{12}$$

TABLE 3 Junction temperature results RMSE.

Model	Semiconductor	T_{jmax}(%)	T_{jmin}(%)
2L-VSC	I1	0.24	0.18
	D1	0.43	0.19
3L-NPC	I1	0.15	0.15
	D1	0.94	0.93
	I2	0.83	0.26
	D2	0.81	1.4
	D5	2.1	0.83

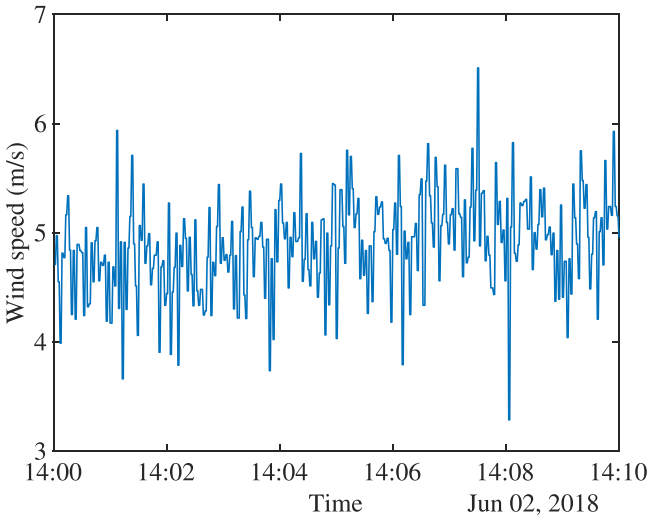

FIGURE 8 Example of 10 min WSTS.

The RMSE value is calculated for each semiconductor's T_{jmax} and T_{jmin} in both WTPC models. The calculated RMSE is shown in Table 3 where most of the values are less than 1 percent which indicates that the results of both WTPC models (2L-VSC and 3L-NPC) are accurate for the WTPC reliability analysis.

3 | EXPERIMENTAL RESULTS AND DISCUSSION

The WTPC reliability analysis is approached by applying a set of WSTS to the simulation model and analyzing the estimated lifetime against the wind properties, U_{avg} and TI. The WSTS are field-recorded wind speed data. Each WSTS is 10 min long and the wind speed is sampled at 1Hz, giving 600 wind speed measurements. The WSTS used in this paper are chosen from year-long wind speed data recorded by ORE Catapult in Blyth, UK. Figure 8 shows an example of one WSTS 4.89 m/s U_{avg} and 9 percent TI.

3.1 | Test 1: WTPC lifetime under WT operating wind speed

The effect of wind properties, U_{avg} and TI on the WTPC lifetime is analyzed in this test. The test includes simulating the

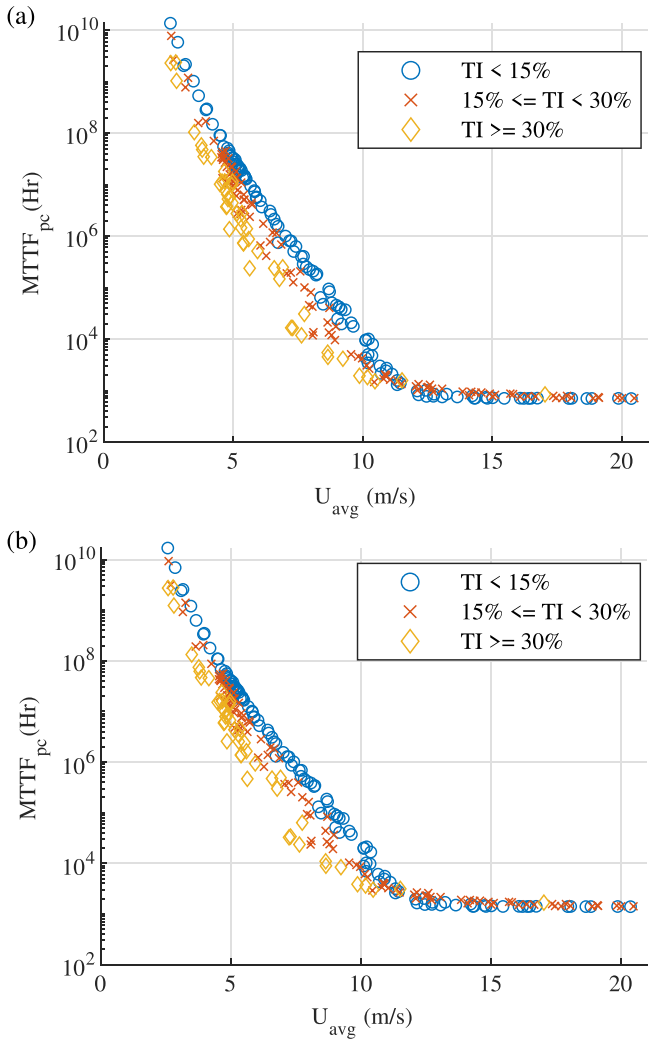

FIGURE 9 WTPC lifetime simulation results, (a) 2L-VSC and (b) 3L-NPC.

WTPC lifetime with a large number of WSTS to cover the WT operating range of wind speed and a wide range of TI. A set of 282 WSTS are selected for this test to cover U_{avg} range from 2.5 to 20.5 m/s and TI range of 1.81–42.36 percent. The simulation results for converter lifetime ($MTTF_{pc}$) are presented in a scatter diagram versus WSTS U_{avg} in Figure 9 for 2L-VSC and 3L-NPC models. To visualize the effect of the TI on the converter lifetime, the WSTS are grouped into three TI levels, less than 15 percent, between 15 and 30 perent, and above 30 percent. The TI groups are plotted in different colours and shapes in the scatter diagrams in Figure 9.

The WSTS U_{avg} shows a clear impact on the WTPC reliability in both WTPC topologies. As U_{avg} increases the MTTF decreases in a log scale until U_{avg} reaches the WT's rated wind speed where the MTTF does not reduce further because the WT pitch control is activated and reduces the blades' angle of attack to limit the WT power. On the other hand, The relationship between the WSTS TI and the WTPC lifetime can be seen in Figure 9 where the group of high TI WSTS (more than 30 percent) shows lower $MTTF_{pc}$ while the group of lower TI WSTS (less than 15 percent) shows higher $MTTF_{pc}$. However, the results overlap among the TI groups which appears because wind speed behaves differently in different WSTS even if they have the same average wind speed and the same TI. They therefore impact WTPC lifetime differently. Statistical methods will provide a better approach to analyze the impact of TI on the WTPC lifetime in the following test.

TABLE 4 Mean and standard deviation of WTPC log(MTTF) for four TI groups of WSTS.

			2L-VSC		3L-NPC	
U_{avg}(m/s)	TI(%)	n	μ	σ	μ	σ
6	10	40	15.47	0.077	15.79	0.068
6	15	34	15.24	0.141	15.58	0.120
6	20	53	14.73	0.250	15.16	0.203
6	25	34	14.02	0.443	14.56	0.372

3.2 | Test 2: the impact of TI on WTPC lifetime

This test analyzes the impact of the TI on the WTPC lifetime. Since the wind TI includes complex patterns of wind speed variations, this test uses a statistical approach to evaluate the impact of TI on WTPC lifetime. For this, four sets of WSTS having the same average wind speed (6 m/s) but varying in their percentage TI (10, 15, 20, and 25) are applied to the simulation models. Each set includes a number of WSTS (n) simulated with WTPC models. The logarithmic values of the WTPC's lifetime ($\log(MTTF_{pc})$) are obtained for each tested WSTS. The statistical mean (μ) and standard deviation (σ) of each set results are calculated by Equations (13) and (14) respectively and shown in Table 4. The simulations' results of each set are applied to the statistical normality distribution test to clarify whether or not they are normally distributed. The Anderson–Darling test (AD test) [26] is selected as it is a widely used normality distribution test. The results of the four TI sets show that they are normally distributed so they can be represented by normal distribution fitting curves as shown in Figure 10 for the 2L-VSC and 3L-NPC.

This test proves that TI has impacted the WTPC lifetime. Although simulating individual WSTS may not show that clearly but the impact is clear when comparing the average WTPC lifetime of many WSTSs for different TI groups. This indicates that WTPC lifetime is impacted by the wind TI in the long run of the WT. Moreover, it can be observed that higher TI groups have a wider distribution curve (larger σ) than lower TI groups. This is because larger TI means higher variation in wind speed which is reflected in a wider distribution of WTPC lifetime estimates. This test examined the impact of TI related to one wind speed (6 m/s), while the next test analyzes the impact of the WTPC lifetime by TI for the range of WT operating wind speeds.

$$\mu = \frac{\sum_{i=1}^{i=n} \log\left(\mathrm{MTTF}_{\mathrm{pc}_i}\right)}{n} \tag{13}$$

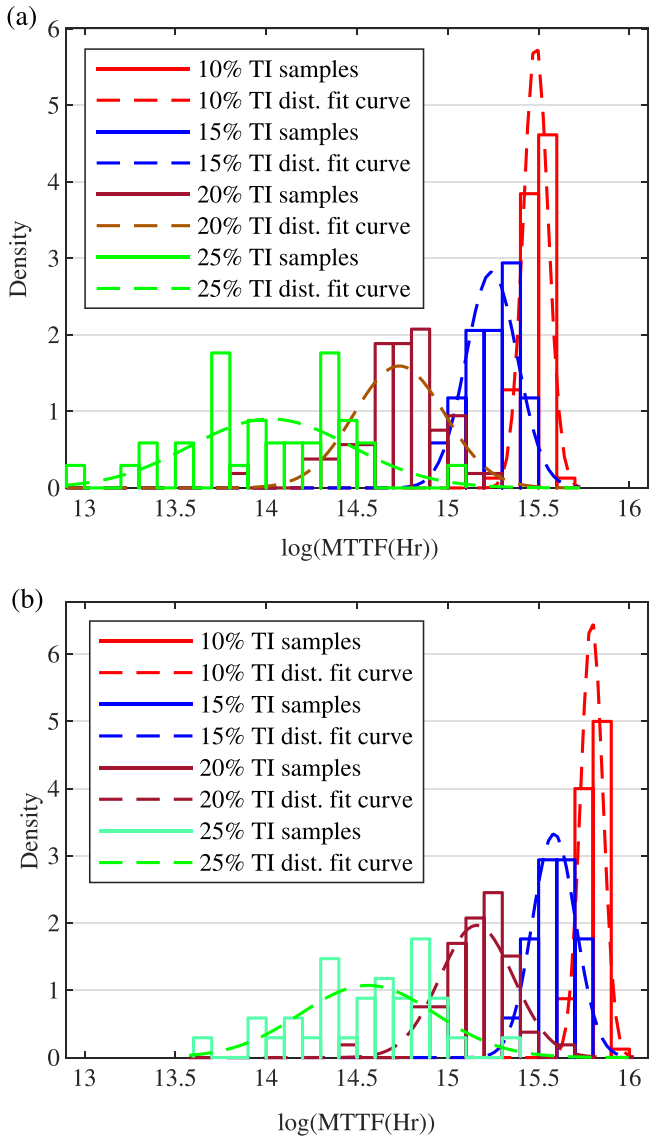

FIGURE 10 WTPC lifetime distributions of 10–25 percent TI WSTS with 6 m/s average wind speed, (a) 2L-VCS and (b) 3L-NPC.

$$\sigma = \sqrt{\frac{\sum_{i=1}^{n}\left(\log\left(\mathrm{MTTF}_{\mathrm{pc}_i}\right) - \mu\right)^2}{n}} \tag{14}$$

This test analyzes the impact of TI on the WTPC lifetime for a range of wind speeds to clarify the significance of TI impacts on the WTPC's lifetime. The test applies ten groups of WSTS on both WT models, 2L-VSC and 3L-NPC. The WSTS groups have U_{avg} of 4, 6, 8, 10, and 12 m/s, and TIs of 10 and 20 percent. The selected WSTS average wind speeds cover the WT variable speed range. The number of WSTS in each group (n) is shown in 5. For each group of WSTS, the average and standard deviation of logarithmic WTPC lifetimes are calculated by Equations (13) and (14) respectively. To analyze the statistical significance in lifetime differences between 10–20 percent TI for each U_{avg}, the confidence intervals (CI) are used. The CI is

TABLE 5 Lifetime comparison of two TI groups.

U_{avg} (m/s)	TI (%)	n	2L-VSC CI	3L-NPC CI
4	10	34	19.33 ± 0.034	19.5 ± 0.036
6		40	15.47 ± 0.024	15.79 ± 0.021
8		35	12.21 ± 0.034	12.84 ± 0.029
10		35	9.09 ± 0.052	9.89 ± 0.054
12		35	6.95 ± 0.012	7.64 ± 0.012
4	20	35	18.83 ± 0.076	19.02 ± 0.072
6		53	14.73 ± 0.067	15.16 ± 0.045
8		35	11.18 ± 0.092	11.89 ± 0.091
10		34	8.17 ± 0.051	8.87 ± 0.051
12		35	7.16 ± 0.017	7.86 ± 0.017

calculated for a selected level of confidence where 95 percent is a widely accepted value in scientific research. The CI of the logarithmic lifetimes of each group is calculated by Equation (15) where z is the confidence level value which equals 1.96 for a 95 percent confidence level. The CI of the tested WSTS groups are shown in Table 5. The lifetime significance difference between the 10 and 20 percent groups can be illustrated using the error bars used to display CI as in Figure 11 for both 2L-VSC and 3L-NPC models. It is clearly shown that the results' CI do not overlap with most of the tested groups which are interpreted as lifetimes differences are significant between the two tested TIs. However, the WTPC lifetime of two TI groups overlapped near the rated wind speed and that is because the higher TI WSTS are more affected by the WT pitch control than the lower TI WSTS resulting in a more regulated rotating speed and therefore achieving higher WTPC lifetime values. This test proved that TI is significantly impacting the WTPC's lifetime for both 2L-VSC and 3L-NPC topologies.

$$\mathrm{CI} = \mu \pm \mathrm{z}\frac{\sigma}{\sqrt{(n)}} \tag{15}$$

3.3 | Lifetime comparison between WTPC topologies

The previous reliability tests show that average wind speed and TI both affect WTPC lifetime for both tested topologies, 2L-VSC and 3L-NPC. Both topologies show similar impacts however the lifetime values ($\mathrm{MTTF}_{\mathrm{pc}}$) were different. The comparison between 2L-VSC and 3L-NPC lifetimes explores which one of them achieves a longer life at the tested conditions. The comparison is evaluated by calculating the lifetime ratio (LTR) of the 3L-NPC to the 2L-VSC as in Equation (16).

$$\mathrm{LTR} = \frac{\mathrm{MTTF}_{\mathrm{3L\text{-}NPC}}}{\mathrm{MTTF}_{\mathrm{2L\text{-}VSC}}} \tag{16}$$

WTPC lifetime results are selected for LTR evaluation covering the WT operating wind speed range and belong to two

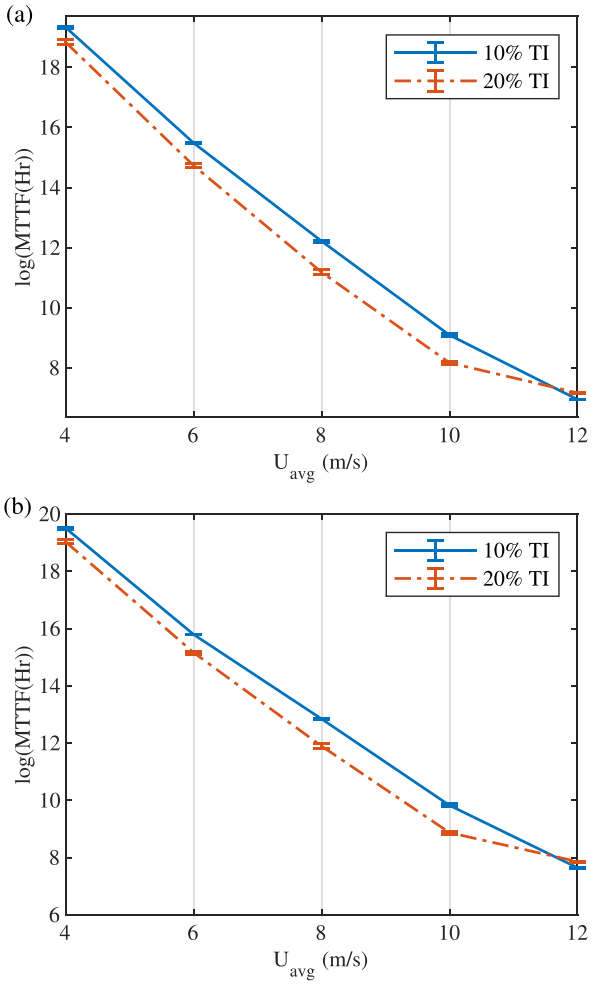

FIGURE 11 Lifetime of WTPC of 10 and 20 percent TI, (a) 2L-VSC and (b) 3L-NPC.

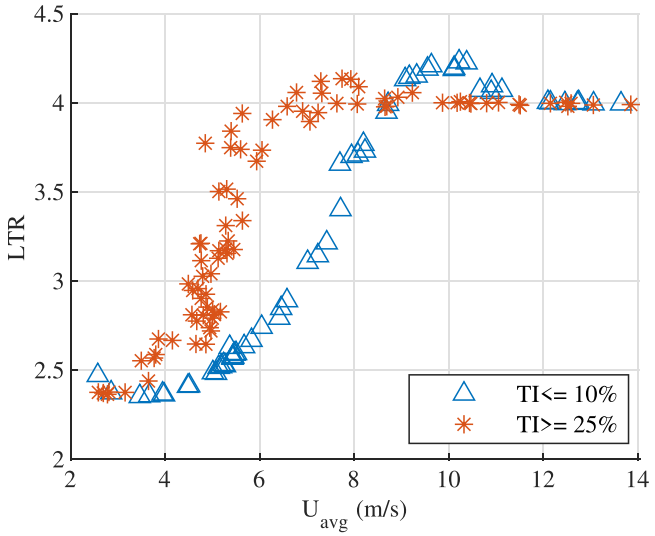

FIGURE 12 Lifetime comparison of 2L-VSC and 3L-NPC. LTR shows the lifetime ratio of 3L-NPC to 2L-VSC.

groups of TI (≤10 percent) and (≥25 percent) for clarity of the comparison. The WTPC lifetime results are presented in the scatter diagram in Figure 12 which clearly shows that LTR is affected by U_{avg} and TI. The results construct two trends for the two TI groups where both are increasing as the U_{avg} increase however the higher TI group (≥25 percent) shows higher LTR values than the ≤10 percent group for similar U_{avg} values. Therefore, it can confidently be concluded that the 3L-NPC WTPC can operate longer in time compared with 2L-VSC WTPC, especially with the high-speed and high-turbulence wind. The 3L-NPC topology shows a longer lifetime than 2L-VSC and that is because the converter load is distributed among more semiconductors in 3L-NPC. This results in lower temperature and therefore longer lifetime for 3L-NPC when compared with the 2L-VSC, particularly when subject to high turbulence intensities.

4 | CONCLUSIONS

This paper has examined the effects of average wind speed (U_{avg}) and turbulence intensity (TI) on the reliabilities of two common WTPC topologies, 2L-VSC and 3L-NPC. The paper has applied statistical analysis to data from detailed electrical and thermal WTPC simulation and lifetime estimation to understand the effects of these two wind characteristics on WTPC lifetime. Lifetime was simulated for 821 10-min WSTS with wind speed sampled at 1Hz. The mean and standard deviation of the simulation results show clearly the relationship between wind conditions and WTPC lifetime. Furthermore, the results reveal how wind conditions interact differently according to the WTPC topology. The paper's conclusions can be summarized as follows:

- Increased average wind speed has a direct and significant negative impact on the lifetime for both WTPC topologies, 2L-VSC and 3L-NPC.
- Higher wind TI causes lower WTPC lifetime in both converter topologies, 3L-NPC and 2L-VSC, however this impact is primarily noticeable over longer periods of WT operation.
- When comparing converter topologies for increasing average wind speed, the 3L-NPC converter achieves better reliability than the 2L-VSC. The 3L-NPC WTPC has an estimated lifetime 2.4 times that of the 2L-VSC WTPC at low average wind speed WSTS; this ratio increases as the WSTS average wind speed increases to reach 4.0 times the estimated lifetime at the WT rated wind speed.
- The 3L-NPC WTPC is more reliable than the 2L-VSC for higher TI wind.
- Wind turbulence and wind speed both have a noticeable effect on the reliability of the WTPC, and both should be considered for WTPC lifetime estimation and converter topology selection.

AUTHOR CONTRIBUTIONS

Sermed Alsaadi: Methodology; software; visualization; writing—original draft. **Christopher J. Crabtree**: Resources; supervision; writing—review and editing. **Peter C. Matthews**:

Supervision; writing—review and editing. **Mahmoud Shahbazi**: Supervision; writing—review and editing.

ACKNOWLEDGEMENTS

This paper is produced as part of the research funded by the UKRI EPSRC Prosperity Partnership in Offshore Wind EP/R0049/1. (npow.group.shef.ac.uk).

CONFLICT OF INTEREST STATEMENT

The authors declare no conflicts of interest.

DATA AVAILABILITY STATEMENT

Data sharing not applicable - no new data generated

ORCID

Sermed Alsaadi https://orcid.org/0000-0002-1923-5358
Christopher J. Crabtree https://orcid.org/0000-0003-0109-5323
Mahmoud Shahbazi https://orcid.org/0000-0002-6057-3228

REFERENCES

1. Dao, C., Kazemtabrizi, B., Crabtree, C.: Wind turbine reliability data review and impacts on levelised cost of energy. Wind Energy 22(12), 1848–1871 (2019)
2. Spinato, F., Tavner, P.J., Van Bussel, G.J.W., Koutoulakos, E.: Reliability of wind turbine subassemblies. IET Renewable Power Gener. 3(4), 387–401 (2009)
3. Fischer, K., Pelka, K., Bartschat, A., Tegtmeier, B., Coronado, D., Broer, C., et al.: Reliability of power converters in wind turbines: Exploratory analysis of failure and operating data from a worldwide turbine fleet. IEEE Trans. Power Electron. 34(7), 6332–6344 (2019)
4. Blaabjerg, F., Liserre, M., Ma, K.: Power electronics converters for wind turbine systems. IEEE Trans. Ind. Appl. 48(2), 708–719 (2012)
5. Kovačević-Badstuebner, I.F., Kolar, J.W., Schilling, U.: Modelling for the lifetime prediction of power semiconductor modules. In: Reliability of Power Electronic Converter Systems, pp. 103–140. IET, London (2016)
6. Ye, S., Zhou, D., Yao, X., Blaabjerg, F.: Component-level reliability assessment of a direct-drive PMSG wind power converter considering two terms of thermal cycles and the parameter sensitivity analysis. IEEE Trans. Power Electron. 36(9), 10037–10050 (2021)
7. Isidoril, A., Rossi, F.M., Blaabjerg, F., Ma, K.: Thermal loading and reliability of 10-MW multilevel wind power converter at different wind roughness classes. IEEE Trans. Ind. Appl. 50(1), 484–494 (2014)
8. Busca, C., Teodorescu, R., Blaabjerg, F., Munk-Nielsen, S., Helle, L., Abeyasekera, T., et al.: An overview of the reliability prediction related aspects of high power IGBTs in wind power applications. Microelectron. Reliab. 51(9–11), 1903–1907 (2011)
9. Wintrich, A., Nicoai, U., Reimann, T., Tursky, W.: Application Manual Power Semiconductors. 2nd ed. ISLE Verlag, Ilmenau (2015)
10. Birk, J., Andresen, B.: Parallel-connected converters for optimizing efficiency, reliability and grid harmonics in a wind turbine. 2007 European Conference on Power Electronics and Applications, pp. 1–7. IEEE, Piscataway, NJ (2007)
11. Bayerer, R., Herrmann, T., Licht, T., Lutz, J., Feller, M.: Model for power cycling lifetime of IGBT modules – various factors influencing lifetime. In: CIPS 2008-5th International Conference on Integrated Power Electronics Systems, pp. 37–42. IEEE, Piscataway, NJ (2008)
12. GE. Haliade-X offshore wind turbine. https://www.ge.com/renewableenergy/wind-energy/offshore-wind/haliade-x-offshore-turbine (2021). Accessed 8 June 2023
13. Samsung Heavy industries. Samsung Wind Energy Solutions (2015). http://www.samsungshi.com/eng/default.aspx. Accessed 4 June 2020
14. Smith, C.J., Crabtree, C.J., Matthews, P.C.: Impact of wind conditions on thermal loading of PMSG wind turbine power converters. IET Power Electron. 10(11), 1268–1278 (2017)
15. Kostandyan, E.E., Ma, K.: Reliability estimation with uncertainties consideration for high power IGBTs in 2.3 MW wind turbine converter system. Microelectron. Reliab. 52, 2403–2408 (2012)
16. Anderson, P.M., Bose, A.: Stability simulation of wind turbine systems. IEEE Power Eng. Rev. 3(12), 32–32 (1983)
17. Li, H., Ji, H., Li, Y., Liu, S., Yang, D., Qin, X., et al.: Reliability evaluation model of wind power converter system considering variable wind profiles. In: 2014 IEEE Energy Conversion Congress and Exposition, ECCE 2014, pp. 3051–3058. IEEE, Piscataway, NJ (2014)
18. Baygildina, E., Peltoniemi, P., Pyrhonen, O., Ma, K., Blaabjerg, F.: Thermal loading of wind power converter considering dynamics of wind speed. In: IECON Proceedings Industrial Electronics Conference, pp. 1362–1367. IEEE, Piscataway, NJ (2013)
19. Wu, B., Lang, Y., Zargari, N., Kouro, S.: Power Conversion and Control of Wind Energy System. vol. 148, Wiley, New York (2011)
20. Fischer, K., Stalin, T., Ramberg, H., Wenske, J., Wetter, G., Karlsson, R., et al.: Field-experience based root-cause analysis of power-converter failure in wind turbines. IEEE Trans. Power Electron. 30(5), 2481–2492 (2015)
21. SEMIKRON DANFOSS. SKM800GA176D IGBT Module. https://www.semikron-danfoss.com/products/product-classes/igbt-modules/detail/skm800ga176d-22890435.html. Accessed 12 June 2023
22. Andresen, B., Birk, J.: A high power density converter system for the Gamesa G10x 4,5 MW wind turbine. In: 2007 European Conference on Power Electronics and Applications, EPE, pp. 1–8. IEEE, Piscataway, NJ (2007)
23. The Mathworks Inc. Semscape 5.0. https://www.mathworks.com/products/simscape.html. Accessed 22 September 2022
24. Miner, M.A.: Cumulative damage in fatigue. J. Appl. Mech., Trans. 12(3), A159–A164 (1945)
25. SEMIKRON INTERNATIONAL GmbH. SemiSel. https://semisel.semikron.com (2021). Accessed 9 Feb 2022
26. Anderson, T.W., Darling, D.A.: A Test of Goodness of Fit. J. Am. Stat. Assoc. 49(268), 765–769 (1954). https://www.tandfonline.com/doi/abs/10.1080/01621459.1954.10501232

How to cite this article: Alsaadi, S., Crabtree, C.J., Matthews, P.C., Shahbazi, M.: Understanding wind turbine power converter reliability under realistic wind conditions. IET Power Electron. 1–10 (2024). https://doi.org/10.1049/pel2.12670

CONTROL STRATEGY ASSESSMENT FOR WIND TURBINE CONVERTER RELIABILITY

Sermed AB R Alsaadi[1], Peter C Matthews[1], Christopher J Crabtree[1]*

[1]*Department of Engineering, Durham University, Durham, UK*

Sermed.a.alsaadi@durham.ac.uk

Keywords: CONVERTER RELIABILITY, WIND TURBINE, WIND TURBINE CONVERTER CONTROL

Abstract

Converter reliability has a high impact on wind turbine reliability and therefore cost of wind energy. The wind turbine industry is adopting two control strategies for power converters, Direct Torque Control (DTC) and Field Oriented Control (FOC). Both control methods show high performance in megawatt-scale, variable speed wind turbines. They have similarities and differences in their way of operating and controlling the power converter. This paper investigates whether or not differences between DTC and FOC are impacting wind turbine power converter reliability. It assesses and compares converter reliability between two identical wind turbine systems, one with DTC and the other with FOC. The comparison is based on simulating a range of constant wind speeds on two wind turbine models and analysing the converter lifetime of each based on the semiconductors' thermal cycling. The results show how the operation of each control strategy affects converter reliability with the interaction of varying wind speeds. The modelled wind turbine converter IGBT lifetime drops by 26% and diode lifetime drops by 15%when the converter is controlled with DTC rather than FOC at the rated wind speed.

1 Introduction

Wind turbine power converter reliability has a high impact on the overall reliability of wind energy systems [1] and increases the cost of wind energy due to maintenance costs and system availability. Multiple papers from academia and industry have discussed wind turbine power converter reliability and researched the possible links between the system design and the operational parameters. The impact of converter control strategy on the converter lifetime, however, has not been fully studied. In particular, the effect of the most popular control approaches (field-oriented control (FOC) and direct torque control (DTC)) might affect converter reliability in wind turbine applications. This paper investigates that impact and compares converter reliability under both control strategies.

With the adoption of permanent magnet synchronous generators (PMSG) in wind turbines, the fully-rated AC-DC-AC voltage source converter became the dominant design of wind turbine conversion systems [2]. It offers frequency and voltage separation between the generator and the grid which is suitable for variable-speed pitch-controlled wind turbines. This converter design also offers separate control of active and reactive power which is a requirement by the grid operators for interconnected renewable generations [3].

The industry adopted two control strategies to operate power converters in wind turbine applications: FOC and DTC. Both controllers were developed for induction machine (IM) applications however both were adapted to work with generators of different types such as the induction generator (IG), doubly-fed induction generator (DFIG) and PMSG.

FOC is first presented in 1972 by Hasse and Blaskchke [4]. This control strategy is based on making the machine rotor and stator magnetic fields perpendicular to achieve the highest possible torque and therefore power. Control of the magnetic field vector is achieved by decomposing it into two components, direct and quadrature vectors, and controlling each one separately to achieve full control of the amplitude and angle of the rotating field [5]. The implementation of this control requires a high computational power of the controller which is currently not a big challenge. The output of the control system is a three-phase sinusoidal wave which is delivered to converter switches by means of pulse width modulation (PWM) or space vector PWM.

DTC is first introduced in 1986 by Takahashi and Noguchi [6]. It operates the machine by energising the right coil at the right time to achieve maximum torque and power. The decision of which coil will be energised is made based on estimating the instantaneous torque and magnetic field of the machine. This control is known for its simplicity and does not require high computational power. However, its output frequency changes rapidly so an updated version of this control method was introduced which uses space vector pulse width modulation (SV-PWM) [7].

For reliability analysis, which is the interest of this paper, DTC and FOC have differences in the way they control the converter switches. Those differences reflect on the semiconductor switches' power losses, and this results in differences in semiconductor junction temperatures. Semiconductor junction temperature values for average and cyclic amplitude have a high impact on semiconductor lifetime. This relation is well explained by the Coffin-Manson Arrhenius law shown in equation (1):

$$N_f = a(\Delta T)^{-n} e^{\left(\frac{E_g}{K_B T_m}\right)} \quad (1)$$

Where N_f is the number of thermal cycles to failure, a and n are empirical constants calculated based on accelerated failure test, ΔT and T_m are semiconductor cycle amplitude and mean junction temperatures, E_g is the semiconductor activation energy, and K_B is the Boltzmann constant.

Due to the complexity of lifetime calculation in relation to wind turbine operating conditions, this paper uses simulation to estimate a converter's semiconductor lifetime and therefore the converter's reliability when operated under the two control strategies of DTC and FOC.

2. Methodology

Power converter reliability is highly impacted by its semiconductor switches [8]; their lifetime is found to be strongly related to semiconductor thermal cycling [9]. The Coffin-Manson Arrhenius equation is widely accepted for semiconductor lifetime estimation and considers both the average and cyclic amplitude of the semiconductor's junction temperature.

Semiconductor junction temperature is a result of the semiconductor power losses and heat dissipation from conduction and switching. Therefore, modelling power losses with the thermal characteristics of the semiconductor and the heatsink is essential for converter lifetime estimation.

For testing both DTC and FOC control strategies on power converter reliability, a wind turbine system is modelled in MATLAB [10] and Simulink [11] with a fully-rated machine-side power converter (MSC). The model includes a two-mass mechanical subsystem for the turbine drive train and the direct-driven PMSG which is necessary to consider the generator electromagnetic torque interaction with wind turbine torque. The model also includes power losses and thermal subsystems for lifetime estimation, a DC source which represents the grid-side converter (GSC) for simulation simplicity as GSCs have reportedly lower failure rates than MSC, and converter control subsystems of both control strategies, FOC and DTC. The model overview is shown in Fig. 1 and the modelled wind turbine parameters are listed in Table 1.

The wind turbine PMSG model parameters are in [12], the FOC subsystem design is based on [13], and the DTC subsystem design is based on [14].

The modelled DTC operates on a fixed switching frequency as it utilizes SVM control scheme [7]. Both modelled control strategies, DTC and FOC, were tested with the same switching frequency.

Table 1: Modelled wind turbine parameters

Parameter	Symbol	value
Cut-in wind speed (m/s)	U_{in}	3.5
Rated wind speed (m/s)	U_r	12
Cut-out wind speed (m/s)	U_{out}	25
Rotor diameter (m)	R_t	32
Rated power (kW)	P_m	2,000
Rated line voltage (V)	V_m	690
DC Bus voltage (V)	V_{DC}	1,150
PMSG pole pairs	P_p	26

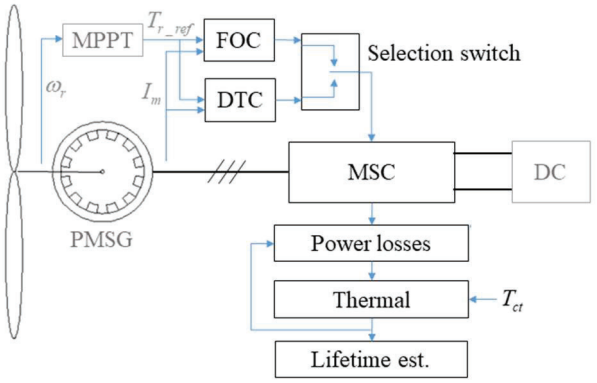

Fig. 1 Wind turbine model overview

The selected converter topology is the two-level voltage source converter (2L-VSC) due to its popularity in the field. The converter consists of six IGBT with freewheeling diode modules. The selected power electronic module is SEMIKRON SKM800GA176D [15]. Fig. 2 shows the schematic diagram of the converter and the attached heatsinks where $sw1$ and $sw2$ are the upper and lower switches of one converter half-bridge. The power rating of the modelled converter is 400 kW while the modelled PMSG is 2 MW, therefore, the simulation considers five paralleled converters to cover the generator rated power. Parallel converters are used with high power wind turbines like in Siemens G10x 4.5MW where six 770 kW converters are paralleled [16].

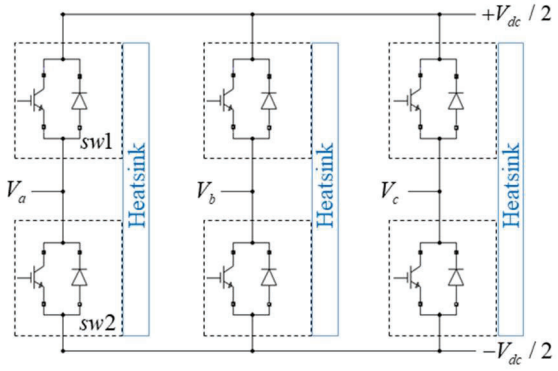

Fig. 2 MSC schematic diagram and heatsink

The converter heatsink is liquid-cooled with an input liquid temperature controlled at 40 C. The heatsink characteristics are listed in Table 2.

Table 2 Converter heatsink details

Cooling method	Liquid (water 50% + glycerine 50%)
Flow rate (L/min)	4
Distance between modules (mm)	20

Thermal impedance 1	$R_{th1} = 0.0122\ K/W, T_{th1} = 6s$
Thermal impedance 2	$R_{th2} = 0.0066\ K/W, T_{th2} = 39.75s$
Total thermal resistance	$R_{hs} = 0.0188\ K/W$

Semiconductor junction temperature is obtained by simulating power losses and considering thermal impedances and heatsink coolant temperature. Fig. *3* shows the thermal equivalent circuit of one converter half-bridge where P_i, P_d are the IGBT and diode power losses, $Z_{th}igbt$, $Z_{th}diode$ are the IGBT and diode thermal impedances, $Z_{th}m$ is the power module thermal impedance, $Z_{th}hs$ is the heatsink thermal impedance, and T_{ct} is the heatsink coolant controlled temperature.

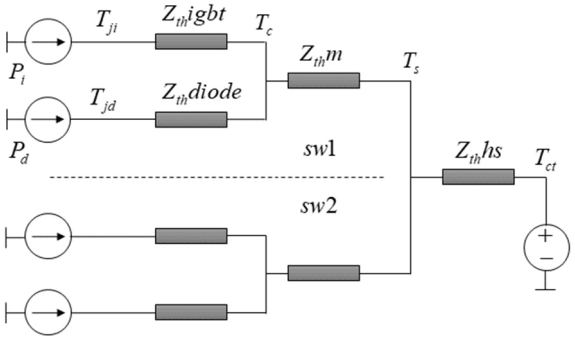

Fig. 3 Thermal equivalent circuit of one converter half-bridge

The experiment is based on simulating a range of constant wind speeds through the wind turbine system model with one of the two control strategies, DTC and FOC, in operation. The impact of the control strategy on the power converter is investigated by comparing converter lifetimes under each control strategy.

3 Results and discussion

The wind turbine model is simulated with five constant wind speeds covering the variable speed region of the wind turbine (4m/s to 12m/s). For each wind speed, the converter IGBT and diode cycles to failure are calculated once with DTC and then with FOC. The simulation outputs IGBT and diode average and cyclic amplitude junction temperature. The estimated cycles to failure for each control approach and wind speed combination are calculated based on the Coffin-Manson Arrhenius law shown in equation (1).

Table 3 lists the converter semiconductor cycles to failure related to wind speed and control strategy where $N_{igbtDTC}$, $N_{igbtFOC}$, $N_{diodeDTC}$, and $N_{diodeFOC}$ are IGBT and diode cycles to failure with the converter controlled by DTC and FOC respectively.

Table 3 converter semiconductors cycles to failure

Wind speed (m/s)	$N_{igbtDTC}$	$N_{igbtFOC}$	$N_{diodeDTC}$	$N_{diodeFOC}$
4	7.93×10^{12}	7.88×10^{12}	1.55×10^{12}	1.55×10^{12}
6	2.05×10^{11}	2.06×10^{11}	4.22×10^{10}	4.24×10^{10}
8	1.35×10^{10}	1.39×10^{10}	1.81×10^{9}	1.86×10^{9}
10	1.27×10^{9}	1.41×10^{9}	7.96×10^{7}	8.48×10^{7}
12	1.27×10^{8}	1.73×10^{8}	2.8×10^{6}	3.28×10^{6}

For the comparison between the semiconductor lifetimes related to the two control strategies, DTC and FOC, the ratio of cycles to failure with DTC to cycles of failure with FOC are defined in equations (2) and (3) for the converter IGBT and diode respectively.

$$\rho_{igbt} = \frac{N_{igbtDTC}}{N_{igbtFOC}} \tag{2}$$

$$\rho_{diode} = \frac{N_{diodeDTC}}{N_{diodeFOC}} \tag{3}$$

Where ρ_{igbt} and ρ_{diode} are lifetime ratios when the converter is operated with DTC and FOC for the IGBT and diode respectively. The results are shown in Table 4.

Table 4 ρ_{igbt} and ρ_{diode} at different wind speeds

Wind speed (m/s)	ρ_{igbt}	ρ_{diode}
4	1.006	1.000
6	0.995	0.996
8	0.969	0.975
10	0.901	0.938
12	0.738	0.852

The converter IGBT and diode lifetime ratios for the two control strategies present the effect of the control strategy on the semiconductors' lifetime across a range of wind speeds as shown in Fig. 4.

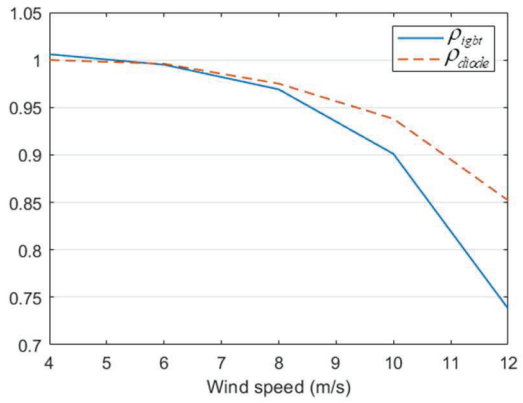

Fig. 4 interaction of ρ_{igbt} and ρ_{diode} with wind speed

At low wind speeds, 4m/s and 6m/s, ρ_{igbt} and ρ_{diode} are approximately 1.00 which means both control strategies, DTC and FOC, do not have a noticeably different impact on the converter lifetime in that wind speed range. However, as the wind speed increases, ρ_{igbt} drops until it reaches 0.743 at rated wind speed (12m/s). This means that the IGBT lifetime will be reduced to 74.3% when the converter is controlled by DTC rather than FOC at rated wind speed. The converter diode shows a similar trend but is less heavily impacted as its lifetime drops to 85.4% when the converter is operated with DTC rather than FOC at rated wind speed.

The MSC's IGBT and diode lifetimes are affected by the converter control strategy as the wind speed reaches the rated value. However, for assessing the converter lifetime, IGBT and the diode lifetimes should be considered together as well as the number of each of them in the converter circuit. The converter lifetime is considered as a system of stressed components which can be evaluated by applying Miner's rule [17] as in equation (4).

$$N_{conv} = \left(\frac{S_{igbt}}{N_{igbt}} + \frac{S_{diode}}{N_{diode}}\right)^{-1} \quad (4)$$

Where N_{conv} is the converter cycles to failure, S_{igbt} and S_{diode} are number of IGBTs and diodes in the converter respectively (equal to 6 in the 2L-VSC), and N_{igbt} and N_{diode} are cycles to failure of the IGBT and diode respectively.
Table 5 lists N_{conv} of both control strategies, DTC and FOC, ($N_{convDTC}$ and $N_{convFOC}$ respectively), and the ratio of them (ρ_{conv}) which is calculated by equation (5).

$$\rho_{conv} = \frac{N_{convDTC}}{N_{convFOC}} \quad (5)$$

Table 5 converter cycles to failure of DTC and FOC and their ratio

Wind speed (m/s)	$N_{convDTC}$	$N_{convFOC}$	ρ_{conv}
4	2.16×10^{11}	2.16×10^{11}	1.001
6	5.84×10^{9}	5.86×10^{9}	0.996
8	2.66×10^{8}	2.73×10^{8}	0.975
10	1.25×10^{7}	1.33×10^{7}	0.936
12	4.56×10^{5}	5.37×10^{5}	0.849

Further analysis can be conducted by comparing ρ_{conv} in Table 5 with ρ_{igbt} and ρ_{diode} in Table 4 and reveals that ρ_{conv} values are close to ρ_{diode} values because the diode shows much lower cycles to failure than the IGBT at higher wind speeds as in Table 3. That indicates that the diode is the dominant risk of failure component in the MSC of PMSG wind turbines.

This result is in line with published research about semiconductor thermal loading and lifetime analysis in wind turbine converters, such as [18] and [8].

Fig. 5 show the trends of ρ_{igbt}, ρ_{diode}, and ρ_{conv} with respect to wind speed which clearly shows how ρ_{conv} is close to ρ_{diode}.

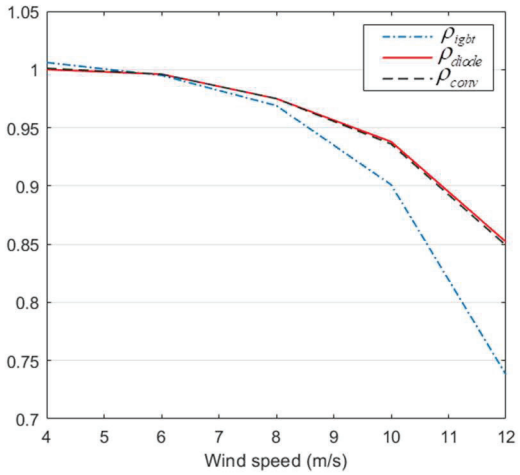

Fig. 5 interaction of ρ_{igbt}, ρ_{diode}, and ρ_{conv} with wind speed

The converter lifetime is highly impacted by its semiconductors' junction temperatures which are influenced by their power losses. Therefore, the changes in lifetime indicate changes in converter semiconductors' power losses. While converter IGBT and diode show different lifetime ratios when operating with DTC compared to FOC, that indicates the control strategy has an impact on the loading of the converter semiconductors.

4 Conclusion

This paper has presented how converter control strategy affects wind turbine power converter lifetime. Comparing the most popular control strategies, DTC and FOC, in PMSG wind turbines reveals how the converter lifetime is reduced to 85% when operated with DTC rather than FOC at the rated wind speed in the modelled wind turbine.

The paper also reveals how converter semiconductors, IGBTs and diodes, are affected differently by the control strategy selection between DTC and FOC. Although the IGBT lifetime is reduced to 74% at rated wind speed, the converter diode continues to be showed the highest risk of failure in the fully-rated MSC. Therefore, the converter lifetime is impacted by a similar percentage of its diode when operated with DTC.

The converter control strategy and wind speed are likely to be interacting and affecting the reliability of fully-rated converters in wind turbine applications.

5 Acknowledgements

This research is funded by the UK EPSRC Prosperity Partnership in Offshore Wind (EP/R004900/1) (npow.group.shef.ac.uk).

6 References

[1] C. Dao, B. Kazemtabrizi, and C. Crabtree, "Wind turbine reliability data review and impacts on levelised cost of energy," *Wind Energy*, vol. 22, no. 12, pp. 1848–1871, 2019, doi: 10.1002/we.2404.

[2] T. R. S. De Freitas, P. J. M. Menegáz, and D. S. L. Simonetti, "Rectifier topologies for permanent magnet synchronous generator on wind energy conversion systems: A review," *Renew. Sustain. Energy Rev.*, vol. 54, pp. 1334–1344, 2016, doi: 10.1016/j.rser.2015.10.112.

[3] I. M. de Alegría, J. Andreu, J. L. Martín, P. Ibañez, J. L. Villate, and H. Camblong, "Connection requirements for wind farms: A survey on technical requierements and regulation," *Renew. Sustain. Energy Rev.*, vol. 11, no. 8, pp. 1858–1872, 2007, doi: 10.1016/j.rser.2006.01.008.

[4] G. S. Buja and M. P. Kazmierkowski, "Direct torque control of PWM inverter-fed AC motors - A survey," *IEEE Trans. Ind. Electron.*, vol. 51, no. 4, pp. 744–757, 2004, doi: 10.1109/TIE.2004.831717.

[5] T. Barisa, D. Sumina, and M. Kutija, "Control of generator-and grid-side converter for the interior permanent magnet synchronous generator," in *2015 International Conference on Renewable Energy Research and Applications, ICRERA 2015*, 2015, pp. 1015–1020, doi: 10.1109/ICRERA.2015.7418563.

[6] I. Takahashi and T. Noguchi, "A New Quick-Response and High-Efficiency Control Strategy of an Induction Motor," *IEEE Trans. Ind. Appl.*, vol. IA-22, no. 5, pp. 820–827, 1986, doi: 10.1109/TIA.1986.4504799.

[7] M. Jasiński and M. P. Kazmierkowski, "Fundamentals of AC-DC-AC converters control and applications," in *Power Electronics and Motor Drives*, no. 2011, 2016, pp. 16.1-16.39.

[8] C. J. Smith, C. J. Crabtree, and P. C. Matthews, "Impact of wind conditions on thermal loading of PMSG wind turbine power converters," *IET Power Electron.*, vol. 10, no. 11, pp. 1268–1278, 2017, doi: 10.1049/iet-pel.2016.0802.

[9] I. F. Kovačević-Badstuebner, J. W. Kolar, and U. Schilling, "Modelling for the lifetime prediction of power semiconductor modules," in *Reliability of Power Electronic Converter Systems*, 2016, pp. 103–140.

[10] The Mathworks Inc, "MATLAB." The Mathworks Inc., Natick, Massachusetts, 2020, [Online]. Available: http://mathworks.com.

[11] The Mathworks Inc, "Simulink." 2020.

[12] B. Wu, Y. Lang, N. Zargari, and S. Kouro, "Appendix B: Generator Parameters," in *Power Conversion and Control of Wind Energy Systems*, A JOHN WILEY & SONS, INC., PUBLICATION, 2011, pp. 319–326.

[13] B. Wu, Y. Lang, N. Zargari, and S. Kouro, *Power Conversion and Control of Wind Energy System*, vol. 148. A JOHN WILEY & SONS, INC., PUBLICATION, 2011.

[14] D. Świerczyński, M. P. Kaźmierkowski, and F. Blaabjerg, "Direct torque control of permanent magnet synchronous motor (PMSM) using space vector modulation (DTC-SVM) - Simulation and experimental results," in *IECON Proceedings (Industrial Electronics Conference)*, 2002, vol. 1, pp. 751–755, doi: 10.1109/iecon.2002.1187601.

[15] SEMIKRON INTERNATIONAL GmbH, "SKM800GA176D." https://www.semikron.com/products/product-classes/igbt-modules/detail/skm800ga176d-22890435.html (accessed Sep. 08, 2021).

[16] B. Andresen and J. Birk, "A high power density converter system for the Gamesa G10x 4,5 MW wind turbine," in *2007 European Conference on Power Electronics and Applications, EPE*, 2007, pp. 1–8, doi: 10.1109/EPE.2007.4417312.

[17] M. A. Miner, "Cumulative Damage in Fatigue," *J. Appl. Mech.*, vol. 12, no. 3, pp. A159–A164, 1945, doi: 10.1115/1.4009458.

[18] E. Baygildina, P. Peltoniemi, O. Pyrhonen, K. Ma, and F. Blaabjerg, "Thermal loading of wind power converter considering dynamics of wind speed," in *IECON Proceedings (Industrial Electronics Conference)*, 2013, pp. 1362–1367, doi: 10.1109/IECON.2013.6699331.

Appendix B

Datasheet

This appendix includes SKM800AG176D power module datasheet:

SKM 800GA176D

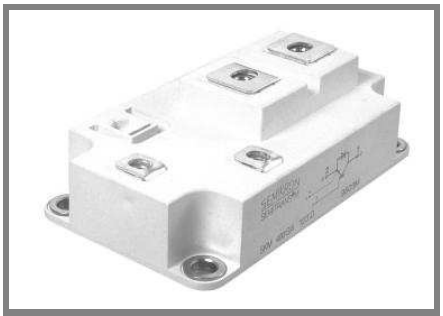

SEMITRANS® 4

Trench IGBT Modules

SKM 800GA176D

Features

- Homogeneous Si
- Trench = Trenchgate technology
- V_{CEsat} with positive temperature coefficient
- High short circuit capability, self limiting to 6 x I_c

Typical Applications*

- AC inverter drives mains 575 - 750 V AC
- Public transport (auxiliary syst.)
- Wind power

Remarks

- $I_{DC} \leq 500$ A limited for $T_{Terminal}$ = 100 °C

Absolute Maximum Ratings T_c = 25 °C, unless otherwise specified

Symbol	Conditions		Values	Units
IGBT				
V_{CES}	T_j = 25 °C		1700	V
I_C	T_j = 150 °C	T_c = 25 °C	830	A
		T_c = 80 °C	590	A
I_{CRM}	I_{CRM}=2xI_{Cnom}		1200	A
V_{GES}			± 20	V
t_{psc}	V_{CC} = 1200 V; $V_{GE} \leq$ 20 V; V_{CES} < 1700 V	T_j = 125 °C	10	µs
Inverse Diode				
I_F	T_j = 150 °C	T_c = 25 °C	630	A
		T_c = 80 °C	440	A
I_{FRM}	I_{FRM}=2xI_{Fnom}		1200	A
I_{FSM}	t_p = 10 ms; sin.	T_j = 150 °C	3600	A
Module				
$I_{t(RMS)}$			500	A
T_{vj}			- 40 ... + 150	°C
T_{stg}			- 40 ... + 125	°C
V_{isol}	AC, 1 min.		4000	V

Characteristics T_c = 25 °C, unless otherwise specified

Symbol	Conditions		min.	typ.	max.	Units
IGBT						
$V_{GE(th)}$	V_{GE} = V_{CE}, I_C = 24 mA		5,2	5,8	6,4	V
I_{CES}	V_{GE} = 0 V, V_{CE} = V_{CES}	T_j = 25 °C			4	mA
V_{CE0}		T_j = 25 °C		1	1,2	V
		T_j = 125 °C		0,9	1,1	V
r_{CE}	V_{GE} = 15 V	T_j = 25°C		1,7	2,1	mΩ
		T_j = 125°C		2,5		mΩ
$V_{CE(sat)}$	I_{Cnom} = 600 A, V_{GE} = 15 V	T_j = 25°C$_{chiplev.}$		2	2,45	V
		T_j = 125°C$_{chiplev.}$		2,45	2,9	V
C_{ies}	V_{CE} = 25, V_{GE} = 0 V	f = 1 MHz		39,6		nF
C_{oes}				2,2		nF
C_{res}				2,5		nF
Q_G	V_{GE} = -8V...+15V			4800		nC
$t_{d(on)}$	R_{Gon} = 3 Ω	V_{CC} = 1200V		230		ns
t_r		I_C= 600A		90		ns
E_{on}		T_j = 125 °C		335		mJ
$t_{d(off)}$	R_{Goff} = 3 Ω	V_{GE} = ± 15V		1030		ns
t_f				160		ns
E_{off}				245		mJ
$R_{th(j-c)}$	per IGBT				0,04	K/W

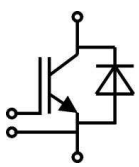

GA

SKM 800GA176D

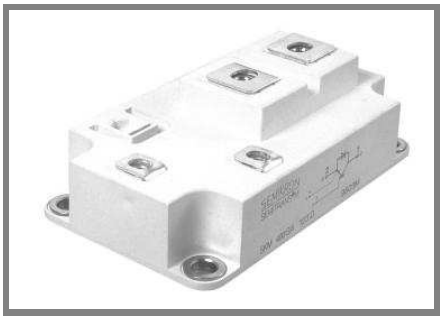

SEMITRANS® 4

Trench IGBT Modules

SKM 800GA176D

Features

- Homogeneous Si
- Trench = Trenchgate technology
- V_{CEsat} with positive temperature coefficient
- High short circuit capability, self limiting to 6 x I_c

Typical Applications*

- AC inverter drives mains 575 - 750 V AC
- Public transport (auxiliary syst.)
- Wind power

Remarks

- $I_{DC} \leq 500$ A limited for $T_{Terminal}$ = 100 °C

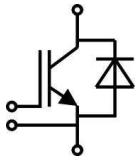

GA

Characteristics						
Symbol	**Conditions**		**min.**	**typ.**	**max.**	**Units**
Inverse Diode						
$V_F = V_{EC}$	I_{Fnom} = 600 A; V_{GE} = 0 V	T_j = 25 °$C_{chiplev.}$		1,6	1,9	V
		T_j = 125 °$C_{chiplev.}$		1,6		V
V_{F0}		T_j = 25 °C		1,1	1,3	V
r_F		T_j = 25 °C		0,83	1	mΩ
I_{RRM}	I_F = 600 A	T_j = 125 °C		650		A
Q_{rr}	di/dt = 6400 A/µs			230		µC
E_{rr}	V_{GE} = -15 V; V_{CC} = 1200 V			155		mJ
$R_{th(j-c)D}$	per diode				0,07	K/W
Module						
L_{CE}				15	20	nH
$R_{CC'+EE'}$	res., terminal-chip	T_{case}= 25 °C		0,18		mΩ
		T_{case}= 125 °C		0,22		mΩ
$R_{th(c-s)}$	per module				0,038	K/W
M_s	to heat sink M6		3		5	Nm
M_t	to terminals M6 (M4)		2,5 (1,1)		5 (2)	Nm
w					330	g

This is an electrostatic discharge sensitive device (ESDS), international standard IEC 60747-1, Chapter IX.

* The specifications of our components may not be considered as an assurance of component characteristics. Components have to be tested for the respective application. Adjustments may be necessary. The use of SEMIKRON products in life support appliances and systems is subject to prior specification and written approval by SEMIKRON. We therefore strongly recommend prior consultation of our personal.

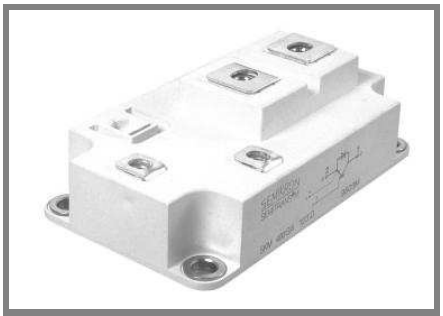

SEMITRANS® 4

Trench IGBT Modules

SKM 800GA176D

Features

- Homogeneous Si
- Trench = Trenchgate technology
- V_{CEsat} with positive temperature coefficient
- High short circuit capability, self limiting to 6 x I_c

Typical Applications*

- AC inverter drives mains 575 - 750 V AC
- Public transport (auxiliary syst.)
- Wind power

Remarks

- $I_{DC} \leq 500$ A limited for $T_{Terminal}$ = 100 °C

GA

Z_{th} Symbol	Conditions	Values	Units
$Z_{th(j-c)I}$			
R_i	i = 1	28	mk/W
R_i	i = 2	9,5	mk/W
R_i	i = 3	2,17	mk/W
R_i	i = 4	0,33	mk/W
tau_i	i = 1	0,0447	s
tau_i	i = 2	0,02	s
tau_i	i = 3	0,0015	s
tau_i	i = 4	0,0025	s
$Z_{th(j-c)D}$			
R_i	i = 1	46	mk/W
R_i	i = 2	17	mk/W
R_i	i = 3	5,9	mk/W
R_i	i = 4	1,1	mk/W
tau_i	i = 1	0,05	s
tau_i	i = 2	0,0075	s
tau_i	i = 3	0,002	s
tau_i	i = 4	0,0002	s

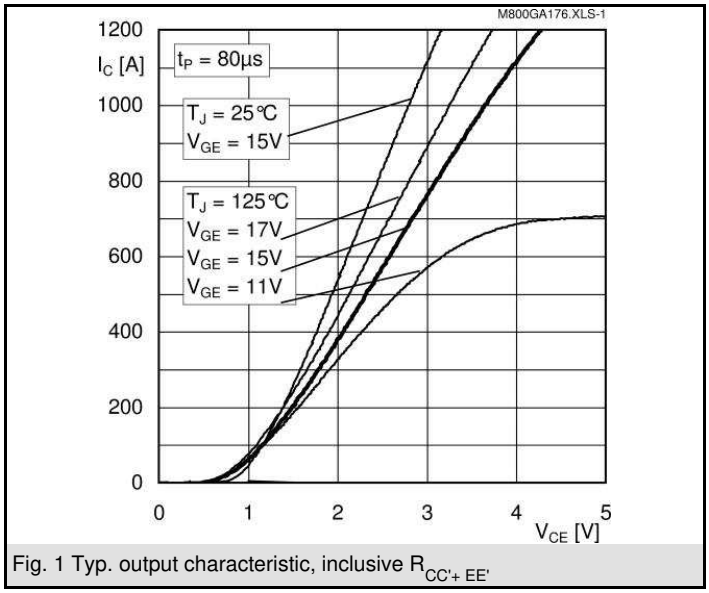

Fig. 1 Typ. output characteristic, inclusive $R_{CC'+EE'}$

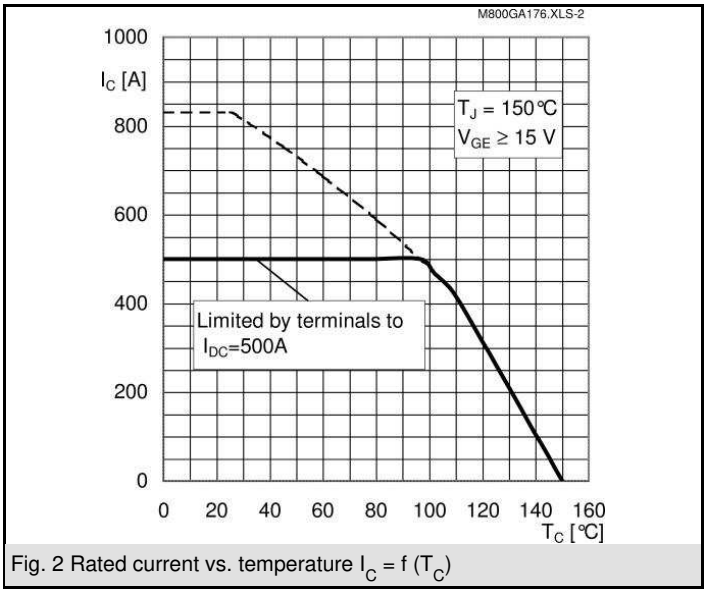

Fig. 2 Rated current vs. temperature $I_C = f(T_C)$

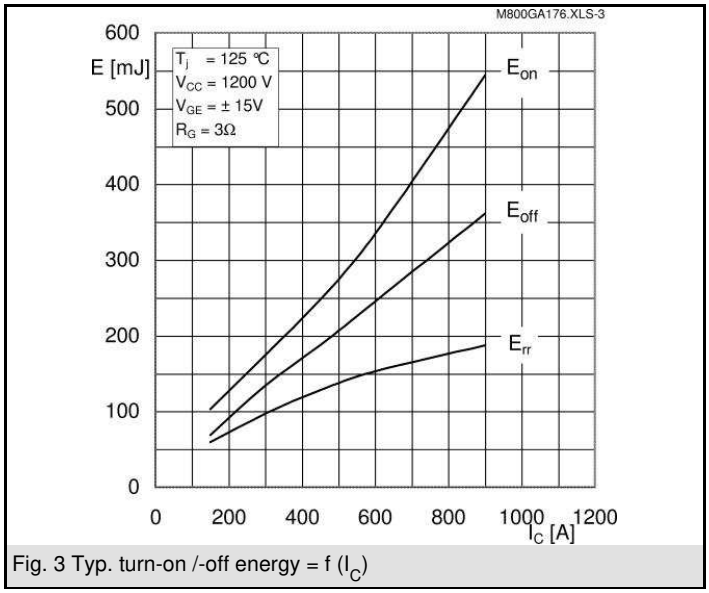

Fig. 3 Typ. turn-on /-off energy = f (I_C)

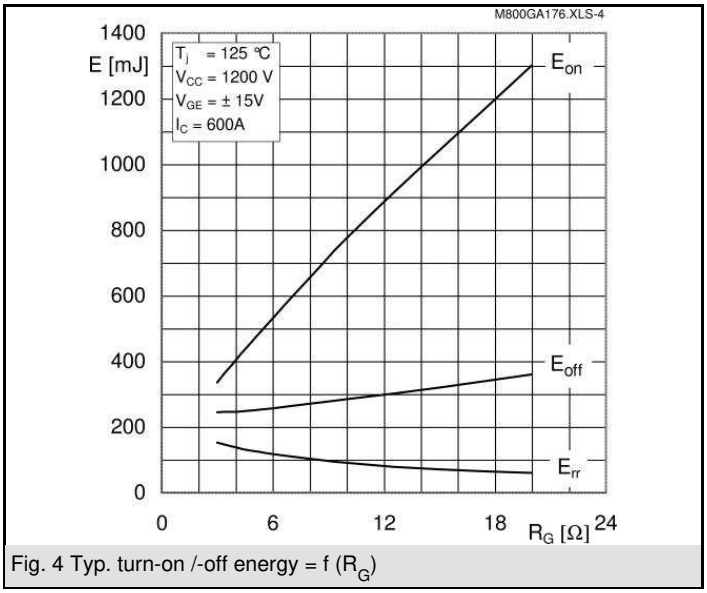

Fig. 4 Typ. turn-on /-off energy = f (R_G)

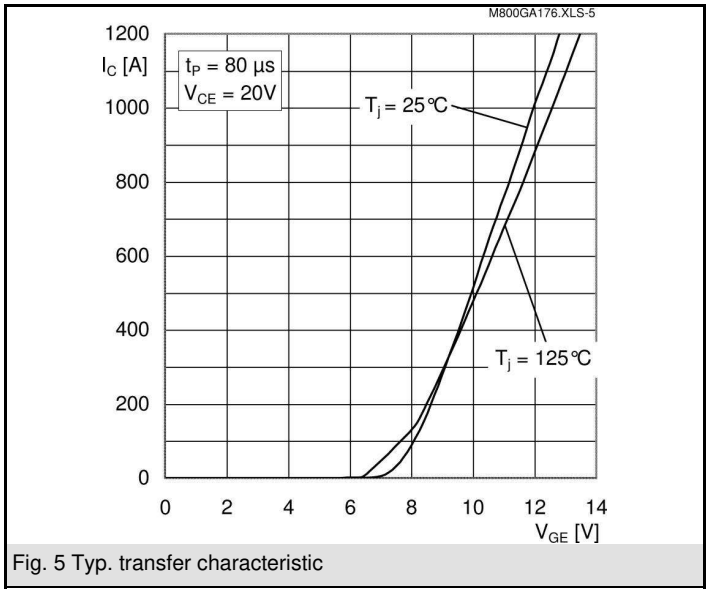

Fig. 5 Typ. transfer characteristic

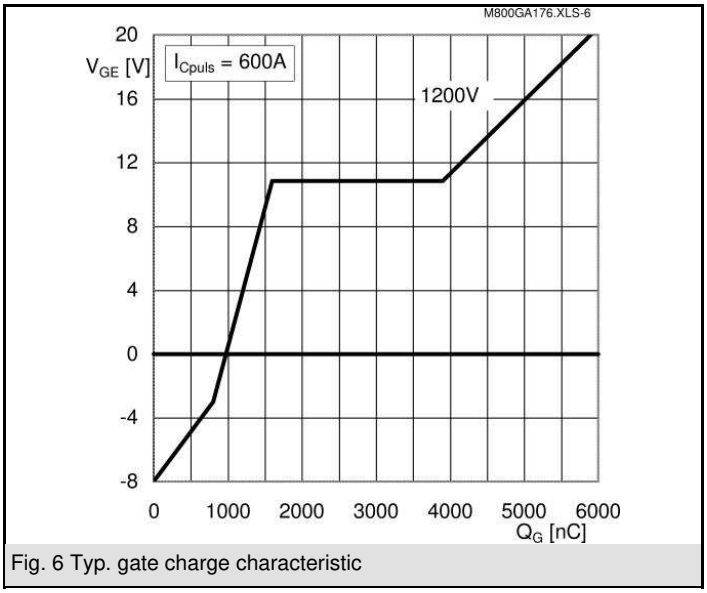

Fig. 6 Typ. gate charge characteristic

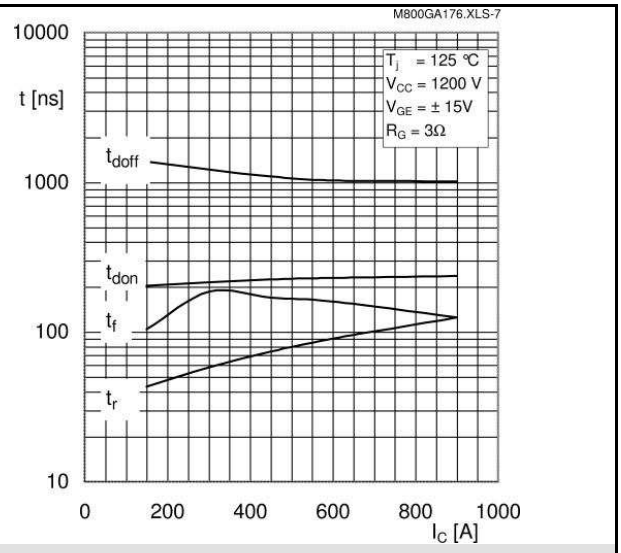

Fig. 7 Typ. switching times vs. I_C

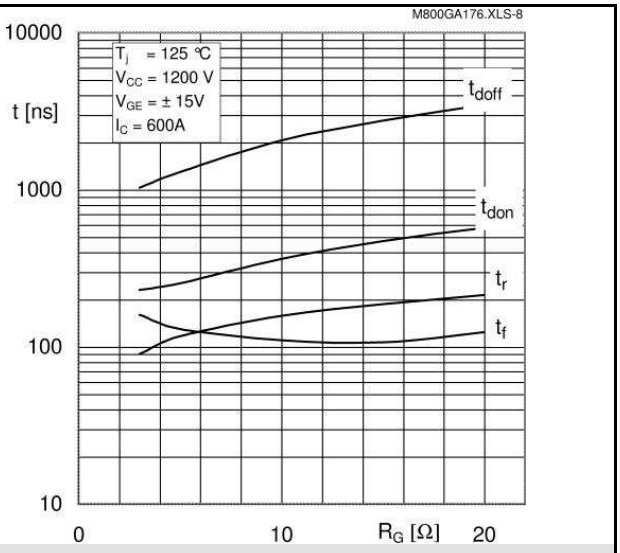

Fig. 8 Typ. switching times vs. gate resistor R_G

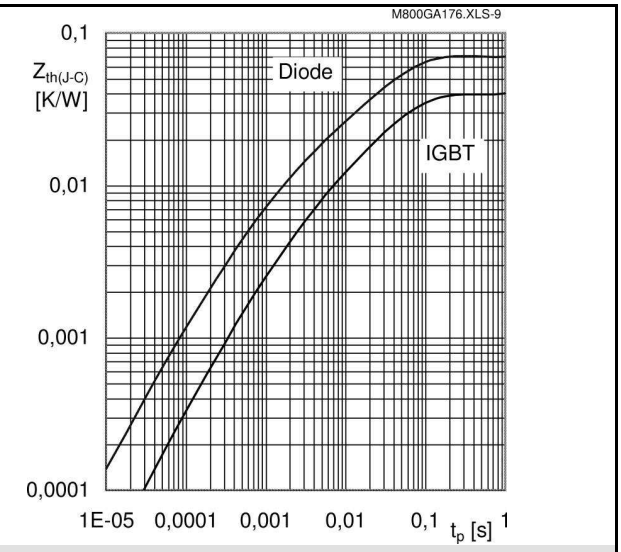

Fig. 9 Transient thermal impedance

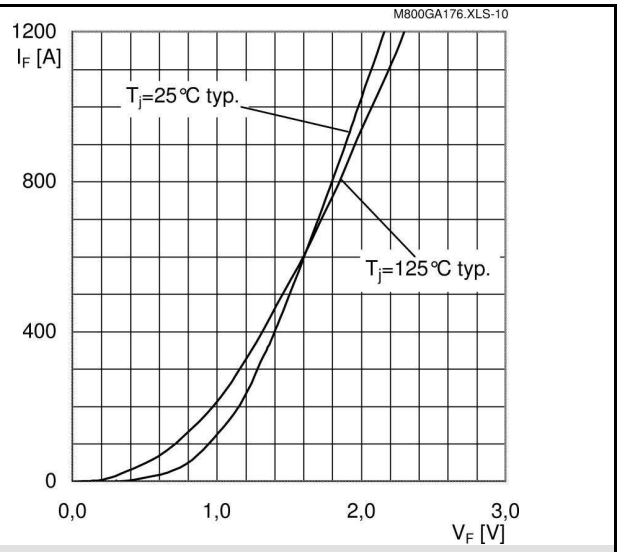

Fig. 10 Typ. CAL diode forward characteristic

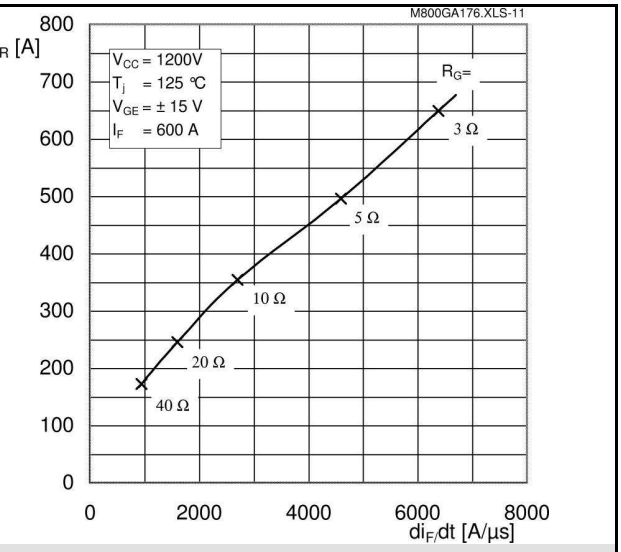

Fig. 11 Typ. CAL diode peak reverse recovery current

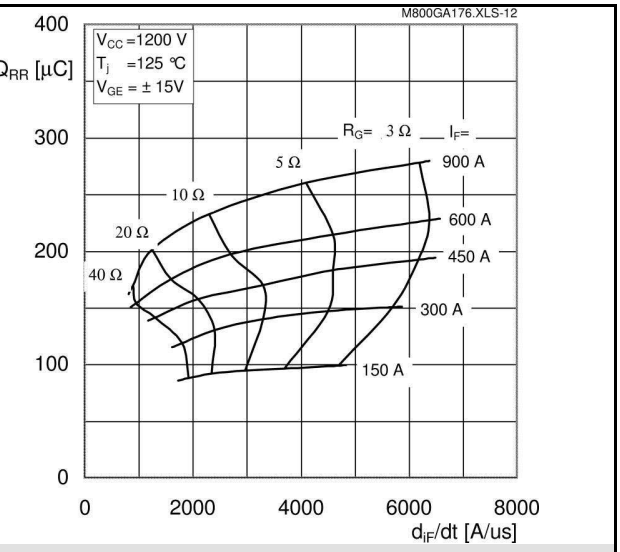

Fig. 12 Typ. CAL diode peak reverse recovery charge

SKM 800GA176D

UL Recognized File no. E 63 532

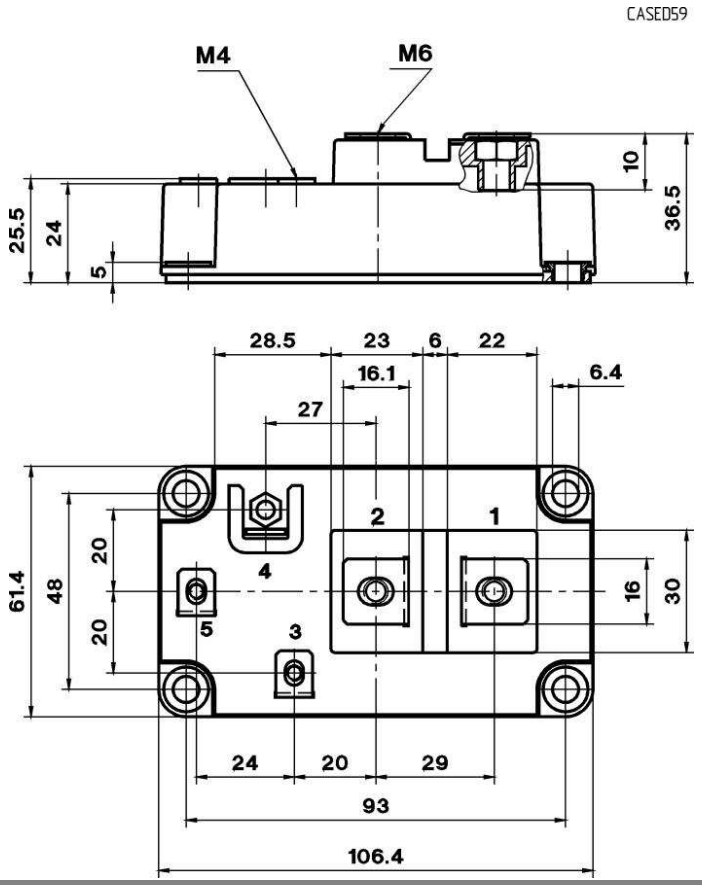

Case D 59

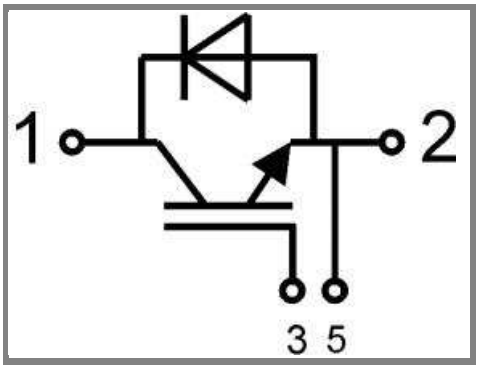

GA Case D 59

